
Analysis of host-pathogen interactions in novel three dimensional surrogate infection models

Christoph Guggenberger

Dissertation
an der Fakultät für Biologie
der Ludwig-Maximilians-Universität
München

vorgelegt von
Christoph Guggenberger
aus München

München, den 8. August 2011

Erster Gutachter	Prof. Dr. Michael Boshart
Zweiter Gutachter	Prof. Dr. Charles David
Sondergutachter	Prof. Dr. Dr. Jürgen Heesemann

Dissertation eingereicht:	8. August 2011
Tag der mündlichen Prüfung:	15. Dezember 2011

To my parents

Contents

Summary	v
Zusammenfassung	vii
List of Figures	x
List of Abbreviations	xi
1 Introduction	1
1.1 Infection models between complexity and accessibility	1
1.2 Neutrophils as the first line of cellular host defense	4
1.2.1 Neutrophil biology	4
1.2.2 Rho GTPases	6
1.2.3 Interstitial leukocyte migration	8
1.3 Paradigmatic pathogenic microorganisms for the study of host cell-pathogen interactions	9
1.3.1 <i>Staphylococcus aureus</i>	9
1.3.2 <i>Yersinia enterocolitica</i>	12
1.3.2.1 <i>Y. enterocolitica</i> pathogenesis	12
1.3.2.2 The pYV plasmid and <i>Yersinia</i> outer proteins (Yops)	13
1.3.3 Uropathogenic <i>Escherichia coli</i>	15
1.3.4 <i>Entamoeba histolytica</i>	17
1.4 Aims of this work	18
2 Materials and Methods	19
2.1 Materials	19
2.1.1 Strains, plasmids and oligonucleotides	19
2.1.1.1 Strains	19
2.1.1.2 Plasmids	22
2.1.1.3 Oligonucleotides	23
2.1.2 Instruments	23
2.1.3 Consumables	25
2.1.4 Chemicals, biochemicals, kits and enzymes	26
2.1.5 Antibodies	28
2.1.6 Animals	28
2.1.6.1 Mouse strains	28

2.1.6.2	Harvesting of organs	29
2.1.6.3	Infection experiments	29
2.2	Methods	29
2.2.1	Microbiological methods	29
2.2.1.1	Microbiological media	29
2.2.1.2	Antibiotics and media supplements	30
2.2.1.3	Cultivation and storage of microorganisms	30
2.2.1.4	Preparation of microorganisms for infection experiments	30
2.2.1.5	Transformation	31
2.2.2	Molecular biological methods	32
2.2.2.1	Isolation of DNA	32
2.2.2.2	Separation of DNA by gel electrophoresis	32
2.2.2.3	Modification of DNA	32
2.2.2.4	Construction of plasmids	32
2.2.2.5	Generation of chromosomal mutants	33
2.2.3	Biochemical and analytical methods	34
2.2.3.1	SDS polyacrylamide gel electrophoresis, SDS-PAGE	34
2.2.3.2	Western blotting	34
2.2.3.3	Precipitation of secreted proteins	34
2.2.3.4	Extraction of membrane-associated <i>S. aureus</i> proteins	35
2.2.3.5	Mass spectrometry	35
2.2.3.6	Transmission electron microscopy	35
2.2.3.7	Immunoassay for cytokine measurements	36
2.2.3.8	Flow cytometry	36
2.2.4	Cell biological methods	36
2.2.4.1	Media and cultivation	36
2.2.4.2	Generation of bone marrow-derived dendritic cells (DCs)	37
2.2.4.3	Generation of bone marrow-derived macrophages (BMMs)	37
2.2.4.4	Isolation of PMNs from peripheral human blood	37
2.2.4.5	HeLa cell culture	38
2.2.4.6	Determination of cell count	38
2.2.4.7	β -lactamase reporter assay	38
2.2.4.8	Lactate dehydrogenase (LDH) release assay	39
2.2.4.9	Transfection of dendritic cells	39
2.2.4.10	Immunocytochemistry ICC	39
2.2.4.11	Live cell stainings	40
2.2.4.11.1	DNA	40
2.2.4.11.2	Surface of epithelial and urothelial cells	40
2.2.4.11.3	Pathogens	40
2.2.4.12	Microscopy and image processing	40
2.2.5	Experimental setups	41

2.2.5.1	3D-CoG spleen slice infection model (3D-CoG/SSIM) . . .	41
2.2.5.2	3D-CoG migration assay	42
2.2.5.3	Under-agarose migration assay	43
2.2.5.4	<i>Ex vivo</i> microscopy in the organ chamber	44
2.3	Statistical analysis	44
3	Results	45
3.1	3D-CoG based <i>in vitro</i> model	45
3.1.1	Development of the 3D-CoG/spleen slice infection model	45
3.1.2	<i>Staphylococcus aureus</i> abscess formation	48
3.1.2.1	Growth of <i>S. aureus</i> in the 3D-CoG system	48
3.1.2.2	Dispersion of microcolonies as a result of fibrin degradation	54
3.1.2.3	Bacterial microcolonies are protected from host immune cells by MAM	57
3.1.2.4	The pseudocapsule acts as a second mechanical barrier against neutrophils	58
3.1.2.5	A therapeutic anticoagulant abrogates barrier activity . . .	61
3.1.3	Inhibition of immune cell migration by <i>Yersinia</i>	64
3.1.3.1	Characteristics of <i>Yersinia</i> microcolony formation in 3D-CoG	64
3.1.3.1.1	Growth of <i>Y. enterocolitica</i> in the 3D-CoG system	64
3.1.3.1.2	Interaction of microcolonies with neutrophils . . .	64
3.1.3.2	Inhibition of cell migration by <i>Y. enterocolitica</i>	66
3.1.3.3	Cell biological characteristics of <i>Y. enterocolitica</i> -infected cells	69
3.1.3.3.1	Analysis of the YopT-mediated elongated morpho- type on the cellular level	69
3.1.3.3.2	RhoA is the YopT target mediating this elongated morphotype	73
3.1.3.3.3	Conservation of the YopT-targeted migration mech- anism	73
3.1.3.4	Comparison of RhoA-active Yops from <i>Y. enterocolitica</i> and <i>Y. pseudotuberculosis</i>	75
3.1.3.4.1	YopE- and YopT-mediated inhibition of cell mi- gration	75
3.1.3.4.2	Analysis on the cellular level	76
3.1.3.4.3	Degradation of plasma membrane integrity	78
3.1.3.4.4	Homology modeling	82
3.2	Organ explant-based <i>ex vivo</i> model	86
3.2.1	The organ chamber	86
3.2.2	Interaction of uropathogenic <i>Escherichia coli</i> with urothelium	88
3.2.2.1	Tissue preservation in the organ chamber	88

3.2.2.2	Properties of intracellular bacterial communities (IBCs) . . .	88
3.2.2.3	The dynamic response of cellular immunity to breach of the urothelial barrier	91
3.2.2.4	Analysis of cytokine release as a result of infection	93
3.2.3	Invasion of caecum epithelia by <i>E. histolytica</i>	93
3.2.4	Extension of the system to other organs and pathogens	95
4	Discussion	99
4.1	3D-CoG based model	99
4.1.1	Development of the 3D-CoG/spleen slice infection model	99
4.1.2	<i>Staphylococcus aureus</i> abscess formation	100
4.1.2.1	Coagulase-mediated encapsulation of microcolonies	100
4.1.2.2	Endogenous degradation of microcolonies	103
4.1.2.3	Coa and vWbp cooperate in shielding microcolonies from neutrophils	103
4.1.2.4	Pharmacological interference with encapsulation	105
4.1.3	Inhibition of immune cell migration by <i>Yersinia</i>	107
4.1.3.1	Implications of <i>Yersinia</i> microcolony formation	107
4.1.3.2	Yop effects on amoeboid leukocyte migration	108
4.1.3.3	<i>Yersinia</i> species-dependent cellular effects of YopE and YopT	113
4.1.3.3.1	Effects on cell migration	113
4.1.3.3.2	Degradation of plasma membrane integrity	116
4.1.3.3.3	Homology modeling	117
4.2	Organ explant-based <i>ex vivo</i> model	118
4.2.1	Development of an <i>ex vivo</i> infection model	118
4.2.2	Pathogenic mechanisms of uropathogenic <i>E. coli</i> and <i>E. histolytica</i> .	121
4.3	Conclusion	123
	References	124
	Appendix: Movie legends	138
	List of Publications	145
	Acknowledgements	147
	Curriculum Vitae	149

Summary

Consideration of a three-dimensional (3D) context is important for understanding host-pathogen interactions. This additional information gained in a 3D system is often sacrificed in two-dimensional (2D) cell culture models for infection biology in favor of improved control of the system. An integrated view of the interplay of single processes during infection is often gained only in *in vivo* infection models, which are difficult to control due to their complexity. The present work combines advantages of cell culture and mouse models in novel *in vitro* and *ex vivo* infection models which provide a more detailed understanding of mechanistic basics already in such simplistic models. In combination with confocal microscopy, these models enable analysis of host-pathogen interactions in high spatial and temporal resolution. The developed models were employed in order to characterize pathogenic mechanisms of exemplary microbial agents with regard to a 3D context.

A 3D-collagen gel/spleen slice infection model (3D-CoG/SSIM) was established, allowing the investigation of microbial growth phenotypes with consideration of a tissue-like 3D context. Moreover, it permits study of the effects of such multicellular bacterial structures on the interaction with neutrophils as the first line of cellular immunity.

In this system it was shown that *Staphylococcus aureus* forms microcolonies which are enclosed by two concentric fibrin structures in the presence of the human plasma protein fibrinogen. These structures resemble staphylococcal abscesses in a published mouse infection model. However, the presented results exceed these *in vivo* observations by assigning distinct functions to the two known staphylocoagulases, which have been regarded as redundant in the mouse model so far: the coagulase vWbp mediated the formation of a fibrin-based microcolony-associated meshwork (MAM) in the periphery, whereas the coagulase Coa influenced the inner pseudocapsule which encloses the microcolony. A barrier function against neutrophils was shown for both structures, indicating that their formation can be considered as a protective mechanism of staphylococci against phagocytes. Finally,

it was exemplarily shown that a thrombin inhibitor in clinical use could be utilized to improve the accessibility of microcolonies to neutrophils.

Yersinia enterocolitica has been demonstrated to form abscess-like microcolonies in 3D-CoG. Application of 3D-CoG/SSIM showed that phagocytosis resistance of *Yersinia* microcolonies is predominantly mediated by the type III secretion system. For neutrophils interacting with yersiniae, a morphotype characterized by strongly elongated cell morphology could be described, causing paralysis of migration in the long term. This inhibition of amoeboid leukocyte migration was analyzed in a migration model based on dendritic cells. The observed paralysis of migration could be assigned to the effector protein YopT and the mediated inhibition of cellular RhoA function by employment of genetically defined *Yersinia* mutants and a ‘toolbox’ strain which is able to translocate single effector proteins. The characterization of the respective effector proteins of *Y. pseudotuberculosis* showed clear differences in the effects on cytoskeleton dynamics, which might result from different Rho GTPase specificity. Eventually, homology-based structure models of the effectors YopE and YopT were generated and evaluated in regard to the known differences in the amino acid sequence.

In the last part of this work, physiological tissue context was included in addition to a 3D context. An *ex vivo* model was established for the analysis of infection of mucous membranes by representative pathogens. The presented model is a further development of tissue explant microscopy and enables, in addition to microscopic characterization, the analysis of secreted proteins, exemplified by cytokine secretion during uropathogenic *Escherichia coli* infection of the urinary bladder. The broad applicability of this model was furthermore proved by demonstrating penetration of intestinal epithelium by *Entamoeba histolytica*.

Taken together, results obtained from the established infection models substantiate the importance of a 3D context for fundamental pathogenic mechanisms of *Staphylococcus aureus*, *Yersinia enterocolitica* and uropathogenic *Escherichia coli*.

Zusammenfassung

Die Berücksichtigung eines dreidimensionalen (3D) Kontexts ist ein wichtiger Faktor für das Verständnis von Wirt-Pathogen-Interaktionen, der in vereinfachten zweidimensionalen (2D) Zellkulturmodellen der Infektionsbiologie oft vernachlässigt wird. Dieser Nachteil wird zugunsten von hoher Kontrollierbarkeit des Systems in Kauf genommen. Ein integrierteres Bild des Zusammenwirkens einzelner Prozesse während einer Infektion ergibt sich oft erst in *in vivo* Infektionsmodellen, die in ihrer Komplexität jedoch schwer zu beherrschen sind. Die vorliegende Arbeit kombiniert Vorteile von Zellkultur- und Mausmodellen in neuartigen *in vitro* und *ex vivo* Infektionsmodellen, die bereits auf dieser Stufe ein detaillierteres Verständnis mechanistischer Grundlagen erzielen können. Als Methode kommt vor allem die Konfokalmikroskopie zum Einsatz, welche eine Analyse dynamischer Wirt-Pathogen-Interaktionen in hoher räumlicher und zeitlicher Auflösung ermöglicht. Die Modelle wurden eingesetzt, um Pathogenitätsmechanismen exemplarischer mikrobieller Erreger unter Berücksichtigung des 3D-Kontexts zu charakterisieren.

Ein 3D-Kollagengel/Milzschnitt-Infektionsmodell (3D-collagen gel/spleen slice infection model, 3D-CoG/SSIM) wurde entwickelt, das die Untersuchung mikrobieller Wachstumsformen unter Berücksichtigung eines Gewebe-ähnlichen 3D-Kontextes erlaubt. Darüber hinaus bietet es die Möglichkeit, die Auswirkung ebensolcher multizellulärer bakterieller Strukturen auf die Interaktion mit Neutrophilen als erste Linie der zellulären Immunität zu untersuchen.

Es wurde gezeigt, dass *Staphylococcus aureus* in diesem Modell in Gegenwart des Plasmaproteins Fibrinogen Mikrokolonien bildet, die von zwei konzentrischen Fibrinstrukturen umschlossen sind. Diese Struktur weist große Ähnlichkeit zu Staphylokokken-Abszessen in einem publizierten Mausmodell auf. Das Ergebnis der vorliegenden Arbeit geht aber über diese *in vivo* Beobachtungen insofern hinaus, als dass den beiden bekannten Staphylokoagulasen, die im Mausmodell bislang als redundant betrachtet wurden, distinkte Funktionen zugeordnet werden konnten: die Koagulase vWbp vermittelt die Ausbildung eines Fibrin-

netzwerkes in der Peripherie, wohingegen die Koagulase Coa einen Einfluss auf die direkt an die Mikrokolonie anliegende innere Pseudokapsel hat. Für beide Strukturen wurde eine Barrierefunktion gegenüber Neutrophilen nachgewiesen, somit handelt es sich hierbei um einen protektiven Mechanismus der Staphylokokken gegen Phagozyten. Abschließend wurde exemplarisch gezeigt, dass ein in klinischer Anwendung befindlicher Thrombininhibitor verwendet werden kann, um die Zugänglichkeit von Mikrokolonien für Neutrophile zu erhöhen.

Für *Yersinia enterocolitica* ist in 3D-CoG eine Ausbildung Abszess-ähnlicher Mikrokolonien gezeigt worden. Die Anwendung des 3D-CoG/SSIM ergab, dass die Phagozytose-resistenz von *Yersinia* Mikrokolonien hauptsächlich auf das Typ III Sekretionssystem zurückzuführen ist. Für mit *Yersinien* interagierende Neutrophile konnte ein durch stark elongierte Zellmorphologie geprägter Morphotyp beschrieben werden, der langfristig zu Migrationsparalyse führt. Diese Inhibition amoeboider Leukozytenmigration wurde in einem auf dendritischen Zellen basierenden Migrationsmodell untersucht. Durch Verwendung genetisch definierter *Yersinia* Mutanten und eines zur Sekretion einzelner Effektorproteine geeigneten "Toolbox-Stammes", konnte die beobachtete Migrationsparalyse auf das Effektorprotein YopT und die hiervon vermittelte Inhibition der zellulären RhoA-Funktion zurückgeführt werden. Eine Untersuchung entsprechender Effektoren aus *Y. pseudotuberculosis* ergab deutliche Unterschiede in den Auswirkungen auf die Dynamik des Zytoskeletts, welche auf unterschiedlicher Spezifität für zelluläre Rho GTPasen beruhen könnten. Abschließend wurden deshalb Homologiestrukturmodelle der Effektoren YopE und YopT erstellt und bezüglich der bekannten Sequenzunterschiede evaluiert.

Der letzte Teil der Arbeit bezieht neben dem 3D-Kontext auch den physiologischen Gewebeverbund mit ein. Es wurde ein *ex vivo* Modell entwickelt, um exemplarische Infektionen von Schleimhautepithelien zu untersuchen. Das Modell stellt eine Weiterentwicklung der Explantatmikroskopie dar und ermöglicht neben mikroskopischen Untersuchungen auch die Analyse freigesetzter Proteine, was beispielhaft für Zytokinsekretion während *ex vivo* Infektion der Harnblase mit uropathogenem *Escherichia coli* durchgeführt wurde. Die breite Adaptierbarkeit des Modells wurde zudem am Beispiel der Penetration von Darmepithel durch *Entamoeba histolytica* gezeigt.

Zusammenfassend betrachtet, belegen die Ergebnisse der entwickelten Infektionsmodelle die Wichtigkeit des 3D-Kontexts für wesentliche Pathogenitätsmechanismen von *Staphylococcus aureus*, *Yersinia enterocolitica* und uropathogenem *Escherichia coli*.

List of Figures

1.1	The role of dimensionality for the interaction of immune cells with extracellular pathogens	3
1.2	The eukaryotic Rho GTPase cycle and interference by <i>Yersinia</i>	7
1.3	Simplified model of the interference of <i>S. aureus</i> proteins with coagulation and fibrinolysis	11
1.4	Simplified model of UPEC infection of urinary bladder urothelium	16
2.1	3D-CoG migration assay setup	42
2.2	Under-agarose migration assay setup	43
3.1	GFP-neutrophils from <i>lys-EGFP</i> spleen slices and structure of 3D-CoG . . .	47
3.2	Stepwise development of the 3D-CoG/SSIM	47
3.3	Growth phenotypes of <i>S. aureus</i> Newman strains in different environments .	49
3.4	Microcolony and MAM diameter of <i>S. aureus</i> Newman strains after growth in 3D-CoG/Fib	50
3.5	<i>S. aureus</i> microcolonies are surrounded by a pseudocapsule in 3D-CoG/Fib	51
3.6	Degradation of fibrin-containing MAM and pseudocapsule by plasmin . . .	51
3.7	Localization of Coa and Emp to <i>S. aureus</i> pseudocapsules	53
3.8	Detection of Coa, vWbp and Emp	54
3.9	vWbp is responsible for formation of the MAM	55
3.10	Pseudocapsule and MAM formation of different <i>S. aureus</i> strains in 3D-CoG/Fib	56
3.11	Degradation of fibrin-containing MAM and pseudocapsule	56
3.12	<i>S. aureus</i> Newman microcolonies are protected from neutrophils by MAM .	59
3.13	Time projection of interaction of neutrophils with Newman <i>sae</i> mutant in 3D-CoG/Fib	60
3.14	The MAM also functions as a barrier against human neutrophils	60
3.15	The pseudocapsule acts as an additional protective barrier	62
3.16	The thrombin inhibitor argatroban antagonizes staphylococcal barrier activity	63
3.17	Invasin is involved in <i>Y. enterocolitica</i> microcolony formation in 3D-CoG . .	65
3.18	Interaction of neutrophils with <i>Yersinia</i> microcolonies in 3D-CoG/SSIM . .	66
3.19	Elongated morphotype in neutrophils after contact with <i>Y. enterocolitica</i> in 3D-CoG	67

3.20	Characteristic elongated morphotype of DCs after contact with YopT _{yen} -producing strains in 3D-CoG	68
3.21	Inhibition of dendritic cell migration by <i>Y. enterocolitica</i>	69
3.22	Migratory behavior of DCs transfected with MLC-GFP constructs after contact with yersiniae in under-agarose assays	71
3.23	Targeting by T3SS destines DCs for the YopT _{yen} -dependent morphotype . .	72
3.24	Inhibition of the RhoA effector ROCK causes a DC morphotype similar to YopT _{yen}	74
3.25	YopT _{yen} -induced morphotype in different cell types	75
3.26	Inhibition of DC migration by <i>Y. enterocolitica</i> and <i>Y. pseudotuberculosis</i> YopE and YopT, respectively	77
3.27	Typical morphotypes of DCs infected with different <i>Yersinia</i> strains in under-agarose assays	79
3.28	Typical morphotype of Lifeact-DCs after contact with WA(pTTSS, pYopT _{yyp}) in an under-agarose assay	80
3.29	T3SS-mediated LDH release in HeLa cells and neutrophils	80
3.30	Effect of the catalytic activity of YopT on T3SS-mediated LDH release in neutrophils	81
3.31	Sequence alignment of YopT and YopE from <i>Y. enterocolitica</i> and <i>Y. pseudotuberculosis</i>	83
3.32	Structure comparison of YopT _{yen} and YopT _{yyp}	84
3.33	Structure comparison of YopE _{yen} and YopE _{yyp}	85
3.34	Depiction of the organ chamber and the membrane oxygenation device . . .	87
3.35	Functionality of the membrane oxygenation device	87
3.36	Preservation of an urinary bladder explant in the organ chamber	89
3.37	Properties of intracellular bacterial communities (IBCs)	90
3.38	Neutrophil recruitment to IBC-containing epithelial cells	92
3.39	Cytokine patterns of <i>ex vivo</i> infected urinary bladders from C57BL/6 mice	94
3.40	Interaction of <i>E. histolytica</i> trophozoites with caecal mucosa surface	95
3.41	Application of the organ chamber to other hollow organs	97
4.1	Proposed model for the differential actions of Coa and vWbp	102
4.2	Effects of <i>Y. enterocolitica</i> YopT-mediated migration of inhibition	112

List of abbreviations

Abbreviation	Meaning
3D-CoG	Three dimensional collagen gel
3D-CoG/SSIM	Three dimensional collagen gel/spleen slice infection model
BSA	Bovine serum albumine
CaaX	C: Cysteine, a: aliphatic amino acid, X: any amino acid
<i>cfu</i>	Colony forming units
Coa	Coagulase
DC	Dendritic cell
DMEM	Dulbecco's Modified Eagle Medium
DP	Densely packed
ECM	extracellular matrix
Eap	Extracellular adherence protein
Emp	Extracellular matrix adhesion protein
FACS	Fluorescence Activated Cell Sorting
FCS	Fetal calf serum
Fib	Fibrinogen
GAP	GTPase activating protein
GEF	Guanine nucleotide exchange factor
GFP	green fluorescent protein
GlcNAc	N-Acetylglucosamine
GTP	Guanosine triphosphate
Inv	Invasin
LDH	Lactate dehydrogenase
LP	loosely packed
LPS	Lipopolysaccharide
MAM	Microcolony-associated meshwork
MOI	Multiplicity of infection
MSCRAMM	Microbial Surface Components Recognizing Adhesive Matrix Molecules
OD	Optical density
p.i.	post infection
PAGE	Polyacrylamide gel electrophoresis
PBS	Phosphate-buffered saline
pYV	Yersinia virulence plasmid
Sae	<i>Staphylococcus aureus</i> exoprotein expression
SERAM	Secretable Expanded Repertoire Adhesive Molecules
T3SS	Type III secretion system
TCA	Trichloroacetic acid
UPEC	Uropathogenic <i>Escherichia coli</i>
vWbp	von Willebrand factor-binding protein
wt	Wildtype
YadA	Yersinia adhesin A
yen	<i>Y. enterocolitica</i>
yps	<i>Y. pseudotuberculosis</i>
Yops	<i>Yersinia</i> outer proteins

Chapter 1

Introduction

1.1 Infection models between complexity and accessibility

The ultimate goal of infection biology is to understand the complex interplay of host and microbe during an infection in order to develop prevention strategies and treatment options for the infectious disease.

However, an infection is a highly complex interaction between the pathogen and the host immune system, also in regard to both spatial and temporal context/dimension. Thus, infection has to be viewed as a sequence of several processes: invasion of the host by a pathogenic organism, defense of the immune system, dissemination of the pathogen inside the host organism and finally eradication or persistence of the pathogen within the host. During (co)evolution both the pathogen and the host have developed sophisticated mechanisms in this struggle for nutrients and clearance, respectively. The sheer diversity of strategies employed by pathogens requires high flexibility of the host immune system (Merrell and Falkow, 2004).

Infection biology relies on distinct experimental approaches to cope with this complexity. The systems biology approach aims at generating a more holistic picture of complex pathogen-host systems, whereas the traditional approach is more or less reductionistic, focussing on few genes, pathogenicity and host response factors (Forst, 2006).

In a first step, the pathogen and the host cell are basically characterized, for instance in regard to the presence of surface proteins.

Next, specific mechanisms of host-pathogen interactions are singled out and studied *in vitro* to gain a basic understanding of the underlying mechanistic principles such as the involvement of a single bacterial surface protein in adhesion to a host cell. Such studies are

conducted with as much reductionism as possible in order to exclude interference with so far uncharacterized cellular mechanisms such as the involvement of further, uncharacterized surface proteins on the host cell. Therefore such studies mostly rely on standardized cell culture of well characterized and often immortalized cell lines, providing a model for specific cell types, e. g. differentiated HL-60 cells for neutrophils. However, this approach often sacrifices physiological conditions in that for instance basic signaling pathways in the model cell type are affected by immortalization or that the model cell type does not completely represent the cell type which is infected under physiological conditions, e. g. by different protein expression (Feuk-Lagerstedt *et al.*, 1999; Hauert *et al.*, 2002).

From the viewpoint of methodology, bioimaging, i. e. microscopy, provides the most direct method to study processes on a cellular and - considering the advancements in fluorescent reporter technology - even molecular level (Frigault *et al.*, 2009).

Findings from basic research can be put together in order to acquire a first understanding of the processes constituting an infection. In the next step, hypotheses are generated and have to be verified in the context of infection, driving the experimental analysis of suitable biological systems (i. e. by providing a host organism instead of exemplary host cells). This is usually achieved with *in vivo* infection models, often relying on mice as experimental animals (Falkow, 2004).

Analysis of host-pathogen interactions in such an *in vivo* system is complex and therefore often relies on end point measurements such as the quantification of colonization of specific organs after a defined amount of time. Dynamic *in vivo* analysis of interactions on the cellular level has been promoted in recent years by advancements in microscopy, launching the field of *in vivo* microscopy. However, these systems suffer from the reciprocal relation of complexity and controllability as well (Germain *et al.*, 2006).

Thus, new infection models for the study of cellular events during host-pathogen interactions are needed to bridge the gap between *in vitro* cell culture studies and *in vivo* imaging involving experimental animals. Such an infection model should, on the one hand include more *in vivo*-like complexity than cell culture models, but on the other also be accessible both for manipulation and dynamic imaging in high spatial and temporal resolution.

One highly important aspect of *in vivo*-like complexity is dimensionality, which exhibits maximal discrepancy between cell culture and a mouse infection model. This aspect is illustrated briefly in the following by the interaction of an extracellularly replicating

bacterial pathogen (e. g. *Staphylococcus aureus* or *Yersinia enterocolitica*) with immune cells (Fig. 1.1):

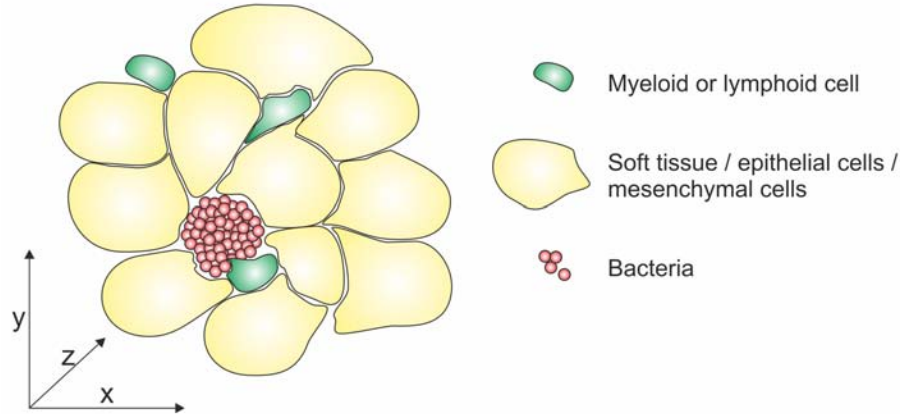


Figure 1.1: The role of dimensionality for the interaction of immune cells with extracellular pathogens. Extracellularly replicating pathogens such as *Staphylococcus aureus* or *Yersinia enterocolitica* establish a tissue-embedded focus of replication which is attacked by cells of the immune system.

Growth of the pathogenic microorganisms in tissue. Bacteria replicate in a three dimensional environment, constituted by the extracellular matrix and embedded host cells. The niche in which they replicate is spatially confined and thus exhibits high cell density in the bacterial population. Furthermore, the liquid phase in this environment is composed of compounds derived both from the host (interstitial fluid) and the pathogen (secreted proteins). Interstitial fluid composition is similar to blood in respect of small molecules (Swartz and Fleury, 2007). Under inflammatory conditions it becomes enriched by exudate due to increased vascular permeability. In comparison to that, cultivation of bacteria in liquid media as used for cell culture infection experiments might trigger a fundamentally different gene expression.

Recruitment of immune cells. Immune cells are recruited to the site of bacterial replication by mediators emitted from either the pathogen itself (chemotactic substances) or from host cells in proximity of the bacteria (chemokines), amplifying the signal. This recruitment involves priming and activation of immune cells which is in both temporal and spatial relation to eventual contact with bacteria and contrasts a cell culture infection system in which immune cells are often pre-stimulated with specific prototype agonists (Lee *et al.*, 2006).

Contact with immune cells. Immune cells get in physical contact with bacteria as a result of their inherent ability to migrate towards the site of infection (Janeway and Medzhitov, 2002). The establishment of contact is mechanistically defined by programs inside the immune cell. Immune cells in cell culture infection models are often mixed with bacteria in liquid suspension or bacteria are brought in contact with adherent cells by a centrifugation step, both of which does not provide the physiological context. Furthermore, neither liquid cell suspension nor two dimensional cell monolayers represent tissue-like environment as a physiological substrate for immune cell migration (Friedl and Weigelin, 2008).

1.2 Neutrophils as the first line of cellular host defense

1.2.1 Neutrophil biology

Neutrophils, together with eosinophils and basophils, represent the polymorphonuclear cell family (PMN), which received its name from their lobulated nuclei. These cells are also referred to as granulocytes because of a multitude of intracellular granula. The term neutrophil derives from characteristic neutral pink staining by hematoxylin and eosin (H&E). Neutrophils are the most abundant leukocytes in human blood. Inflammatory stimuli induce activation of neutrophils and their subsequent transepithelial migration from the blood into underlying tissue, where they arrive as the first cell type of the innate immune system at sites of inflammation and consequently represent the first line of cellular defense of the innate immune system (Witko-Sarsat *et al.*, 2000; Nathan, 2006). But their function outreaches their role in direct combatting of pathogens in that they are also crucial for activation and regulation of other cells of innate or adaptive immunity (Kobayashi and DeLeo, 2009; Mantovani *et al.*, 2011).

Chemoattraction to inflammatory foci is mediated by receptors for stimuli deriving either directly from pathogens or indirectly by amplification of a danger signal by host cells. Bacteria-derived chemotactic compounds such as fMLP or LPS are termed pathogen-associated molecular patterns (PAMPs). Neutrophils are endowed with an arsenal of receptors for such molecules, for instance Toll-like receptors or NOD-like receptors (Kaisho and Wagner, 2008).

Host cells produce and release chemokines and complement fragments in consequence of infection. Chemokine receptors are usually G protein-coupled receptors (GPCRs) which

undergo a conformational change upon ligand binding allowing interaction with so called heterotrimeric G proteins. These proteins release their G α subunits (Rosenbaum *et al.*, 2009), which further transmits the signal into reshaping of the cytoskeleton which can eventually promote cell locomotion.

Upon reaching sites of inflammation, neutrophils exert their antimicrobial functions either intra- or extracellularly. The prerequisite for intracellular killing is uptake of pathogens into specialized organelles, so called phagosomes. There are two major receptor classes involved in this process: firstly, Fc γ -receptors which bind to the Fc-domain of antibodies which are bound to pathogens via their Fab-domain and secondly, complement receptors which bind to complement fragments deposited on the surface of pathogens. In both cases, Rho GTPases are involved in transmitting the binding event into remodeling of the cytoskeleton leading to the actual uptake and formation of a phagosome. Eventually phagosomes fuse with lysosomes, resulting in acidification of the phagolysosome (Witko-Sarsat *et al.*, 2000).

The microbicidal compounds released into nascent phagolysosomes can be divided into two classes: antimicrobial proteins stored in granules and reactive oxygen species (ROS) generated by the NADPH-dependent oxidase. Granules are subdivided into four morphologically distinct populations: azurophil granules, specific granules, gelatinase granules and secretory vesicles. However, this strict classification is outdated and granules can be considered as a continuum with subsets based on selected marker proteins (Borregaard *et al.*, 2007). Granule fusion with phagolysosomes releases both proteins stored in the granule lumen into the phagolysosome but it also recruits functionally important integral membrane proteins to neutrophil membranes (Nauseef, 2007). Granule proteins comprise a plethora of antimicrobial molecules such as defensins, proteases (elastase, cathepsin G, proteinase 3), lysozyme and MPO, amongst others (Borregaard *et al.*, 2007).

Alternatively, granule proteins can also be released into the extracellular space in a process termed granule exocytosis. Another mechanism of neutrophil-mediated killing is the formation of so called neutrophil extracellular traps (NETs) which result from a novel kind of cell death, NETosis. In short, cell lysis leads to formation of net-like structures of DNA, histones and granule proteins covering nearby pathogens (Brinkmann *et al.*, 2004).

The process of reactive oxygen species (ROS) production is also termed respiratory or oxidative burst and is the consequence of NADPH-dependent oxidase assembly at the cytoplasmic membrane or at the phagolysosome membrane. NADPH oxidase reduces molecular

oxygen to generate the superoxide anion (O_2^-) which eventually dismutates into H_2O_2 . This compound is in turn converted to hypochlorous acid (HOCl) by myeloperoxidase (MPO) (Witko-Sarsat *et al.*, 2000).

1.2.2 Rho GTPases

Stimuli from the environment are sensed via receptors inserted in the cell membrane. These receptors undergo conformational changes upon binding and in turn activate regulatory proteins in signaling pathways in the cytosol which eventually leads to adaptation of the cell to the external stimulus.

One such group of regulatory proteins is the Rho family of GTPases, a subfamily of the Ras superfamily. Its 20 so far identified members are grouped into several subclasses. Rho GTPases control various cell functions such as migration, adhesion, phagocytosis, neuronal development, cell division, microtubule dynamics, respiratory burst and finally gene expression (Jaffe and Hall, 2005). The best characterized Rho GTPases are Rac1 (Rac subclass), RhoA (Rho subclass) and Cdc42 (Cdc42 subclass) (Heasman and Ridley, 2008). One of their prominent functions is the coordination of the actin cytoskeleton.

Members of the Rac family are crucial for actin polymerization, e. g. demonstrated by deletion of Rac1 and Rac2 in mature dendritic cells which completely suppresses actin dynamics in these cells (Benvenuti *et al.*, 2004). In contrast to that, inhibition of RhoA downstream signaling does not affect actin protrusion at the leading edge but paralyzes the trailing edge of migrating dendritic cells by abrogation of actomyosin contractility (Lämmermann *et al.*, 2008). Cdc42 is involved in filopodia regulation in some cell types (Wang and Zheng, 2007) and in regulation of protrusions in dendritic cells, thus establishment of the leading edge (Lämmermann *et al.*, 2009). Taken together, Rac1, RhoA and Cdc42 are essential for the correct temporal and spatial coordination of cytoskeletal rearrangements, which are linked to migration and uptake of bacteria.

On a molecular level, most Rho GTPases exert their function as binary molecular switches. The signaling state is defined by binding of GTP ('on') or GDP ('off'), respectively (Fig. 1.2). Conversion of both activation states is mediated by three regulatory mechanisms: Firstly, GTPase-activating proteins (GAPs) increase the intrinsic GTPase activity of Rho GTPases resulting in bound GDP ('off'). Secondly, Rho GTPases with bound GDP can be kept in an inactive state by guanine nucleotide-dissociation inhibitors (GDIs) which bind specifically to the C-terminal prenyl group (detailed in the next paragraph). This

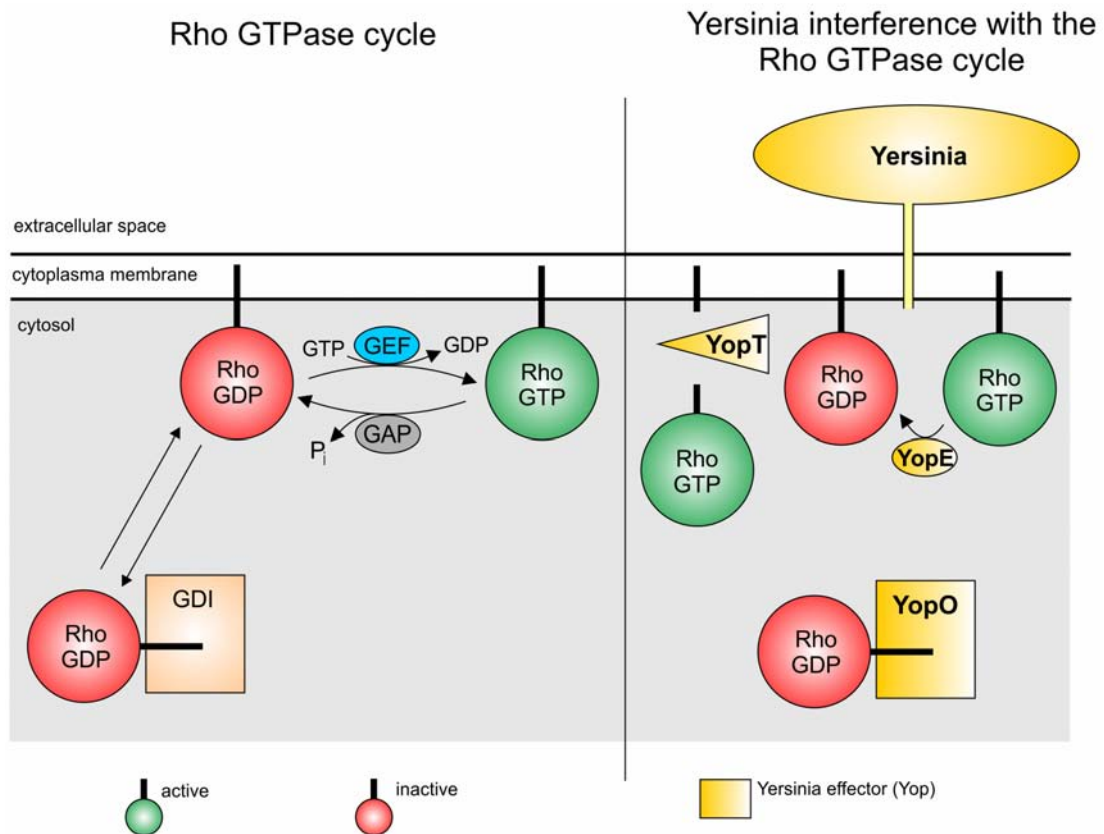


Figure 1.2: The eukaryotic Rho GTPase cycle and interference by *Yersinia*. Rho GTPases are binary molecular switches, their activation state is dependent on binding to GTP (active) or GDP (inactive). Three regulatory mechanisms are depicted: GTPase-activating proteins (GAPs) inactivate Rho GTPases by promoting the conversion of GTP to GDP. Guanine nucleotide-dissociation inhibitors (GDIs) inhibit membrane localization by binding to the C-terminal prenyl group. Guanine nucleotide-exchange factors (GEFs) activate Rho GTPases by catalyzing the release of GDP which allows subsequent binding of GTP. Three *Yersinia* effectors interfere with this regulation: YopE acts as a GAP, YopO acts as a GDI and YopT is a protease cleaving the prenylated residue of membrane-bound Rho GTPases, thereby mislocalizing them.

inhibits Rho GTPase insertion into the cytoplasmic membrane and sequesters them in the cytosol. This equilibrium of GDI-bound Rho GTPases and membrane-bound Rho GTPases is tightly regulated. Thirdly, activation is achieved by guanine nucleotide-exchange factors (GEFs) which catalyze the release of GDP and facilitate subsequent binding of GTP. More than 70 GEFs, 80 GAPs and three GDIs are described in humans. Of note, several of these regulators can bind to more than one Rho GTPase, demonstrating that this regulatory network is highly complex (Heasman and Ridley, 2008).

Correct subcellular localization is crucial for the modulatory effect of Rho GTPases as they have to be in spatial proximity with their interaction partners. Rho GTPases harbor

a C-terminal CaaX box (C: cysteine, a: aliphatic residue, X: any residue) which has to be post-translationally modified: geranylgeranyl transferase type I (GGT-I) mediates isoprenylation of the cysteine. Subsequently, Ras converting enzyme 1 (RCE1) cleaves the terminal three amino acid residues of the CAAX box and in the following, the carboxyl group of the remaining terminal cysteine is methylated by isoprenylcysteine carboxyl methyltransferase (IcMT). The prenyl residue serves as a membrane anchor for the respective Rho GTPase (Fueller and Schmidt, 2008).

1.2.3 Interstitial leukocyte migration

Rapid leukocyte recruitment to sites of infection is a critical event for the host as it has to cope with theoretically exponential bacterial growth. Thus, leukocytes have to reach their destination as fast as possible. There are two main strategies which enable the host to reach this goal: firstly, leukocyte migration is highly flexible in that it can alternate between adhesion receptor-dependent and adhesion receptor-independent amoeboid leukocyte migration and thus is independent of the molecular composition of the tissue (Renkawitz and Sixt, 2010). Secondly, leukocyte guidance is mediated by a highly intricate system of soluble chemoattractant gradients providing migrating leukocytes with ‘up-to-date’ information on the shortest way to the site of inflammation (Witko-Sarsat *et al.*, 2000).

In two dimensional environments cells are often attached to the substrate via integrin receptors forming focal adhesions. Polymerization of actin filaments at the leading edge of the migrating cell in cooperation with myosin II-mediated contraction in more distal areas pull the substrate-ligated integrin receptors backward and by this propel the cell body forward. For this purpose, the actin network and the adhesion receptor have to be connected by a so called molecular ‘clutch’ (Renkawitz *et al.*, 2009).

In contrast to that, in three dimensional environments leukocytes can also switch to a migration mode independent of transmembrane force coupling via this molecular integrin-‘clutch’. When integrin-mediated adhesion is possible, actin polymerization can be transformed almost 1:1 into forward movement, similar to the situation in two dimensional environments. However, in the absence of integrin ligands (‘uncoupling’) in such confined environments, cells do not ‘run on the spot’ but continue migration, while intriguingly neither overall cell shape nor speed is affected. The underlying mechanics are an increase in actin polymerization rate and force transduction to the substrate via friction generated by deformation of the cell in the 3D environment instead of receptor-binding. In this case,

a certain amount of retrograde actin movement is observed ('slippage') as the generated force cannot be transduced to the substrate efficiently (Renkawitz *et al.*, 2009).

The involvement of Rho GTPases is also relevant for interstitial leukocyte migration, in that Cdc42 plays a role in regulation of polarity, Rac is needed for chemotaxis and Rho is necessary for tail retraction (Bokoch, 2005).

1.3 Paradigmatic pathogenic microorganisms for the study of host cell-pathogen interactions

For the study of host cell-pathogen interactions in three dimensional infection models, three genetically well-defined pathogens were chosen of which the major pathogenicity factors are known and a set of mutants carrying defined deletions of genes encoding pathogenicity factors are available. For this purpose, the extracellularly replicating *Staphylococcus aureus* and *Yersinia enterocolitica* were chosen, as well as the facultative intracellular uropathogenic *Escherichia coli* (pathotype UPEC). Additionally, *Entamoeba histolytica* was used as an enteropathogenic protozoan.

1.3.1 *Staphylococcus aureus*

Staphylococcus aureus is a Gram-positive common human colonizer of skin and nasopharynx. More than 50% of healthy adults are colonized without showing symptoms. Upon breaching the natural barrier of the skin, *S. aureus* can gain access to underlying tissue. Especially carriers with impaired immune defense are at increased risk for subsequent infections, ranging from localized soft tissue infections to severe infections such as endocarditis, metastatic infections of joints, kidneys and lungs with progression to sepsis (Lowy, 1998). Treatment of staphylococcal infections has been further complicated by the massive development of antibiotic resistances in recent years, in particular methicillin resistance. Primarily observed with hospital-associated infections, methicillin-resistant *S. aureus* (MRSA) strains are meanwhile also community-associated (Hiramatsu *et al.*, 2001).

Adherence to host endothelium is crucial for invasion and metastatic dissemination. Thus, *S. aureus* can be considered a pathogen with preferential extracellular life style during the infection process. In regard of this complex host-pathogen interaction, *S. aureus* has evolved a highly adaptive and versatile strategy. Survival and replication in beneficial as well as in hostile environments is facilitated by a large set of fine-tuned virulence-associated

genes of which gene products can be roughly classified into several groups, among those are adhesins/invasins (mainly involved in the interaction with extracellular matrix (ECM) proteins), pore-forming toxins, superantigens and immune evasion factors (Bartlett and Hulten, 2010). The adhesins/invasins consist of two subgroups: cell wall anchored proteins, termed MSCRAMMs (Microbial Surface Components Recognizing Adhesive Matrix Molecules) and SERAMs (Secretable Expanded Repertoire Adhesive Molecules) which are released but mainly surface-associated proteins (Foster and Höök, 1998; Chavakis *et al.*, 2005).

The MSCRAMM subgroup includes fibronectin binding proteins (FnbpA, FnbpB), fibrinogen/fibrin binding proteins such as the clumping factor A and B (ClfA, ClfB), the collagen binding protein (Cna) and *Staphylococcus* protein A (Spa), which binds immunoglobulin G (IgG) and von Willebrand factor (vWF) (Foster and Höök, 1998; Hartleib *et al.*, 2000).

The SERAM subgroup includes further fibrinogen/fibronectin binding proteins such as the extracellular adherence protein (Eap) and the extracellular matrix binding protein (Emp) (Chavakis *et al.*, 2005; Hussain *et al.*, 2001; Palma *et al.*, 1999) but also prothrombin-activating proteins such as coagulase (Coa) and von Willebrand factor binding protein (vWbp). The latter has been identified and named by its property of binding to von Willebrand factor but has been shown to be a coagulase homologous to Coa (Friedrich *et al.*, 2003; Bjerketorp *et al.*, 2004).

At a first glance MSCRAMMs and SERAMs may be of redundant function in the context of colonization and infection. However, there must be a selective pressure for maintenance of virulence-associated genes with apparent redundant functions, suggesting different spatial and/or temporal roles in the complex life style of *S. aureus*. Different global regulatory systems (Agr, Sar, Sae) responding to environmental cues control the virulon of *S. aureus* (Cheung *et al.*, 2004). Genes encoding several MSCRAMMs, SERAMs and hemolysins (*hla* and *hly*) are regulated by the Sae system (*S. aureus* exoprotein expression) which does not affect the Agr and Sar systems (Mainiero *et al.*, 2010).

In order to investigate the contribution of these virulence-associated factors to disease initiation and progression, various *in vitro* and *in vivo* infection models are utilized. Recently, some molecular mechanisms of *S. aureus* abscess formation in the mouse infection model were elucidated in an approach based on defined mutants deficient in production of e. g. Coa, vWbp and Emp (Cheng *et al.*, 2009, 2010). It could be demonstrated that mature

abscesses in the kidney are composed of a core structure (termed staphylococcal abscess community, SAC) which is enclosed by a pseudocapsule of fibrin deposits and several layers of neutrophils of different viability in the periphery. This supports a more differentiated concept of abscess formation by pointing to an exploitation of host clotting machinery by staphylococcal virulence factors in order to establish a protective niche for the pathogen (Cheng *et al.*, 2011).

However, it is difficult to assess the role of single MSCRAMM or SERAM proteins during infection *in vivo* because of the complexity of the infection process and coevolution-driven host specificity of *S. aureus* (e.g. species specificity of coagulase and human-specific hemoglobin utilization) (Friedrich *et al.*, 2006; Pishchany *et al.*, 2010). In a physiological context, coagulation is necessary for hemostasis by sealing off damaged blood vessels. Platelets form a plug at the site of injury (primary hemostasis) and simultaneously plasma proteins, so called clotting factors, interact in formation of a fibrin meshwork enforcing the plug (secondary hemostasis). Soluble fibrinogen is cleaved by thrombin to form insoluble fibrin. In the process of wound healing, fibrin clots are degraded by the protease plasmin. Its zymogen precursor plasminogen is activated in a process termed fibrinolysis (Fig. 1.3). The regulation of these processes is highly conserved in mammals and involves a sophisticated cascade of proteolytically activated factors (Furie and Furie, 1988; Dahlbäck, 2000; Mosesson, 2005).

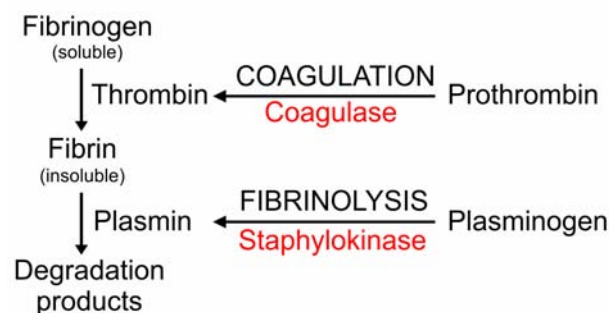


Figure 1.3: Simplified model of the interference of *S. aureus* proteins with coagulation and fibrinolysis. The generation of fibrin as well as its degradation is closely controlled by the mechanisms of coagulation and fibrinolysis. *S. aureus* can initiate these processes independently of the host regulation.

S. aureus targets these mechanisms at several key points (Fig. 1.3): Staphylococcal coagulases Coa and vWbp are able to activate prothrombin in a non-proteolytic manner, opposed to physiological prothrombin activation. The resulting Coa- or vWbp-prothrombin complex converts soluble fibrinogen into insoluble fibrin fibers (Friedrich *et al.*, 2003; Kroh

et al., 2009). The opposed mechanism of fibrinolysis can be initiated by staphylokinase (Giraud *et al.*, 1997), the secretion of which is positively regulated by the Agr system (Sun *et al.*, 2010), thus peaking in stationary phase (Bokarewa *et al.*, 2006).

1.3.2 *Yersinia enterocolitica*

1.3.2.1 *Y. enterocolitica* pathogenesis

Yersiniae are Gram-negative rod-shaped members of the family *Enterobacteriaceae*. The genus *Yersinia* comprises at present 17 species (Skurnik and Toivonen, 2011), among those are three human pathogenic species: *Y. pseudotuberculosis*, *Y. enterocolitica* and *Y. pestis*. *Y. pestis* is the etiologic agent of bubonic and pneumonic plague and is transmitted via flea bites, whereas *Y. pseudotuberculosis* and *Y. enterocolitica* are food-borne enteropathogens causing mostly self-limiting gastroenteritis. Pigs are frequently colonized with *Y. enterocolitica*. Pathogenic *Y. enterocolitica* strains are further subdivided according to their mouse virulence: biotype 2 and 4 comprise the low-virulence group and biotype 1B represents the high-virulence group (Oberhettinger *et al.*, 2011; Chain *et al.*, 2004; Aepfelbacher and Heesemann, 2001).

Y. enterocolitica infection is initiated by uptake of contaminated food or water. After passage of the stomach yersiniae multiply in the lumen of the small intestine from where they colonize the Peyer's patches. Passage through the epithelium is mediated by binding of the outer membrane protein Invasin (Inv) to β 1-integrins on microfold cells (M cells) which are located in follicle-associated epithelia (FAE) (Autenrieth and Firsching, 1996; Viboud and Bliska, 2005). Dissemination to spleen and liver via the blood stream does not sequentially result from colonization of regional lymph nodes but depends on a replicating population inside the intestine (Barnes *et al.*, 2006). In these organs abscesses are formed due to predominantly extracellular replication (Oellerich *et al.*, 2007). Thus, yersiniae are mostly extracellular pathogens which in contrast to intracellular pathogens such as *Salmonella* or *Shigella* do not replicate in secluded niches but have to face both the cellular and the humoral immune system. This lifestyle is possible due to virulence factors encoded on a \sim 70 kb *Yersinia* virulence plasmid (pYV). Outside the host, yersiniae replicate optimally at 27 °C, whereas many virulence-associated genes are temperature-controlled and upregulated upon entry into the host (37 °C) (Aepfelbacher and Heesemann, 2001).

1.3.2.2 The pYV plasmid and *Yersinia* outer proteins (Yops)

The pYV virulence plasmid (termed pCD1 in *Y. pestis*) is present in all three human pathogenic *Yersinia* species and encodes several virulence factors. Among those are YadA (exclusively in enteropathogenic *Yersinia*), an adhesin mediating adherence to host cells, and a type III secretion system (T3SS). This system functions as an injection device allowing Gram-negative bacteria to translocate bacterial effector proteins into the cytosol of the host cell. Such effector proteins are often orthologous to eukaryotic proteins involved in cellular signaling pathways and can thus be considered as a bacterial means to manipulate host cells (Aepfelbacher and Heesemann, 2001).

The classical view of T3SS is a conduit model of translocation: the T3SS apparatus consists of rings inserted into the bacterial inner membrane, peptidoglycan layer and outer membrane and extending into the extracellular space in the form of a needle. Effector proteins are either directly injected into the host cell via puncturing of the cell membrane by the needle or via pores consisting of YopB and YopD (Cornelis, 2002; Galán and Wolf-Watz, 2006). The respective type III effector proteins in *Yersinia* are called Yersinia outer proteins (Yops) and are also encoded on the pYV plasmid. There are at least six Yops which interfere with several important host cell functions as detailed in the following paragraph. Their ultimate aim is to promote extracellular growth, which is achieved most prominently by inhibition of phagocytosis (Aepfelbacher *et al.*, 2007).

YopH. YopH is a protein tyrosine phosphatase (PTP) targeting p130Cas, focal adhesion kinase (Fak), paxillin, Fyn-binding protein (Fyb) and SKAP-HOM, among others. These tyrosine-phosphorylated proteins are involved in the focal adhesion complex which relays signals from β 1-integrins on the cell surface to remodelling of the cytoskeleton via Rac1. In consequence, integrin-triggered bacterial internalization in epithelial and phagocytic cells is inhibited (Aepfelbacher *et al.*, 2007). YopH is thus considered a key player in antiphagocytosis. Furthermore, YopH inhibits the oxidative burst in macrophages and neutrophils (Shao, 2008).

YopO. The cellular effects of YopO result from its biochemical activity as a serine threonine kinase as well as from guanidine nucleotide dissociation inhibitor (GDI) activity towards Rac1 and RhoA (Barz *et al.*, 2000; Prehna *et al.*, 2006). Kinase activity is stimulated by binding to monomeric actin and is directed towards G α q (Navarro *et al.*, 2005). YopO is involved in disruption of the cytoskeleton and thereby in antiphagocyto-

sis, although the exact contributions of the two distinct molecular functions remain to be elucidated (Shao, 2008).

YopM. The exact mode of action of YopM is not understood yet. Different studies found binding to thrombin (Viboud and Bliska, 2005) or to the kinases PRK2 and RSK1 (McDonald *et al.*, 2003), as well as nuclear localization signals in the protein (Benabdillah *et al.*, 2004).

YopP. YopP is a potent suppressor of cytokine production by inactivating several MAPK pathways and the NF- κ B pathway, including the anti-apoptosis response. The underlying biochemical reaction is Ser/Thr acetylation of several MKKs and IKKs, thus blocking their phosphorylation site for activation by kinases (Mittal *et al.*, 2006). Furthermore, YopP possesses protease activity which mediates deubiquitination of several factors involved in NF- κ B signaling. Finally, YopP initiates apoptosis in macrophages and inhibits maturation of dendritic cells (Shao, 2008).

YopE. YopE belongs to a group of bacterial virulence factors structurally mimicking eukaryotic Rho GTPase activating proteins (GAPs, compare 1.2.2, p. 6). For this purpose, it is endowed with a specific amino acid sequence motif termed ‘arginine finger’, which supports the GTPase activity of Rho GTPases (enhanced GTP hydrolysis). Rac1 is its main target, Cdc42 and RhoA have been shown to be targeted *in vitro* as well (Aepfelbacher *et al.*, 2007). Recently, targeting of another Rho GTPase, RhoG, has been shown (Ropenser *et al.*, 2009). Binding of activated RhoG to the Elmo-Dock180 complex increases the GEF activity of Dock180 towards Rac1. Thus, YopE is able to inactivate Rac1 directly as well as upstream via inactivation of RhoG. On a cellular level, Rac1-inactivation of YopE mediates disruption of the actin cytoskeleton and thereby phagocytosis (Aepfelbacher *et al.*, 2011).

YopT. The cysteine protease YopT also targets Rho GTPases (mainly RhoA) and, by interfering with the involved signaling pathways, ultimately disrupts the actin cytoskeleton. Upon translocation into the host cell cytosol, it specifically cleaves distinct Rho GTPases proximal of the post-translationally prenylated C-terminal cysteine which mediates membrane attachment (Shao *et al.*, 2002; Fueller and Schmidt, 2008). Removal of RhoA from the cytoplasmic membrane inhibits its function. Additionally, it has been shown that YopT-modified GTP-Rac1 localizes to the nucleus after cleavage where it is not accessible to inactivation via YopE, thus demonstrating a competition for substrate between YopE

and YopT (Wong and Isberg, 2005). In a *Yersinia* mouse infection model it has been shown that YopE is more important than YopT for splenic colonization (Viboud *et al.*, 2006).

YopQ. Another translocated protein is YopQ (YopK in *Y. pseudotuberculosis*) which does not interact with host proteins but instead interacts with the part of the T3SS which is extending into the host cytoplasm. This masking of the T3SS prevents its recognition by the host cell and eventually results in prolonged bacterial survival *in vivo* (Brodsky *et al.*, 2010).

Taken together, three Yop proteins, namely YopE, YopT and YopO, interfere with the eukaryotic Rho GTPase cycle (Fig. 1.2).

1.3.3 Uropathogenic *Escherichia coli*

Escherichia coli pathotype UPEC (Uropathogenic *Escherichia coli*) is the causative agent of almost 90% of diagnosed urinary tract infections (UTI). Typically the infection is confined to urethra and urinary bladder (cystitis), but infection can also ascend to the kidneys and cause pyelonephritis and in rare cases even disseminate into the circulation (urosepsis) (Hunstad and Justice, 2010). The urothelium of the bladder is a transitional epithelial tissue which is composed of several cell layers. The surface layer contains multinucleate large cells, termed umbrella cells, which are eventually replaced by the underlying transitional cell layer (Apodaca, 2004).

Bacteria enter the urinary tract via the urethra and attach to epithelial and urothelial cells. This adhesion is a key event of the infection, arising from the necessity to literally swim against the current. Prominent members of the adhesin family are type 1 pili, binding to mannosylated uroplakin proteins on bladder epithelia (Zhou *et al.*, 2001), and P pili involved in establishing pyelonephritis (Roberts *et al.*, 1994). Inside the urinary bladder, bacteria are not restricted to the lumen and surface but also invade superficial bladder urothelial cells (umbrella cells), probably via Rab27b-positive fusiform vesicles (Hunstad and Justice, 2010). A critical step in establishment of infection is the access of bacteria to the cytoplasm where exponential growth can be initiated (Fig. 1.4). Intracellular bacterial communities (IBCs) arise as densely packed bacterial clusters in the cytosol of urothelial cells, in particular in umbrella cells. During this stage, cell division results in coccoid morphology of the bacteria which allows a denser packaging compared to rod-shaped bacteria (Justice *et al.*, 2004). IBCs are often considered as ‘intracellular biofilms’ despite the lack of underlying substrate. However, intracellular membrane structures (Golgi, nuclear

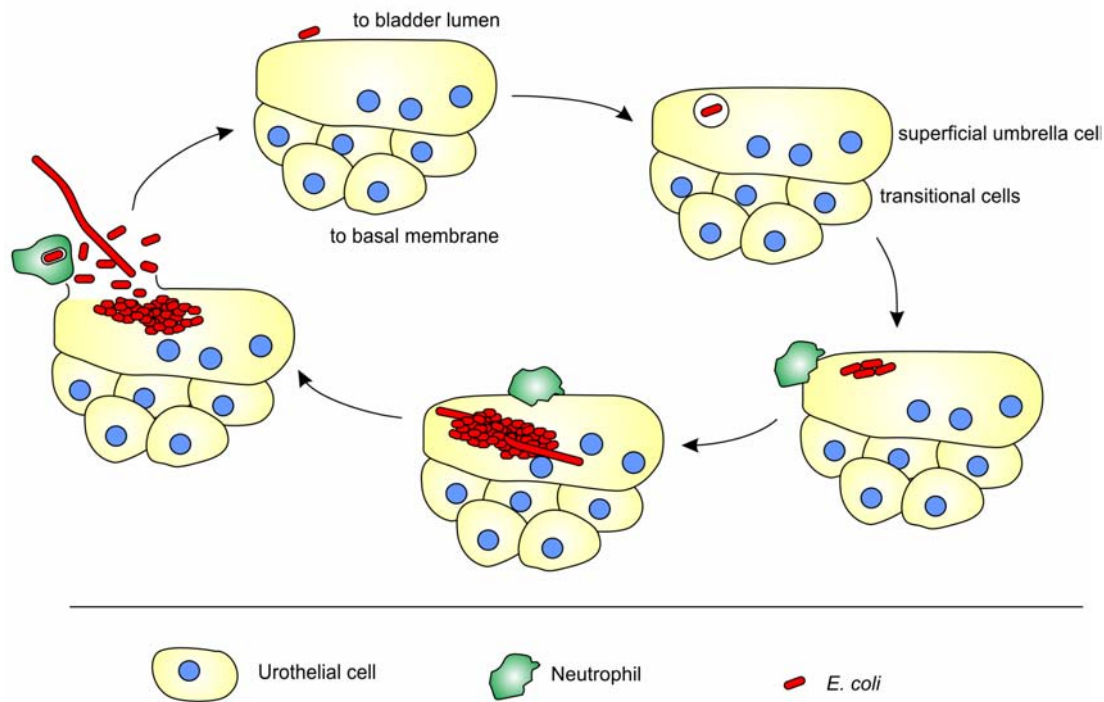


Figure 1.4: Simplified model of UPEC infection of urinary bladder urothelium.

UPEC cells adhere to and invade epithelial cells and subsequently gain access to the cytosol where exponential growth is initiated, resulting in intracellular bacterial communities (IBCs). Some bacteria give rise to filamentous bacteria. Eventually, infected epithelial cells exfoliate and/or lyse, releasing UPEC into the lumen of the urinary bladder where they are able to infect new cells. Neutrophils are recruited to infected cells but are not able to gain access to the IBC. Phagocytosis is initiated upon cell lysis.

membrane) could be considered as substrates for bacterial biofilm formation (Hunstad and Justice, 2010). Few bacterial cells in IBCs undergo a different differentiation program giving rise to filamentous bacteria of up to 80 μm in length. Finally, infected umbrella cells are exfoliated and bacteria are released from IBCs into the bladder lumen. From there, a new infection cycle can arise (Justice *et al.*, 2004). Alternatively, during exfoliation of a superficial umbrella cell, bacteria can gain access to underlying transitional epithelial cell layer which replaces superficial umbrella cells. In these cells they can remain in a membrane-enclosed compartment, undergo growth arrest and form quiescent intracellular reservoirs (QIR) from where recurrent infections are suggested to arise (Justice *et al.*, 2004; Mysorekar and Hultgren, 2006).

Neutrophil influx in response to UPEC infection is a rapid and important step during infection (Ingersoll *et al.*, 2008). However, suppression of proinflammatory cytokine production by UPEC via alterations in LPS (Billips *et al.*, 2007) and via partially unidentified

direct mechanisms (Hunstad *et al.*, 2005) counteracts neutrophil recruitment. Furthermore, IBCs are considered as protected niches from neutrophil attack (Justice *et al.*, 2004).

1.3.4 *Entamoeba histolytica*

E. histolytica is an enteropathogenic protozoan parasite and humans and primates are the only natural hosts. Its lifecycle consists of two stages, infectious cysts and amoeboid trophozoites. Cysts are ingested with fecally contaminated food or water and survive passage through the stomach unharmed due to their stable wall. Upon reaching the large intestine the parasite excysts and releases the active form, trophozoites. These are highly motile due to their pleomorphic shape which led to their name ‘amoeba’. Normally, they reside within the intestine, ingest bacteria and partly digested food particles and multiply by binary fission. The lifecycle is completed by encystation of trophozoites within the colon, which are then excreted in stool. Trophozoites are not viable outside the host, whereas cysts can survive for months in the environment (Stanley, 2003; Pritt and Clark, 2008).

E. histolytica is the causative agent of amoebiasis in humans, a leading parasitic disease causing up to 100,000 deaths per year. This is mostly the result of tissue invasion and systemic dissemination of *E. histolytica* (Stanley, 2003). Interestingly, most infections remain asymptomatic, suggesting a low occurrence of tissue invasion but also pointing out that this is a determinative event in the progression to fatal outcome (Pritt and Clark, 2008).

The first step of invasion is adherence to colonic epithelial cells, mediated by specific lectins on the amoebae (Mann, 2002). Subsequently, cytolysis is initiated by several factors, for instance amoebapores which cause pores in the host cell membrane, terminating in necrosis. Other factors involved in invasion are cysteine proteinases of *E. histolytica* (Que and Reed, 2000). Epithelial barrier integrity can be further decreased by mediators released from recruited neutrophils. Finally, penetration of the mucosal barrier by *E. histolytica* can lead to dissemination via the blood stream and terminate in liver abscesses (Stanley, 2003).

1.4 Aims of this work

Surrogate infection models for the study of host-pathogen interactions should be developed and established to bridge the gap between *in vitro* and *in vivo* infection models. A special focus should be put on the three dimensional context of such models in that they should both be able to induce *in vivo*-like growth behavior of pathogens and to study the subsequent interaction of various pathogens with cells of the innate immune system, namely neutrophils.

For this purpose, the collagen gel system (3D-CoG) which had been established for growth studies on *Yersinia enterocolitica* (Freund *et al.*, 2008), should be further developed for phagocyte-pathogen interaction studies.

The broad applicability of such a model in infection biology was to be utilized for the study of another extracellularly replicating pathogen, *Staphylococcus aureus*. Specifically, the role of secreted proteins (SERAMs) on conversion of host fibrinogen to fibrin was to be studied in regard to interaction with neutrophils. It was to be analyzed if such a model can serve to simulate specific stages of *S. aureus* abscess formation.

The effect of plasmid-encoded pathogenicity factors of *Y. enterocolitica* on migratory behavior of neutrophils was to be analyzed in this 3D-CoG infection model. The *in vivo*-like dimensionality of the setup was to be exploited in order to evaluate *Yersinia*-mediated cellular effects in an appropriate context regarding interstitial leukocyte migration.

As a step beyond the artificial 3D-CoG infection model, an organ explant-based *ex vivo* infection model should be developed for the study of host-pathogen interactions on bladder and intestinal epithelia. The model should be validated with the paradigmatic pathogens uropathogenic *Escherichia coli* and *Entamoeba histolytica*, which cause disease in these tissues.

Chapter 2

Materials and Methods

2.1 Materials

2.1.1 Strains, plasmids and oligonucleotides

2.1.1.1 Strains

The organisms and strains used in this study are listed in Tab. 2.1-2.3.

Table 2.1: *Staphylococcus aureus* strains

Strain	Properties	Reference
Newman	reference strain	Duthie and Lorenz (1952)
Newman-29	$\Delta saePQRS::kan$	Mainiero <i>et al.</i> (2010)
Newman-29, 33	complementation of Newman-29	Mainiero <i>et al.</i> (2010)
Newman <i>coa</i>	$\Delta coa::tetK$	McDevitt <i>et al.</i> (1992)
Newman <i>vWbp emp</i> *	$\Delta emp::erm$	Johnson <i>et al.</i> (2008)
Newman <i>eap</i>	$\Delta eap::erm$	Hussain <i>et al.</i> (2002)
Newman <i>ica</i>	$\Delta ica::tet$	Kropec <i>et al.</i> (2005)
CA-MRSA USA300	$\Delta saePQRS::kan$	Diep <i>et al.</i> (2006)
RN4220	restriction-deficient derivative of <i>S. aureus</i> 8325-4	Kreiswirth <i>et al.</i> (1983)

* Formerly denoted as Newman *emp* (Johnson *et al.*, 2008). Sequencing analysis revealed that assumedly by phage transduction not only the *emp* gene but also the neighboring functional *vWbp* gene of strain Newman has been replaced by a truncated version of *vWbp* from strain RN4220. This was further confirmed by the fact that *vWbp* could be

detected in the supernatants of 3 h Newman wildtype cultures but not of this *emp* mutant strain (Fig. 3.8, p. 54).

Table 2.2: *Yersinia enterocolitica* strains

Strain	Properties	Reference
WA(pYV)	clinical isolate WA-314, serotype O:8	Heesemann <i>et al.</i> (1983)
WA-C	plasmid-cured derivative of WA(pYV)	Heesemann <i>et al.</i> (1983)
WA(pYV Δ <i>lcrD</i>)	T3SS-deficient by Tn5 insertion in <i>lcrD</i> (pYV-515)	Heesemann <i>et al.</i> (1983)
WA Δ <i>inv</i> (pYV)	Δ <i>inv::kan</i> , WA-C- <i>inv</i> (pYV)	Ruckdeschel <i>et al.</i> (1996)
WA(pYV Δ <i>yadA</i>)	Δ <i>yadA::kan</i> ; WA(pYVO8-A-0)	Roggenkamp <i>et al.</i> (1995)
WA Δ <i>inv</i> (pYV Δ <i>yadA</i>)	Δ <i>inv::spec</i> , Δ <i>yadA::kan</i>	This work
WA(pYV, pRFP)	WA-314 harboring pLACrfp	Oellerich <i>et al.</i> (2007)
WA(pYV Δ <i>yadA</i> , pRFP)	WA(pYV Δ <i>yadA</i>) harboring pLACrfp	Oellerich <i>et al.</i> (2007)
WA(pYV Δ <i>yopH</i>)	<i>yopH</i> mutant WA-C(pYV Δ H)	Trülsch <i>et al.</i> (2004)
WA(pYV Δ <i>yopO</i>)	<i>yopO</i> mutant WA-C(pYV Δ O)	Trülsch <i>et al.</i> (2004)
WA(pYV Δ <i>yopP</i>)	<i>yopP</i> mutant WA-C(pYV Δ P)	Trülsch <i>et al.</i> (2004)
WA(pYV Δ <i>yopE</i>)	<i>yopE</i> mutant WA-C(pYV Δ E)	Trülsch <i>et al.</i> (2004)
WA(pYV Δ <i>yopT</i>)	<i>yopT</i> mutant WA-C(pYV Δ T)	Trülsch <i>et al.</i> (2004)
WA(pTTSS)	WA-C harboring pTTSS which encodes the T3SS apparatus of WA-314 but no <i>yop</i> genes	Trülsch <i>et al.</i> (2003)
WA(pTTSS, pYopHSycH)	secretion of YopH	Trülsch <i>et al.</i> (2003)
WA(pTTSS, pYopO)	secretion of YopO	Trülsch <i>et al.</i> (2003)
WA(pTTSS, pYopP-bla)	secretion of YopP-bla	MvPI*, H. Bouabe
WA(pTTSS, pYopE _{yen})	secretion of YopE _{yen}	Trülsch <i>et al.</i> (2003)
WA(pTTSS, pYopT _{yen})	secretion of YopT _{yen}	MvPI*, K. Trülsch
WA(pTTSS, pYopE _{yps})	secretion of YopE _{yps}	MvPI*, B. Czech

(Y. enterocolitica strains, continued)

Strain	Properties	Reference
WA(pTTSS, pYopT _{yps})	secretion of YopT _{yps}	MvPI*, B. Czech
WA(pTTSS, pYopT _{yenC139S})	secretion of YopT _{yenC139S}	MvPI*, B. Czech
WA(pTTSS, pYopE _{ypsR144A})	secretion of YopE _{ypsR144A}	MvPI*, B. Czech
WA(pTTSS, pYopT _{ypsC139S})	secretion of YopT _{ypsC139S}	MvPI*, B. Czech and this work
WA(pTTSS, pYopE _{yenK62R,K75Q})	secretion of YopE _{yenK62R,K75Q}	Hentschke <i>et al.</i> (2007)
WA(pYV, pYopH-bla)	WA(pYV) harboring pYopH-bla: secretion of a <i>yopH-bla</i> fusion	Cvetanovic (2011)
WA(pYV Δ <i>lcrD</i> , pYopH-bla)	WA(pYV Δ <i>lcrD</i>) harboring pYopH-bla: secretion of a <i>yopH-bla</i> fusion	Cvetanovic (2011)

* MvPI = Strain collection Max von Pettenkofer-Institute

yop genes for expression in WA(pTTSS) are derived from *Y. enterocolitica* serotype O:8 or from *Y. pseudotuberculosis* serotype O:3, strain IP32953, and cloned in pACYC184. Chapter 3.1.3.1-3.1.3.3 deals only with *Y. enterocolitica*-derived *yop* genes, therefore YopE_{yen} and YopT_{yen} and the respective plasmids are referred to as YopE and YopT only in this section.

Table 2.3: Other microorganisms

Strain	Properties	Reference
<i>Escherichia coli</i> DH5 α	strain for plasmid modifications, <i>recA1</i> , <i>hsdR17</i>	Hanahan (1983)
<i>Escherichia coli</i> NU14	clinical UPEC isolate	Hultgren <i>et al.</i> (1986)
<i>Yersinia pseudotuberculosis</i> YPIII(pIB1)	wildtype strain	Logsdon and Mecsas (2003)
<i>Yersinia pseudotuberculosis</i> IP32953	wildtype strain	Chain <i>et al.</i> (2004)
<i>Salmonella enterica</i> serovar Typhimurium SB824	Δ <i>aroA</i> , <i>sptP::kan</i>	Rüssmann <i>et al.</i> (1998)

(Other microorganisms, continued)

Strain	Properties	Reference
<i>Entamoeba histolytica</i> HK 9	clinical isolate	Geiman and Becker (1953)

2.1.1.2 Plasmids

The plasmids used in this study are listed in Tab. 2.4.

Table 2.4: Plasmids

Plasmid	Properties	Reference
pSK236	Shuttle vector containing pUC19 cloned into the <i>HindIII</i> site of the <i>S. aureus</i> plasmid pC194	Gaskill and Khan (1988)
pEmp	a 1.3 kb fragment containing the <i>emp</i> gene from strain Newman was cloned into pSK236 (<i>BamHI/PstI</i>)	This work
pvWbp	a 1.9 kb fragment containing the <i>vWbp</i> gene from strain Newman was cloned into pSK236 (<i>EcoRI/SalI</i>)	This work
pvWbpEmp	a 1.9 kb fragment containing the <i>vWbp</i> gene (<i>EcoRI/BamHI</i>) and a 1.3 kb fragment containing the <i>emp</i> gene (<i>BamHI/PstI</i>) from strain Newman were cloned into pSK236	This work
pBLUESCRIPT II KS(+)	cloning plasmid	Fermentas, Walldorf
pBS-YopT _{yps}	<i>yopTsyncT_{yps}</i> in pBLUESCRIPT II KS(+)	This work
pBS-YopT _{ypsC139S}	<i>yopTsyncT_{ypsC139S}</i> in pBLUESCRIPT II KS(+)	This work
pFPV-mCherry/2	mCherry expression vector	Drecktrah <i>et al.</i> (2008)
pM965-4 eGFP	eGFP expression vector	Stecher <i>et al.</i> (2004)
pTurboYFP-B	turboYFP expression vector	Evrogen, Moscow, Russia
MLC-GFP	myosin light chain-GFP fusion for expression in eukaryotic cells	Croft <i>et al.</i> (2005)

2.1.1.3 Oligonucleotides

The oligonucleotides used in this study are listed in Tab. 2.5.

Table 2.5: Oligonucleotides

Oligonucleotide	Sequence
vWbp-f-EcoRI	AAA GAATTC TAATGATATTAATTAATCATATG
vWbp-r-SalI	AAA GTCGAC AATTATTGATATTGATAGTTAAGC
vwbp-r-BamHI	AAA GGATCC AATTATTGATATTGATAGTTAAGC
emp-f-BamHI	AAA GGATCC AAGCTGAAAAACAATAAAAATGTT
emp-r-PstI	AAA CTGCAG TGTTACTTCCAAC TTTCAAAGTAG
invETfor	CGCATTAGATTAATGCATCGTGAAAAATGCAGAGAG TCTATTTTATGAGAAGTGGCGGTTTTTCATGGCTTG
invETrev	GGTCACGCTAAAGGTGCCAGTTTGCTGGGCGCAA GATTGGTATTTAGCACATTATTTGCCGACTACCTTG
pKD46betFOR	CCTTTCCTGATAAGCAGAATG
pKD46betREV	AATCCAAGAGCTTTTACTGC
IP32953 pYV 29282 XbaI forward	AATCTAGATAACATCACTGTCCCCATAAG
IP32953 pYV 30915 SalI reverse	TATGTCGACAGATATTATTGTA ACTATGTAGTG
YopT C139S Yps Forward	CTAGCGGTGTCAGCGAGGCTTTATGTG
YopT C139S Yps Reverse	GTGCACATAAAGCCTCGCTGACACGCCTAG
Pbs-f	GCAAGGCGATTAAGTTGGGTAAC
Pbs-r	GCGCGCAATTAACCCTCAD
pACYC184-1356-forward	CAGAGCAAGAGATTACGCGCAG
pACYC184-2312-reverse	AAAATACAAAACGCCCGA

‘invETfor’-‘invETrev’were designed by K. Trülsch, ‘pKD46betFOR/REV’ were designed by E. Schriefer. ‘IP32953 pYV 29282 XbaI forward’-‘Pbs-r’ were designed by B. Czech.

2.1.2 Instruments

All instruments are listed in Tab. 2.6.

Table 2.6: Instruments

Instrument	Model	Manufacturer
Agarose gel documentation	GelDoc EQ	Bio-Rad, Munich
Centrifuge	3K30, 1K15, 112	Sigma, Osterode
Centrifuge	Varifuge 3.OR	Heraeus, Hanau
Centrifuge (Table top)	5415D, 5424R	Eppendorf, Hamburg
Developing machine	Kodak Imager	Kodak
Electrophoresis cell DNA	miniRapide	OLS, Bremen
Electroporation device	GenePulser II	Bio-Rad, Munich
Electrophoresis cell SDS-PAGE	Mini-PROTEAN 3	Bio-Rad, Munich
Flow cytometer	FACSCanto II + FACS Diva Software	BD, Heidelberg
Fluorescence reader	Sunrise Tecan, Magellan3 Software	Tecan, Mennedorf, Switzerland
Hemocytometer	Neubauer improved 0,1 mm	Marienfeld, Lauda-Königshofen
Incubation chamber for microscopy	The Cube & The Box	Life Imaging Services, Basel, Switzerland
Incubator shaker	Excella E24	New Brunswick, Nürtingen
Incubator	Typ B20	Heraeus, Hanau
Laboratory scales	1203 MP, type 1801	Sartorius, Göttingen
Laminar flow hood	Herasafe HS 12	Thermo Electron Corporation, Langenselbold
Microscope	SP5 confocal	Leica, Wetzlar
Mixer	Thermomixer compact	Eppendorf, Hamburg
Oxygen sensor	PSt3 Oxygen Optodes	PreSens, Regensburg
PCR cycler	Uno Cycler	VWR, Darmstadt
pH meter	320 pH-Meter	Mettler Toledo, Giessen
Pipettes	10, 20, 100, 200, 1000 µl	Eppendorf, Hamburg
Power supplies	Power Pac 300	Bio-Rad, Munich
Spectrophotometer	Ultrospec 3100 pro	Amersham Biosciences, Freiburg
Spectrophotometer	NanoDrop ND 1000	Spectronic instruments, Rochester, United States

(Instruments, continued)

Instrument	Model	Manufacturer
Transfection device	Nucleofector I	Lonza, Cologne
Transilluminator	UVT-20M/W	Herolab, Wiesloch
Vibrating blade micro-tome	VT1200S	Leica, Wetzlar
Western blotting system	Mini Trans-Blot System	Bio-Rad, Munich

2.1.3 Consumables

Consumables used in this study are listed in Tab. 2.7.

Table 2.7: Consumables

Consumables	Manufacturer
12/24/48/96 well plates	TPP, Trasadingen, Switzerland
Cell culture flasks	Nunc, Langenselbold
Electroporation cuvettes	Thermo Fisher Scientific, Schwerte
FACS tubes	BD, Heidelberg
Filter paper	Whatman, Dassel
μ -slide 8 well	ibidi, Munich
Needles	Braun, Melsungen
PCR tubes	Eppendorf, Hamburg
Petri dishes (plastic)	Greiner bio-one, Frickenhausen
Pipettes (Falcon)	BD, Heidelberg
Reaction tubes (1.5 and 2 ml)	Eppendorf, Hamburg
Reaction tubes (15 and 50 ml, Falcon)	BD, Heidelberg
Scalpels	Braun, Melsungen
Sterile filtration devices	TPP, Trasadingen, Switzerland
Syringe driven filter unit 0.22 and 0.45 μ m	Millipore, Schwalbach
Syringes	Braun, Melsungen

2.1.4 Chemicals, biochemicals, kits and enzymes

Chemicals, biochemicals, kits and enzymes used in this study are listed in Tab. 2.8.

Table 2.8: Chemicals, biochemicals, kits and enzymes

Name	Manufacturer
Acetic acid	Merck, Darmstadt
Aceton	Roth, Karlsruhe
Acrylamide	Serva, Heidelberg
Agarose (Premium)	Serva, Heidelberg
Antibiotics	Sigma-Aldrich, Hamburg
APS, Ammonium persulfate	Sigma-Aldrich, Hamburg
Argatroban	Santa Cruz, Heidelberg
Bacto Tryptone	BD, Heidelberg
Bacto Yeast extract	BD, Heidelberg
BHI	BD, Heidelberg
Bromphenol blue	Roth, Karlsruhe
BSA	Roth, Karlsruhe
CCL19	Peptotech, Hamburg
Coomassie Brillant Blue	Merck, Darmstadt
Cytometric Bead Array (CBA) Flex Set (IL-6, KC, MCP-1, TNF- α)	BD, Heidelberg
CytoTox 96 Non-Radioactive Cytotoxicity assay	Promega, Mannheim
DAPI	Invitrogen, Karlsruhe
DMEM	Sigma-Aldrich, Hamburg
DNA standard (GeneRuler 1kb DNA Ladder)	Fermentas, Walldorf
D-PBS (PBS)	Invitrogen, Karlsruhe
ECL Western blotting detection reagent	GE Healthcare, Munich
EDTA	Sigma-Aldrich, Hamburg
EGTA	Sigma-Aldrich, Hamburg
Ethanol p.a.	Roth, Karlsruhe
Ethidium bromide	Sigma-Aldrich, Hamburg
FCS	Invitrogen, Karlsruhe
Fibrinogen from human plasma	Merck, Darmstadt
Ficoll	GE Healthcare, Munich
FM 4-64	Invitrogen, Karlsruhe
Gentamicin	Sigma-Aldrich, Hamburg

(Chemicals, biochemicals, kits and enzymes, continued)

Name	Manufacturer
Glycerol	Roth, Karlsruhe
Glutaraldehyde	Roth, Karlsruhe
Glycin	MP, Ohio, United States
GM-CSF	Peptotech, Hamburg
H ₂ SO ₄	Roth, Karlsruhe
HBSS (2x)	Invitrogen, Karlsruhe
HCl	Roth, Karlsruhe
High fidelity PCR enzyme mix	Fermentas, Walldorf
Isopropanol	Merck, Darmstadt
KCl	Roth, Karlsruhe
K ₂ HPO ₄	Roth, Karlsruhe
KHCO ₃	Roth, Karlsruhe
L-glutamine	Invitrogen, Karlsruhe
Lectin (<i>T. vulgaris</i> , FITC-labeled)	Sigma-Aldrich, Hamburg
Liveblazer-FRET B/G Loading Kit	Invitrogen, Karlsruhe
LPS (<i>E. coli</i> K12)	Invivogen, San Diego, United States
Lysostaphin	Sigma-Aldrich, Hamburg
M-CSF	Peptotech, Hamburg
Methanol	Merck, Darmstadt
Mouse Dendritic Cell Nucleofector Kit	Amaxa/Lonza, Cologne
NaCl	Roth, Karlsruhe
NaOH	Merck, Darmstadt
NH ₄ Cl	Roth, Karlsruhe
NucleoSpin PlasmidPure kit	Macherey & Nagel, Düren
NuSieve GTG agarose	Lonza, Cologne
Mercaptoethanol	Sigma-Aldrich, Hamburg
Oligonucleotides (custom)	Metabion, Martinsried
Paraformaldehyde	Merck, Darmstadt
PCR purification kit	Qiagen, Hilden
Plasmin	Merck, Darmstadt
Presto Spin D bug kit	Molzylm, Bremen
Protein standard (PageRuler protein Ladder)	Fermentas, Walldorf
Purecol	Advanced Biomatrix, San Diego, United States

(Chemicals, biochemicals, kits and enzymes, continued)

Name	Manufacturer
Restriction enzymes	Fermentas, Walldorf
RPMI 1640 (no phenol red)	Invitrogen, Karlsruhe
rWGA (Alexa 680-labeled)	Invitrogen, Karlsruhe
SDS	Serva, Heidelberg
T4 DNA-Ligase	Fermentas, Walldorf
TEMED (Tetramethylethylenediamin)	Sigma-Aldrich, Hamburg
Trichloroacetic acid (TCA)	Roth, Karlsruhe
Tris	MP, Ohio, United States
Triton X-100	Roth, Karlsruhe
Trypan blue solution	Invitrogen, Karlsruhe
Tryptone soya agar	Roth, Karlsruhe
Trypsin-EDTA	Invitrogen, Karlsruhe
Tween 20	Sigma-Aldrich, Hamburg
Ultra-pure agarose	Invitrogen, Karlsruhe
X-ray films type SuperRX	Fujifilm
Y-27632 (ROCK inhibitor)	Merck, Darmstadt

2.1.5 Antibodies

Polyclonal rabbit antisera against *Staphylococcus aureus* Coa or Emp were provided by O. Schneewind, Chicago. Alexa 555 anti-rabbit from goat was purchased from Invitrogen, Karlsruhe. Polyclonal rabbit antisera against YopT were provided by J. Heesemann. HRP-linked secondary antibody (ECL α -Rabbit IgG, HRP-linked) was purchased from GE Healthcare.

2.1.6 Animals

2.1.6.1 Mouse strains

C57BL/6, *Lys-EGFP* (Faust *et al.*, 2000), Lifeact-GFP mice (Riedl *et al.*, 2010) and *CX₃CRI-GFP* mice (Jung *et al.*, 2000) were bred and maintained at the Max von Pettenkofer Institute in isolated ventilated cages (Tecniplast, Hohenpeißenberg) under SPF conditions. All animal work was conducted according to the relevant national and international guidelines. Mice were sacrificed by CO₂ asphyxiation.

2.1.6.2 Harvesting of organs

Mice were sacrificed by inhalation of CO₂. In order to remove organs, mice were fixed to a stage immediately after death and disinfected with ethanol. Organs were removed under sterile conditions and stored on ice. For spleen explantation, mice were opened and the spleen was removed using sterile tweezers and scissors. For urinary bladder explantation, sacrificed mice were catheterized with a custom made catheter tip and the urinary bladder was gently inflated using 150 µl of pre-warmed saline. Ureters and urethra were ligated with a micro-surgical clip and the organ was removed from the mouse. For explantation of gut tissue, gut sections were ligated on both ends before removal. The section was cut open along the opposite side of the attachment line of the mesothelium. Intestinal content was removed by flushing gently with PBS. Caecum and stomach were removed similarly as described for the gut.

2.1.6.3 Infection experiments

Mice were anesthetized with a ketamin/xylacin mixture injected intraperitoneally according to laboratory animal guidelines. For intravesical infection of mice, 3×10^8 cfu were administered in a volume of 50 µl pre-warmed PBS.

2.2 Methods

2.2.1 Microbiological methods

2.2.1.1 Microbiological media

Microbiological media used in this work are listed in Tab. 2.9.

Table 2.9: Microbiological media

Name	Composition
Lysogeny broth (LB)	1% tryptone, 0.5% yeast extract, 0.5% NaCl
Basic medium (BM)	1% peptone, 0.5% yeast extract, 0.1% glucose, 0.5% NaCl, 0.1% K ₂ HPO ₄
Brain Heart Infusion medium (BHI)	37 g/l brain heart infusion

(Microbiological media, continued)

Name	Composition
SOC medium	2% tryptone, 0.5% yeast extract, 0.05% NaCl, 250 mM KCl, 20 mM Glucose
Tryptone soya agar (TSA)	40 g/l tryptone soya agar
High salt LB medium	LB with 300 mM NaCl
TYI-S-33: Trypticase, yeast extract, iron-serum	(Diamond <i>et al.</i> , 1978), provided by M. Pritsch
Storage medium	20% glycerol in LB

Solid media were prepared by adding 15 g/l agar to the respective media.

Media were sterilized by autoclaving before use (121 °C, 1 bar, 20 min).

2.2.1.2 Antibiotics and media supplements

Antibiotics were added to the media when appropriate at the following concentrations: 50 µg/ml kanamycin, 10 µg/ml erythromycin, 20 µg/ml tetracycline (5 µg/ml for staphylococci), 10 µg/ml chloramphenicol, 100 µg/ml ampicillin, 50 µg/ml spectinomycin.

2.2.1.3 Cultivation and storage of microorganisms

Bacteria were routinely cultured under aerobic conditions in the media specified in the following, supplemented with antibiotics if appropriate (shaking 190 rpm): LB (*E. coli*, *S. aureus*), BM (*S. aureus*), BHI (*Yersinia*), High salt LB (*S. enterica*). All strains were incubated at 37 °C except for *Yersinia* strains which were cultivated routinely at 27 °C. The optical density at 600 nm (OD₆₀₀) of bacterial suspensions was determined by spectrophotometry. If the OD₆₀₀ was above 0.8, the samples were diluted for the measurement.

E. histolytica was cultured at 37 °C without shaking in cell culture flasks under anaerobic conditions in TYI-S-33.

Bacteria were stored at -80 °C in storage medium.

2.2.1.4 Preparation of microorganisms for infection experiments

Bacteria were prepared for infection experiments as follows. The number of colony forming units (*cfu*) was determined by plating of dilutions of the infection samples.

***S. aureus*:** Bacteria were harvested by centrifugation (1800 x g, 3 min) from overnight

cultures.

***Yersinia*:** Overnight cultures were diluted 1:20 in medium, cultivated for 3-4 h at 37 °C until an OD₆₀₀ of ~0.5 was reached and harvested by centrifugation (1800 x g, 3 min).

***E. coli* NU14:** Bacteria were harvested by centrifugation (2300 x g, 5 min) from overnight cultures and washed in PBS. Heat inactivation was conducted at 100 °C for 5 min.

***S. enterica*:** Bacteria were harvested by centrifugation (2300 x g, 5 min) at an OD₆₀₀ of 0.8-1 and washed in PBS.

***E. histolytica*:** Amoebae were harvested from cell culture bottles by ice shock for 30 s and centrifuged (200 x g, 2 min) to remove medium. Amoebae were resuspended in pre-warmed PBS and counted using a hemocytometer.

2.2.1.5 Transformation

Preparation of electrocompetent cells. Bacteria were grown overnight under standard conditions (starter culture) and inoculated (1:50) the following day in the appropriate media. After reaching the logarithmic growth phase (OD₆₀₀ 0.5-0.8, depending on the species after 3-5 h), bacteria were placed on ice for 10 min. All subsequent steps were performed at 4 °C. Subsequently, bacteria were harvested by centrifugation (10 min, 3000 x g) and washed three times in the same volume of H₂O bidest and once in 1/10 volume of 10% glycerol. Bacteria were finally resuspended in 1/300 volume of 10% glycerol and immediately used for electroporation or stored at -80 °C in 50-100 µl aliquots.

Electroporation. For transformation of plasmids by electroporation, 50-100 µl of electrocompetent cells were thawed on ice, gently mixed with DNA in solution (1 µl, usually 200-700 ng), and transferred into cuvettes for electroporation. *E. coli* and *Y. enterocolitica* cells were kept on ice and electroporated immediately, *S. aureus* was incubated with DNA for 30 min at room temperature before electroporation. Electroporation was performed with a Gene Pulser at $U = 2.5 \text{ kV}$, $R = 200\Omega$, $C = 25 \mu\text{F}$ and $t \sim 4 \text{ ms}$ (*E. coli*, *Y. enterocolitica*). For *S. aureus* the voltage was set to $U = 2.0 \text{ kV}$. Immediately after electroporation, cells were resuspended in SOC medium (*E. coli*, *Y. enterocolitica*) or BM medium supplemented with 0.5% BSA (*S. aureus*), incubated for 1 h (*E. coli*, *S. aureus*: 37 °C; *Y. enterocolitica*: 27 °C) and subsequently plated on the corresponding selective agar plates (*E. coli*, *Y. enterocolitica*: LB Agar; *S. aureus*: TSA).

2.2.2 Molecular biological methods

2.2.2.1 Isolation of DNA

Plasmids were isolated with the NucleoSpin PlasmidPure kit (Macherey & Nagel, Düren) according to the manufacturer's protocol and stored at -20 °C. In short, bacterial cells were lysed by alkaline lysis, proteins were denatured and removed by centrifugation. DNA contained in the liquid supernatant is bound to a silica membrane for washing and eluted with H₂O bidest. Chromosomal DNA from *S. aureus* was isolated with the Presto Spin D bug kit (Molzym, Bremen) after treatment with lysostaphin (10 µg/ml, 1 h, 37 °C). DNA concentrations were measured with a NanoDrop ND1000.

2.2.2.2 Separation of DNA by gel electrophoresis

DNA was separated by electrophoresis (90 V, 30-60 min) in 1% agarose gels in TAE buffer [40 mM Tris; 40 mM acetic acid; 1 mM EDTA]. DNA samples were mixed with 10x DNA sample buffer [50% (v/v) glycerol; 0.1 M EDTA; 1% (w/v) SDS; 0.1% (w/v) bromphenol blue]. The size of DNA fragments was determined by comparison with a DNA standard (GeneRuler™ 1kb DNA Ladder, Fermentas). Gels were stained with ethidium bromide and DNA staining was visualized on a UV-transilluminator at 254 nm.

2.2.2.3 Modification of DNA

Modification of DNA was performed according to standard protocols based on Maniatis *et al.* (1989). Restriction enzymes, T4 DNA ligase and all corresponding buffers were purchased from Fermentas and used according to the protocols provided by the manufacturer. Polymerase chain reaction (PCR) was performed with High Fidelity PCR enzyme mix (Fermentas, Walldorf) according to the protocol provided by the manufacturer.

2.2.2.4 Construction of plasmids

***S. aureus* plasmids pVwbp, pEmp and pvWbpEmp:** The *vWbp* gene and the *emp* gene were amplified from chromosomal DNA of strain Newman by PCR (High Fidelity PCR Enzyme Mix, Fermentas) using the primer pairs *vWbp*-f-EcoRI / *vWbp*-r-SalI (1), *vWbp*-f-EcoRI / *vwb*-r-BamHI (2) and *emp*-f-BamHI / *emp*-r-PstI (3), respectively. The PCR products (1) and (3) were digested with EcoRI / SalI and BamHI / PstI, respectively, and ligated into pSK236 isolated from DH5α digested in the same way, resulting in the

plasmids pvWbp and pEmp. In order to produce pvWbpEmp, the PCR product from (2) was cloned into pSK236 via EcoRI / BamHI, followed by cloning of the PCR product from (3) into the resulting plasmid. Ligation products were transformed into electrocompetent DH5 α . Transformants were screened for growth with ampicillin. The resulting plasmids were isolated from DH5 α and transformed into electrocompetent RN4220, isolated again and then transformed into electrocompetent Newman wildtype or *vWbp emp* mutant strain.

***Y. enterocolitica* plasmid pYopT_{ypsC139S}:** The *yopT* gene from pYopT_{yps} was amplified by PCR using the primer pair "IP32953 pYV 29282 XbaI forward" and "IP32953 pYV 30915 SalI reverse". The fragment was digested with XbaI / SalI and ligated into pBLUE-SCRIPT II KS(+) digested with XbaI / SalI, creating pBS-YopT_{yps}. The amino acid exchange C139S in YopT_{yps} was generated by mutation of the corresponding DNA sequence from TGT to AGC by PCR with the primer pair "YopT C139S Yps Forward" and "YopT C139S Yps Reverse" from pBS-YopT_{yps}. The PCR product containing pBS-YopT_{ypsC139S} was digested with DpnI to remove unmodified pBS-YopT_{yps}, purified with a PCR purification kit and transformed into DH5 α . pBS-YopT_{ypsC139S} was isolated from DH5 α , the *yopT_{ypsC139S}* gene was excised with XbaI / SalI and ligated into pACY184 digested with XbaI / SalI, resulting in pYopT_{ypsC139S}. pBS-YopT_{ypsC139S} and pYopT_{ypsC139S} were confirmed by DNA sequencing at GATC (Konstanz) with the primer pairs Pbs-f/r and pACYC184-1356-forward/pACYC184-2312-reverse, respectively.

2.2.2.5 Generation of chromosomal mutants

Y. enterocolitica WA Δ inv(pYV Δ yadA) was generated by deletion of the *inv* gene in strain WA-C by Red recombination (Datsenko and Wanner, 2000) as described in Trcek *et al.* (2010) and subsequent transformation of pYVO8-A-0 into the resulting WA-C Δ inv mutant. In short, the primers invETfor and invETrev were used to amplify the spectinomycin cassette from the Ω plasmid (Prentki and Krisch, 1984) by PCR. 20 bp at the 3'-end of the primers were complementary to the regions flanking the spectinomycin cassette from the Ω plasmid. 50 bp at the 5'-end of the primers were homologous to the regions on the chromosome of *Y. enterocolitica* WA-314 flanking the *inv* gene (homology arms). This PCR construct was used to replace the *inv* gene by the spectinomycin cassette as described in Trülsch *et al.* (2004) by the Red recombinase system provided by the plasmid pKD46.

This plasmid is not replicated at 37 °C and can thus be removed by incubation of bacteria at 37 °C, which was checked by PCR (primer pair pKD46betFOR/REV).

2.2.3 Biochemical and analytical methods

2.2.3.1 SDS polyacrylamide gel electrophoresis, SDS-PAGE

Proteins were separated under denaturing conditions in SDS-PAGE (Laemmli, 1970) in 7 x 10 cm gels. Gels consisted of 5 % stacking gels and 10-15 % resolving gels, depending on the protein size. Protein samples were mixed with sample buffer before loading (final concentration: 62.5 mM Tris/HCl (pH 6.9), 10 % (v/v) glycerol, 2 % (w/v) SDS, 5 % (v/v) 2-mercaptoethanol, 0.005 % (w/v) bromphenol blue). Electrophoresis was performed in a Bio-Rad system in Laemmli buffer [250 mM glycine, 0.1 % SDS, 25 mM Tris/HCl, pH 8.3] at 40 V for 20 min and 120 V for approximately 2 h, depending on protein size. For the visualization of proteins, gels were stained in Coomassie solution (0.275 % Coomassie brilliant blue R250, 50 % methanol, 10 % acetic acid) for 30 min and subsequently destained in destaining solution (10 % methanol, 10 % ethanol, 7.5 % acetic acid) until adequate contrast was achieved (Weber and Osborn, 1969).

2.2.3.2 Western blotting

Proteins were transferred from SDS polyacrylamide gels to nitrocellulose membranes by Western blotting in a Mini Trans-Blot System (Bio-Rad) for 50 min at 100 V. SDS polyacrylamide gels, nitrocellulose membrane and filter paper were equilibrated in blotting buffer [25 mM Tris, 192 mM Glycine, 10 % methanol, p.a. (v/v)]. After transfer, the membrane was incubated over night in blocking buffer [0.5 % Tween 20, 1 % milk powder, 1 % BSA in 1 x PBS] at 4 °C. Proteins were detected by immunostaining with primary antibody (1:10,000, 1 h, RT), followed by three washing steps in washing buffer [0.5 % tween 20 in 1 x PBS], incubation with horseradish peroxidase (HRP)-linked secondary antibody (1:10,000, 1 h, RT), followed by three washing steps. HRP was detected with ECL Western blotting detection reagents and visualized on x-ray films.

2.2.3.3 Precipitation of secreted proteins

For analysis of secreted *S. aureus* proteins, overnight cultures were diluted 1:25 in 5 ml medium. For the analysis of secreted *Yersinia* proteins, overnight cultures were diluted

1:40 in fresh medium, cultivated for 2 h at 27 °C and then 5 mM EGTA was added to the cultures and temperature was shifted to 37 °C. After 3-5 h of growth, secreted proteins were precipitated from 3.6 ml culture supernatants with 10 % trichloroacetic acid for 1 h on ice. The pellets were washed three times in 1 ml -20 °C acetone (12.000 x g, 10 min, 4 °C), followed by a final washing step in H₂O. The pellet was dried and resuspended in SDS sample buffer. Equal amounts of supernatant according to the OD₆₀₀ before harvesting were separated by 10-12 % SDS-PAGE.

2.2.3.4 Extraction of membrane-associated *S. aureus* proteins

Presence of Emp on the *S. aureus* cell surface was detected as described previously with some modifications (Hussain *et al.*, 2002): *S. aureus* was cultivated in 10 ml of BM medium for 18 h. Differences in OD₆₀₀ were adjusted by addition of BM medium. Cells were harvested by centrifugation at 4,000 x g for 10 min. The pellets were resuspended in 300 µl of 2 % SDS (Sigma) and incubated at 95 °C for 5 min shaking at 750 rpm. The supernatant was then isolated in two sequential centrifugation steps at 10,000 x g for 5 min and stored at -80 °C. Equal amounts were mixed with sample buffer and proteins were separated by 12 % SDS-PAGE.

2.2.3.5 Mass spectrometry

Identification of proteins was performed with MALDI-TOF. Proteins were manually isolated from SDS-PAGE. Subsequent sample preparation and mass spectrometric analysis was conducted by staff at the Protein Analysis Unit (ZfP), LMU Munich, in a Voyager DE STR (Applied Biosystems, Foster City, United States).

2.2.3.6 Transmission electron microscopy

Samples for transmission electron microscopy were fixed in 3.5 % glutaraldehyde in 0.1 M phosphate buffer (pH 7.4) for 2.5 h at 4 °C and then transferred to 1 % glutaraldehyde in 0.1 M phosphate buffer (pH 7.4). Further processing and imaging was performed by staff at the electron microscopy unit at the Anatomy Institute, LMU Munich as follows: Samples were washed in phosphate buffer and incubated with 2 % osmium tetroxide in H₂O bidest for 2 h at 4 °C followed by a further washing step at room temperature. Dehydration was performed in a graded series of ethanol (30, 50, 70, 90 and 100 %). Subsequently, samples were embedded in araldite (polymerization for 48 h at 60 °C), thin sectioned and stained

with 2% unbuffered uranyl acetate. Imaging was performed in a Philips CM-10 electron microscope.

2.2.3.7 Immunoassay for cytokine measurements

Cytokine concentrations in the flow through of the basal compartment of the organ chamber were measured using multiplexed BD Cytometric Bead Array (CBA) Flex Sets (BD, Heidelberg). IL-6, KC, MCP-1 and TNF- α were analyzed using the respective BD CBA Mouse Soluble Protein Flex Sets in combination with the BD CBA Mouse Soluble Protein Master Buffer Kit. 50 μ l of sample were collected at defined time points, stored at -80 °C and analyzed according to the manufacturer's protocol.

2.2.3.8 Flow cytometry

FACS analysis of the CBA Flex Set (BD, Heidelberg) was conducted with a BD FACSCanto™ II flow cytometer. Data were evaluated with FCAP Array™ software (Soft Flow Hungary).

2.2.4 Cell biological methods

2.2.4.1 Media and cultivation

Cell culture media used in this work are listed in Tab. 2.10.

Table 2.10: Cell culture media

Name	Composition
RPMI 1640	no phenol red
M-CSF DMEM	DMEM high glucose (4.5 g/l), 10% FCS, 5% horse serum, 1% HEPES, 1% Na-Pyruvate, 1% L-glutamine, 2 ng/ml M-CSF
RPMI GM-CSF	RPMI 1640, 2 mM L-glutamine, 50 μ M β -mercaptoethanol, 10% FCS, 20 ng/ml GM-CSF

Eukaryotic cells were cultured in an incubator at 37 °C, 5% CO₂ and saturated humidity. Bone marrow-derived dendritic cells or macrophages were cultured in petri dishes, HeLa cells were cultured in cell culture flasks

2.2.4.2 Generation of bone marrow-derived dendritic cells (DCs)

DCs were cultured as described previously (Lutz *et al.*, 1999). In short, femurs of 8-12 weeks old mice were prepared and disinfected in 70% ethanol for 2-3 min. Subsequently, both ends of the bones were cut with a scalpel and flushed with PBS with a syringe to isolate bone marrow cells. Cells were seeded at 2×10^6 cells per 100 mm petri dish in 10 ml RPMI GM-CSF. At day 3, 10 ml RPMI GM-CSF were added to the dish. At day 6 and 8, 10 ml cell suspension was removed from the dish, centrifuged (200 x g, 5 min), resuspended in 10 ml fresh RPMI GM-CSF and returned to the dish. At day 8-10, non-adherent cells were harvested, resuspended in 10 ml fresh RPMI GM-CSF and seeded in 100 mm petri dishes for cell culture. Cells were stimulated with 200 ng/ml LPS (*E. coli* K12) overnight and used for experiments the following day.

2.2.4.3 Generation of bone marrow-derived macrophages (BMMs)

Bone marrow was isolated as described for DCs. Cells were seeded at 5×10^6 cells per 100 mm petri dish in 8 ml DMEM M-CSF. At day 3 and 7, 4 ml fresh DMEM M-CSF were added. At day 10, the medium was replaced by fresh DMEM M-CSF. At day 12, 4 ml fresh DMEM M-CSF were added. At day 15, cells were used for experiments.

2.2.4.4 Isolation of PMNs from peripheral human blood

20 ml blood from voluntary donors was drawn into syringes pre-filled with heparin (final concentration: 10 U/ml). Blood was transferred to 50 ml Falcon tubes and filled to 50 ml with PBS. Two 50 ml Falcon tubes were filled with 15 ml Ficoll each and 25 ml blood suspension was slowly added on top of the Ficoll. The tubes were centrifuged at 400 x g for 30 min at room temperature without braking. Supernatant and the opaque layer were removed and the bottom phase (ca. 5 ml) was resuspended in 50 ml PBS. Tubes were centrifuged at 350 x g for 10 min at 4 °C without braking and the supernatant was discarded. The bottom phases of both tubes were combined and 40 ml lysis buffer [4.15 g NH_4Cl , 500 mg KHCO_3 , 18 mg EDTA ad 500 ml H_2O ; pH adjusted to 7.4] was added. The solution was incubated at 4 °C for 30 min and centrifuged at 350 x g for 10 min at 4 °C. The supernatant was removed and the pellet was resuspended in 50 ml of lysis buffer and incubated for 10 min at 4 °C. After a final washing step at 350 x g for 10 min at 4 °C, the pellet was resuspended in RPMI / 1% FCS and cells were used for experiments.

2.2.4.5 HeLa cell culture

HeLa cells were cultivated in DMEM supplemented with 10 % FCS in cell culture flasks. Cells were split every 2-3 days before reaching confluency by washing in PBS and subsequent trypsin-EDTA treatment (3 ml, 3 min, 37 °C, 5% CO₂). Trypsin was inactivated by addition of 5 ml DMEM / 10 % FCS. An aliquot was inoculated in a fresh cell culture flask with DMEM / 10 % FCS.

2.2.4.6 Determination of cell count

The concentration of cells in solution was determined in a hemocytometer (Neubauer chamber). Prior to counting, cells were stained with trypan blue and cell solutions were diluted with PBS in order to reach cell counts of 30-300 cells per large square of the hemocytometer. Trypan blue is a vital stain selectively staining dead cells in dark blue.

2.2.4.7 β -lactamase reporter assay

Translocation of fusion proteins of the *yopH* gene from *Y. enterocolitica* with the TEM-1 β -lactamase (*bla*) gene from *E. coli* was analyzed in DCs in under-agarose assays. The constructs were provided by Cvetanovic (2011). β -lactamase activity after translocation of the fusion proteins into eukaryotic cells was detected with LiveBLAzer™-FRET B/G Loading Kit (Invitrogen) according to the manufacturer's recommendations. In short, CCF4 is a FRET (Fluorescence Resonance Energy Transfer) substrate in which a fluorescein is linked via a cephalosporin core to 7-hydroxycoumarin. Uncleaved CCF4 exhibits FRET when excited at 409 nm: the coumarin is excited, transfers the energy to the fluoresceine which emits green fluorescence (520 nm). Upon cleavage of the cephalosporin core by β -lactamase, FRET is disrupted and the coumarin emits blue fluorescence (450 nm).

CCF4-AM (a lipophilic, esterified version of CCF4) enters eukaryotic cells and is subsequently cleaved to CCF4 by endogenous cytoplasmic esterases, hindering its diffusion from the cell.

6x CCF4 staining solution (sufficient for ca. 0.8×10^6 cells in 800 μ l) was prepared from 2 μ l solution A, 10 μ l solution B, 150 μ l solution C and 12 μ l solution D. DCs were washed, resuspended in PBS and mixed with 6x CCF4 staining solution in a 12 well plate. Cell suspensions were incubated at room temperature in the dark for 90 min. Cell suspensions were subsequently transferred to 1.5 ml tubes, filled to 1.5 ml with RPMI/10 % FCS and

centrifuged (200 x g, 3min). The cell pellets were resuspended in 4 μ l RPMI/10 % FCS and used for under-agarose migration experiments.

2.2.4.8 Lactate dehydrogenase (LDH) release assay

LDH release from HeLa cells or neutrophils as a result of infection with different *Yersinia* strains was analyzed. LDH is a stable cytosolic enzyme which is released as a result of cell membrane damage, typically a primary stage of cell lysis. The CytoTox 96 Non-Radioactive Cytotoxicity Assay (Promega) was used for quantitative analysis of cell lysis according to the manufacturer's recommendations. It is based on an enzymatic reaction converting a tetrazolium salt into a red formazan which can be measured at 490 nm in a 96 well plate reader.

For neutrophils isolated from human blood, 50 μ l cell suspension (4×10^6 cells/ml RPMI/2 % FCS) were incubated for 1 h at 37 °C, 5% CO₂ in a 96 well plate. 50 μ l bacteria suspension (8×10^7 /ml RPMI) were added.

For HeLa cells, 2×10^4 cells/well were seeded the day before the assay in a 96 well pate. After 24 h the cells had doubled (4×10^4 cells/well), and the medium was replaced by 100 μ l infection medium (8×10^6 /ml RPMI/1 % FCS).

Cells were infected for 4 h at an MOI of 20, cells in the control were lysed with lysis buffer during the last 10 min of incubation. 96 well plates were centrifuged (5 min, 200 x g) in order to sediment cells and bacteria. 50 μ l supernatant were mixed with 50 μ l assay buffer, incubated for 20 min in the dark at room temperature and the enzymatic reaction was stopped by addition of 50 μ l stopping solution. The absorption at 490 nm was measured in a 96 well plate reader.

2.2.4.9 Transfection of dendritic cells

DCs were transfected with MLC-GFP using the Amaxa Mouse Dendritic Cell Nucleofector Kit (Lonza) and the Amaxa Nucleofector I (program Y-01) at day 8-10 of culture. DCs were transfected according to the protocol provided by the manufacturer. After transfection, DCs were incubated for 3 h and then stimulated with 200 ng/ml LPS.

2.2.4.10 Immunocytochemistry ICC

ICC in 3D-CoG was performed in microscopic dishes (μ -slide 8 well, ibidi) at room temperature. If not mentioned otherwise, solutions were applied in a volume of 150 μ l. 3D-CoG

were fixed with 4% paraformaldehyde for 20 min at room temperature and then washed three times (PBS, 5 min each). Samples were blocked in blocking buffer [PBS with 3% bovine serum albumine and 5% human serum from donors] for 1 h. Primary antibody was added to the samples (1:100 rabbit anti-Coa, 1:333 rabbit anti-Emp; both were kindly provided by O. Schneewind) and incubated for 1.5 h, followed by three washing steps (PBS, 5 min each). Secondary antibody (1:200 Alexa 555 anti-rabbit from goat, Invitrogen) was diluted in blocking buffer, added to the samples and incubated for 1 h in the dark, followed by three washing steps (PBS, 5 min each). 1 $\mu\text{g}/\text{ml}$ DAPI was used for staining of DNA. Cell surface of staphylococci was stained with 5 $\mu\text{g}/\text{ml}$ FITC-labeled lectin from *T. vulgaris*, specific for N-Acetyl-glucosamine (Sigma-Aldrich). Additional stainings were performed in parallel to incubation with secondary antibody.

2.2.4.11 Live cell stainings

2.2.4.11.1 DNA Nuclei were stained with DAPI at concentrations ranging from 0.02 to 1 $\mu\text{g}/\text{ml}$ for 5-10 min. Nuclei of cells with corrupted cell membrane were stained with 1 μM Sytox Blue (Invitrogen), which was added to the medium.

2.2.4.11.2 Surface of epithelial and urothelial cells Cell membranes were stained with the lipophilic styryl dye FM 4-64 (Invitrogen) for 15 min at room temperature or by additional supplement of the medium with FM 4-64. Concentrations were chosen according to the setting: urinary bladder and small intestine of the mouse 4 $\mu\text{g}/\text{ml}$; stomach and cecum 10 $\mu\text{g}/\text{ml}$. Alternatively, epithelial staining was performed with Alexa 680-labeled rWGA (Invitrogen) applied at 15 $\mu\text{g}/\text{ml}$ for 15 min at room temperature.

2.2.4.11.3 Pathogens Amoebae were stained with Alexa 680-labeled rWGA at 50 $\mu\text{g}/\text{ml}$ for 5 min at 37 $^{\circ}\text{C}$ to facilitate phagocytic uptake of the dye. The dye accumulated in vesicles inside the amoeba.

Bacteria were expressing fluorescent proteins (see Tab. 2.1-2.3, p. 19) or detected as mentioned in the text.

2.2.4.12 Microscopy and image processing

Microscopy was performed on a Leica SP5 microscope (Leica, Germany) equipped with an incubation chamber (The Cube & The Box, Life Imaging Services, Switzerland). Images were acquired with a 63x oil immersion objective, a 40x oil immersion objective,

a 20x immersion objective or a 10x objective. Image acquisition, processing and quantification was performed with LAS AF software (Leica, Germany) and ImageJ software (<http://rsb.info.nih.gov/ij/>). Velocity measurements were performed with the Manual Tracking plugin for ImageJ (F. Cordelières). Kymographs were generated using ImageJ. Confocal reflection contrast microscopy was used to visualize unstained collagen and fibrin fibers as described previously (Friedl *et al.*, 1997). The dimensions of z projections from xyz stacks are mentioned in the figure legends. Time projections of xyzt series were performed by projecting all single xy frames onto a single one.

2.2.5 Experimental setups

2.2.5.1 3D-CoG spleen slice infection model (3D-CoG/SSIM)

Collagen gels (3D-CoG) were generated as described previously (Freund *et al.*, 2008) and incubated without agitation. Bacteria were prepared as described in chapter 2.2.1.4 (p. 30) and subsequently suspended in liquid collagen solution (about 2×10^4 /ml). Liquid collagen solution consisted of 1.78 mg/ml bovine type I collagen (Purecol, Advanced Biomatrix) in RPMI 1640 medium adjusted to pH 7.4. 10 μ l of this solution were dispersed on the bottom of a microscopic dish (9.4 x 10.7 mm, μ -slide 8 well, ibidi). The samples were allowed to polymerize for 45 min (37 °C; 5 % CO₂). 3D-CoGs were overlaid with 150 μ l cell culture medium (RPMI 1640).

For neutrophil challenge of microcolonies in 3D-CoG, native spleens from 8-12 weeks old heterozygous *lys-EGFP* mice (Faust *et al.*, 2000) were used. Mice were sacrificed by CO₂ asphyxiation and spleens were harvested and cut into 300 μ m slices with a vibrating blade microtome (Leica) at 4 °C. Supernatants from 3D-CoG samples were removed and then 3D-CoG were overlaid with spleen slices. To immobilize the slices on the 3D-CoG, a drop of 4 % NuSieve GTG agarose (Lonza) was applied. After solidification, 150 μ l of RPMI 1640 were added.

The manual process of overlaying 3D-CoG with tissue slices can partially result in compression or injury of some areas of the collagen gel. To compensate for artifacts, only microcolonies in a lateral distance of about 200 μ m to the tissue slice-collagen gel interface were analyzed after verifying that the collagen gel in this area was not compressed or injured. This was achieved by visualization of the 3D-CoG structure with confocal reflection microscopy. The samples were incubated at 37 °C, 5 % CO₂ and saturated humidity in a cell culture incubator or in the microscope incubation chamber.

For experiments with *S. aureus*, the medium for overlaying 3D-CoG was supplemented with 3 mg/ml fibrinogen from human plasma (Calbiochem) (3D-CoG/Fib). Optionally, argatroban (Santa Cruz) was added to the growth medium at the concentrations mentioned in the text.

2.2.5.2 3D-CoG migration assay

LPS-stimulated dendritic cells were infected with *Y. enterocolitica* and their ability to migrate after infection was analyzed in custom-built migration chamber (Fig. 2.1). 6×10^5 DCs were infected for 30 min at an MOI of 20 with the respective *Yersinia* strains in a volume of 200 μ l RPMI/10% FCS in 24 well plates. After infection, PBS with 20 μ g/ml gentamicin was added to the wells, the cell suspension was transferred to 1.5 ml tubes and cells were washed two times with 1 ml PBS/Genta. Cells were resuspended in 100 μ l RPMI/10% FCS and incorporated in 3D-CoG in a custom-built setup (final cell concentration in 3D-CoG ca. 7×10^5 DCs/ml). After polymerization of the 3D-CoG, a CCL19 gradient was established by applying 20 μ l 0.6 μ g/ml CCL19 (Peprotech, Hamburg) to the open side of the 3D-CoG. Cell migration was recorded with a microscope at 37 °C, 5% CO₂ for 3 h.

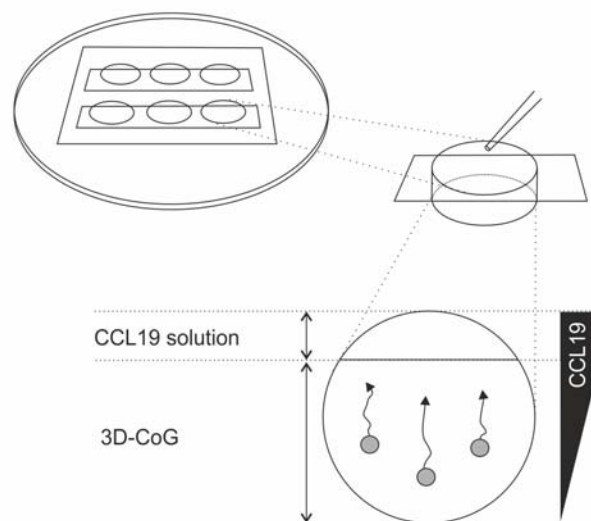


Figure 2.1: 3D-CoG migration assay setup. 6 holes (ca. 6 mm in diameter) were drilled in the bottom of a 35 mm cell culture dish. To the bottom they were closed by attaching a coverslip. On top, ca. 70 % of the hole were covered with a broken coverslip. Collagen solution was applied with a pipette and the setup was tilted 90 degrees so that the collagen sank to the side of the well opposite of the opening. After polymerization, chemoattractant solution (CCL19) was applied to the residual space in the well, establishing a CCL19 gradient in the 3D-CoG. Cells migrated towards the gradient in 3D-CoG.

2.2.5.3 Under-agarose migration assay

The under-agarose migration assay (Fig. 2.2) provides a setup for quantitative and qualitative analysis of cell migration and was conducted according to Heit and Kubes (2003) and Lämmermann *et al.* (2009). In the present work it has been used to characterize the effects of *Yersinia* effector proteins on migratory behavior of single dendritic cells. 5 ml 2x HBSS buffer and 10 ml RPMI 1640/20% FCS were mixed and heated to 68 °C in a water bath. In a separate tube, 0.125 g ultra-pure agarose was dissolved in 5 ml H₂O by boiling in a microwave. Both solutions were combined and 1.8 ml were pipetted into custom-made chambers composed of a ring cut from a 50 ml Falcon tube fixed to a small petri dish. After solidification of the 0.625% agarose, wells were punched in the gel (ca. 2 mm in diameter). Gels were equilibrated for 1 h at 37 °C; 5% CO₂. Usually a central well (attractor well) was filled with 5 µl chemoattractant (1.2 µg/ml CCL19; Peprotech, Hamburg) and in a distance of 5 mm 1-3 wells were punched (responder wells). The chemokine diffuses through the agarose and thereby a chemokine gradient from the attractor to the responder wells is created. The responder wells were filled with 5 µl DC suspension (10⁵ cells/well). Alternatively, cells directly injected under the agarose for transfected cells or if initial cell migration from the responder well under the agarose was inhibited, e. g. due to pre-infection. Bacteria were prepared as described in in chapter 2.2.1.4 (p. 30) and injected under the agarose with a fine pipette tip in 0.5 µl.

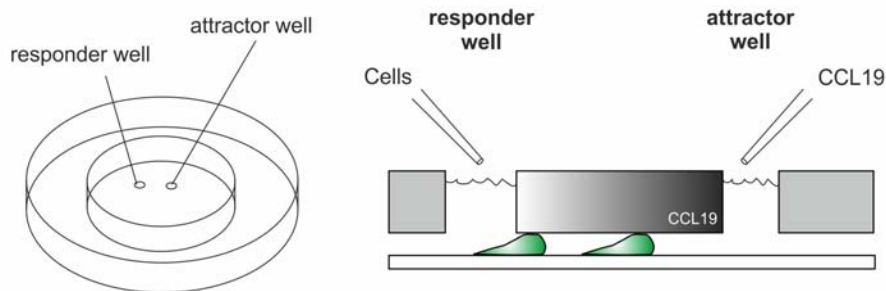


Figure 2.2: Under-agarose migration assay setup. 0.625 % agarose was poured in a well constructed by a section of a 50 ml Falcon tube. After solidification of the agarose, small wells were punched in the gel. Usually, a central well was filled with chemoattractant (CCL19) and acted as the attractor well and wells in the periphery were filled with dendritic cells in solution. A gradient is established outward from the attractor well, causing the DCs to squeeze underneath the agarose and migrate towards the gradient.

2.2.5.4 *Ex vivo* microscopy in the organ chamber

The organ chamber (Fig. 3.34 A, B, p. 87) was conceived by A. Wieser, designed and optimized by A. Wieser and C. Guggenberger and machined from aluminum and anodized by A. Wieser and Dipl. ing. Michael Achtelik. It is suitable for standard cross tables for ISO 8037/I microscope slides (76 x 26 mm) and consists of four main parts which are held together by screws. The chamber is sealed water and gas tight against the environment by two glass coverslips (32 x 24 mm) and can be used on both inverted and upright microscope setups. All connectors of the organ chamber are in the Luer-Lock system to allow usage of standard medical infusion tubing. Gas composition is adjusted by a custom-built membrane oxygenation device (Fig. 3.34 C, p. 87, constructed by A. Wieser) and an active gas supply system (The Brick, Life Imaging Services, Basel). Oxygen concentration and pH values in the medium were measured with PSt3 Oxygen Optodes (PreSens, Regensburg, Germany) and a pH electrode (320 pH-Meter, Eppendorf, Hamburg), respectively.

Ex vivo cultivation of organ explants was performed in DMEM (Sigma-Aldrich, Hamburg, Germany) supplemented with 10% fetal calf serum (Invitrogen). *Ex vivo* infection in the organ chamber was performed with *E. coli* NU14, *S. enterica* and *E. histolytica*, respectively; intravesical *in vivo* infection was performed with *E. coli* NU14 as described in chapter 2.1.6.3 (p. 29). Bacterial counts were determined by photometric measurements and subsequent determination of *cfu*.

E. coli NU14 About 3×10^8 *cfu* in 30 μ l PBS were injected into the apical compartment of the urinary bladder explant in the organ chamber.

S. enterica About 2×10^5 *cfu* in a volume of 50 μ l PBS were injected into the apical compartment of the gut explant inside the organ chamber.

E. histolytica 3.8×10^4 *cfu* amoebae in a volume of 50 μ l PBS were injected into the apical compartment of the organ chamber containing the caecum explant and incubated for 20 min before starting perfusion.

2.3 Statistical analysis

Statistical significance calculations were performed with Student's unpaired t-test (Graph Pad Prism 5.0, Graph Pad Software Inc, La Jolla, USA).

Chapter 3

Results

3.1 3D-CoG based *in vitro* model

3.1.1 Development of the 3D-CoG/spleen slice infection model

In order to mimic *in vivo* dimensionality, a previously published collagen gel system (3D-CoG) was chosen as the basis for the presented setup (Islam *et al.*, 1985; Freund *et al.*, 2008). Collagen fibers constitute a three dimensional scaffold (Fig. 3.1 B). It has been shown that *Y. enterocolitica* exhibits unique *in vivo*-like microcolony formation in 3D-CoG (Freund *et al.*, 2008). The task of this work was to extend this system to the study of neutrophil interactions with different bacterial species.

The previous model was based on custom-constructed gel chambers holding 66-100 μ l 3D-CoG in between a microscope slide and a coverslip. For standardization and easier access to the 3D-CoG, this setup was modified: 10 μ l collagen solution were dispensed on the bottom of standardized dishes (μ -slide 8 well, ibidi) to a ca. 4 x 4 mm nearly flat plane. The collagen solution was allowed to polymerize for 45 min (37 °C; 5 % CO₂) as described previously (Islam *et al.*, 1985; Freund *et al.*, 2008). 3D-CoG were overlaid with 150 μ l cell culture medium (RPMI, 1640) and incubated for the desired time as indicated.

As the first line of cellular defense of the host immune system is represented by neutrophils (Nathan, 2006), the interactions of this professional phagocyte with bacterial microcolonies were studied. As source of neutrophils spleen slices from transgenic *lys-EGFP* mice were used. In this mouse strain, GFP is expressed under control of the endogenous lysozyme M-promoter, resulting in GFP-positive myelomonocytic cells (Faust *et al.*, 2000). It has been shown that cells expressing high levels of GFP are neutrophils, whereas cells

expressing low levels of GFP belong to the monocyte/macrophage population (Peters *et al.*, 2008). As the spleen is heavily vascularized and the red pulp is thus expected to contain high amounts of neutrophils from blood, this organ was used for the generation of native thin tissue slices (300 μm) with a vibrating blade microtome. These spleen slices from *lys-EGFP* mice were found to contain a sufficient density of bright GFP-positive cells in the red pulp (Fig. 3.1 A1, A2; blue arrowhead). A population of more dimly fluorescent and differently shaped GFP-positive cells was found mainly in the white pulp (Fig. 3.1 A1, A2; yellow arrowhead). When incubated under cell culture conditions on the microscope, the population of bright GFP-positive cells was found to emigrate from the spleen slice and to be highly migratory on the coverslip. This cell type contained lobulated nuclei which are typical for neutrophils (Movie 1). Addition of DsRed-expressing bacteria WA-C(pRFP) to the coverslip before addition of the spleen slice induced phagocytosis of bacteria after emigration of GFP-positive cells (Fig. 3.2 A, Movie 2). In the next step, spleen slices were layered on top of pre-formed 3D-CoG and immobilized with a drop of Low Melting agarose (Fig. 3.2 B). GFP-positive cells migrated steadily into the 3D-CoG (Fig. 3.1 A). In the presence of bacteria, phagocytosis was observed. As a control, bone marrow-derived macrophages were incorporated into 3D-CoG together with WA-C. The migratory behavior (Movie 3) of this cell type was different and much slower compared to the spleen-derived GFP-positive cells, demonstrating that the GFP-positive cells, which migrated into the 3D-CoG, were exclusively neutrophils. Non-fluorescent cells immigrating into the 3D-CoG were rarely observed and not further characterized.

Taken together, the 3D-CoG/spleen slice infection model (3D-CoG/SSIM) is suitable for the study of bacterial growth behaviour in a tissue-like environment and subsequent interactions with neutrophils. Moreover, observations from this model can be compared to *in vivo* characteristics by analyzing tissue sections from infected organs in future studies (Fig. 3.2 C).

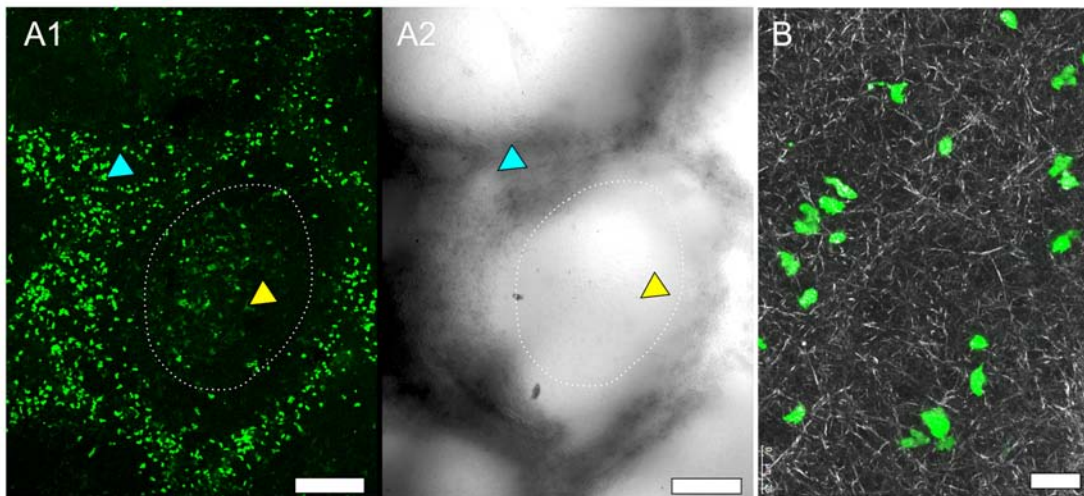


Figure 3.1: GFP-neutrophils from *lys-EGFP* spleen slices and structure of 3D-CoG. **A:** Overview of a 300 μm thin spleen slice produced with a vibrating blade microtome. Scale bar 200 μm . **A1:** GFP channel. GFP-positive cells in the spleen. A bright population of GFP-positive cells is mainly localized in the red pulp (blue arrowhead), whereas a population of more dimly fluorescent and differently shaped GFP-positive cells was found mainly in the white pulp (yellow arrowhead). The border of red and white pulp is marked by a dashed white line. **A2:** Bright field channel. Red pulp (blue arrowhead) and white pulp (yellow arrowhead) can be clearly distinguished by their different opacity. **B:** Fibrillar structure of the 3D-CoG, serving as a migration substrate for neutrophils. z projection of 13 z sections spanning a total depth of 45 μm . 3 h after mounting of a *lys-EGFP* spleen slice. Scale bar 25 μm .

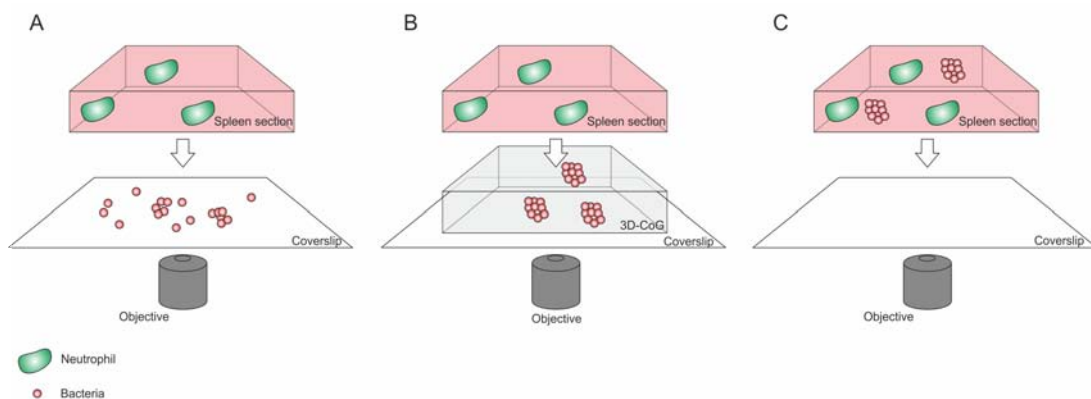


Figure 3.2: Stepwise development of the 3D-CoG/SSIM. **A:** Spleen slices are mounted on dishes suitable for microscopy. Migratory cells emigrate from the tissue section and interact with bacteria on the coverslip (compare Movie 1 and 2). **B:** Spleen slices are layered on top of pre-formed 3D-CoG. Neutrophils enter the 3D-CoG matrix. **C:** Infected tissue slices can be mounted as well and *in vivo* phenotypes can be compared to observations from **B**.

3.1.2 *Staphylococcus aureus* abscess formation

3.1.2.1 Growth of *S. aureus* in the 3D-CoG system

In a first approach to establish the collagen gel-system (3D-CoG/SSIM) for studying staphylococci-neutrophil interactions, the growth behavior of *S. aureus* strain Newman was analyzed. When growing strain Newman for 16 h in RPMI 1640 medium without agitation, single bacterial cells gave rise to irregularly shaped bacterial clusters of variable size (Fig. 3.3 A). In the next step, monodispersed staphylococci were mixed with neutralized collagen type I solutions, followed by incubation at 37 °C. Gelling occurred within 45 min and resulted in a rigid collagen matrix which was then overlaid with medium (3D-CoG). Staphylococci replicated and formed clusters similar to those observed in RPMI 1640 without collagen after 16 h (Fig. 3.3 B). Moreover, specific interaction of staphylococci with collagen fibers was not observed by confocal microscopy. Thus, the 3D-CoG system is suitable for studying growth of *S. aureus* in a rigid matrix by microscopy.

In order to supply a more tissue-like environment, fibrinogen corresponding to normal serum concentration (3 mg/ml) was added to the growth medium (3D-CoG/Fib). This led to dramatic changes in the growth behavior of staphylococci (Fig. 3.3 C):

Firstly, single staphylococci gave rise to discrete microcolonies of uniform size after 16 h of growth which were surrounded by a spherical pseudocapsule (35 µm in diameter and 1-3 µm in thickness, Fig. 3.3 C and 3.4). The encapsulated microcolonies consisted of densely packed staphylococci and appeared to be free of collagen fibers. Staphylococci were embedded in disperse material inside the pseudocapsule (Fig. 3.5).

Secondly, the pseudocapsules were embedded in an outer dense microcolony-associated meshwork (MAM) surrounding the microcolonies (approximately 150 µm in diameter, Fig. 3.4). Both of these concentric structures, the inner pseudocapsule and the outer MAM, were only formed in the presence of fibrinogen. The observation that these structures - in contrast to collagen fibers - were rapidly degraded after the addition of plasmin (8 µg/ml) suggests that they are at least in part composed of fibrin (Fig. 3.6, Movie 4).

As the observed pseudocapsule and the MAM appeared to consist of fibrinogen/fibrin components, an involvement of secreted proteins belonging to the SERAM family was assumed (Chavakis *et al.*, 2005). Most, if not all of these genes have been shown to be transcriptionally activated by the *saeRS* two-component system (Mainiero *et al.*, 2010; Harraghy *et al.*, 2005). Therefore, the Newman *sae* mutant with severe repression of

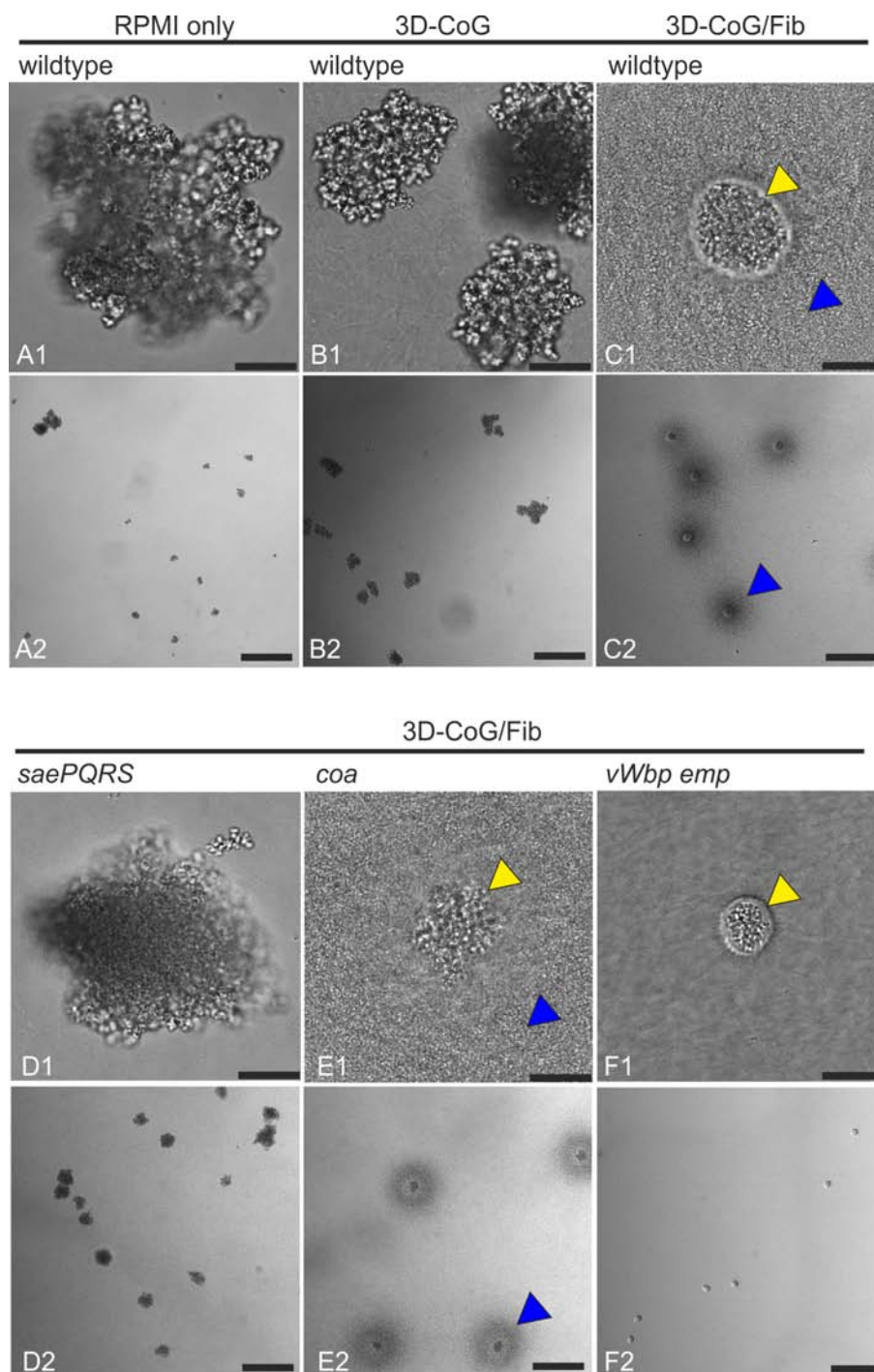


Figure 3.3: Growth phenotypes of *S. aureus* Newman strains in different environments. Growth phenotypes of *S. aureus* Newman strains under different growth conditions were analyzed 16 h after inoculation without agitation. **A:** Growth in RPMI 1640 leads to cluster formation of variable size. **B:** Growth in 3D-CoG leads to similar cluster formation. **C:** Addition of 3 mg/ml fibrinogen to the medium (3D-CoG/Fib) resulted in the formation of discrete microcolonies of uniform diameter, surrounded by an inner pseudocapsule (yellow arrowhead) and an outer dense microcolony-associated meshwork MAM (blue arrowhead). **D:** The *sae* mutant (Newman-29) formed clusters comparable to the wildtype, even in 3D-CoG/Fib. **E:** The *coa* mutant formed microcolonies which were irregularly shaped in comparison to the wildtype, MAM formation was unaffected. **F:** The *vWbp emp* double mutant was unaffected in formation of the inner pseudocapsule but was devoid of any outer MAM. A1-F1: 40x oil immersion objective, scale bar 25 μ m. A2-F2: 10x objective, scale bar 200 μ m.

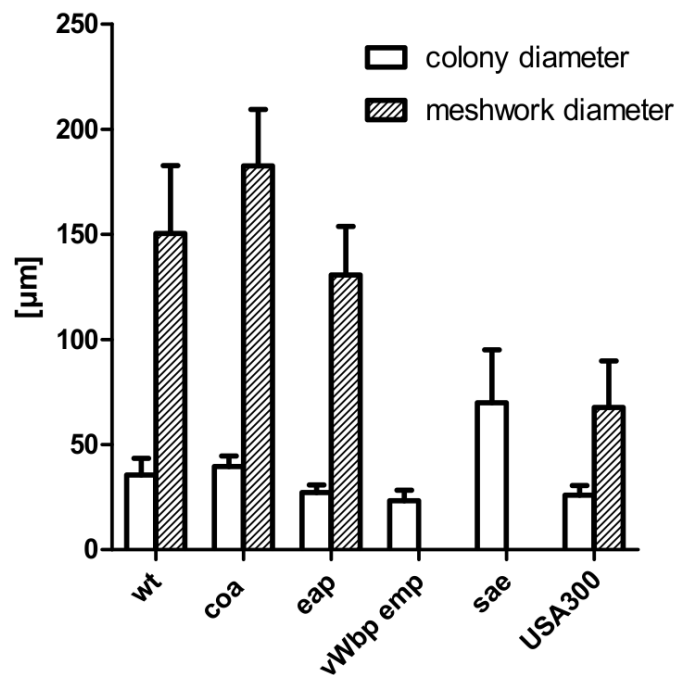


Figure 3.4: Microcolony and MAM diameter of *S. aureus* Newman strains after growth in 3D-CoG/Fib. The average diameter of microcolonies and MAM was determined after 16 h of growth in 3D-CoG/Fib. Wildtype (wt), *coa* mutant and *eap* mutant formed microcolonies and microcolony-associated meshwork (MAM) of comparable size. The *vWbp emp* double mutant did not form any MAM, despite being unaffected in pseudocapsule formation. A *sae* mutant (Newman-29) neither formed pseudocapsules nor MAM but grew in clusters significantly larger than wt colonies. USA300 microcolonies were comparable in size to wt, pseudocapsule formation was present, but the diameter of the MAM was significantly smaller compared to wt. Data are averaged from at least three independent experiments.

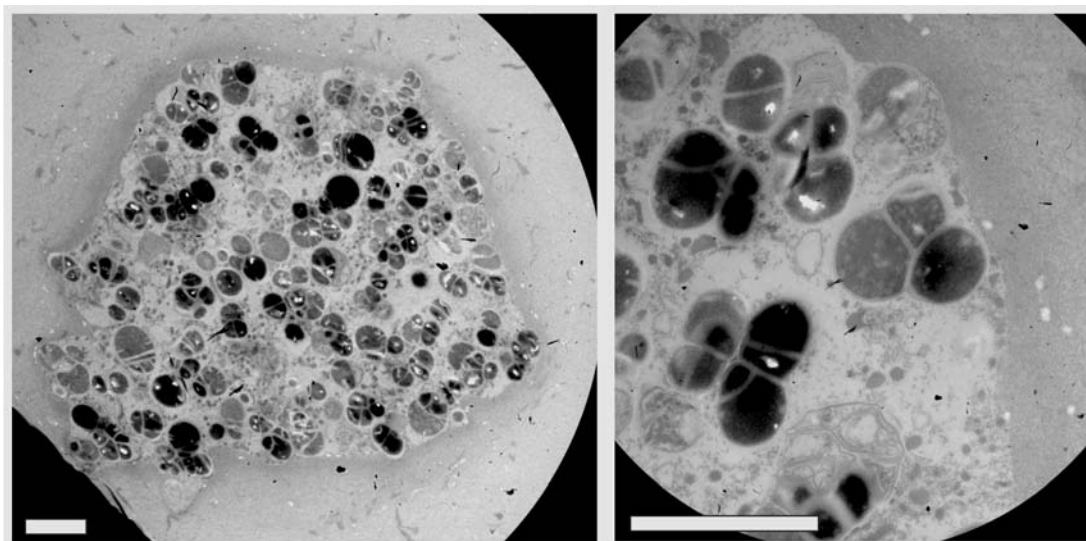


Figure 3.5: *S. aureus* microcolonies are surrounded by a pseudocapsule in 3D-CoG/Fib. *S. aureus* Newman microcolonies grown in 3D-CoG were analyzed by transmission electron microscopy 16 h after inoculation without agitation. A fibrillar structure surrounding the microcolony is visible, the inner of the microcolony consists of staphylococci and extracellular material. Scale bar 5 μm .

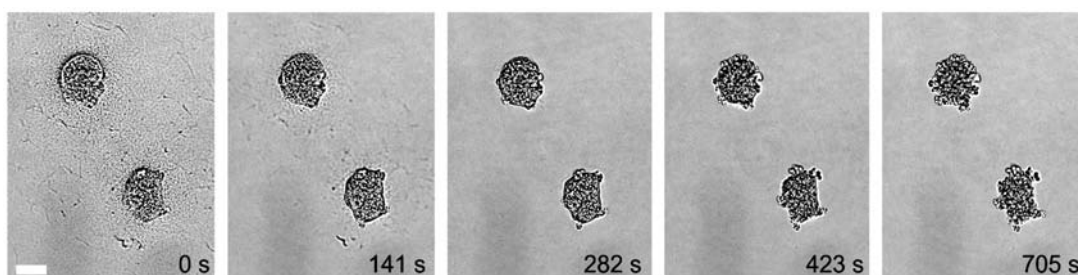


Figure 3.6: Degradation of fibrin-containing MAM and pseudocapsule by plasmin. Addition of plasmin (8 $\mu\text{g}/\text{ml}$) led to rapid degradation of both pseudocapsule and MAM surrounding *S. aureus* Newman colonies grown in 3D-CoG/Fib for 17 h. The timestamp in the single panels is relative to plasmin addition. This suggested that fibrin is a main component of these structures.

SERAM-encoding genes (Newman-29, Mainiero *et al.* (2010)) was analyzed for its growth behavior in 3D-CoG/Fib (Fig. 3.3 D, 3.4). Both pseudocapsule and MAM formation were completely abrogated; the growth phenotype resembled cluster formation of strain Newman in 3D-CoG without fibrinogen. Of note, cell wall-anchored fibrinogen binding proteins ClfA and ClfB are not affected in the *sae* mutant (Goerke *et al.*, 2001). Thus, SERAM family members activated by the *saeRS* two-component system appeared to be involved in the formation of these putatively fibrin-based structures.

Immunostaining of Emp and Coa revealed their localization on or within the pseudocapsule (Fig. 3.7). In order to elucidate the pseudocapsule and MAM formation process, a set of Newman mutants in *coa*, *vWbp*, *eap*, and *emp* was analyzed. Emp and Eap production were confirmed by SDS surface extracts (Fig. 3.8 A), Coa and vWbp were detected in culture supernatants and confirmed by MALDI-TOF (Fig. 3.8 B).

A *coa* mutant was still able to form pseudocapsules and MAM, although the pseudocapsules and the enclosed microcolonies were considerably more irregularly shaped than those of the parental Newman strain (Fig. 3.3 E, 3.4). Obviously, Coa was partially involved in the formation of the pseudocapsule.

The *vWbp emp* double mutant was able to form a pseudocapsule similar to that of the parent strain (Fig. 3.3 F, 3.4). However, the microcolonies were completely devoid of the MAM. Ectopic complementation studies with a set of plasmids (encoding *vWbp* or *emp* or both) showed that this phenotype was solely dependent on vWbp (Fig. 3.9). The increased MAM diameter compared to the parental strain could be explained by the increased secretion of vWbp due to the multicopy ectopic complementation (Fig. 3.8).

Interestingly, the *eap* mutant and an *ica* mutant were phenotypically indiscernible from the parent strain when grown in 3D-CoG/Fib (Fig. 3.4, 3.10).

It has been reported that strain Newman is dysregulated in SERAM-production because of an amino acid exchange in SaeS, the sensor kinase of the *saeRS* two-component system, compared to other *S. aureus* strains (Mainiero *et al.*, 2010). Therefore, the community-associated MRSA (CA-MRSA) strain USA300 was also assessed for its growth behavior (Diep *et al.*, 2006). Both the pseudocapsule and the MAM were present in USA300 (Fig. 3.10), although the pseudocapsule was less regularly shaped in comparison to strain Newman. Moreover, the MAM of USA300 was considerably less prominent in diameter than for strain Newman (Fig. 3.4). Thus, the formation of microcolonies sur-

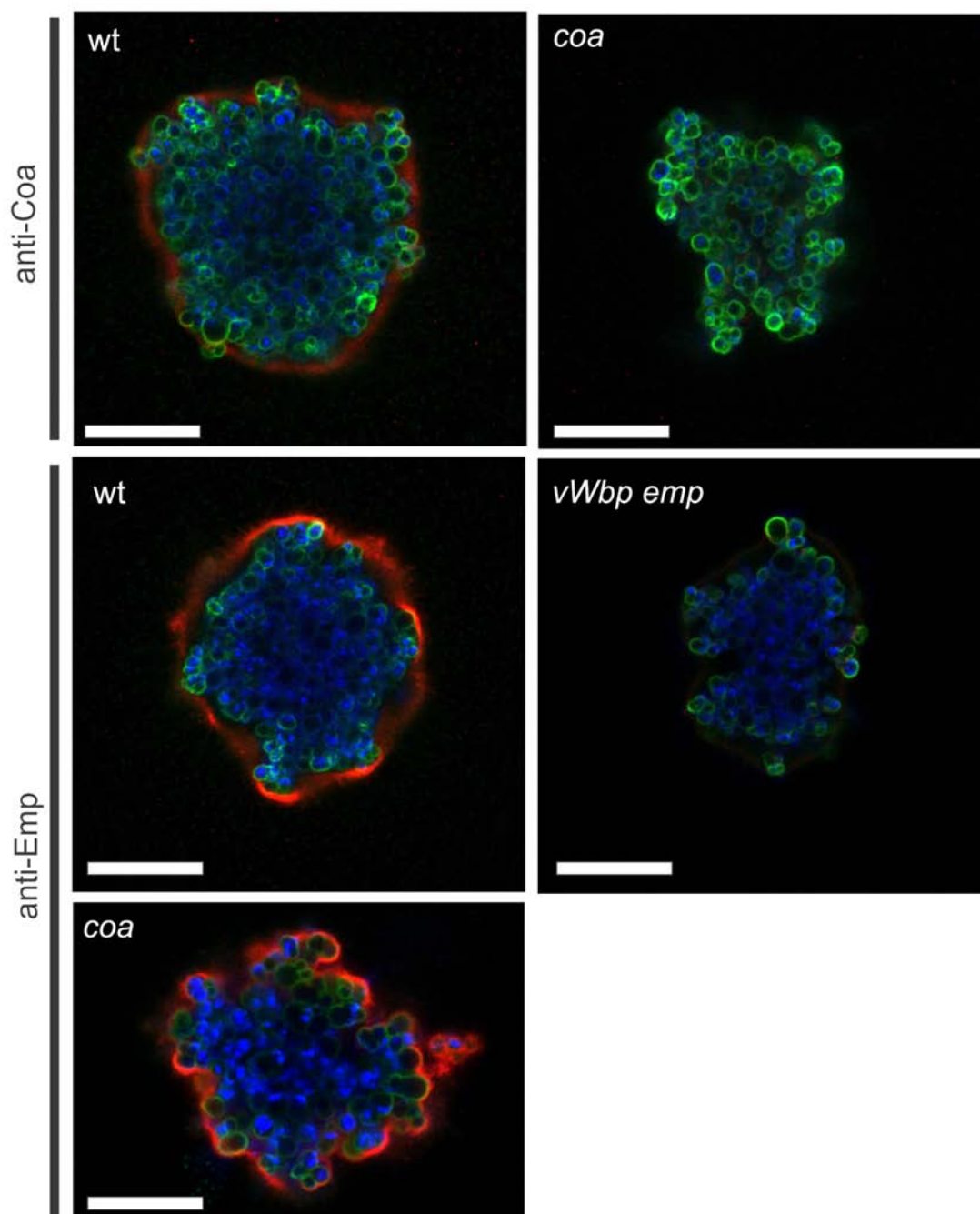


Figure 3.7: Localization of Coa and Emp to *S. aureus* pseudocapsules. Coa and Emp were detected in pseudocapsules by immunocytochemistry using rabbit antibodies specific for coagulase (anti-Coa) or Emp (anti-Emp). Staphylococci were grown in RPMI/Fib for 16 h and then fixed with 4% paraformaldehyde. Primary antibodies were detected by Alexa 555 anti-rabbit antibodies. Staphylococci were detected by staining DNA with DAPI (Blue) and N-acetyl-glucosamine with FITC-Lectin (*T. vulgaris*) (Green). Coa could be detected as localized to the pseudocapsule in Newman wildtype, Emp was similarly localized. Staining of Coa and Emp was specific as the *coa* and *vWbp emp* mutant were not stained with the respective antisera. The *coa* mutant formed an irregularly shaped pseudocapsule as seen from anti-Emp staining. Scale bar 15 μ m.

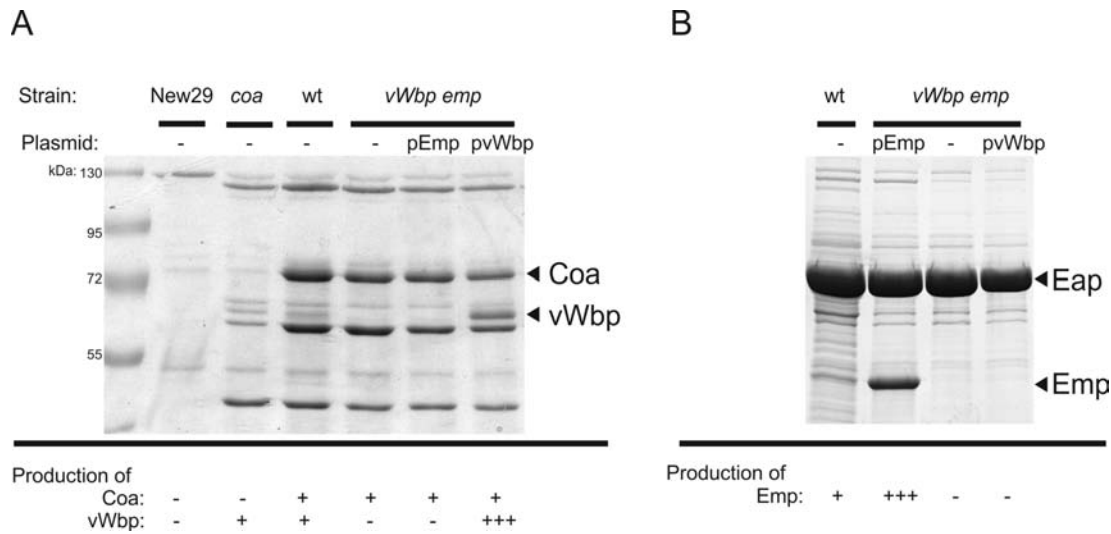


Figure 3.8: Detection of Coa, vWbp and Emp. **A:** Coa and vWbp were detected in supernatants of 3 h cultures and verified by MALDI-TOF. The *vWbp emp* double mutant secreted no vWbp, the *coa* mutant secreted no Coa, the *sae* mutant (New29) secreted neither detectable Coa nor vWbp. Ectopic expression of *vWbp* from *pvWbp* led to hypersecretion of vWbp. **B:** Emp and Eap were detected in SDS surface extracts. The *vWbp emp* double mutant is defective in Emp production. *pEmp* restores this defect and causes hypersecretion of Emp.

rounded by fibrin-containing pseudocapsules and MAM in 3D-CoG/Fib was not specific for strain Newman but it was also found with the CA-MRSA strain USA300.

Taken together, *S. aureus* Newman microcolonies grown in a 3D-CoG matrix in the presence of fibrinogen were surrounded by two distinguishable concentric structures: an inner pseudocapsule and an outer dense microcolony-associated meshwork which was termed MAM.

3.1.2.2 Dispersion of microcolonies as a result of fibrin degradation

It could be shown that at later time points (>20-40 h) single *S. aureus* Newman microcolonies transit from relative growth arrest to massive growth and dispersion (Fig. 3.11 A, B). This event was accompanied by degradation of both the pseudocapsule and the MAM, probably by releasing or activating a soluble fibrin-specific protease as the underlying collagen matrix was not degraded. Similar fibrin degradation was observed occasionally with USA300 microcolonies (Fig. 3.11 C, Movie 5). Degradation of fibrin structures of nearby colonies did not induce their growth immediately.

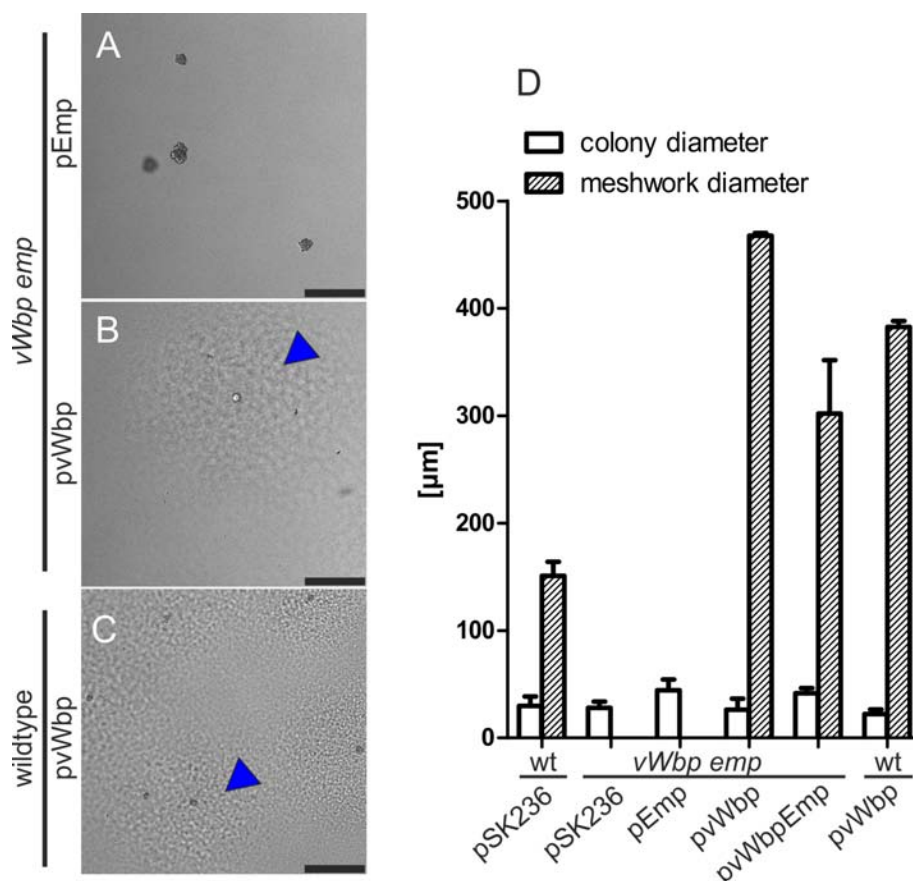


Figure 3.9: *vWbp* is responsible for formation of the MAM. The *vWbp emp* double mutant was complemented with plasmids encoding *emp* (pEmp) or *vWbp* (pvWbp) alone or both (pvWbpEmp) under their native promoters (A, B, C). This *in trans* approach led to overproduction of the respective proteins (compare Fig. 3.8). **A:** *vWbp emp* double mutant complemented with pEmp. Expression of Emp from the plasmid caused increased size and more irregular shape of microcolonies but did not complement the lacking MAM. **B:** *vWbp emp* double mutant complemented with pvWbp. Expression of *vWbp* from the plasmid restored the MAM phenotype (blue arrowhead) and led to an increased MAM diameter. **C:** Overproduction of *vWbp* in the wildtype also increased the MAM diameter. Scale bar 150 μm . The images (A-C) are representative of three independent experiments. **D:** Quantification of microcolony and MAM diameter. Data are averaged from two independent experiments.

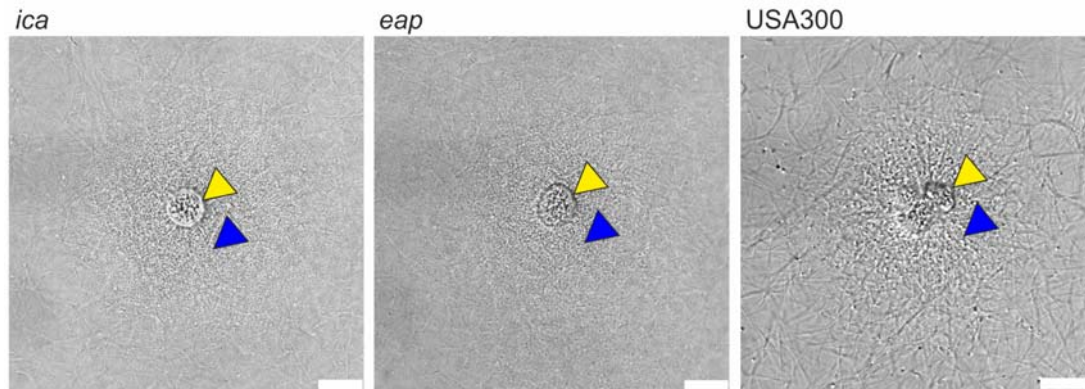


Figure 3.10: Pseudocapsule and MAM formation of different *S. aureus* strains in 3D-CoG/Fib. Growth phenotypes were analyzed 16 h after inoculation without agitation in 3D-CoG/Fib. Pseudocapsule (yellow arrowhead) and MAM (blue arrowhead) formation were independent of *ica* or *eap* in strain Newman and also present in the CA-MRSA strain USA300. Scale bar 25 μm .

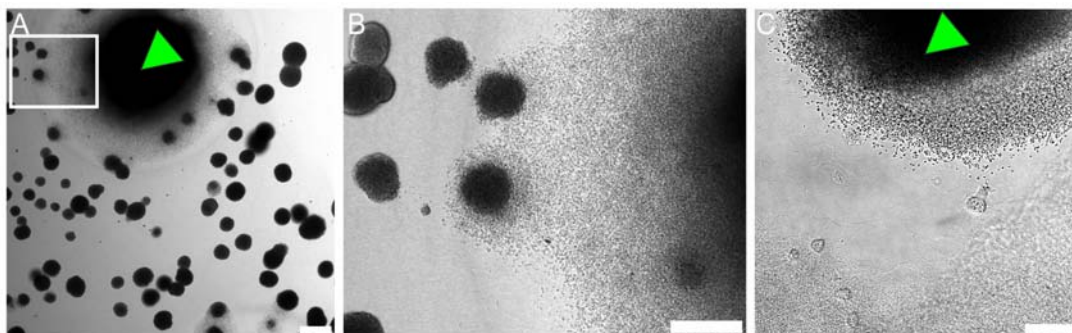


Figure 3.11: Degradation of fibrin-containing MAM and pseudocapsule. **A:** At later time points (here: 43 h after inoculation) single *S. aureus* Newman microcolonies (green arrowhead) started massive growth and dispersion by fibrinolytical degradation of both structures. **B:** Magnification of the inset in **A**. **C:** Similar mechanisms were observed in CA-MRSA USA300. Scale bar sizes: A 150 μm , B 75 μm , C 50 μm .

3.1.2.3 Bacterial microcolonies are protected from host immune cells by MAM

Bacterial pathogens shield themselves from humoral and cellular factors of the host defense system by formation of exopolysaccharide or proteinaceous capsules. Therefore, the *S. aureus* pseudocapsule and the MAM were assessed for affecting the interaction of neutrophils with staphylococcal microcolonies. For this purpose, the 3D-CoG/spleen slice infection model (3D-CoG/SSIM, 3.1.1, p. 45) was applied. In short, native spleen explants of *lys-EGFP* mice were cut into thin slices (300 μm) using a vibrating blade microtome and layered upon the surface of the 3D-CoG. Subsequently, neutrophils presumably originating from the red pulp migrated into the collagen matrix (see also Fig. 3.2 B and Fig. 3.1). Staphylococci were grown in 3D-CoG/Fib for 16-17 h before challenge with murine neutrophils.

In the absence of fibrinogen (3D-CoG), neutrophils migrated towards and invaded bacterial clusters of strain Newman, followed by immediate phagocytosis of staphylococci (Fig. 3.12 A). A high ratio of these neutrophils lost their fluorescence and their nuclei became stainable by Sytox Blue, a cytoplasmic membrane impermeable fluorescent dye, indicating necrotic neutrophils.

In contrast to that, neutrophils were not able to approach and contact strain Newman microcolonies grown in 3D-CoG/Fib (Fig. 3.12 C, D and Movie 6). In order to visualize the dynamics of neutrophil migration, all single time frames of this image sequence were projected onto one another, producing a time projection (Fig. 3.12 E). The microcolonies exhibited a halo (101 \pm 46 μm) free of neutrophils during the observation period of >3 h after neutrophil challenge. The Newman *sae* mutant, which neither formed pseudocapsule nor MAM in 3D-CoG/Fib, was immediately invaded by neutrophils (Fig. 3.12 B, Fig. 3.13 and Movie 7), similarly to strain Newman in the absence of fibrinogen (Fig. 3.12 A). The microcolonies of *eap* and *coa* mutant strains grown in 3D-CoG/Fib appeared to be protected from neutrophils similarly as strain Newman (Fig. 3.12 I). In contrast to this, microcolonies of Newman *vWbp emp* double mutant did not exhibit such a neutrophil-free halo, instead the neutrophils were able to reach the pseudocapsule surrounding the microcolonies (Fig. 3.12 F-I and Movie 8). Thus, the presence of the neutrophil-free halo correlated with the presence of the *vWbp*-dependent MAM surrounding bacterial microcolonies. Obviously, the MAM functioned as a mechanical barrier inhibiting neutrophil immigration into this zone. A possible artifact resulting from the combination of murine

neutrophils with human fibrinogen could be ruled out by reproducing the same migration restriction for human neutrophils isolated from peripheral blood (Fig. 3.14).

Taken together, *vWbp*-producing staphylococci grown in 3D-CoG/Fib produce a MAM surrounding the microcolonies which inhibits the migration of neutrophils, thus acting as a mechanical barrier.

3.1.2.4 The pseudocapsule acts as a second mechanical barrier against neutrophils

In order to assess whether the pseudocapsule also contributed to shielding from neutrophils, the Newman *vWbp emp* mutant strain which was unable of MAM formation but still produced a pseudocapsule (Fig. 3.12 F-I) was used. As shown in (Fig. 3.15 A), immigrating neutrophils were not able to directly contact staphylococci of the microcolony. Instead, they were kept on short distance, as can be seen from a narrow gap between neutrophils and staphylococcal fluorescence signal in single z sections (Movie 9). The dimension of this gap roughly equaled the dimension of the pseudocapsule (compare Fig. 3.4 and 3.12 I). This suggests that the pseudocapsule acts as a second mechanical barrier sequestering the bacterial microcolonies from phagocytic cell attack. However, after about 4 h microcolony-associated neutrophils started penetrating the pseudocapsule and phagocytosing staphylococci. Typically, invasion of the pseudocapsule started with a localized invasive event, that is, only a single or few neutrophils squeezed through a narrow hole in the pseudocapsule.

Once in direct contact with staphylococci, they immediately started phagocytosis (Fig. 3.15 B and Movie 9). This initial breakthrough of neutrophils resulted in recruitment of a wave of neutrophils and disruption of the entire colony. With some microcolonies it was observed that initially a larger fragment of the pseudocapsule ruptured, allowing access of a number of neutrophils to the staphylococci. This led to a rapid dispersion of staphylococci from the ruptured pseudocapsule, while massive phagocytosis was observed (Fig. 3.15 C and Movie 10). Interestingly, phagocytosis of staphylococci after pseudocapsule rupture was frequently associated with neutrophil cell lysis/necrosis (Fig. 3.15 E-H and Movie 11). This was in agreement with neutrophil/microcolony-interaction of strain Newman grown in 3D-CoG (Fig. 3.12 A). In the very rare case that strain Newman wild-type or *coa* mutant microcolonies were encountered by neutrophils which had penetrated disrupted MAM, similar events were observed. Such mechanical injury can be occasionally observed when overlaying the 3D-CoG with a spleen slice. In the case of the *coa* mutant

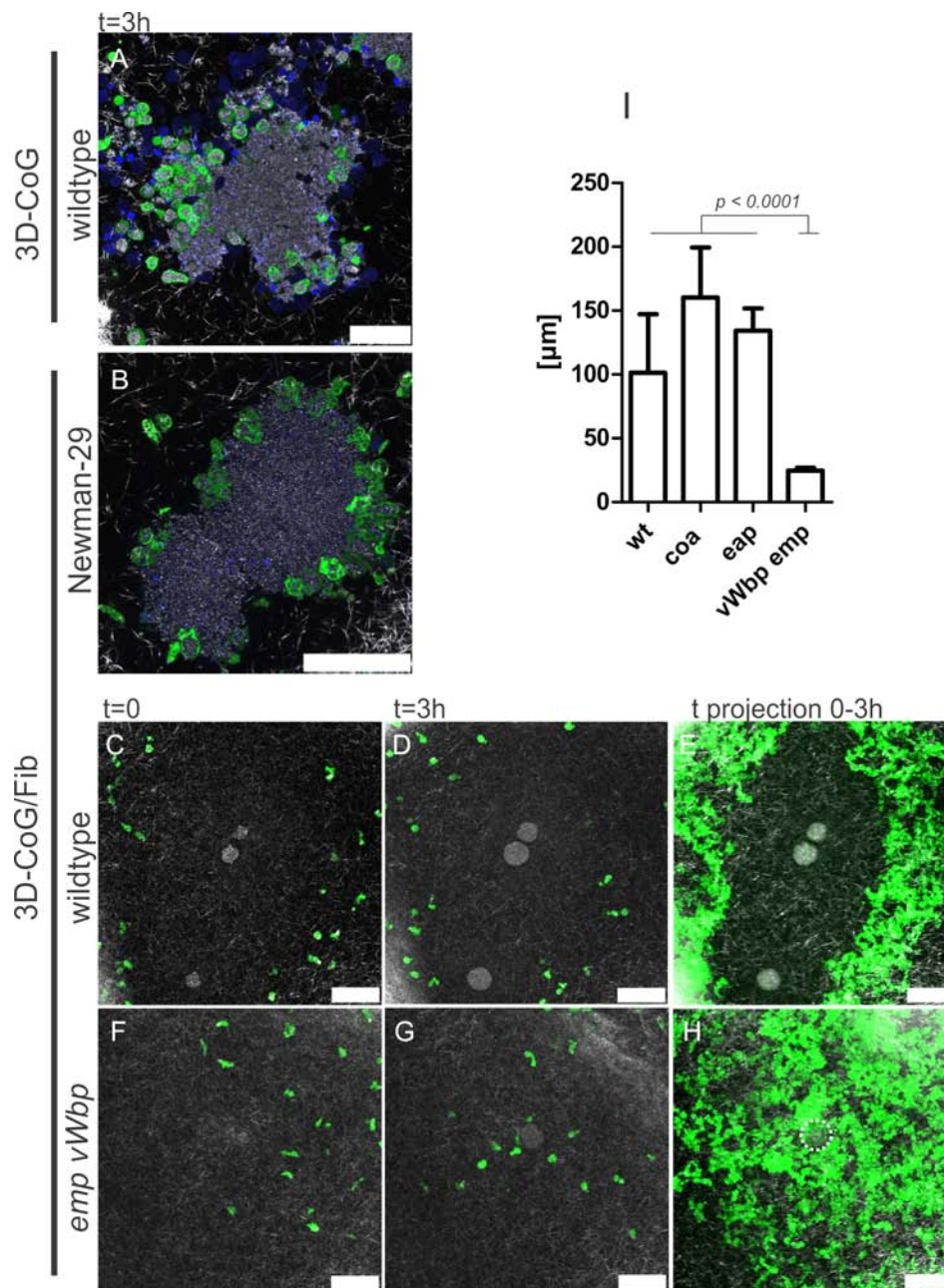


Figure 3.12: *S. aureus* Newman microcolonies are protected from neutrophils by MAM. **A:** Neutrophils approached Newman wildtype microcolonies grown in 3D-CoG and immediately started phagocytosis (picture 3 h after challenge with neutrophils). **B:** The *sae* mutant (Newman-29) grown in 3D-CoG/Fib was attacked in the same way (picture 3 h after challenge with neutrophils). **C-E:** Wildtype microcolonies grown in 3D-CoG/Fib were not approached by neutrophils within 3 h. This can be depicted more clearly by time projection (0-3 h) of single frames from Movie 6 (**E**). **F-H:** In contrast to this, the *vWbp emp* double mutant was readily approached by neutrophils which were only held back by the pseudocapsule (Movie 8). **I:** This neutrophil-free halo surrounding the microcolonies was measured and revealed a correlation with the MAM. Green: GFP-neutrophils; Blue: Sytox Blue-stained DNA; White: confocal reflection microscopy showing collagen fibers. Scale bar 50 μm. The microcolony in H is illustrated by a dotted line. The images are representative of at least three independent experiments. Data in I are averaged from three independent experiments.

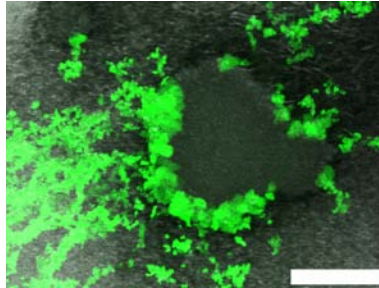


Figure 3.13: Time projection of interaction of neutrophils with Newman *sae* mutant in 3D-CoG/Fib. *S. aureus sae* mutant clusters grown in 3D-CoG/Fib for 17 h were invaded and phagocytosed by neutrophils without delay. This figure shows a time projection of the whole observation period (87 min) of Movie 7 (projection of two sections spanning a total depth of 5.3 μm). Green: GFP-neutrophils; White: confocal reflection microscopy showing collagen fibers. Scale bar 75 μm .

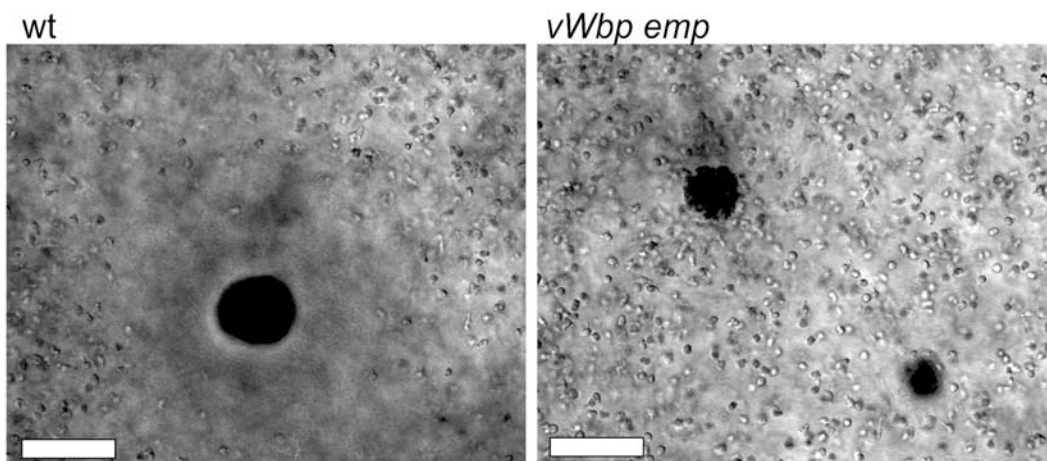


Figure 3.14: The MAM also functions as a barrier against human neutrophils. Newman wildtype and *vWbp emp* mutant were grown in 3D-CoG/Fib for 22 h. Then, human neutrophils isolated from peripheral blood were pipetted on top of the 3D-CoG/Fib ($\sim 3 \times 10^6$ per well) and incubated at 37 $^\circ\text{C}/5\% \text{CO}_2$. After 2 h, neutrophils had migrated towards microcolonies of the *vWbp emp* mutant but not of the wildtype.

strain, the more irregularly shaped pseudocapsule retained residual barrier function (Movie 12).

As shown above, formation of both a pseudocapsule and a MAM is not exclusive for strain Newman but is also present in strain USA300, albeit to a lesser extent (Fig. 3.4, 3.10). After challenging microcolonies pre-grown in 3D-CoG/Fib, neutrophils reached the USA300 pseudocapsule interface more easily compared to strain Newman (Fig. 3.15 D and Movie 13). Moreover, the barrier function of the USA300 pseudocapsule for neutrophils was less effective, as neutrophil invasion of the microcolony was more prevalent. Thus, strain USA300 was able to exploit a similar strategy as strain Newman in 3D-CoG/Fib to protect itself from neutrophils, though its impact was less pronounced.

Taken together, the pseudocapsule acts as a second mechanical barrier protecting staphylococcal microcolonies from neutrophil attack.

3.1.2.5 A therapeutic anticoagulant abrogates barrier activity

Several synthetic thrombin inhibitors in clinical use have been shown to inhibit *S. aureus* coagulase activity (dabigatran (Vanassche *et al.*, 2010); argatroban (Hijikata-Okunomiya and Kataoka, 2003)), but inhibition of vWbp-mediated clotting has not been addressed yet. Therefore, it was investigated whether argatroban could interfere with Coa-mediated pseudocapsule and vWbp-dependent MAM formation.

By supplementing the growth medium (3D-CoG/Fib) with 10 nM argatroban, MAM formation was affected (Fig. 3.16 A). Marked impairment of pseudocapsule formation required about 50 nM argatroban. These results demonstrate that argatroban is able to prevent the formation of the outer and the inner barrier generated by staphylococci grown in 3D-CoG/Fib. In consequence, microcolonies became prone to neutrophil attack: at 10 nM argatroban, 75% of the microcolonies were protected from neutrophil attack by the MAM, at 50 nM only 16% retained this barrier function, at 100 nM all microcolonies were accessible to neutrophils (Fig. 3.16 B). Pseudocapsule function was diminished in the same argatroban concentration-dependent manner (Fig. 3.16 B).

Thus, argatroban inhibits both pseudocapsule and MAM formation, probably by inhibiting the proteolytic activity of Coa- and vWbp-activated prothrombin. This inhibitory effect supports the disruption of microcolonies by neutrophils.

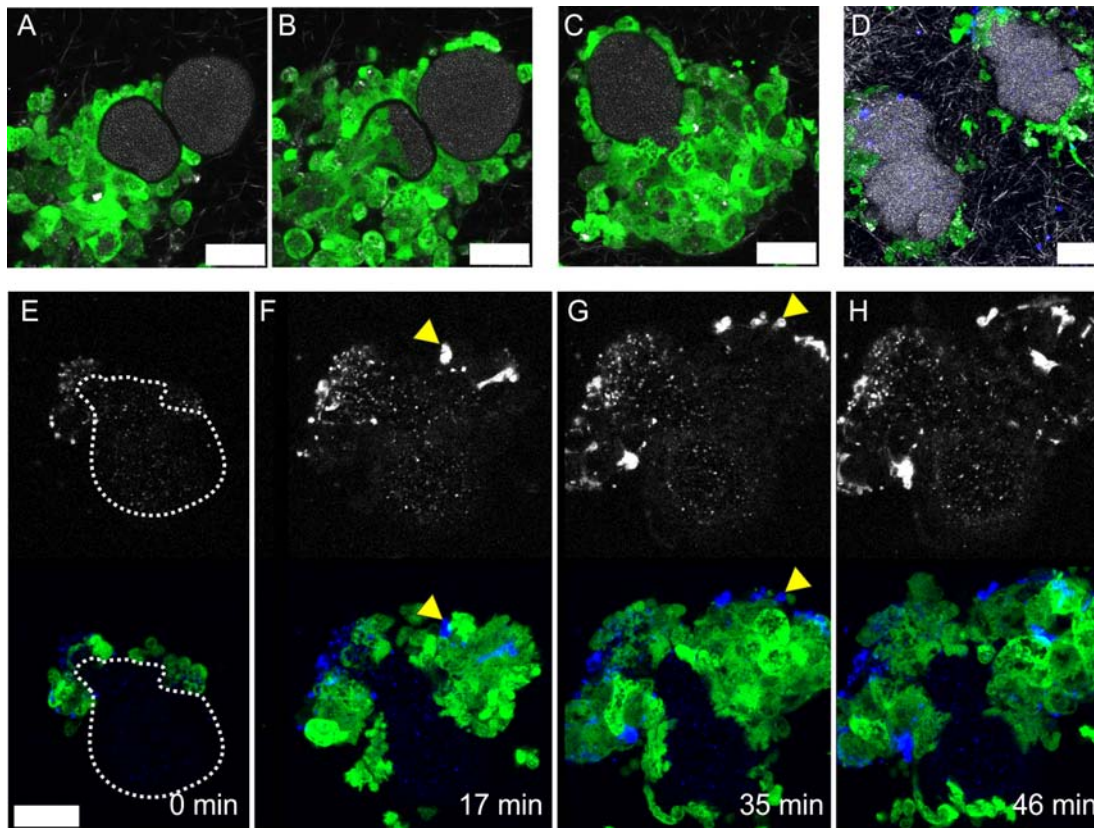


Figure 3.15: The pseudocapsule acts as an additional protective barrier. **A:** The pseudocapsule of *vWbp emp* double mutant microcolonies are protective against direct invasion of neutrophils into the microcolony (single frame from Movie 9, 5 h after neutrophil challenge). **B:** After punctual rupture of the pseudocapsule, phagocytosis is initiated (single frame from Movie 9, 45 min after **A**). **C:** After pseudocapsule rupture, phagocytosis is a rapid event (single frame from Movie 10, 5 h after neutrophil challenge). **D:** USA300 barriers fulfill similar functions (single frame from Movie 13, 3.5-5 h after neutrophil challenge). **E-H:** Direct contact of staphylococci with neutrophils leads to massive neutrophil cell lysis/necrosis, visualized by Sytox Blue staining (yellow arrowheads, single frames from Movie 11, 5 h after neutrophil challenge). The top panes in E-H represent the isolated Sytox Blue channel. In **E**, the microcolony outline is illustrated by a dotted line. Green: GFP-neutrophils; Blue: Sytox Blue-stained DNA; White: confocal reflection microscopy showing collagen fibers. Scale bar 20 μm .

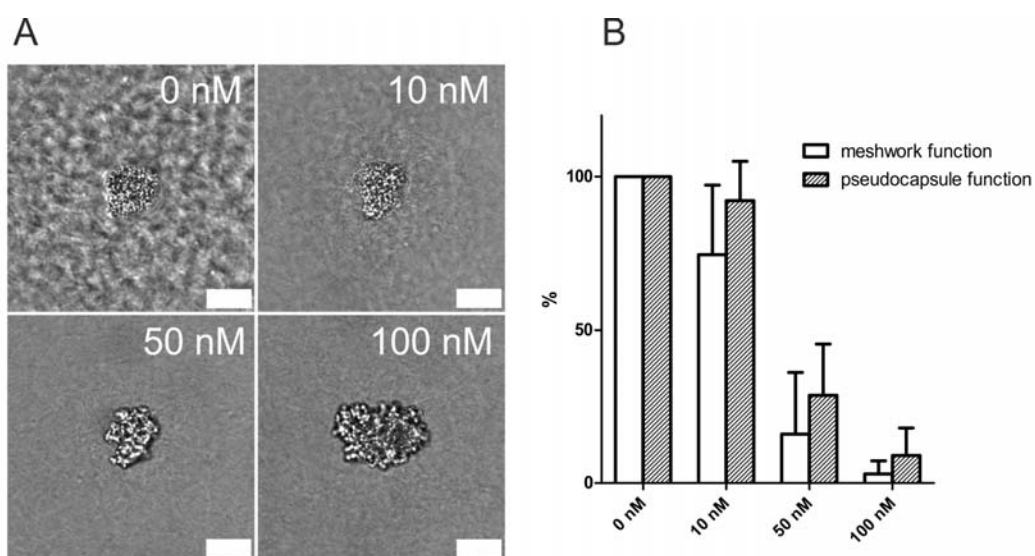


Figure 3.16: The thrombin inhibitor argatroban antagonizes staphylococcal barrier activity. *S. aureus* **A:** Newman was grown in 3D-CoG/Fib in the presence of different argatroban concentrations. After 16 h of growth, the growth phenotypes were analyzed: at 10 nM argatroban, the MAM was diminished and at higher concentrations also pseudocapsule formation was absent. **B:** Challenging the system with neutrophils revealed loss of both barrier functions in a concentration-dependent manner. Scale bar 25 μ m. The images are representative of three independent experiments. Data are averaged from three independent experiments.

3.1.3 Inhibition of immune cell migration by *Yersinia*

3.1.3.1 Characteristics of *Yersinia* microcolony formation in 3D-CoG

3.1.3.1.1 Growth of *Y. enterocolitica* in the 3D-CoG system It has been shown by Freund *et al.* (2008) that *Y. enterocolitica* WA(pYV) forms densely packed (DP) microcolonies in 3D-CoG, whereas a strain devoid of the virulence plasmid (WA-C) exhibits planktonic growth. A deletion of the *yadA* gene obviously diminishes interbacterial adhesion insofar as that the microcolonies are more loosely packed (LP) compared to the wildtype. A deletion of the invasin gene (*inv*) does not change the DP phenotype.

In order to further characterize the different microcolony morphologies, time-lapse microscopy was performed and microcolonies were compared after 4 h 20 min (Fig. 3.17 A). Single WA(pYV) cells appeared to not separate after cell division but formed chains which eventually coiled up to a DP microcolony. The pYV-cured strain WA-C sank to the bottom of the wells and short chains resulting from cell division separated quickly, giving rise to a planktonic population. The *yadA* mutant WA(pYV Δ *yadA*) was seldomly located in the depth of the 3D-CoG but rather sank to the bottom (Fig. 3.17 B). Curling up of bacterial chains was not as prominent as in the wildtype, resulting in more elongated chains which eventually formed LP microcolonies. Moreover, an *inv yadA* double mutant was constructed and assessed for its growth behavior. Surprisingly, WA Δ *inv* (pYV Δ *yadA*) showed preferentially planktonic growth behavior, similar to the pYV-cured strain (WA-C).

3.1.3.1.2 Interaction of microcolonies with neutrophils In the next step, the 3D-CoG/SSIM (section 3.1.1, p. 45) was used to analyze the impact of microcolony formation on the interaction with neutrophils. WA(pYV) or the T3SS-deficient mutant WA(pYV Δ *lcrD*) were grown for 17 h in 3D-CoG and subsequently challenged with neutrophils by overlaying the 3D-CoG with spleen slices. Neutrophils migrated towards microcolonies of WA(pYV) and WA(pYV Δ *lcrD*), respectively. WA(pYV) microcolonies were resistant against phagocytosis and invasion by neutrophils, in contrast to WA(pYV Δ *lcrD*) microcolonies (Fig. 3.18). As WA(pYV Δ *lcrD*) is T3SS-deficient, it can be concluded that effectors injected by the T3SS into contacted neutrophils were responsible for this resistance of WA(pYV). WA(pYV Δ *yadA*) microcolonies were also protected from neutrophil phagocytosis and invasion despite their LP morphology (Fig. 3.18) although few neutrophils appeared to migrate into the outer layer of the microcolony.

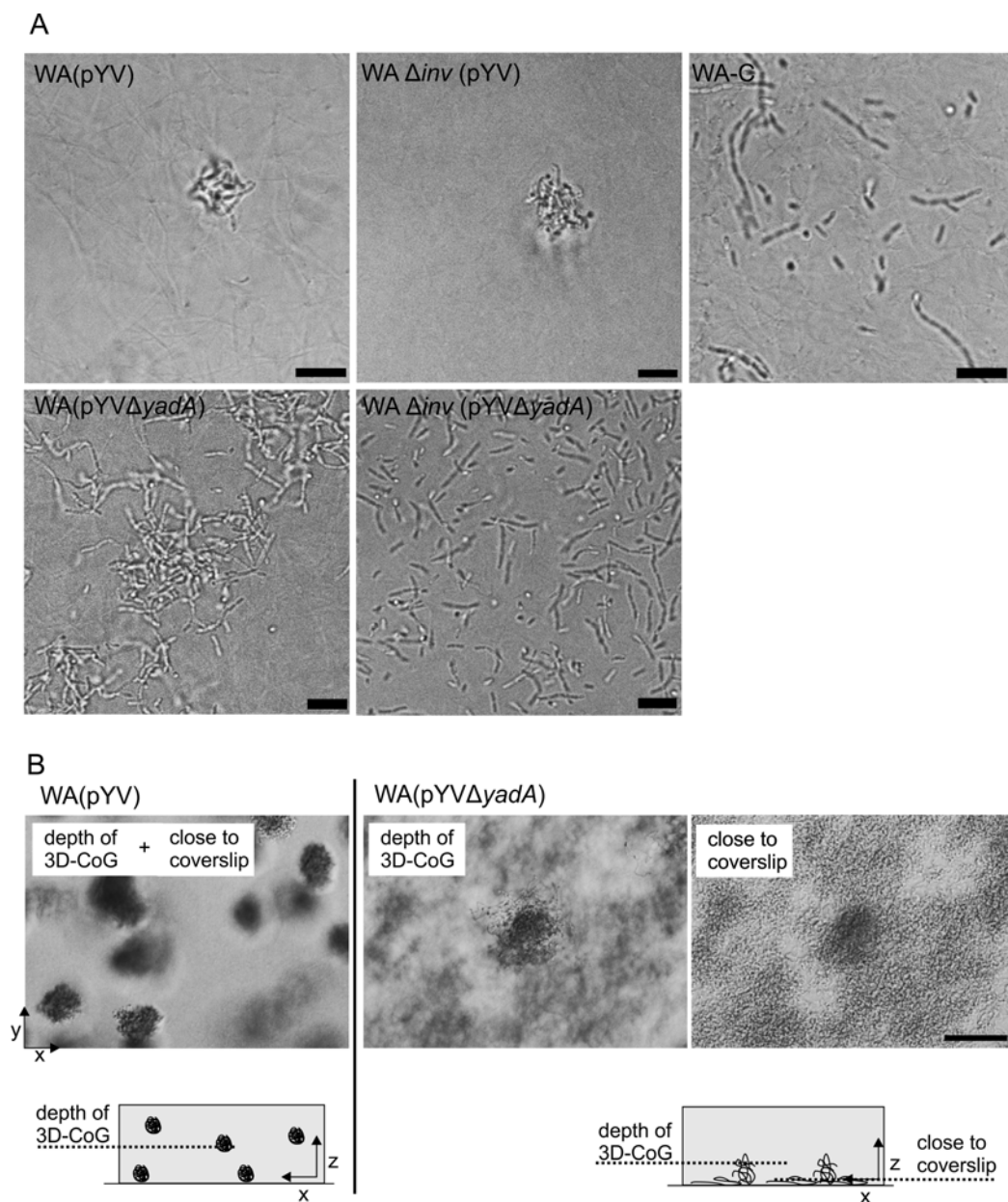


Figure 3.17: Invasin is involved in *Y. enterocolitica* microcolony formation in 3D-CoG. **A:** As shown in Freund *et al.* (2008), WA(pYV) and WA Δ inv(pYV) formed densely packed (DP) microcolonies in 3D-CoG, WA(pYV Δ yadA) formed loosely packed (LP) microcolonies and WA-C consisted of a planktonic population. Deletion of the *inv* and *yadA* gene caused planktonic growth in WA Δ inv(pYV Δ yadA), similar to WA-C. Images 4 h 20 min after inoculation. **B:** The majority of WA(pYV Δ yadA) microcolonies was localized at the bottom of the 3D-CoG, whereas WA Δ inv(pYV) microcolonies were dispersed over the 3D-CoG. Images 14 h after inoculation. Scale bar **A** 5 μ m, **B** 25 μ m.

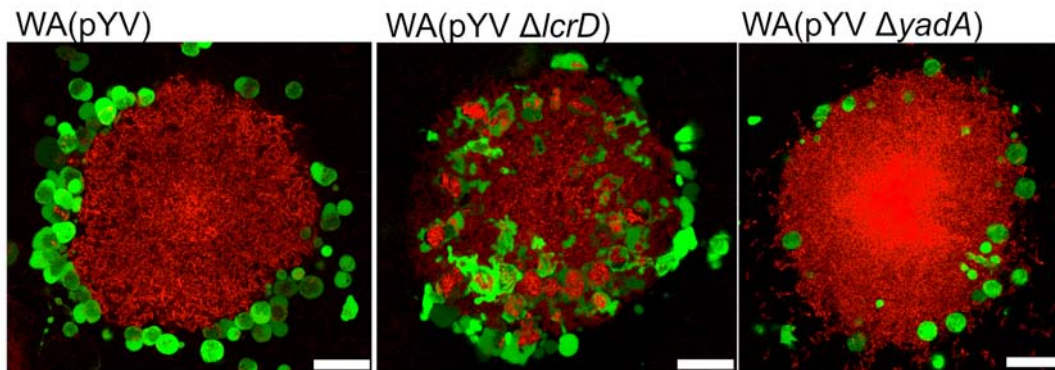


Figure 3.18: Interaction of neutrophils with *Y. enterocolitica* microcolonies in 3D-CoG/SSIM. After microcolony formation (17 h), 3D-CoGs were overlaid with spleen slices from a *lys-EGFP* mouse (3D-CoG/SSIM). Neutrophils (green) migrated into the collagen matrix towards *Yersinia* microcolonies (red). In the case of WA(pYV), neutrophils were not able to invade the microcolony. In contrast, neutrophils invaded WA(pYV Δ *lcrD*) microcolonies by squeezing between bacteria and subsequently phagocytosed bacteria. WA(pYV Δ *yadA*) microcolonies were protected similarly to WA(pYV) microcolonies, though the separation of yersiniae and neutrophils was not as strict, due to the LP microcolony morphology. Single optical sections of the microcolonies are shown, demonstrating the invasion of WA(pYV Δ *lcrD*) microcolonies. Images taken 6 h after spleen slice mounting. Green: GFP-expressing neutrophils. Red: DsRed-expressing yersiniae. Scale bar 20 μ m.

3.1.3.2 Inhibition of cell migration by *Y. enterocolitica*

The 3D-CoG/SSIM enables the study of neutrophil/*Yersinia* microcolony-interactions for several hours. In such experiments it was observed that after contact with yersiniae neutrophils became massively elongated and sometimes rugged by developing an additional independent leading edge in 3D-CoG (Fig. 3.19 and Movie 57).

This morphotype occurred only after interaction with *Yersinia* strains which are able to translocate Yops, indicating the involvement of one or several Yops acting on neutrophil migration. The occurrence of this morphotype was independent of microcolony formation and was also observed when neutrophils encountered single yersiniae in 3D-CoG. This rules out a crucial role of microcolony formation and allows the application of other *in vitro* systems to study this elongated morphotype. Furthermore, WA(pYV Δ *yadA*) led to a practically identical morphotype (compare also Fig. 3.20 B).

In order to identify the responsible Yops, a migration assay for analysis of long term migration defects was set up. Bone marrow-derived dendritic cells (DCs) were used as a model cell type due to their stable migration towards CCL19 gradients. Together with CCL21, this chemokine is involved in guidance of DC migration by binding to the CC-chemokine receptor 7 (CCR7) which is upregulated in activated DCs (Förster *et al.*, 1999). Both neu-

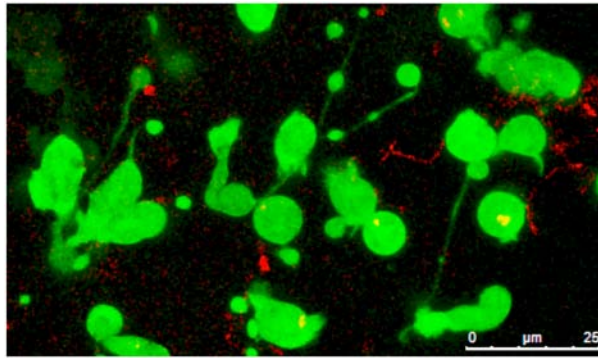


Figure 3.19: Elongated morphotype in neutrophils after contact with *Y. enterocolitica* in 3D-CoG. WA(pYV Δ yadA) grown in 3D-CoG was challenged with neutrophils from a *lys-EGFP* mouse. After 2 h most neutrophils in contact with bacteria were elongated with their trailing edge often stuck to substrate or bacteria. Green: GFP-expressing neutrophils. Red: DsRed-expressing yersiniae.

trophils and DCs rely on the principles of amoeboid migration in 3D-CoG (Lämmermann *et al.*, 2008).

DCs were infected *in vitro* with *Yersinia* strains (MOI 20) for 30 min in cell culture dishes, subsequently washed and incorporated in 3D-CoG in custom-built tracking dishes. After polymerization of the 3D-CoG, a CCL19 gradient was established and migratory behavior of DCs was recorded using time-lapse microscopy for 3 h. Approximately 70 % of DCs migrated continuously towards the gradient as assessed by translocation of their nucleus for at least 100 μ m during the assay time (Movie 14). If cells were pre-infected with WA(pYV), this ratio dropped to 20 %, as most of the cells became highly elongated, developed several leading edges and were not able to translocate their cell body (Fig. 3.20 A, Fig. 3.21 and Movie 15). In contrast to this, DCs pre-infected with WA(pYV Δ lcrD) were not affected in their migratory behavior as 70 % of cells were migratory (compare Movie 16). From this it was concluded that translocation of Yops via the T3SS affects migratory behavior of DCs. In order to identify Yops involved in this migration inhibition, DCs were infected with mutant strains lacking single *yop* genes (WA(pYV Δ yopX)). The percentage of migratory cells was calculated by assessing at least 100 cells for their migratory behavior. Samples pre-infected with WA(pYV Δ lcrD) were set to 100 %. The severe inhibition of migration was only neutralized in the Δ yopT mutant (Fig. 3.21 A, Movie 17). Mutants with deletions in *yopH*, *yopO*, *yopP* or *yopE* were not affected in a similar manner in mediating this severe inhibition of migration.

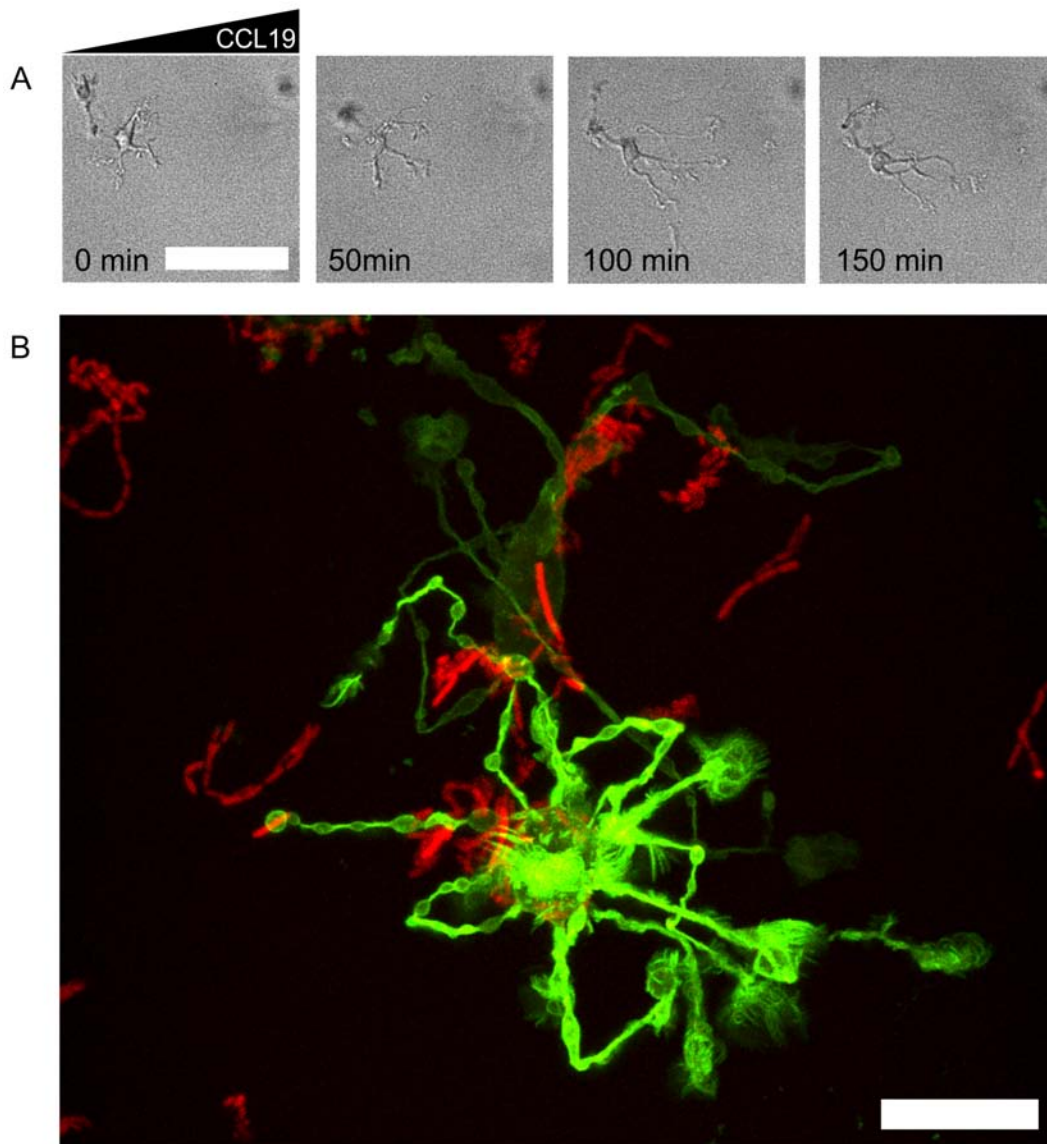


Figure 3.20: Characteristic elongated morphotype of DCs after contact with $YopT_{yen}$ -producing strains in 3D-CoG. **A:** Typical elongated morphotype of WA(pYV)-infected DCs in 3D-CoG. Indicated time after casting of 3D-CoG. CCL19 gradient decreases from right to left. Bright field channel. Scale bar 75 μm . **B:** Lifeact-GFP DCs were mixed with WA(pYV $\Delta yadA$, pRFP) and incorporated into 3D-CoG. After several hours DCs exhibit the $YopT_{yen}$ -specific elongated morphotype but there is no clear cell polarity due to the lack of a CCL19 gradient. Green: Lifeact-GFP DCs. Red: WA(pYV $\Delta yadA$, pRFP). z projection of 13 z sections spanning a total depth of 38 μm . Scale bar 10 μm .

In order to confirm the prominent role of YopT in rapid inhibition of migration, DCs were pre-infected with the ‘toolbox strain’ WA(pTTSS, pYopX), expressing a functional T3SS and only single Yops (Trülzsch *et al.*, 2003; Wölke *et al.*, 2011). Solely the YopT secreting strain WA(pTTSS, pYopT_{gen}) inhibited cell migration comparably to WA(pYV) (Fig. 3.21 B, Movie 18). In conclusion, YopT appears to be the dominant Yop in mediating long term inhibition of DC migration in *Y. enterocolitica*.

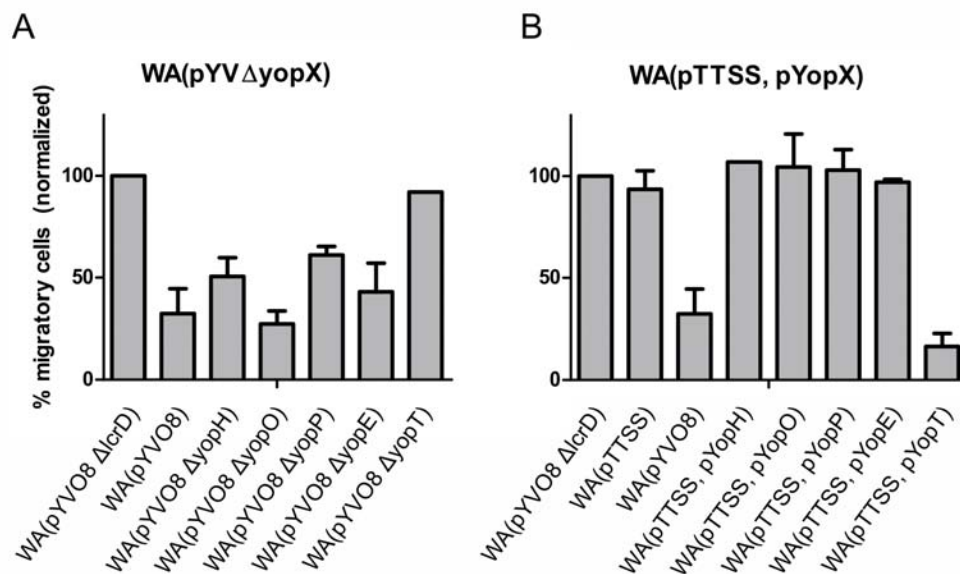


Figure 3.21: Inhibition of dendritic cell migration by *Y. enterocolitica*. DCs were infected with *Yersinia* strains *in vitro* for 30 min (MOI 20). Cells were then washed to remove bacteria and mixed with neutralized collagen solution. After polymerization of the 3D-CoG, cell migration was recorded using time lapse microscopy for 3 h. Cells were considered as migratory when they translocated their nucleus for at least 100 μm during the assay time. **A:** DCs were infected with mutant strains lacking single Yops, WA(pYVΔyopX). **B:** Cell were infected with strains expressing a functional T3SS but only single Yops, WA(pTTSS, pYopX). The ratio of migratory cells was normalized to DCs infected with the T3SS-deficient strain WA(pYVΔlcrD). YopT appeared to be the prominent Yop mediating long term inhibition of migration under these conditions. Data represent two independent experiments.

3.1.3.3 Cell biological characteristics of *Y. enterocolitica*-infected cells

3.1.3.3.1 Analysis of the YopT-mediated elongated morphotype on the cellular level In order to elucidate the molecular events which cause this *Y. enterocolitica* YopT-mediated migration inhibition in DCs, GFP-expressing DCs were employed:

Transgenic Lifeact mice produce the 17-amino-acid Lifeact peptide fused to EGFP driven by the chicken actin promoter (Riedl *et al.*, 2010). The Lifeact-GFP binds to filamentous actin (F-actin) in living cells, thus rendering the F-actin network visible in

fluorescence microscopy. DCs from Lifeact mice were incorporated together with yersiniae into 3D-CoG without a CCL19 gradient. After several hours, DCs exhibited the YopT-specific morphotype described above but due to the lack of a chemotactic gradient, the multiple leading edges protruded uncoordinatedly and randomly. A z projection of an infected cell is shown in (Fig. 3.20 B). Several highly active protrusions of the DC in the foreground can be seen.

In a next step, under-agarose cell migration assays (Heit and Kubes, 2003) were conducted to answer the question if myosin II localization is perturbed after contact with yersiniae. Myosin II is a component of the actomyosin complex generating force for cell locomotion (Vicente-Manzanares *et al.*, 2009). It is activated via RhoA, preferentially in the trailing edge of the cell where it is involved in contractility of the actin cytoskeleton (Lämmermann *et al.*, 2008). To elucidate myosin II localization in response to contact with yersiniae, C57BL/6-derived DCs were transfected with a MLC-GFP construct (Croft *et al.*, 2005) which tags myosin II, and coincubated with yersiniae in under-agarose assays. During the early contact phase neither contact with WA(pYV) (Fig. 3.22 A1 and Movie 19) nor contact with WA(pYV Δ lcrD) (Fig. 3.22 A2 and Movie 20) affected MLC-GFP localization in transfected cells. Besides, both strains were sometimes dragged by DCs but there was no uptake of yersiniae. This supports that LPS-stimulated DCs do not take up yersiniae under these conditions, and thus regulatory interference of phagocytic events with migratory behavior could be ruled out. However, about 5-10 min after the first contact with WA(pYV), DCs became elongated and subsequently exhibited a peculiar morphology reminiscent of the elongated morphotype observed in 3D-CoG: DCs were massively elongated, formed several highly active protrusions at the same time but locomotion of the cell body was impeded. Fig. 3.22 B shows a single DC which is $>500 \mu\text{m}$ long. Interestingly, cell protrusions were highly active even 3 h after first cell elongation events occurred (Movie 21). A similar morphotype was observed after infection with WA(pTTSS, pYopT_{yen}) (compare Movie 43).

In order to prove T3SS-mediated translocation of Yops under these conditions a β -lactamase (bla) reporter system was employed (Cvetanovic, 2011). DCs from C57BL/6 mice were loaded with Förster resonance energy transfer (FRET) substrate CCF4-AM and subsequently coincubated with WA(pYV, pYopH-bla) or WA(pYV Δ lcrD, pYopH-bla) in under-agarose assays. Within minutes after contact with WA(pYV, pYopH-bla), cell elongation could be observed, followed by a change in fluorescence wavelength, proving

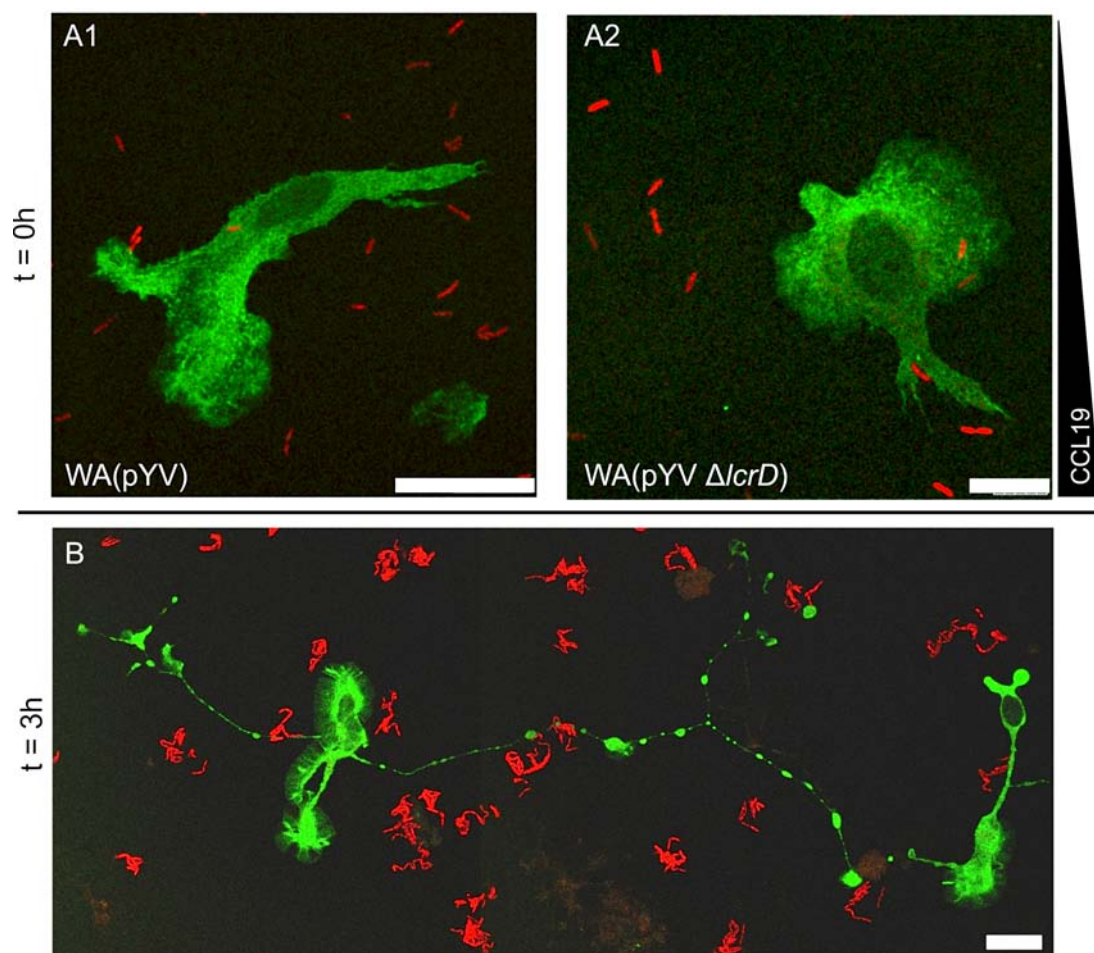


Figure 3.22: Migratory behavior of DCs transfected with MLC-GFP constructs after contact with yersiniae in under-agarose assays. **A:** First contact of DCs with yersiniae. DCs and bacteria were inoculated under agarose using pipet tips. DCs were inoculated at a distance of 4-5 mm from the attractor well. Bacteria were inoculated between responder and attractor well. **A1:** WA(pYV, pRFP). Single frame from Movie 19. **A2:** WA(pYVΔlcrD, pRFP). Single frame from Movie 20. **B:** DCs 3 h after first occurrence of elongated cells due to contact with WA(pYVΔyadA, pRFP). Green: MLC-GFP. Red: yersiniae with pRFP. Scale bar 25 μm.

translocation of the reporter construct YopH-bla into the DC cytosol (Fig. 3.23 and Movie 22). Coincubation with WA(pYV Δ lcrD, pYopH-bla) neither caused cell elongation nor a change in fluorescence wavelength (Fig. 3.23 and Movie 23). The gradual decline of fluorescence is due to diffusion of CCF4 out of the cells. However, this proves that translocation via the T3SS is present prior to development of the YopT-mediated elongated morphotype in DCs.

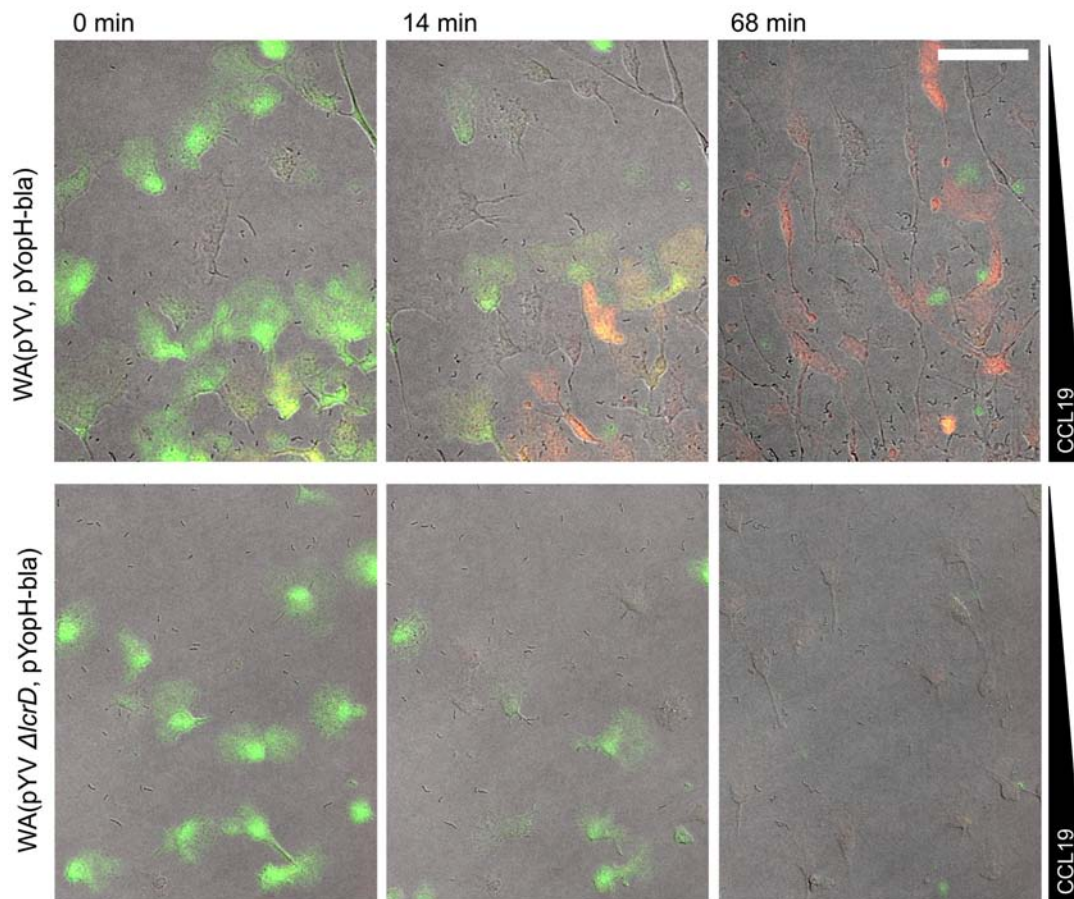


Figure 3.23: Targeting by T3SS destines DCs for the YopT_{yen}-dependent morphotype. CCF4-loaded DCs were infected in under-agarose assays with WA(pYV, pYopH-bla) or WA(pYV Δ lcrD, pYopH-bla) carrying a plasmid encoding for a fusion of YopH and β -lactamase. Successful translocation of this construct cleaves the FRET substrate CCF4 inside the DCs. Cell elongation could be observed within minutes with WA(pYV, pYopH-bla), followed by a change in fluorescence wavelength. WA(pYV Δ lcrD, pYopH-bla) caused neither cell elongation nor change in fluorescence wavelength. For better visibility, the fluorescence of uncleaved and cleaved CCF4 is depicted in green and red, respectively. Green: fluorescence of CCF4 prior to cleavage by β -lactamase. Red: fluorescence of CCF4 after cleavage by β -lactamase. Overlay with bright field channel. Scale bar 75 μ m.

3.1.3.3.2 RhoA is the YopT target mediating this elongated morphotype The predominant target of *Y. enterocolitica* YopT is probably RhoA (Zumbihl *et al.*, 1999). Upon translocation into the cytosol, YopT removes the isoprenylated C-terminal cysteine of membrane-anchored RhoA, thus delocalizing it from the membrane or even disrupting its catalytic activity. Further experiments were conducted in order to confirm that RhoA inactivation leads to the observed elongated morphotype. When DCs were inoculated together with WA(pYV) in the responder well in under-agarose assays, the cell front was able to squeeze underneath the agarose, whereas the trailing edge of the cell, obviously containing the nucleus, could not be dragged into the gap between coverslip and agarose (Fig. 3.24 A). As a consequence, trailing edges of infected cells were lined up along the edge of the well.

All previous migration experiments in 3D-CoG were carried out at a concentration of 1.7 mg/ml collagen. The experiment was repeated in 3D-CoG of reduced meshwork density (0.86 mg/ml collagen) for strains WA(pYV) and WA(pYV Δ lcrD). As shown in Fig. 3.24 B, the increased pore size due to the lower collagen concentration attenuated the migration defect mediated by WA(pYV) (1.7 mg/ml: 21% migratory cells, 0.86 mg/ml: 58% migratory cells) and increased migration of DCs infected with WA(pYV Δ lcrD) (1.7 mg/ml: 70% migratory, 0.86 mg/ml: 89% migratory).

Next, the effect of the ROCK inhibitor Y27632 on DC morphology in under-agarose assays was evaluated. ROCK is a downstream component of the RhoA-signaling pathway. Fig. 3.24 C shows that uninfected cells pre-incubated with the ROCK inhibitor Y27632 appear rugged and possess multiple highly elongated protrusions, similar to *Y. enterocolitica* YopT-infected cells.

3.1.3.3.3 Conservation of the YopT-targeted migration mechanism So far, the presented migration experiments were conducted with DCs as a model cell type not affected by phagocytosis and showing stable migration in chemokine gradients. In the next step it was analyzed if this elongated morphotype initially observed with neutrophils from murine spleens is specific for these two cell types or if it also occurs with other cell types. To this end, the YopT_{yen}-morphotype as observed in under-agarose assays was chosen exemplarily.

In a first step murine bone marrow cells from Lifeact-GFP mice were used. It has been shown that murine bone marrow contains a large amount of functionally competent neutrophils (Boxio *et al.*, 2004). Under the same conditions as DCs, cells entering the

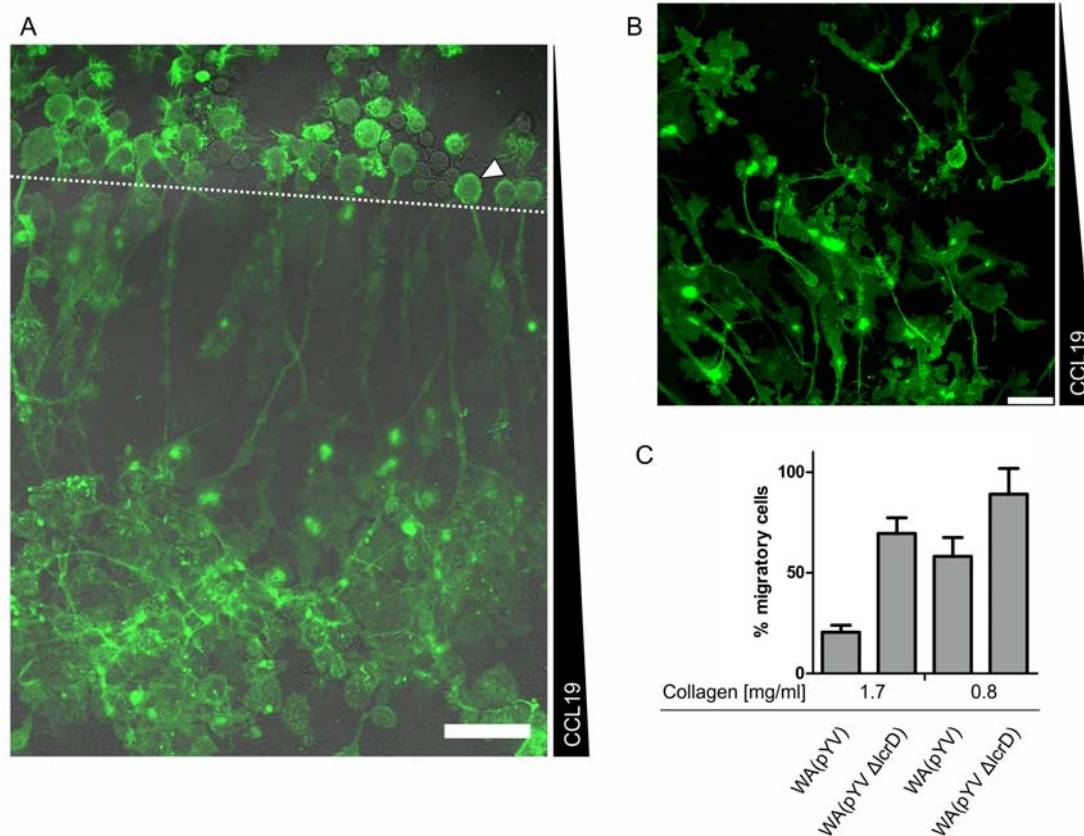


Figure 3.24: Inhibition of the RhoA effector ROCK causes a DC morphotype similar to *YopT_{yen}*. **A:** Trailing edges of WA(pYV)-infected DCs are not able to enter the gap between coverslip and agarose in under-agarose assays. DCs were infected with WA(pYV) directly in the responder well. The border of the agarose well is depicted by a dashed white line (the well is above the line). A trailing edge of an DC which is stuck at this border is highlighted by a white arrowhead. Green: Lifeact DCs. Greyscale: bright field. Scale bar 50 μ m. **B:** Native DCs were pre-incubated with ROCK inhibitor Y27632 and then directly injected between the coverslip and the agarose in under-agarose assays. After 2 h of incubation, DCs formed long and partially branched protrusions. Green: Lifeact DCs. Scale bar 50 μ m. **C:** Lowering the collagen concentration (from 1.7 to 0.86 mg/ml), and thereby increasing the pore size of the collagen meshwork, alleviates the migration inhibition mediated by WA(pYV). Infected cells were incorporated into 3D-CoG and their migratory behavior was evaluated for 3 h.

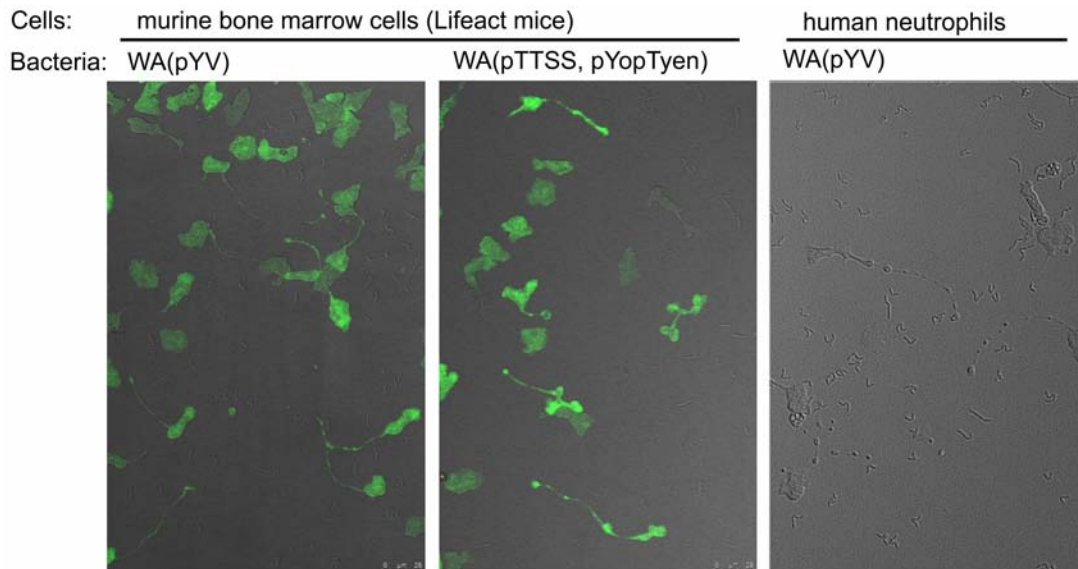


Figure 3.25: YopT_{yen}-induced morphotype in different cell types. Murine bone marrow cells and human neutrophils from peripheral blood were coincubated with WA(pYV) or WA(pTTSS, pYopT_{yen}) in under-agarose assays. 75 min after inoculation massive cell elongation could be observed. Murine cells were expressing Lifeact-GFP (green).

liquid-filled gap between coverslip and agarose (thus migration-competent bone marrow cells) also formed elongated cells with mostly unaffected dynamics in actin polymerization in protrusions after infection with WA(pYV) or WA(pTTSS, pYopT_{yen}) (Fig. 3.25 and Movie 24, 25).

Human neutrophils isolated from peripheral blood were also prone to this morphotype after contact with WA(pYV) (Fig. 3.25 and Movie 26). Taken together, the YopT_{yen}-morphotype is similar in different cell types relying on amoeboid migration. Furthermore, there was no significant difference between murine and human neutrophils.

3.1.3.4 Comparison of RhoA-active Yops from *Y. enterocolitica* and *Y. pseudotuberculosis*

3.1.3.4.1 YopE- and YopT-mediated inhibition of cell migration

Previous studies produced conflicting results concerning the Rho GTPase targets of YopE and YopT of *Y. enterocolitica* (*yen*, YopE_{yen} and YopT_{yen}) compared with *Y. pseudotuberculosis* (*yps*, YopE_{yps} and YopT_{yps}). Amino acid sequence comparison of the respective Yops further fueled the hypothesis of different Rho GTPase specificity. As the presented results demonstrate a unique role of YopT_{yen} in long term migration inhibition of DCs, suggesting preferential targeting of RhoA, the effects of YopE_{yen}/YopE_{yps} and YopT_{yen}/YopT_{yps} on

mammalian cells were compared in the 3D-CoG migration assay. In order to translocate single Yops, the ‘toolbox strain’ WA(pTTSS) secreting single Yops was utilized.

The results of these 3D-CoG migration experiments are shown in Fig. 3.26. Both tested *Y. pseudotuberculosis* strains, YPIII(pIB1) and IP32953, showed an inhibitory effect on DC migration similarly to WA(pYV). In the next step, the individual effect of YopE_{yyp}s and YopT_{yyp}s from strain IP32953 were analyzed. YopT_{yyp}s mediated inhibition of migration to a similar extent as YopT_{yen}. Interestingly, YopE_{yyp}s also had a comparable inhibitory effect, in contrast to YopE_{yen}. It has been shown that two lysin residues (K62 and K75) in YopE_{yen} from serogroup O:8 serve as polyubiquitination sites which leads to degradation of YopE_{yen} by the proteasome in the host cell cytosol. Amino acid exchanges (K62R, K75Q) have been introduced and shown to prevent ubiquitination and subsequent proteasomal degradation (Hentschke *et al.*, 2007). As shown in Fig. 3.26, YopE_{yenK62R,K75Q} caused an intermediate inhibition of migration (66.5% migration-positive cells), when compared to wildtype YopE_{yen} (97%) and YopE_{yyp}s (27%). Finally, it was checked if the inhibitory effect of YopT_{yen}, YopE_{yyp}s and YopT_{yyp}s was due to the respective inhibitory activity towards Rho-GTPases. Abrogation of GAP-activity in YopE (amino acid exchange R144A in the arginine finger) or abrogation of the proteolytic activity of YopT (amino acid exchange C139S in the catalytic triad) abolished their inhibitory effect on DC migration (Fig. 3.26).

Microscopic analysis of these pre-infected cells during the 3D-CoG migration assay revealed that infection with *Y. pseudotuberculosis* strains resulted in the early stage in formation of cell protrusions associated with the inability to translocate the nucleus, resembling frustrated migration (Movie 27, 28). In contrast to that, WA(pTTSS, pYopT_{yyp}s)-infected cells were even unable to form protrusions (Movie 29). WA(pTTSS, pYopE_{yyp}s)-infected cells behaved phenotypically similar to IP32953-infected cells (Movie 30).

Compared to these morphotypes, WA(pYV)- and WA(pTTSS, pYopT_{yen})-infected cells appeared more active in formation and dynamics of protrusions, also in regard to cell polarization in the CCL19-gradient (Movie 15, 18).

3.1.3.4.2 Analysis on the cellular level In order to study these morphotypes in more detail, Lifeact-DCs were co-cultured with yersiniae in under-agarose assays. Interaction with *Y. pseudotuberculosis* strains YPIII(pIB1) and IP32953 produced fundamentally different DC morphotypes compared to *Y. enterocolitica* WA(pYV), as shown in Fig. 3.27: *Y. pseudotuberculosis*-infected cells did not become elongated but formed small

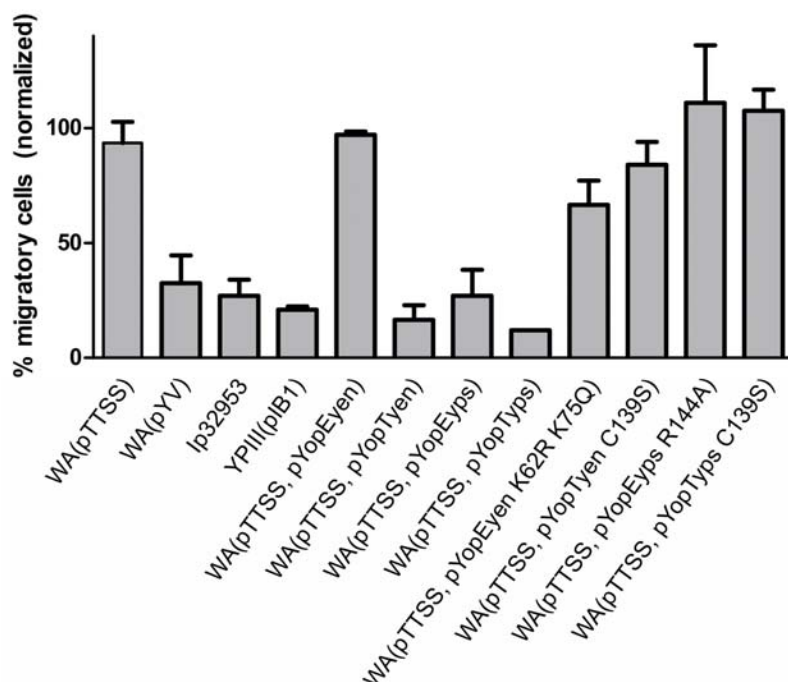


Figure 3.26: Inhibition of DC migration by *Y. enterocolitica* and *Y. pseudotuberculosis* YopE and YopT, respectively. Experiments were performed as described in Fig. 3.21, ratios were normalized to DCs infected with WA(pYV Δ lcrD). WA(pTTSS) harboring YopE- or YopT-constructs as indicated was utilized to translocate single Yops into DCs. YPIII(pIB1) and IP32953 are *Y. pseudotuberculosis* strains. The lysin exchanges in YopE_{yenK62R,K75Q} abrogate ubiquitination for proteasomal degradation. R144A and C139S are amino acid substitutions abrogating the GAP activity of YopE and the proteolytic activity of YopT, respectively. YopE_{ypS} also mediates strong inhibition of migration, similar to YopT from either strain. Data represent two independent experiments.

filopodia-like structures along the entire cell outline while no dynamic actin polymerization could be observed anymore (Movie 31-36). After coincubation with single Yop-producing strains, WA(pTTSS, pYopE_{yen}) caused no obvious defect (Fig. 3.27, Movie 37-39), while WA(pTTSS, pYopE_{yyp}) led to cell morphologies reminiscent of cells infected with IP32953 (Movie 40-42). WA(pTTSS, pYopT_{yen}) led to highly elongated cells (Movie 43-45), while WA(pTTSS, pYopT_{yyp}) led to cells more prone to form lamellipodia-like structures spanning the entire cell outline. Still, cell elongation occurred also with these cells occasionally (Movie 46-48). Interestingly, actin polymerization was observed over the entire cell outline. By producing kymographs from time-lapse experiments with WA(pTTSS, pYopT_{yyp})-coincubated DCs, actin polymerization rates of over 15 $\mu\text{m}/\text{min}$ were determined in these cells (Fig. 3.28 and Movie 49, 50).

3.1.3.4.3 Degradation of plasma membrane integrity It has been shown that the T3SS causes pore formation in HeLa cells by insertion of the translocator proteins YopB and YopD into the host cell membrane. This pore is suggested to be regulated by YopQ (YopK in *Y. pseudotuberculosis*) and translocation of YopE and YopT have been shown to counteract cellular effects of this pore formation. One hypothesis of the underlying pore ‘healing mechanism’ is YopE- and YopT-mediated inactivation of Rho GTPases (Holmström *et al.*, 1997; Viboud and Bliska, 2001; Wölke *et al.*, 2011). Pores in the host cell membrane can eventually lead to disintegration of the cytoplasmic membrane and release of cytosolic proteins, e. g. lactate dehydrogenase (LDH). The concentration of LDH can be determined in an enzymatic assay. Most of the studies mentioned above were done with *Y. pseudotuberculosis* strains. The results in section 3.1.3.4.1 suggest substantial differences between YopE and YopT from *Y. enterocolitica* compared to *Y. pseudotuberculosis*, possibly due to Rho GTPase specificity. Therefore LDH release experiments were conducted with HeLa cells infected with different *Yersinia* strains. The results published by Viboud and Bliska (2001) and Wölke *et al.* (2011) could be confirmed: WA(pTTSS) but not WA(pYV) caused LDH release by infected HeLa cells (Fig. 3.29). WA(pTTSS, pYopE_{yyp}) or WA(pTTSS, pYopT_{yyp}) did not cause LDH release. WA(pTTSS, pYopE_{yen}) or WA(pTTSS, pYopT_{yen}) had the same effect as their *Y. pseudotuberculosis* counterparts, that is a low rate of LDH release.

So far, the effect of T3SS-dependent pore formation on neutrophils has not been addressed yet. Therefore human neutrophils isolated from peripheral blood were infected

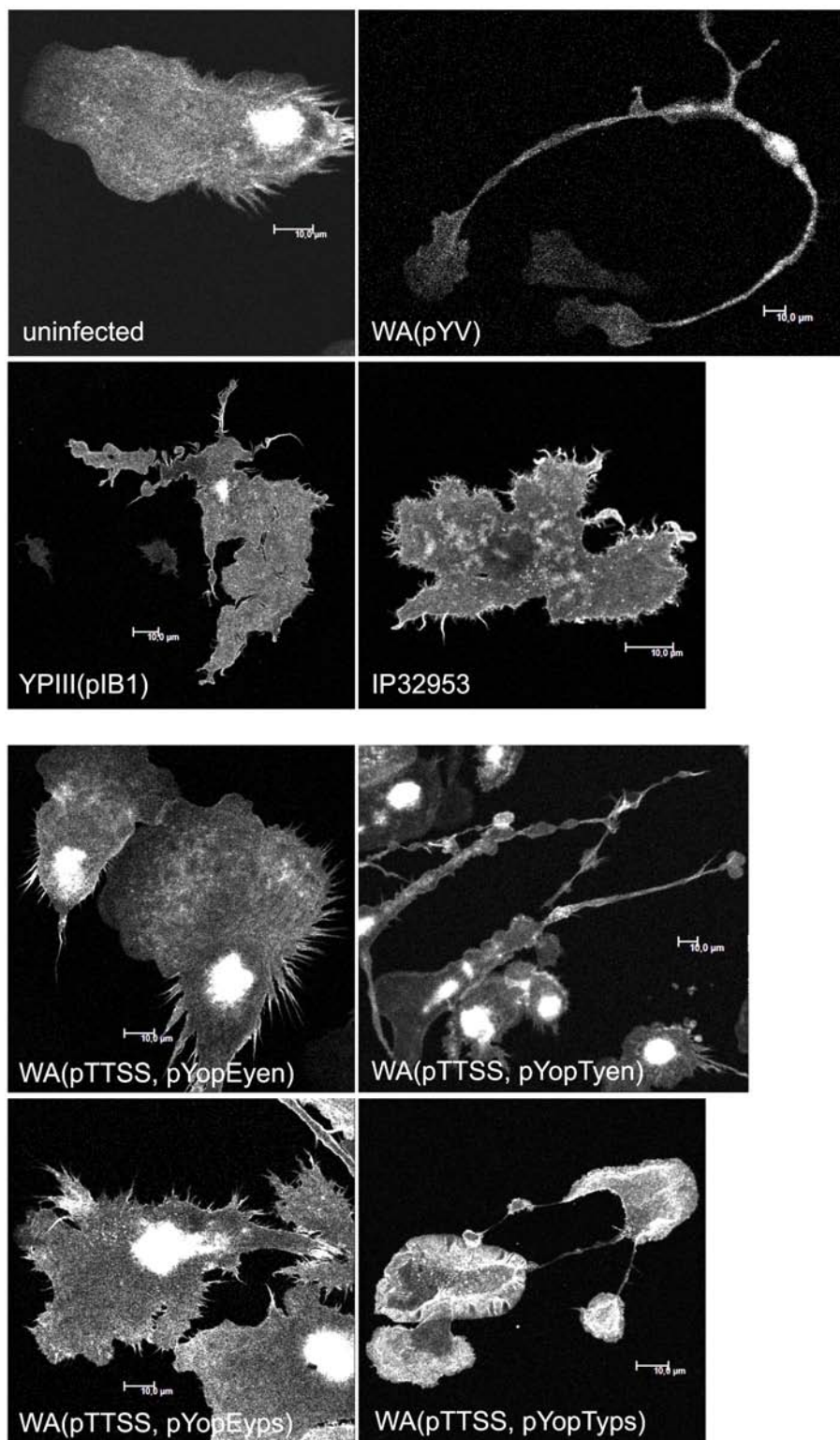


Figure 3.27: Typical morphotypes of DCs infected with different *Yersinia* strains in under-agarose assays. Lifact-DCs were infected with WA(pYV), YPIII(pIB1), IP32953, WA(pTTSS, pYopE_{yen}), WA(pTTSS, pYopE_{yps}), WA(pTTSS, pYopT_{yen}) or WA(pTTSS, pYopT_{yps}). DC morphotypes caused by the different *Yersinia* strains are clearly distinguishable and so are morphotypes caused by YopE_{yen}/YopE_{yps} and YopT_{yen}/YopT_{yps}. White: Lifact-GFP.

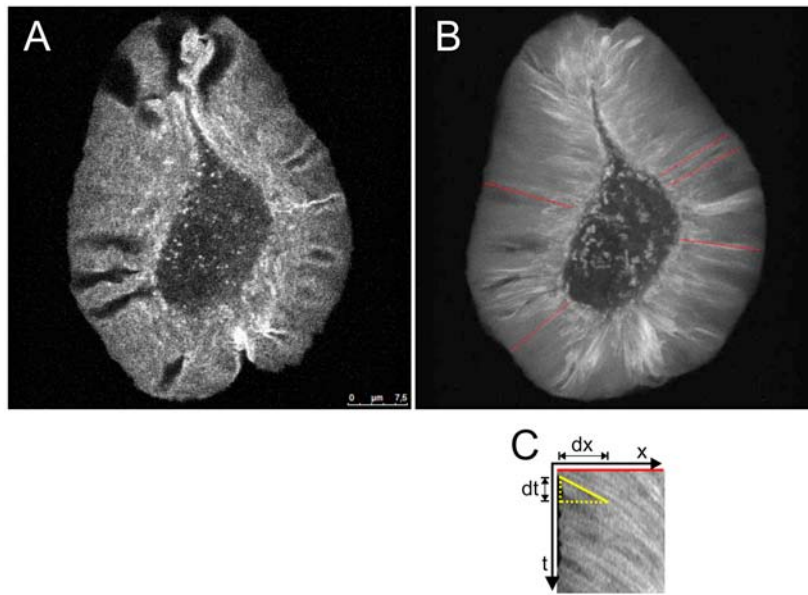


Figure 3.28: Typical morphotype of Lifeact-DCs after contact with WA(pTTSS, pYopT_{yps}) in an under-agarose assay. After contact with WA(pTTSS, pYopT_{yps}), DCs round up and show no net migration. Instead, constant actin treadmilling can be observed in the lamellipodium-like protrusion which can span the entire cell outline. **A:** Typical YopT_{yps}-morphotype, a time lapse is shown in Movie 49. **B:** Time projection of the dynamics of the cell in **A** over 87 s. Kymographs of this experiment have been generated from the positions marked by red lines. Actin treadmilling is parallel to these lines. **C:** Representative kymograph. The intensity signal of the red line (x) is plotted against time (t). From linear areas in this kymograph, the rate of actin polymerization can be calculated.

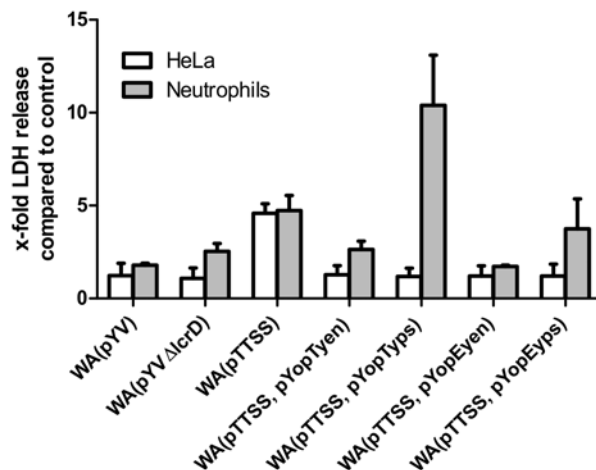


Figure 3.29: T3SS-mediated LDH release in HeLa cells and neutrophils. Cells were infected for 4 h at a MOI of 20 with the strains mentioned in the figure. In HeLa cells, only WA(pTTSS) caused LDH release, whereas in neutrophils WA(pTTSS, pYopT_{yps}) caused an even stronger effect. For the comparison of neutrophils and HeLa cells, the increase in LDH release compared to uninfected cells is indicated.

with WA(pTTSS)-derived strains (Fig. 3.29). Infection with WA(pTTSS) caused a similar increase in LDH release as with HeLa cells (4-5 fold compared to uninfected cells), whereas WA(pYV)-infected neutrophils did not release significantly more LDH (<1.8 fold). WA(pTTSS, pYopE_{yen}) or WA(pTTSS, pYopT_{yen}) efficiently inhibited LDH release as demonstrated for HeLa cells, whereas WA(pTTSS, pYopE_{yps}) appeared to be less efficient. Surprisingly, WA(pTTSS, pYopT_{yps}) caused >10 fold LDH release compared to uninfected cells. This discrepancy between HeLa cells and neutrophils suggests a certain cell type specificity of the effects of YopE and YopT.

In order to assess whether the massive LDH release caused by YopT_{yps} in neutrophils is the result of its activity towards Rho GTPases, the catalytically inactive mutants YopT_{yenC139S} and YopT_{ypsC139S} were tested. Both strains failed to induce LDH release (Fig. 3.30 A). To exclude fundamental differences in secretion between YopT_{yps} and YopT_{yen} from strain WA(pTTSS), secretion during growth in liquid medium was induced and the amount of secreted YopT was analyzed. Secretion of YopT_{yps} and YopT_{yen} by WA(pTTSS) in the medium was practically identical (Fig. 3.30 B).

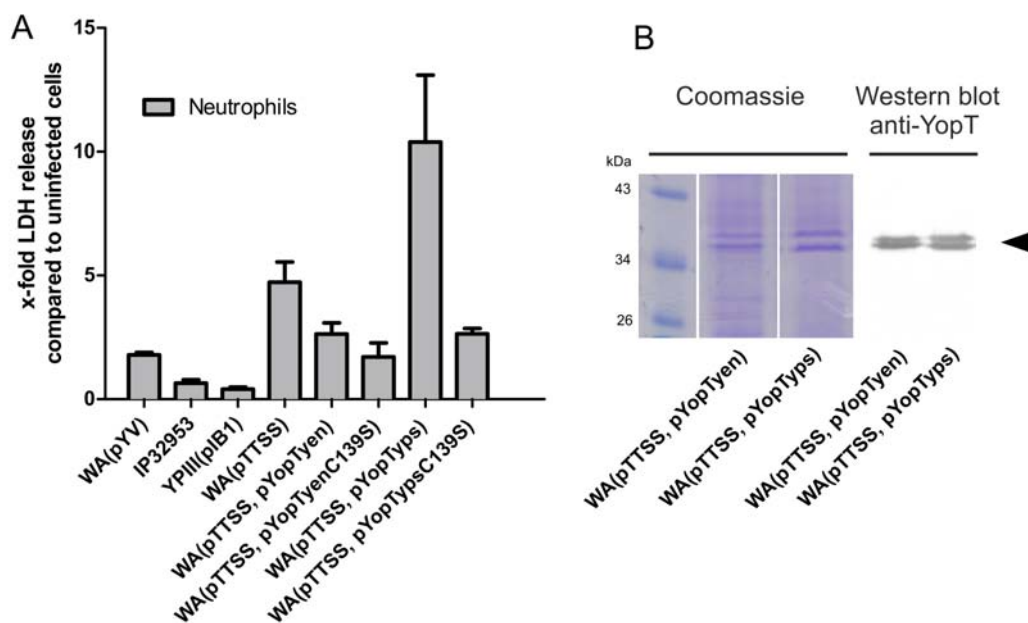


Figure 3.30: Effect of the catalytic activity of YopT on T3SS-mediated LDH release in neutrophils. **A:** Cells were infected for 4 h at MOI 20 with the strains mentioned in the figure. WA(pTTSS, pYopT_{yps}) induced more LDH release than the catalytically inactive mutant WA(pTTSS, pYopT_{ypsC139S}) or WA(pTTSS). **B:** Secretion of YopT by WA(pTTSS, pYopT_{yen}) or WA(pTTSS, pYopT_{yps}) was analyzed as described in section 2.2.3.3, p. 34 by precipitation of secreted proteins by TCA and Western blot analysis. The expected size of YopT is marked by an arrowhead. The amount of secreted YopT was practically identical for WA(pTTSS, pYopT_{yen}) and WA(pTTSS, pYopT_{yps}).

Of note, *Y. pseudotuberculosis* wildtype strains IP32953 and YPIII(pIB1) caused even less cell lysis than *Y. enterocolitica* WA(pYV) in neutrophils. These results demonstrate that translocation of YopT_{yps} induces neutrophil necrosis, in contrast to YopT_{yen}.

3.1.3.4.4 Homology modeling The demonstrated species-dependent cellular effects of YopT and YopE might arise from differences in the amino acid sequence (Fig. 3.31). Homology models of the protein structure were generated with the web tool HHpred (Söding *et al.* (2005), available at toolkit.tuebingen.mpg.de/hhpred) in order to establish a basis for the interpretation of the observed discrepancies.

YopT. Structure models based on amino acid residues 134-294 of YopT_{yen} and YopT_{yps} were generated using the crystal structure of the related cysteine protease AvrPphB from *Pseudomonas syringae* (Zhu *et al.*, 2004) as a template (Fig. 3.32, 22.5% sequence identity of the sequences used for modeling). Within this conserved structure there were 13 amino acid exchanges between YopT_{yen} and YopT_{yps}, some conferring differences in electric charge. The surface in the vicinity of the catalytic triad (C139/H258/D274) exhibited a slightly altered morphology in the model.

YopE. YopE_{yen} and YopE_{yps} structure models encompassing amino acid residues 102-219 were derived from the crystal structure of the YopE GAP domain of *Y. pestis* (Evdokimov *et al.*, 2002) as a template (Fig. 3.33, 94.9% sequence identity of the sequences used for modeling). The two proteins appear more conserved within *Y. pseudotuberculosis* and *Y. enterocolitica* than the YopT proteins. There are six amino acid exchanges within the GAP domain, strikingly all of them are situated on one side of the structure. Moreover, this side is opposite of the arginine finger (R144) involved in GAP function. Amino acid exchanges in position 213 and 214 cause a charge reversal on the protein surface which might result in different binding properties to cellular proteins.

A second accumulation of amino acid sequence differences is found outside of the modeled GAP domain at position 60-75 (7 differences in 15 residues). Strikingly, this section represents the membrane localization domain (MLD, AA 54-75) of YopE (Krall *et al.*, 2004).

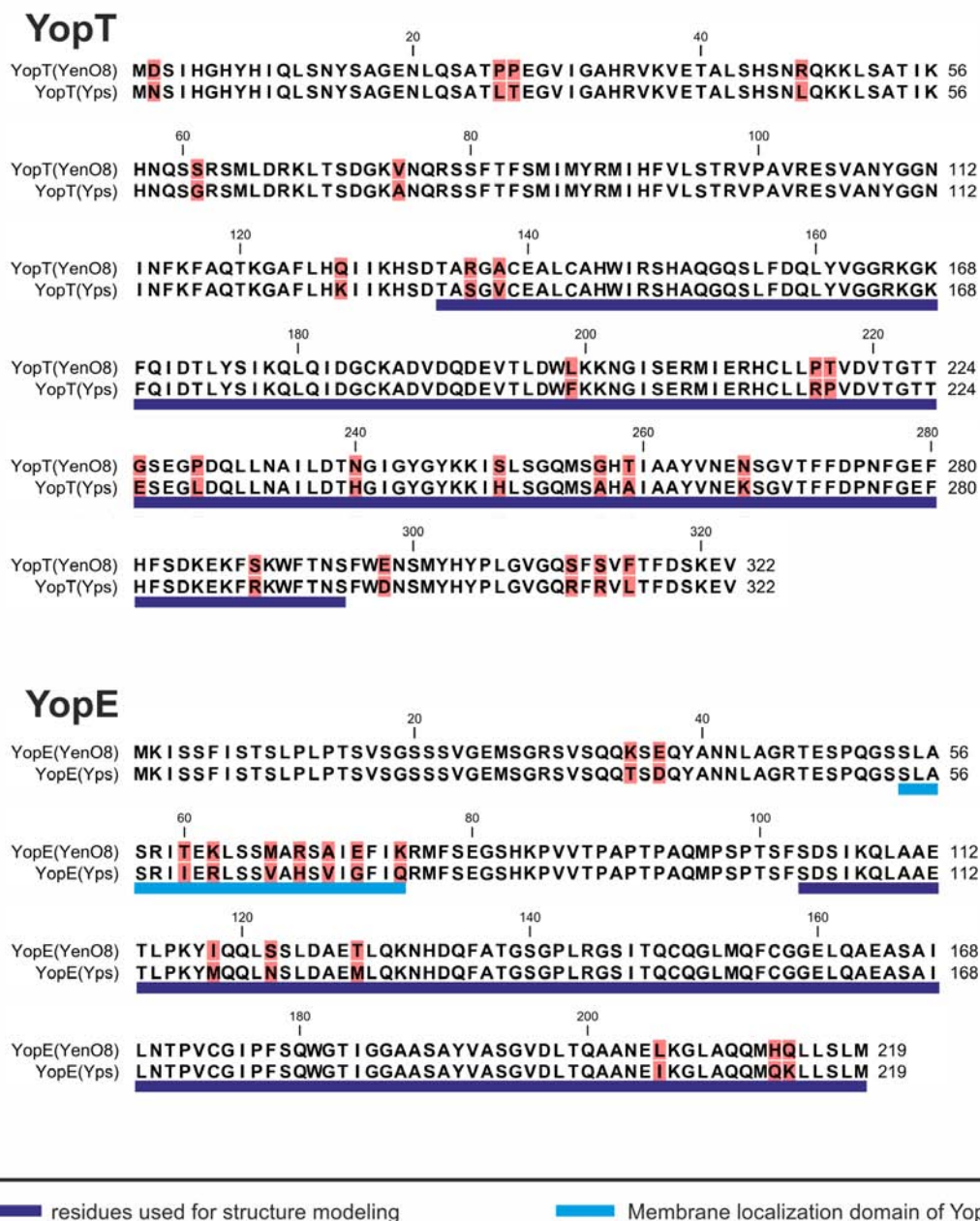


Figure 3.31: Sequence alignment of YopT and YopE from *Y. enterocolitica* and *Y. pseudotuberculosis*. Sequence alignment of YopT and YopE from *Y. enterocolitica* serotype O8 and *Y. pseudotuberculosis* (strain IP32953). The amino acid residues represented in the structure model in Fig. 3.33 and 3.32 are marked in purple, the residues constituting the MLD of YopE are marked in light blue.

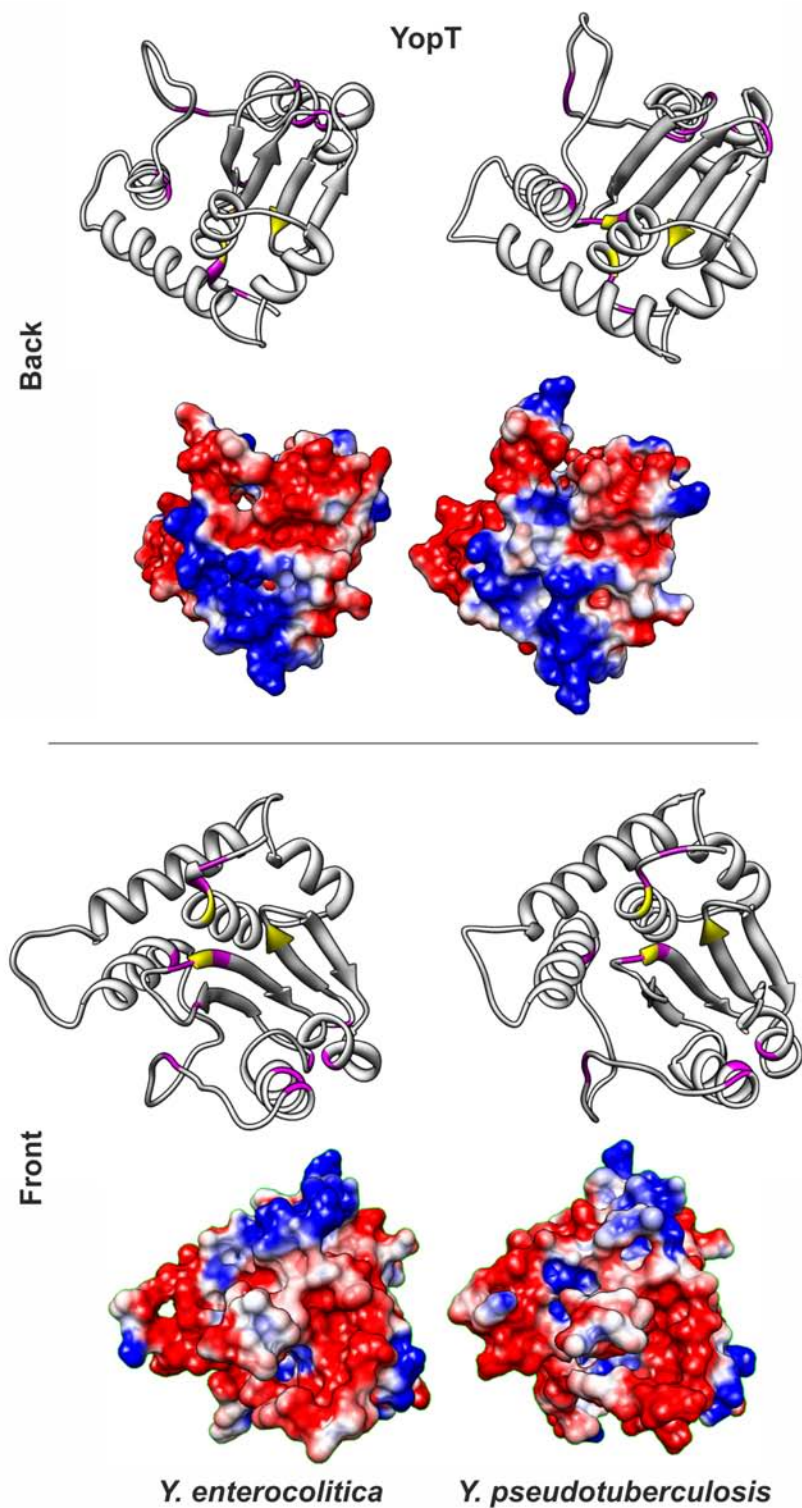


Figure 3.32: Structure comparison of YopT from *Y. enterocolitica* and *Y. pseudotuberculosis*. The structure model (amino acid residues 134-294) was generated by structure prediction with HHpred based on the crystal structure of the homologous protein AvrPphB from *Pseudomonas syringae*. The catalytic triad C139/H258/D274 is colored yellow, differences in amino acid sequence are colored magenta. The electrostatic potential surface is colored according to its charge (blue: positive, red: negative).

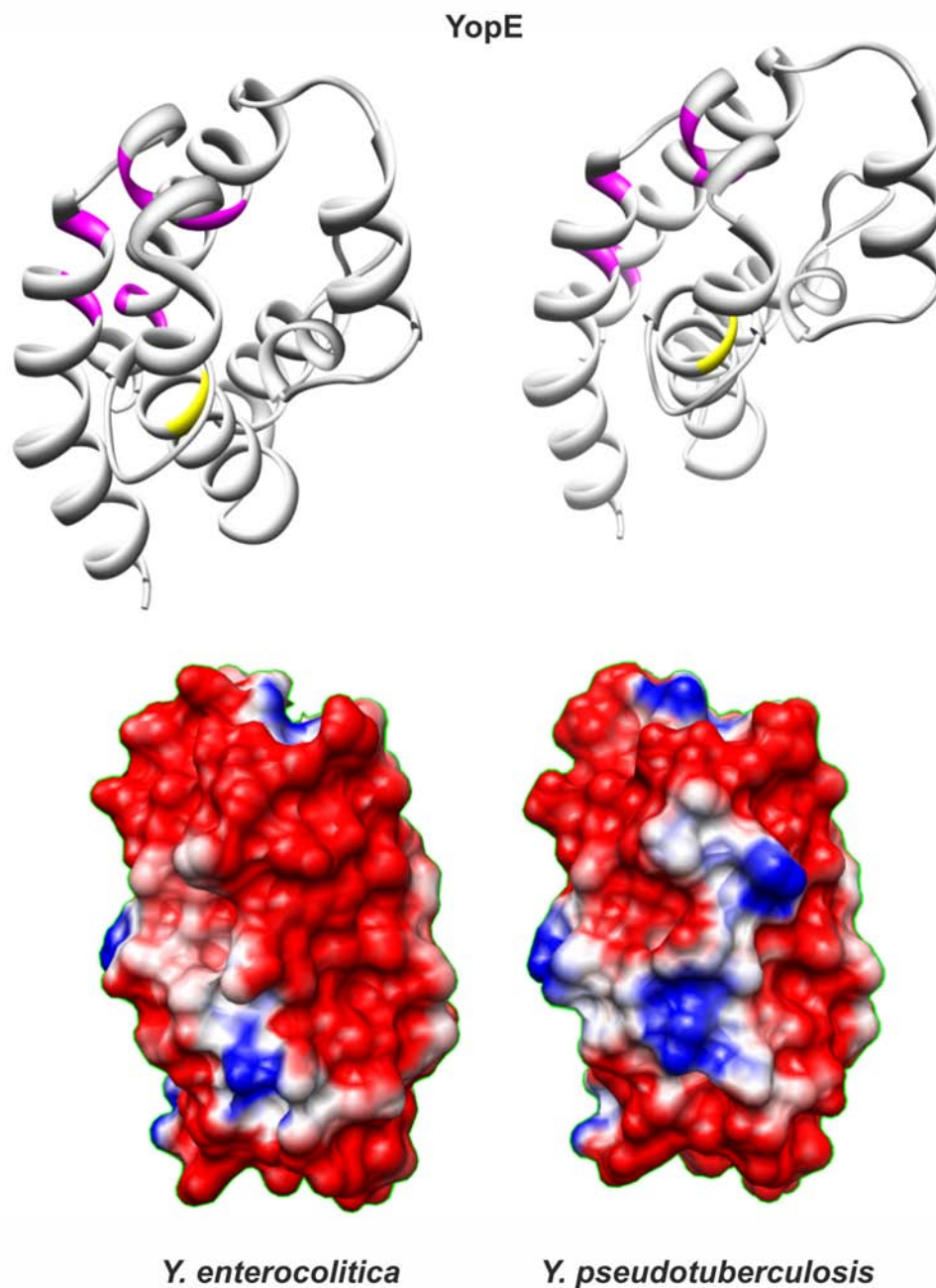


Figure 3.33: Structure comparison of YopE from *Y. enterocolitica* and *Y. pseudotuberculosis*. The structure model (amino acid residues 102-219) was generated by structure prediction with HHpred based on the crystal structure of YopE from *Y. pestis*. The arginine finger R144 is colored yellow, differences in amino acid sequence are colored magenta. The electrostatic potential surface is colored according to its charge (blue: positive, red: negative).

3.2 Organ explant-based *ex vivo* model

In the last part of this work, another infection model was established for the study of infections at mucous membranes. This exceeds the approach of supplying a 3D context by also taking into account the physiological environment of epithelial tissue in regard to cell type composition and polarity.

3.2.1 The organ chamber

The system (Fig. 3.34 A, B, detailed description in section 2.2.5.4, p. 44) is based on a microscopy-compatible organ chamber for mounting explanted tissue and supplying it with nutrients and oxygen for the duration of the experiments. The organ is fixed between the two inner aluminum parts with custom-modified syringe tips and separates the chamber into two main compartments, termed apical and basal chamber in respect to the orientation of the mucosa. Both compartments have an inlet and an outlet, the basal compartment has an additional inlet. The two compartments are connected to separate syringe pumps which provide perfusion. The basal compartment is supplied with medium containing nutrients and oxygen, the apical compartment can be flushed with PBS or appropriate solutions which mimic the physiological milieu of the organs (e. g. artificial urine media for bladder tissue). Both compartments of the organ chamber drain through separate outlets to collect and analyze the flow-through independently at given time points. The additional inlet of the basal compartment enables addition of pharmacological agents during experiments.

In order to regulate oxygen and carbon dioxide concentrations, the medium is channelled through a custom-built membrane oxygenation device (Fig. 3.34 C, detailed description in section 2.2.5.4, p. 44) before entering the basal compartment. Gas concentrations are adjusted by an active gas supply system. For media based on physiological hydrogen carbonate-based buffers (i. e. RPMI 1640 medium), the pH level can be regulated by the carbon dioxide concentration. The effect of different conditions on oxygen-saturation and pH of the medium were analyzed (Fig. 3.35). An increase of carbon dioxide in the gas mixture from 5 % to 15 % lowered the pH in the medium from ca. 7.7 to 7.4. Ambient air concentration of oxygen (21 %) resulted in 9-11 mg/l in the medium, maximizing the oxygen concentration (95 %) increased this value to ca. 20 mg/l. In order to buffer explanted tissue at pH 7.4, experiments were conducted with 85 % oxygen and 15 % carbon dioxide for membrane oxygenation, providing 18 mg/l oxygen in the medium.

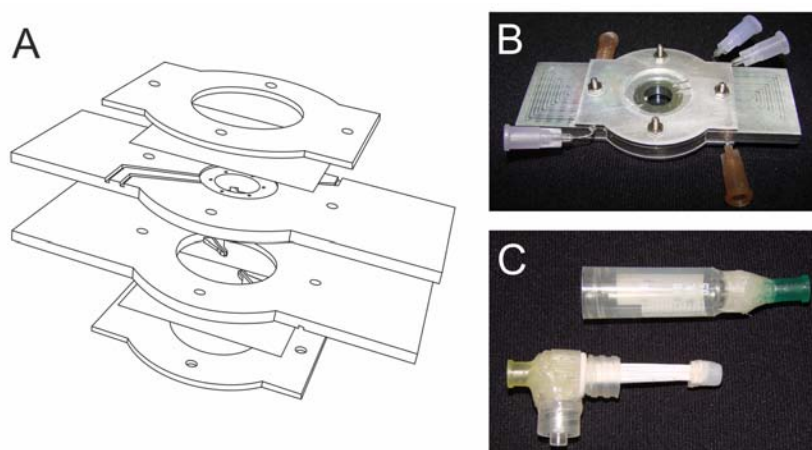


Figure 3.34: Depiction of the organ chamber and the membrane oxygenation device. **A:** Sketch of the organ chamber, based on the original blueprint, on the basis of Wieser *et al.* (2011). **B:** Photograph of the assembled organ chamber. Three violet syringes connect to the basal compartment, two brown syringes connect to the apical compartment. **C:** Photograph of the membrane oxygenation unit. Medium is channeled through the unit via the green and yellow connectors. The hollow fibers are connected to the gas flow via the connector at the bottom of the picture.

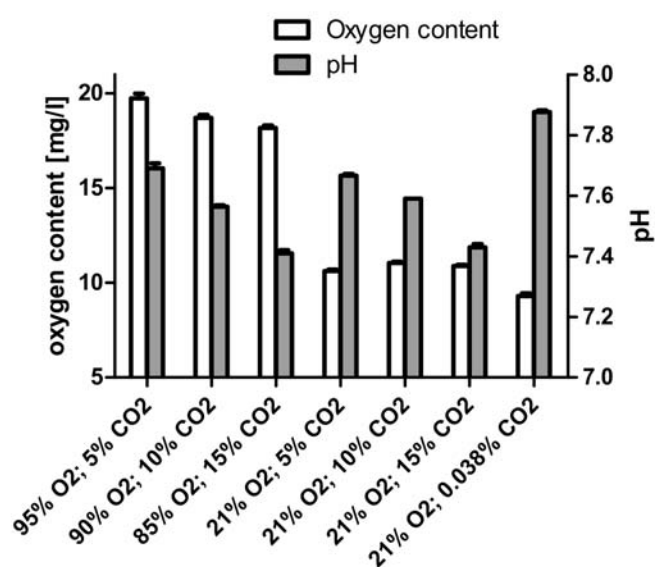


Figure 3.35: Functionality of the membrane oxygenation device. The medium content of oxygen and carbon dioxide was controlled by a custom-built membrane oxygenation device. pH and oxygen content were measured using a pH electrode and oxygen Optodes (PreSens, Regensburg, Germany). pH was set to 7.4 by supply of 15 % carbon dioxide.

By default, a flow rate of 5 ml/h and 0.5 ml/h was applied to the basal and apical compartment, respectively. To simulate a stationary filled bladder in the beginning of experiments and to allow *E. coli* NU14 to establish contact with epithelial cells, perfusion of the apical compartment was established 2 h after infection. For *E. histolytica*, perfusion of the apical compartment was established 30 min after *ex vivo* infection. If necessary for microscopy, flow rates in the apical compartment can be lowered or increased (0.1-4 ml/h) for short periods of time.

3.2.2 Interaction of uropathogenic *Escherichia coli* with urothelium

3.2.2.1 Tissue preservation in the organ chamber

Native urinary bladders were explanted from C57BL/6 mice and cultivated for 8.5 h in the organ chamber (Fig. 3.36). Staining was achieved by supplementing the buffer in the apical compartment with FM 4-64. In Fig. 3.36 A, an overview of bladder epithelium 8.5 h after explantation is shown. Fig. 3.36 B shows a detail from the tissue at 1, 3, 5.5 and 8 h after explantation. Tissue integrity is generally preserved well as evaluated by the preservation of the superficial umbrella cell layer. Starting from 3 h after explantation, a certain extent of disintegration of the epithelial layer can be observed: single cells are detached from the epithelium (compare white arrowhead in Fig. 3.36 A). Furthermore, the cell surface staining appears more granular with increasing time. From these data a time frame until 5 h after explantation was chosen for further experiments in order to minimize experimental artifacts caused by longer incubation.

3.2.2.2 Properties of intracellular bacterial communities (IBCs)

In order to analyze intracellular bacterial communities (IBCs) established by UPEC, urinary bladders were removed from uninfected mice or 5 h after intravesical infection with 3×10^8 cfu of UPEC strain NU14(pFPV-mCherry/2) or NU14(pM965-4 eGFP). Explants were cultivated in the organ chamber for a total of 5 h and subjected to microscopical analysis. Several IBCs could be detected per organ. They were contained within superficial umbrella cells and appeared very densely packed (Fig. 3.37 A). Overall cell morphology of the infected cell appeared unchanged in comparison to uninfected tissue (Fig. 3.37 B). More detailed analysis of IBCs revealed that about 50 % of the bacterial population inside IBCs was motile to a certain degree (Movie 51). In contrast to this, bacteria adhering to the cell surface were immotile.

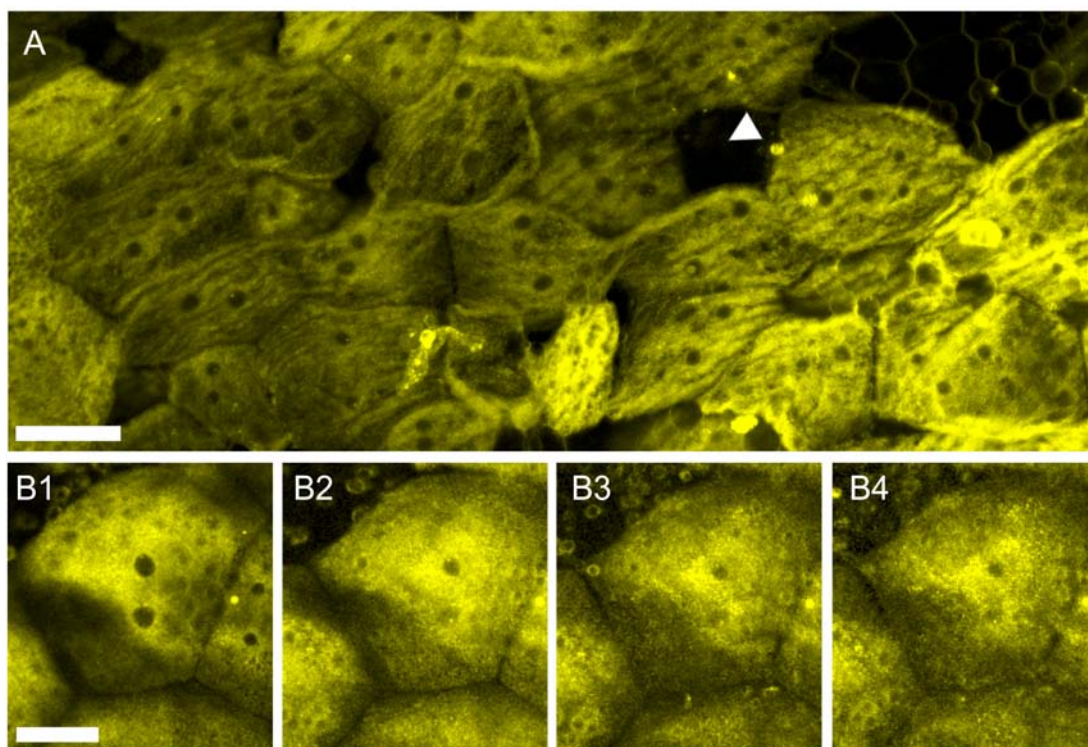


Figure 3.36: Preservation of an urinary bladder explant in the organ chamber. Urinary bladder tissue from a C57BL/6 mouse was explanted, stained with FM 4-64 (shown in yellow) and cultivated in the organ chamber for 8.5 h. Tissue preservation was considered as good, if only a low number of epithelial cells was detached (white arrowhead). **A:** Overview of the tissue. **B1-B5:** Details of a superficial umbrella cell after 1, 3, 5.5 and 8 h, respectively. Scale bar 75 μm .

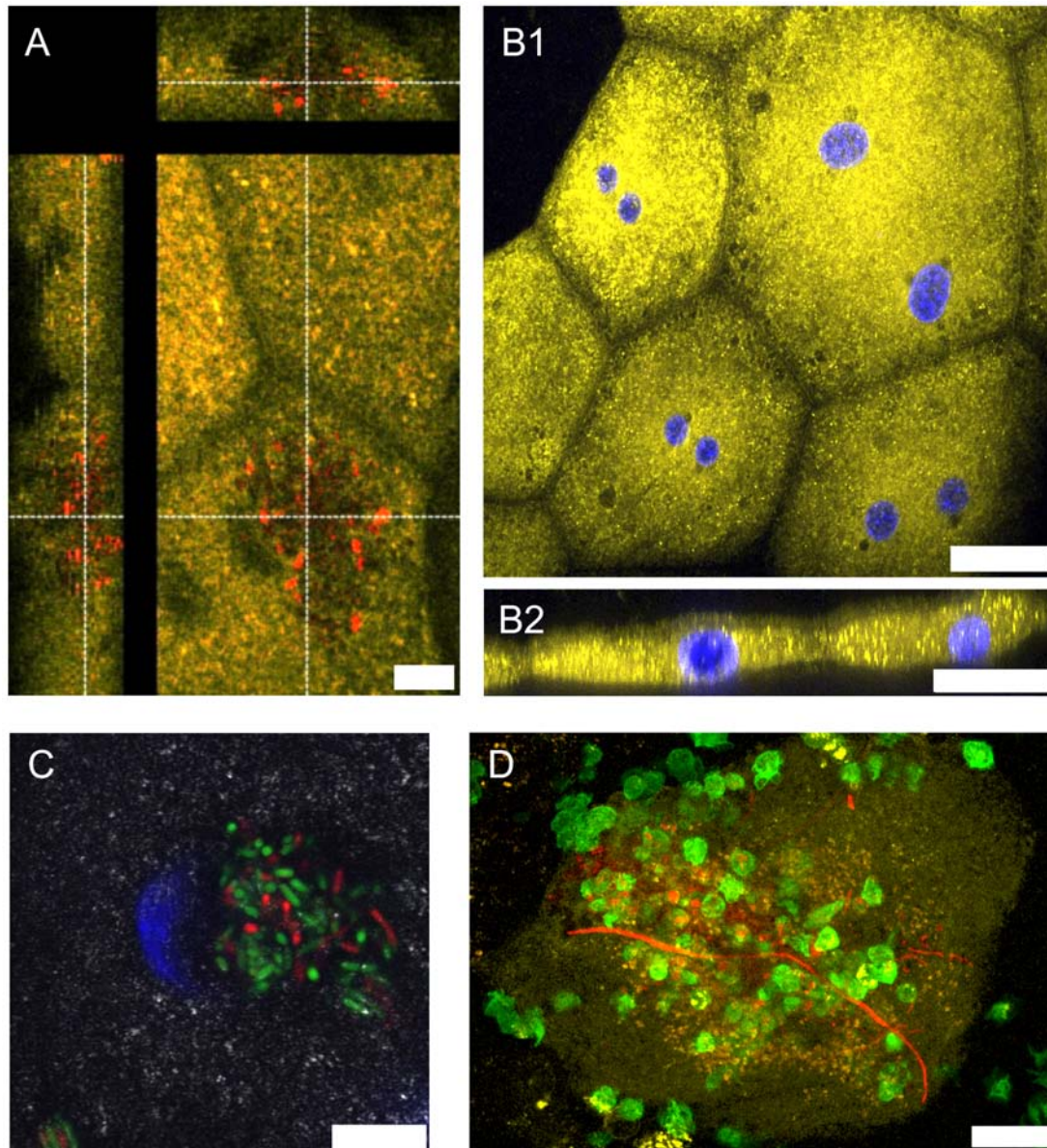


Figure 3.37: Properties of intracellular bacterial communities (IBCs). If not indicated otherwise, *lys-EGFP* mice were infected intravesically with 3×10^8 *cfu* NU14(pM965-4 eGFP or pFPV-mCherry/2), sacrificed 5 h p.i., and urinary bladders were removed. **A:** An IBC inside a superficial umbrella cell of a C57BL/6 mouse. The panes next to the central pane are xz and yz sections, illustrated by the crosshair. Yellow: FM 4-64-stained cell membranes. Red: NU14(pFPV-mCherry/2). 2 h after explantation. Scale bar 10 μm . **B1:** Uninfected superficial umbrella cells of a C57BL/6 mouse. **B2:** z section of B1. Yellow: FM 4-64-stained cell membranes. Blue: DAPI-stained nuclei. 30 min after explantation. Scale bar 50 μm . **C:** Coinfection experiments of a *lys-EGFP* mouse with a 1:2 mixture of GFP- and mCherry-expressing NU14 ($\sim 5 \times 10^8$ *cfu*) (NU14(pM965-4 eGFP) or NU14(pFPV-mCherry/2)). Most of the IBCs consist of both populations. Blue: DAPI-stained nuclei. Green: NU14(pM965-4 eGFP). Red: NU14(pFPV-mCherry/2). White: Confocal reflection microscopy. 2 h after explantation. Scale bar 10 μm . **D:** Filamentous NU14(pFPV-mCherry/2) in association with an IBC-containing superficial umbrella cell of a *lys-EGFP* mouse. Neutrophils are recruited to the infected focus in high numbers. Yellow: FM 4-64-stained cell membranes. Red: NU14(pFPV-mCherry/2). Green: GFP-positive cells from a *lys-EGFP* mouse. 3 h after explantation. Scale bar 25 μm .

In the next step, the uptake mechanism of UPEC into epithelial cells was analyzed. C57BL/6 mice were infected intravesically with a 1:2 mixture of GFP- and mCherry-expressing NU14(pM965-4 eGFP or pFPV-mCherry/2) (5×10^8 cfu). Mice were sacrificed 5 h p.i. and urinary bladders were mounted in the organ chamber. Most of the IBCs consisted of both GFP- and mCherry-expressing bacteria (Fig. 3.37 C). This suggests that IBCs arise from the uptake of two or more bacteria by a cell. Monochrome IBCs were rare and can result from a single uptake of a bacterium, as well as from uptake of multiple bacteria of the same population, which is stochastically possible. Single filamentous bacteria ($>140 \mu\text{m}$) were detected, adhering to mostly ruptured IBC-containing epithelial cells (Fig. 3.37 D).

3.2.2.3 The dynamic response of cellular immunity to breach of the urothelial barrier

Subsequent stages of UPEC infection involve establishment of inflammation and recruitment of immune cells to the epithelium. *Lys-EGFP* mice were infected as stated above. In this mouse strain, GFP is expressed under control of the *lysM*-promoter (Faust *et al.*, 2000). Thus, neutrophils express high levels of GFP, monocytes and macrophages express lower levels of GFP. Neutrophils are the first cell type recruited to infectious lesions, followed by macrophages (Nathan, 2006). For the presented experiments, urinary bladders were removed 5 h p.i., as at this time point neutrophils were present in high numbers in infected epithelium. In uninfected tissue no neutrophils could be detected on or under superficial umbrella cells (appearance similar to Fig. 3.37 B). In contrast to this, infected explants revealed a strong influx of neutrophils (Fig. 3.38 A, B). They were present both in cell layers below superficial umbrella cells, on the epithelium and transmigrating between epithelial cells. Migratory behavior could be detected for more than 7 h after explantation. Neutrophils were attracted to extracellular bacteria and ruptured IBC-containing cells where they ingested bacteria (Fig. 3.38 A-D). Neutrophils were also found inside IBCs and taking up bacteria from within (Fig. 3.38 B, C). It is possible that they crossed the cell membrane autonomously or due to damage of cell membranes as a result of partial IBC rupture. These events are also shown in Movie 52.

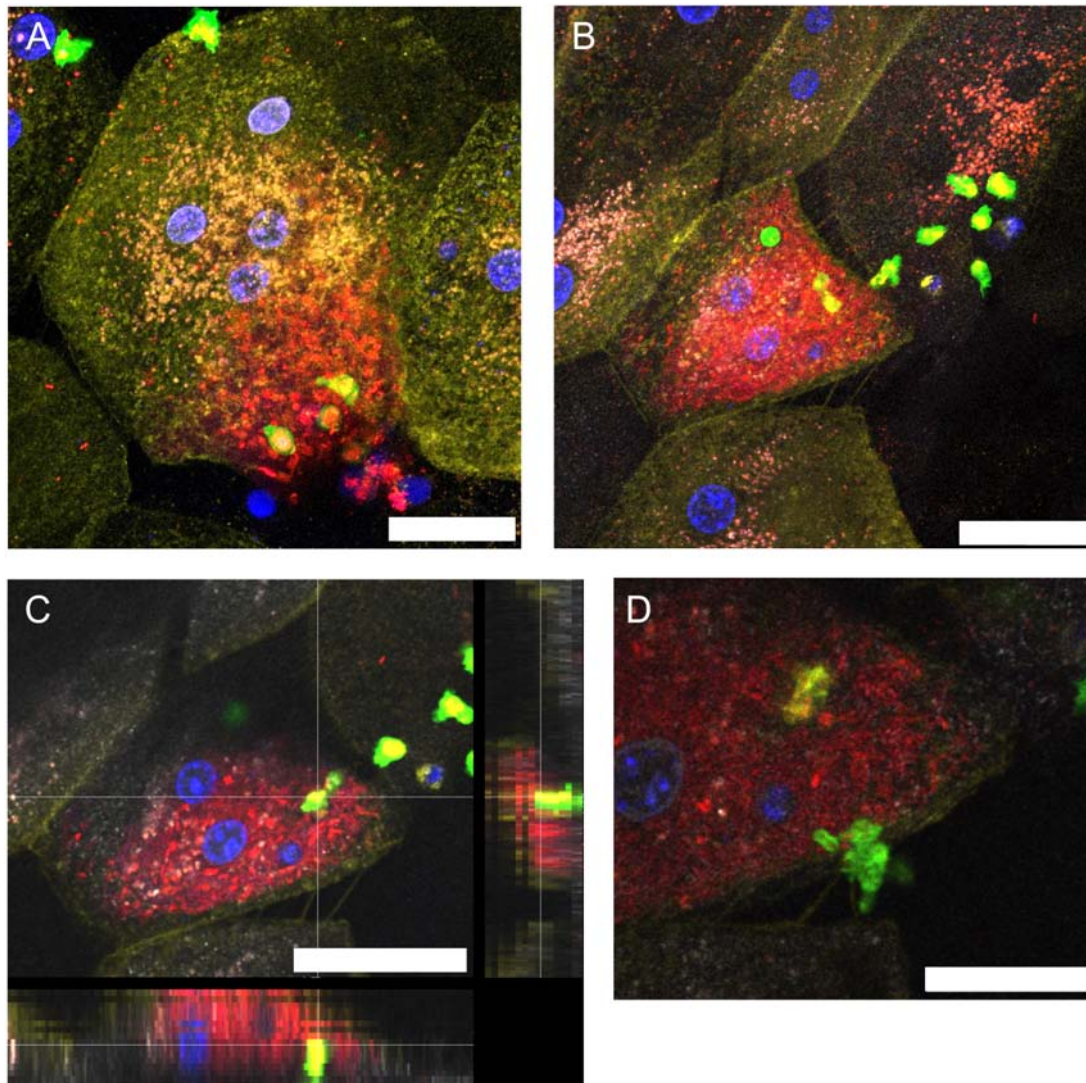


Figure 3.38: Neutrophil recruitment to IBC-containing epithelial cells. *Lys-EGFP* mice were infected intravesically with 3×10^8 cfu NU14(pFPV-mCherry/2), sacrificed 5 h p.i. and urinary bladders were removed. **A:** Neutrophils are recruited to a ruptured IBC-containing superficial umbrella cell of a *lys-EGFP* mouse. Neutrophils appear to have ingested bacteria. 4.5 h after explantation. Scale bar 50 μ m. **B:** Initial frame from Movie 52. The IBC is bright red, whereas granular contents of neighboring cells appear more white due to a strong signal in confocal reflection microscopy. Neutrophils are observed on top of the cells and obviously inside IBCs. 30 min after explantation. Scale bar 50 μ m. **C:** Single neutrophils penetrate the IBC. Depth reconstruction of the cell in B. xz and yz sections demonstrate suggested intracellular localization of the neutrophil indicated by the crosshair. 15 min after explantation. Scale bar 50 μ m. **D:** Single frame from Movie 52. A neutrophil invades the IBC and ingests a rod-shaped red bacterium. Scale bar 25 μ m. Blue: DAPI-stained nuclei. Yellow: FM 4-64-stained cell membranes. Green: GFP-positive cells from a *lys-EGFP* mouse. Red: NU14(pFPV-mCherry/2). White: Confocal reflection microscopy.

3.2.2.4 Analysis of cytokine release as a result of infection

UPEC infection influences cytokine secretion patterns of urinary bladder epithelia (Ingersoll *et al.*, 2008). The organ chamber system presented here is designed to permit measurements of secreted proteins in the flow-through, in parallel to microscopy. This functionality is utilized to analyze cytokine profiles of *ex vivo* infected urinary bladders. Native urinary bladders were mounted in the organ chamber and infected with 3×10^8 cfu NU14 from stationary phase or the same amount of heat-inactivated NU14. 50 μ l samples were taken at time points 1 h, 2 h, 3 h and 4 h post *ex vivo* infection from the outlet of the basal compartment. Samples were stored at -80°C and cytokine concentrations for IL-6, MCP-1, KC and TNF- α were determined with BD Cytometric Bead Arrays (CBA) (Fig. 3.39). IL-6, MCP-1 and KC release increased over 4 h after infection with NU14 (IL-6: 645 pg/ml, MCP-1: 129 pg/ml, KC: 210 pg/ml). Heat-inactivated NU14 also stimulated cytokine secretion (IL-6: 754 pg/ml, MCP-1: 217 pg/ml, KC: 223 pg/ml), whereas native explants did not show a comparable increase in these cytokines over 4 h. TNF- α levels remained relatively low both for native and infected urinary bladders.

3.2.3 Invasion of caecum epithelia by *E. histolytica*

Entamoeba histolytica was chosen as an invasive protozoan parasite. Caecum explants from C57BL/6 mice were washed extensively with PBS to remove caecum contents and mucus. Epithelial staining was done with FM 4-64. *E. histolytica* trophozoites were stained with rWGA-Alexa680. Trophozoites were found to exhibit a granular staining by this method. This suggests active uptake of labeled rWGA during the staining step. Caecum explants were infected with 3.8×10^4 amoebae. In order to facilitate initial contact with the epithelium, flow in the apical compartment was established after 30 min. Trophozoites were found to migrate on the epithelium at high velocity (average 1.2 ± 0.3 $\mu\text{m/s}$, maximum 1.8 $\mu\text{m/s}$) (Movie 53). *E. histolytica* is an anaerobic protozoan and the caecum offers such an anaerobic milieu. Nevertheless, in this setup trophozoites did not appear restricted in their migratory behavior for several hours, and from this basal applicability of the applied aerobic conditions (the same as for the urinary bladder) for analysis of amoeba interactions with caecum epithelia was concluded. Although the majority of trophozoites were motile over hours, some trophozoites became sessile (Fig. 3.40 A). This behavior was mostly observed in crypts, possibly due to lower flow rates in this protected location. This is supported by the observation that some trophozoites could be flushed by increasing

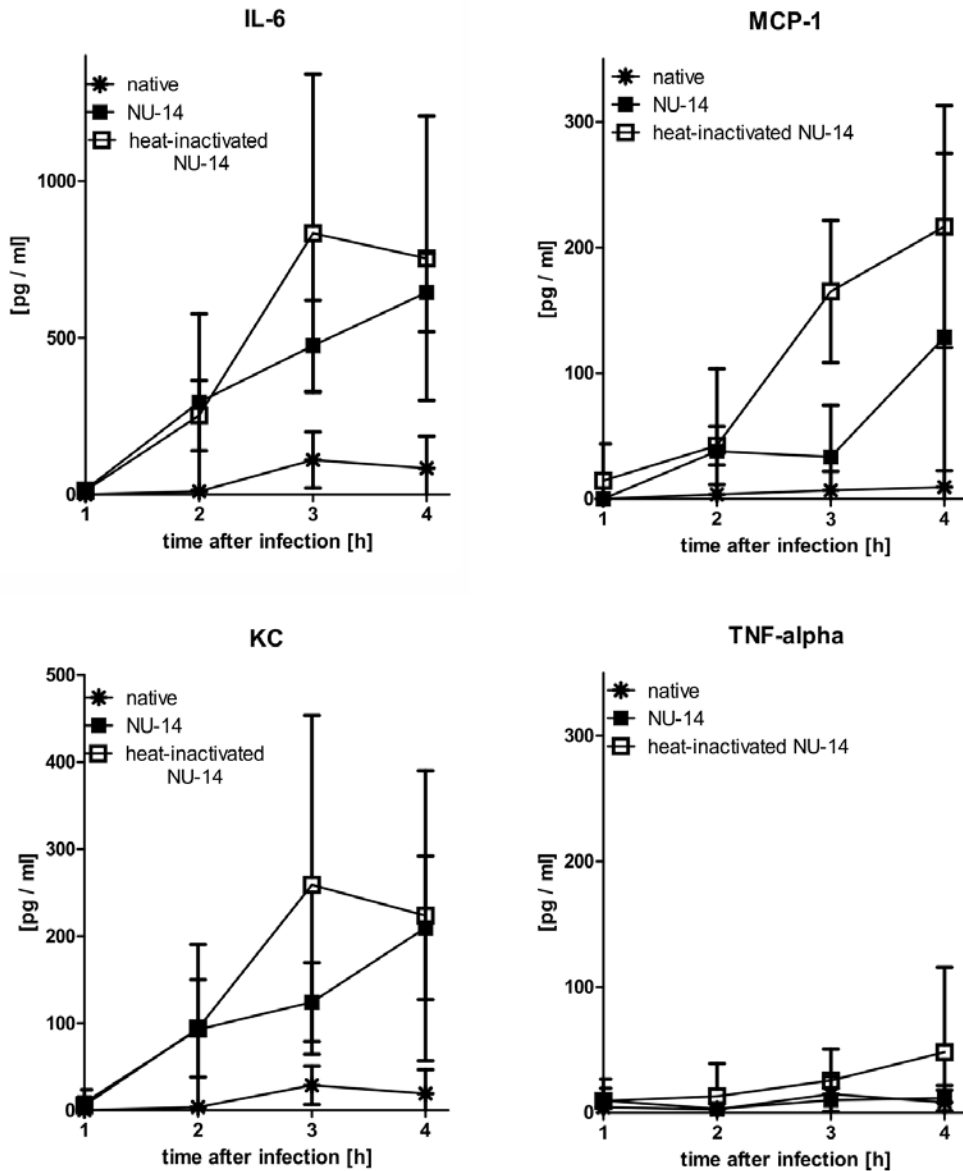


Figure 3.39: Cytokine patterns of ex vivo infected urinary bladders from C57BL/6 mice. Urinary bladders were explanted and infected with 3×10^8 cfu NU14 from stationary phase or the same amount of heat-inactivated bacteria. IL-6, MCP-1, KC and TNF- α release were measured at 1, 2, 3 and 4 h post ex vivo infection. Infection with both live and heat-inactivated NU14 led to dramatic increase in IL-6, MCP-1 and KC release. Sample size 50 μ l. Native mice: n = 5; infected mice: n = 3.

the flow rate in the apical compartment (Movie 54). 2 h p.i. single detached enterocytes could be detected, similar observations have been described *in vivo* due to extracellular amoeba proteases (Stanley, 2001). A low proportion of trophozoites succeeded in invading the mucosal barrier. Representatively shown are an amoeba invading caecum mucosa (Fig. 3.40 B and Movie 55) and an amoeba located in the lamina propria after successful penetration of the epithelial barrier (Fig. 3.40 C).

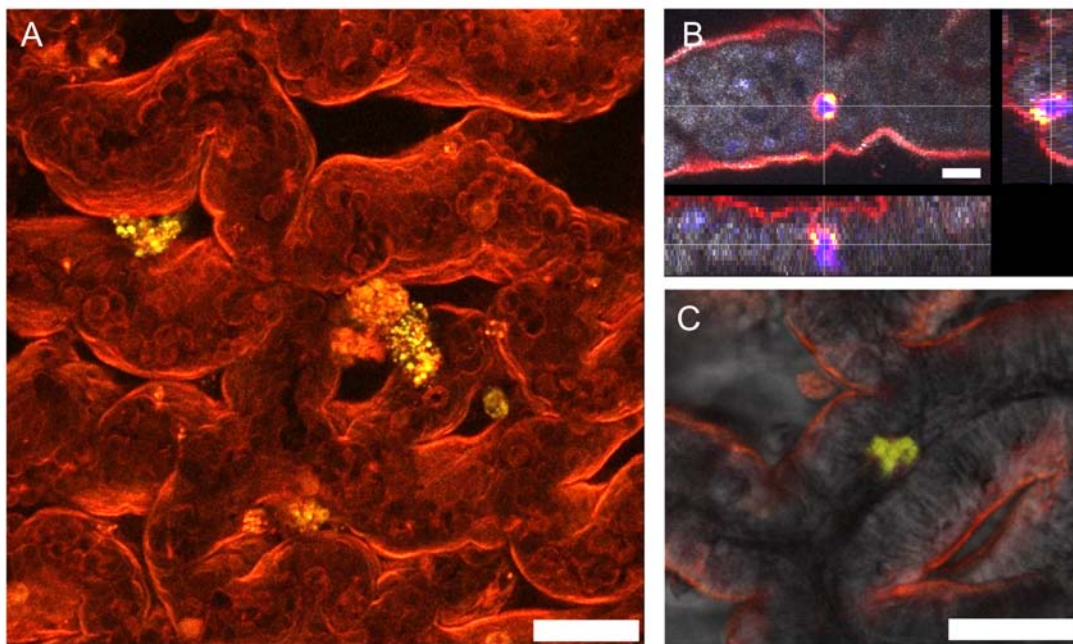


Figure 3.40: Interaction of *E. histolytica* trophozoites with caecal mucosa surface. Caecum explants from C57BL/6 mice were infected with 3.8×10^4 amoebae and analyzed by confocal microscopy. **A:** Sessile trophozoites in crypts of the mucosa. Amoebae staining is granular, presumably due to endocytic uptake of the dye into vacuoles. z projection of 9 z sections spanning a total depth of 48 μm . Scale bar 50 μm . **B:** Trophozoite after invasion of the mucosa. The localization can be seen in more detail in Movie 55. Scale bar 10 μm . **C:** Trophozoite after penetration of the epithelium inside the lamina propria. Scale bar 50 μm . Red: FM 4-64-stained cell membranes. Yellow: rWGA-Alexa680-stained *E. histolytica* trophozoites. Blue: DAPI-stained nuclei. White: Confocal reflection microscopy.

3.2.4 Extension of the system to other organs and pathogens

In order to prove applicability of the presented organ chamber system to other hollow organs, it was adapted to gut and stomach explants from *lys-EGFP* and *CX₃CR1-GFP* mice. Analysis of villi revealed presence of *lysM*- and *CX₃CR1*-positive cells in the depth of the villus (Fig. 3.41 A, C). During *ex vivo* infection of a C57BL/6 small intestine explant with *S. enterica* serovar typhimurium (pTurboYFP-B), adherence to the villus

mucosa could be shown (Fig. 3.41 B, arrowhead). Dendritic cell extensions as small as 0.5 μm in diameter were detected in villi from *CX₃CR1-GFP* mice (Fig. 3.41 D). Putatively endogenous small filamentous bacteria (Gaboriau-Routhiau *et al.*, 2009) were detected in terminal ileum explants of *lys-EGFP* mice (Fig. 3.41 E). They were firmly anchored to the mucosa and were found to be in contact with neutrophils (Movie 56). Stomach explants from a *lys-EGFP* mouse exhibited a reticular arrangement of GFP-positive cells in the lamina propria (Fig. 3.41 F).

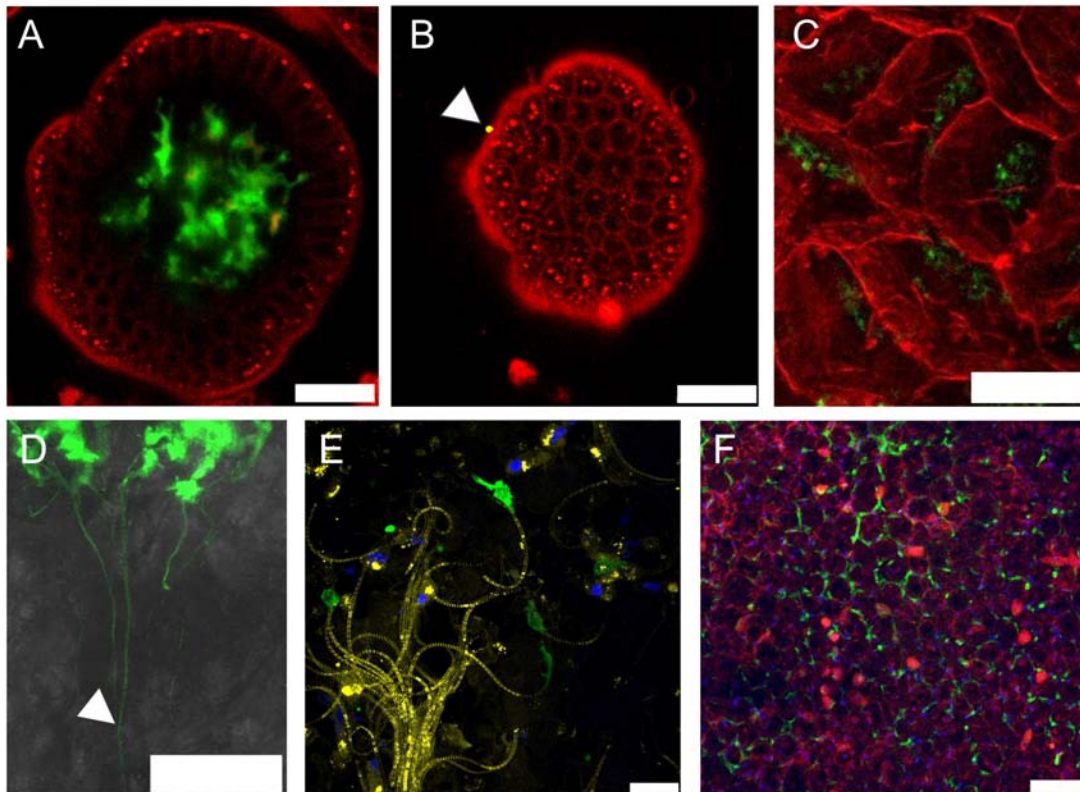


Figure 3.41: Application of the organ chamber to other hollow organs. The organ chamber can be adapted to the study of host-pathogen interactions in other hollow organs. Various tissues were explanted and mounted in the organ chamber. **A:** Section of a villus of the small intestine of a *CX₃CR1-GFP* mouse. In the depth of the villus, a network of putatively *CX₃CR1*-positive dendritic cells can be seen. Red: FM 4-64-stained cell membranes. Green: GFP-positive cells. Scale bar 25 μ m. **B:** Section of a villus of the small intestine of a C57BL/6 mouse. After *ex vivo* infection, a *S. enterica* cell was found in association with the villus surface. Red: FM 4-64-stained cell membranes. Yellow: *S. enterica*(pTurboYFP-B). Scale bar 25 μ m. **C:** z projection of several sections of small intestine tissue from a *lys-EGFP* mouse. In the depth of the villi, *lysM*-positive cells were located. Red: FM 4-64-stained cell membranes. Green: GFP-positive cells. Scale bar 100 μ m. **D:** Detail of dendritic cell extensions of a *CX₃CR1-GFP* mouse in the small intestine. Green: GFP-positive cells. White: bright field channel. Scale bar 25 μ m. **E:** Endogenous population of putatively small filamentous bacteria (SFB) on gut epithelium. SFBs were found in gut tissue from *lys-EGFP* mice. Neutrophils adhere to and try to ingest SFBs. The movie from which this frame was taken is shown in Movie 56. Yellow: FM 4-64-stained cell membranes. Green: GFP-positive cells. Blue: DAPI-stained nuclei. Scale bar 25 μ m. **F:** z projection of several sections of a stomach explant from a *lys-EGFP* mouse. *lysM*-positive cells are arranged in a reticular network below the mucosal cell layer. Red: FM 4-64-stained cell membranes. Green: GFP-positive cells. Blue: DAPI-stained nuclei. Scale bar 100 μ m.

Chapter 4

Discussion

4.1 3D-CoG based model

4.1.1 Development of the 3D-CoG/spleen slice infection model

3D-CoG-based systems have been used in various fields of cell biological research for many years. Hereby, the predominant aspect is the introduction of a third dimension in cell culture systems (Saltzman *et al.*, 1992). Fundamental aspects of the mechanics of amoeboid immune cell migration have been revealed in this system (Lämmermann *et al.*, 2008). Another study reported on the role of environmental dimensionality in host cell-fungi interactions (Behnsen *et al.*, 2007). Furthermore, it has been shown that even growth behavior of bacteria in 3D-CoG differs from that in suspension, e. g. *Y. enterocolitica* exhibits tissue-like growth behaviour in this system (Freund *et al.*, 2008). However, the implication of such bacterial microcolony formation for the recruitment of neutrophils in a three dimensional setup has not been addressed yet. Therefore, such a system was further developed to allow the study of neutrophil-pathogen interactions in a 3D-CoG setup. For this purpose, a novel approach for the recovery of neutrophils from native spleen slices for *in vitro* assays has been established for the first time (3D-CoG/SSIM, Fig. 3.2, p. 47). This setup promises several advantages in comparison to the application of neutrophils isolated from blood or bone marrow: Firstly, manipulation of neutrophils due to an isolation procedure is avoided and thus prevents unwanted stimulation of neutrophils. Moreover, their inherent ability of amoeboid migration in 3D-CoG leads to neutrophil enrichment due to migration into the 3D-CoG. Secondly, spleen slices provide a steady supply of native murine neutrophils throughout the experiments by acting as ‘neutrophil-

soaked sponges' (Fig. 3.1, p. 47). However, this model can be used with isolated neutrophils from other sources as well (e. g. human neutrophils isolated from peripheral blood, dHL60 cell line). Thirdly, neutrophils from various transgenic or knock out mouse strains can be used in this system in future studies to assess the impact of gene deletions on specific host-pathogen interactions.

4.1.2 *Staphylococcus aureus* abscess formation

4.1.2.1 Coagulase-mediated encapsulation of microcolonies

In this work, growth behavior of *S. aureus* in a 3D-CoG setup supplemented with fibrinogen as a surrogate of host tissue environment was analyzed. When *S. aureus* Newman is cultivated in liquid cell culture medium RPMI 1640 without agitation, bacterial clusters of variable size are formed. This is independent of the gene products of *ica*, *eap*, *emp*, *vWbp* or *coa*. Similar growth behavior of *S. aureus* was observed in 3D-CoG. The bacterial clusters were somewhat more compact due to spatial restriction by collagen fibers. Attachment of single staphylococci to collagen fibers was not observed. This can be explained by the fact that strain Newman lacks the collagen binding adhesin CNA (Mascari and Ross, 2003). This leads to the conclusion that the 3D-CoG serves as an almost inert fibrillar collagen meshwork for strain Newman. Consequently, the 3D-CoG can be used as a migration substrate for neutrophils when studying staphylococci-neutrophil interactions.

A characteristic feature of *S. aureus* is its capability to convert fibrinogen into fibrin by activating prothrombin via the secreted proteins Coa and vWbp. Therefore human fibrinogen was added to the assay (3D-CoG/Fib). Under these conditions, *S. aureus* strain Newman formed regular microcolonies which are surrounded by two concentric structures: an inner spherical pseudocapsule and an outer dense microcolony-associated meshwork (MAM) (Fig. 3.3, p. 49). Both obviously contained fibrin as they could be degraded by plasmin (Fig. 3.6, p. 51). This architecture resembled that of staphylococcal abscess communities (SAC) in experimental murine infection described by Cheng *et al.* (2009, 2010) and Sawai *et al.* (1997). The staphylococcal clotting factors Coa and vWbp could be shown to be required for the formation of these structures.

Firstly, Coa was detected in association with the pseudocapsule by immunostaining (Fig. 3.7, p. 53). This suggests that Coa is retained and accumulated in the vicinity of the pseudocapsule where it is likely involved in cleaving fibrinogen to fibrin by forming a proteolytic complex with prothrombin. Furthermore, it was demonstrated that a *coa*

mutant strain formed more irregularly shaped pseudocapsules. This seems to influence the shape of the microcolony.

Secondly, formation of the MAM was not affected in a *coa* mutant but completely abolished in a *vWbp* mutant (Fig. 3.9, p. 55). From this, one can conclude that *vWbp*, and not *Coa*, is the clotting factor involved in MAM formation. Assuming that the *coa* mutant is producing only *vWbp* as clotting factor, this means that *vWbp* is also able to partially take over *Coa* function by supporting partial formation of the pseudocapsule.

Based on these observations the following model is proposed (Fig. 4.1): single *S. aureus* cells give rise to microcolonies during growth in 3D-CoG/Fib. Staphylococcal clotting factors *Coa* and *vWbp* mediate conversion of soluble fibrinogen to insoluble fibrin. This leads to fibrin deposition in the vicinity of the microcolony, resulting in two independent structures: an inner pseudocapsule and an outer MAM. *Eap* and *Emp* are apparently not required for the formation of these structures, though *Emp* localized on or within the pseudocapsule in a similar manner to *Coa*.

It is of note that both *Coa* and *vWbp* have no direct proteolytic activity for fibrinogen conversion but they hijack the host clotting machinery by activating prothrombin independently of the coagulation cascade (Friedrich *et al.*, 2003; Kroh *et al.*, 2009). Traces of prothrombin, plasminogen and vWF can be present in commercially available fibrinogen prepared from human plasma. Obviously, even these prothrombin traces appear to be sufficient for the observed clotting activity of *S. aureus* in 3D-CoG. However, during the study a fibrinogen batch was encountered which did not induce the described encapsulation. In that case addition of 2-5 µg/ml prothrombin to 3D-CoG/Fib restored the phenotype.

Both *Coa* and *vWbp* are members of the bifunctional zymogen activator and adhesion protein (ZAAP) family: besides their prothrombin-binding and -activating function, they possess binding properties for other host proteins such as fibrinogen and vWF (Bjerketorp *et al.*, 2004). Moreover, vWF is capable of binding collagen fibers (Cruz *et al.*, 1995). It has been discussed that such binding activities might be responsible for localized coagulation activity by acting as a homing device to direct these proteins to a certain spatial context after release from staphylococci. The presented results support this hypothesis by spatial dissection of the clotting activity due to the formation of two discrete capsule-like structures. This is further corroborated by a recent study in a mouse infection model which reports that *Coa* is localized to a pseudocapsule enclosing the staphylococci, whereas *vWbp* was also found more distant in the abscesses (Cheng *et al.*, 2010). In consequence, *Coa* activity

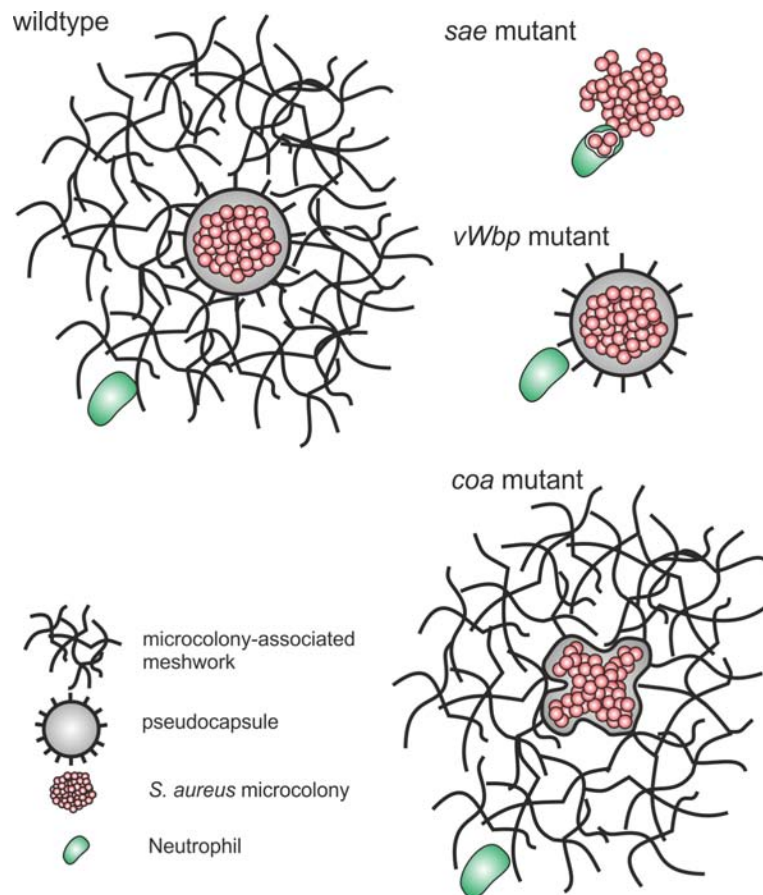


Figure 4.1: Proposed model for the differential actions of Coa and vWbp. *S. aureus* Newman forms two concentric barriers in the presence of fibrinogen in the growth medium: the outer MAM and the inner pseudocapsule; both contain fibrin. The MAM is dependent on vWbp and inhibits neutrophil immigration into the vicinity of the microcolony. The pseudocapsule is partially dependent on Coa and acts as a second barrier preventing neutrophil invasion of the microcolony.

might be restricted to a narrow zone of the microcolony interface, probably by binding to a released staphylococcal protein or via a host-derived bridging molecule. From this localization it might exert a short-distance effect on fibrinogen conversion, resulting in pseudocapsule formation. In contrast, vWbp acts preferentially in the periphery of the microcolony, mediating the formation of the MAM (long-distance effect).

These conclusions are supported by the growth behavior of the *saeRS*-mutant which is impaired in secretion of Coa and vWbp and thus is unable to form the MAM or the pseudocapsule. This supports that *saeRS* directly or indirectly controls *coa* and *vWbp* expression.

4.1.2.2 Endogenous degradation of microcolonies

Another important virulence mechanism of *S. aureus* is its ability to degrade fibrin clots which play a role in sequestering infected foci from healthy tissue in abscesses. This can lead to dissemination of staphylococci into deeper and more remote tissue. After extended periods of growth (20-40 h), single microcolonies were detected which exhibited massive growth and subsequent dispersion probably after disintegration of the pseudocapsule and MAM (Fig. 3.11, p. 56). *S. aureus* is able to induce fibrin degradation by activation of host plasminogen by staphylokinase (Giraud *et al.*, 1997). Staphylokinase secretion is positively regulated by the agr system (Sun *et al.*, 2010) and its production peaks in stationary phase (Bokarewa *et al.*, 2006). The observed occasional dispersion of a few single colonies after incubation for extended periods of time might be mediated by staphylokinase. However, staphylokinase requires plasminogen for conversion into plasmin which in turn degrades fibrin. Commercially available fibrinogen purified from human plasma is known to contain traces of plasminogen, supporting this suggestion.

4.1.2.3 Coa and vWbp cooperate in shielding microcolonies from neutrophils

Only recently, the concept of *S. aureus* hijacking the host clotting machinery to establish a protective niche has gained support from experimental mouse infection (Cheng *et al.*, 2009, 2010). In corroboration of this concept, it was of interest whether the observed two discrete fibrin capsule-like structures mediate any barrier function for immigrating phagocytes and whether pseudocapsule and MAM function differently in regard to phagocyte invasion.

Neutrophils are considered to be the first line of cellular defense of localized infections. Moreover, their predominance in abscesses formed by staphylococci has been shown

(Cheng *et al.*, 2009). As shown previously, neutrophils migrate randomly in 3D-CoG (Islam *et al.*, 1985). In the present study, unrestricted neutrophil migration towards *S. aureus* microcolonies pre-grown in 3D-CoG was observed, followed by high rates of phagocytosis. However, in the presence of fibrinogen, the vWbp-mediated MAM acted as a mechanical barrier and prevented neutrophil migration towards the staphylococcal microcolony (Fig. 3.12, p. 59). In addition to mechanical restraints imposed onto neutrophils, it is also conceivable that released *S. aureus* proteins bind to the fibrin meshwork and interfere with neutrophil signaling pathways involved in chemotaxis. This remains to be elucidated.

Strikingly, the pseudocapsule turned out to be a second safety barrier against neutrophil attack: in the absence of the MAM, neutrophils approached the interface of microcolonies but were unable to invade the pseudocapsule directly (Fig. 3.15, p. 62). The pseudocapsule appeared to be very resistant to neutrophil penetration and only after accumulation of a higher number of neutrophils at the interface of the microcolony, selected neutrophils were able to penetrate. This might be due to a bacteria-mediated dispersion mechanism degrading the pseudocapsule, or more likely due to direct degradation of the pseudocapsule by released neutrophil proteases. These neutrophils obviously gained entry to the microcolony by squeezing through small holes. The penetration of such a ‘pioneer neutrophil’ elicited a massive attraction and invasion of neutrophils to the interior of the microcolony.

Interestingly, a high rate of neutrophil cell lysis/necrosis was observed after direct contact of neutrophils with staphylococci, regardless of whether microcolonies were previously surrounded by a pseudocapsule or not (Fig. 3.15, p. 62). Probably neutrophils are killed after phagocytosis and oxidative burst or by toxic substances released by staphylococci. It is also conceivable that staphylococci reached stationary phase after pseudocapsule formation and start toxin production, resulting in ‘caged toxins’. By using mutants affected in toxin production (e. g. α -hemolysin), it should be possible to unravel the mechanism of this staphylococci-induced neutrophil cell death after pseudocapsule rupture. Of note, it has been reported recently that CA-MRSA strains induce a form of programmed necrosis (Kobayashi *et al.*, 2010).

Taken together, both the pseudocapsule and the MAM exert a strong barrier function for neutrophils and protect staphylococci against phagocytosis. However, compared to the rapid phagocytosis of staphylococci after barrier breakdown, this suggests that other reported anti-phagocytosis activities, e.g. ClfA-mediated phagocytosis inhibition (Higgins *et al.*, 2006), are minimal compared to this massive phagocytosis inhibition.

Various studies have shown that strain Newman differs from other *S. aureus* model strains, mainly due to a missense mutation in *saeS* resulting in derepression of protein secretion (Mainiero *et al.*, 2010). In order to clarify, whether the results obtained with strain Newman are unique, experiments with the CA-MRSA strain USA300 were performed and revealed similar characteristics. This is in line with the reported pseudocapsule of strain USA300 in the mouse infection model (Cheng *et al.*, 2009).

4.1.2.4 Pharmacological interference with encapsulation

Several thrombin inhibitors have been reported to inhibit Coa-mediated activation of prothrombin (Vanassche *et al.*, 2010; Hijikata-Okunomiya and Kataoka, 2003). The degradability of the pseudocapsule and the MAM by plasmin suggests a possible impact of such agents on the growth phenotypes of *S. aureus* in 3D-CoG/Fib and on the barrier functions for neutrophils. Indeed, argatroban, a thrombin inhibitor in clinical use, prevented pseudocapsule and MAM formation in a concentration-dependent manner, and thereby enhanced neutrophil access to staphylococci (Fig. 3.16, p. 63). As MAM formation could be assigned exclusively to vWbp, an indirect inhibitory effect of this drug on vWbp-mediated fibrin formation could be shown for the first time.

This result provides one with an attractive therapeutic option in combating staphylococcal infections: By hijacking host machinery and relying on this mechanism for virulence, *S. aureus* offers a specific host-derived target. This target is well characterized, not least for its importance in coagulation-associated diseases. Early access of neutrophils to staphylococci can be expected to counteract this virulence advantage gained by usurping host machinery. Future studies based on 3D-CoG/Fib and the mouse infection model should be initiated to study the effect of thrombin inhibitors on antibiotic sensitivity of *S. aureus* microcolonies.

Furthermore, it should be mentioned that a species specificity for various clotting-related *S. aureus* proteins has been shown: staphylokinase shows high activity towards human but only limited activity towards murine plasminogen (Kwieciński *et al.*, 2010), coagulase activates bovine and rabbit prothrombin only weakly compared to human prothrombin (Friedrich *et al.*, 2006), and recently it has been shown, that certain *S. aureus* strains carry species-specific vWbp alleles (Viana *et al.*, 2010). Thus, the presented 3D-CoG infection model can be useful in the study of such host specificities by supplementing the system with the protein or cell of interest.

Taken together, the 3D-CoG model in combination with native spleen slices is a suitable *in vitro* infection model to study both *in vivo*-like growth characteristics and the resulting phagocyte-microbe interactions. It opens a broad field of applications by complementing established animal infection models for the development of new treatment options for infections.

4.1.3 Inhibition of immune cell migration by *Yersinia*

4.1.3.1 Implications of *Yersinia* microcolony formation

Previously, the 3D-CoG system has been established to study pYV-dependent *Yersinia* growth behavior (Freund *et al.*, 2008). pYV-dependent microcolony formation resembling *in vivo* microcolonies (e. g. in spleen lesions) was observed. The head domain of YadA has been shown to be crucial for the formation of densely packed (DP) microcolonies, whereas Invasin had no effect. In order to gain a better understanding of this microcolony formation, the first hours of of this event were analyzed by microscopy (Fig. 3.17, p. 65). Single *Yersinia* cells undergo cell division and do not separate thereafter, but form chains of rods. These curl up and eventually form ‘ball of wool-like’ microcolonies. In the absence of YadA, the curling up is less close, leading to the previously described loosely packed (LP) microcolonies. Furthermore, WA(pYV Δ yadA) microcolonies were preferentially found on the bottom of the wells (Fig. 3.17, p. 65), suggesting a lack of interaction with collagen fibers and thereby emphasizing the role of YadA in collagen binding (Roggenkamp *et al.*, 1995). Interestingly, a newly constructed *inv yadA* double mutant formed unstable bacterial chains and thus completely lost the ability of microcolony formation, similar to the pYV-cured strain WA-C. This suggests either secondary regulatory effects of this deletion or an involvement of Inv in inhibition of cell-cell separation and thereby microcolony formation. In the latter scenario, bacterial aggregation via YadA must be able to compensate for a loss of Inv in regard to microcolony formation but not vice versa because deletion of *inv* alone had no effect on microcolony formation. Moreover, this would suggest that LP microcolonies of WA(pYV Δ yadA) are held together solely via Inv. One might also speculate a mutual influence of these two proteins on their localization in the bacterial membrane which might lead to this growth phenotype. For instance, polar localization of non-fimbrial bacterial adhesins with autotransporter properties has been shown and thus might impair cell-cell separation during replication (Charles *et al.*, 2001; Jain *et al.*, 2006).

In order to analyze whether the microcolony structure (DP or LP) predominantly affects the interaction with neutrophils, WA(pYV) and WA(pYV Δ yadA) were compared in 3D-CoG/SSIM in regard to phagocytosis inhibition (Fig. 3.18, p. 66). Both strains appeared to be resistant to phagocytosis, pointing to the T3SS as the primary mechanism of antiphagocytosis in this setup, in line with results from cell culture infection models (Grosdent *et al.*, 2002).

Taken together, the established 3D-CoG/SSIM is able to monitor both microcolony formation and subsequent neutrophil interaction. It thus opens up new possibilities to study the effects of T3SS effectors in a context with tissue-like dimensionality which will be of high relevance for understanding the involvement of microcolony formation in *Yersinia* infection.

4.1.3.2 Yop effects on amoeboid leukocyte migration

The effects of Yops on various mammalian cell types have been studied in detail and revealed an impressive anti host-stratagem of *Yersinia* (Heesemann *et al.*, 2006). Eukaryotic cells are affected on many levels, such as adhesion, signaling pathways and cytoskeletal integrity. One focus of this work was to study the interaction of *Yersinia* with migratory immune cells in a more tissue-like context in regard to dimensionality, compared to classical cell culture assays based on cell suspensions or adherent cell monolayers. To this end, neutrophils were chosen as they are the first line of the cellular host immune defense. *Yersinia*-neutrophil interactions in 3D-CoG resulted in a peculiar elongated morphotype of neutrophils, suggesting *Yersinia*-specific inhibition of amoeboid neutrophil migration (Fig. 3.19, p. 67 and Movie 57). This elongated morphotype includes both properties of a postulated ‘tranquilizing kiss’, in that cells became partially stuck to yersiniae, and of a ‘kiss & run’ mechanism, in that neutrophil leading edges remained highly active (Heesemann *et al.*, 2006). This feature of ‘frustrated migration’ was studied further to clarify which individual Yops are involved in the cell biological mechanisms of this neutrophil morphotype.

Neutrophils are endowed with the capacity to migrate towards bacteria and subsequently take up and destroy the pathogen (Nathan, 2006). They are equipped with various receptors specific for pathogen associated molecular patterns (PAMPs) and chemotactic oligopeptides (fMLP) which orchestrate chemotactic behavior. Upon reaching the bacteria, various receptors on the neutrophil can bind to the microbe and trigger phagocytosis. There is overlap between regulation of these events and migration. Thus, prevention of phagocytic events is a prerequisite for a cell biological analysis of single Yop effects on migratory behavior of the phagocyte. For this purpose, dendritic cells (DCs) were chosen as a model system for amoeboid migration. After LPS-stimulation, dendritic cells downregulate endocytic machinery and upregulate CCR7 chemokine receptor which is responsive to CCL19 (Garrett *et al.*, 2000; Platt *et al.*, 2010; e Sousa, 2006). Furthermore, LPS-

stimulated DCs are not responsive to the bacteria-derived chemotactic compound fMLP, which is introduced into the system with bacteria during *in vitro* infection (Foti *et al.*, 1999; Yang *et al.*, 2000). Most importantly, DCs exhibit similar migration mechanics as neutrophils by relying on amoeboid migration in 3D-CoG (Lämmermann *et al.*, 2008).

The validity of this model was proven by the fact that pre-infection with the T3SS-deficient strain WA(pYV Δ *lcrD*) did not decrease the percentage of migratory cells in 3D-CoG ($\sim 70\%$), whereas WA(pYV) strongly affected migratory behavior ($\sim 21\%$). Using a set of *Y. enterocolitica* mutants it could be shown for the first time that solely YopT was responsible for long-term inhibition of migration in *Y. enterocolitica* (Fig. 3.21, p. 69). YopT is a cysteine protease, cleaving the isoprenylated C-terminal cysteine of membrane-anchored RhoA (Zumbihl *et al.*, 1999; Shao *et al.*, 2003). This delocalization from the membrane probably results in inhibition of coordinated RhoA signaling which is involved in detachment of the uropod (Lämmermann *et al.*, 2008). Additional experiments with a ROCK inhibitor supported the contribution of RhoA-inhibition by YopT to this morphotype (Fig. 3.24, p. 74).

For cell biological analysis of this morphotype, DCs expressing fluorescent probes (Lifeact-GFP, MLC-GFP) were analyzed in under-agarose assays. This is a conventional assay to study amoeboid migration of leukocytes similar to 3D-CoG. However, dimensional restriction to a plane perpendicular to the microscope light path allows analysis of fluorescent probes distribution at higher temporal resolution.

After contact with WA(pYV), DCs became elongated and occasionally developed uncoordinated multiple leading edges (Fig. 3.22, p. 71) instead of maintaining a single stable leading edge supporting constant forward motion in the direction of the chemokine gradient (Renkawitz *et al.*, 2009). Moreover, retraction of the trailing edge appeared to be paralyzed.

Myosin II distribution in DCs, visualized by MLC-GFP, was not immediately affected after contact with yersiniae, irrespective of T3SS function (Fig. 3.22, p. 71 and Movie 19, 20) (Renkawitz *et al.*, 2009). This suggests normal assembly of myosin II structures immediately after Yop translocation. Indeed, contraction of actomyosin filaments is regulated by the RhoA effector ROCK, mediating downstream phosphorylation events which increase Mg^{2+} -ATPase activity of myosin, rather than by myosin II localization (Vicente-Manzanares *et al.*, 2009).

Actin dynamics could be visualized in DCs expressing Lifeact-GFP. Normally, force generation by actin polymerization is coupled to the substrate via receptors and leads to forward movement of cell protrusions (Renkawitz *et al.*, 2009). Strikingly, after massive cell elongation induced by WA(pYV), the uncoordinated multiple leading edges of DCs were highly active (Movie 21). However, instead of forward movement of the protrusions, actin tread-milling was observed in these structures. Either force coupling to the substrate might be affected due to membrane stress resulting from the massive cell elongation or the respective receptors might have been targeted by Yops. Further studies have to clarify this.

Taken together, YopT is the unique *Y. enterocolitica* Yop which affects amoeboid cell migration rapidly after translocation. Strikingly, other Yops known to interfere with Rho GTPase family members, such as YopE or YopO, did not show such a pronounced and immediate effect on LPS-stimulated DCs as YopT. According to the literature, RhoA is the main target of *Y. enterocolitica* YopT (Aepfelbacher *et al.*, 2003) and the described results are in line with this effect on DCs.

Until now, the effects of *Y. enterocolitica* YopT on amoeboid cell migration have not been addressed yet. The following mechanistic model is suggested: Upon translocation to the cytosol, YopT_{yen}-mediated cleavage of membrane-anchored RhoA disrupts its spatially restricted signaling function (Shao *et al.*, 2003). This impedes the downstream function of RhoA in mediating contractility in the trailing edge of the migrating cell (Lämmermann *et al.*, 2008). Furthermore, polar organization of the cytoskeleton in infected cells is lost in that multiple leading edges can be developed in an uncoordinated manner. This process is physiologically regulated by e. g. Cdc42 (Lämmermann *et al.*, 2009). As Cdc42 is not a primary target of YopT (Aepfelbacher *et al.*, 2003; Fueller and Schmidt, 2008), involvement of other Rho GTPases has to be addressed in further studies. However, actin polymerization in the leading edge(s) of infected cells was unaffected, although force coupling to the substrate seems to be defective, possibly due to the reasons mentioned above. This observation does not contradict the so called ‘cytotoxic’ effect of YopT (Trosky *et al.*, 2008) but rather demonstrates a more fine-tuned interference with cellular signaling pathways. Moreover, there is evidence that GTPase-targeting by YopT depends on the infected cell type (Schmidt, 2011). Previous results showed selective disintegration of actin stress fibers by YopT in endothelial cells (Zumbihl *et al.*, 1999) and pronounced ruffling in human macrophages (Aepfelbacher *et al.*, 2003). RhoA has two major effectors in cells,

Rho kinase ROCK and the formin mDia. In short, mDia catalyzes actin nucleation and polymerization, whereas ROCK kinase amongst other effects increases myosin light chain phosphorylation, which leads to cross-linking of actin by myosin and enhances actomyosin contractility. Potential antagonism of these two pathways is suggested and might result in RhoA exerting both stimulatory and inhibitory actions on Rac, depending on the downstream signaling events (Narumiya *et al.*, 2009). Of note, it is still unclear, if GTP-bound RhoA retains activity after delocalization from the membrane, similar to Rac1 (Wong and Isberg, 2005). This might shift RhoA signaling towards either of the two branches. However, there is experimental evidence that complete inhibition of RhoA with C3 exoenzyme or specific inhibition of ROCK with Y-27632 leads to elongated cell shape in e. g. neutrophils (Yoshinaga-Ohara *et al.*, 2002). Moreover, Cdc42 and Rac, which are probably not directly targeted by *Y. enterocolitica* YopT (Fueller and Schmidt, 2008), induce lamellipodia formation via Arp2/3-mediated nucleation of branched actin filaments (Ridley, 2006; Mejía *et al.*, 2008).

Finally, the initial question of whether a ‘kiss & run’ or a ‘tranquilizing kiss’ mechanism predominates, has to be answered in an appropriate, three dimensional context (Fig. 4.2, p. 112): *Y. enterocolitica* affects the cytoskeleton profoundly via YopT, causing a ‘tranquilized’ trailing edge of the cell, while leaving the leading edge ‘run’. Additionally, coordination of the leading edge is occasionally disturbed due to the lack of the negative control element RhoA. In under-agarose assays, DCs located in the liquid-filled gap between agarose and coverslip retain their ability to translocate their nuclei until overall cell length is massively increased. In contrast to this, DCs develop multiple actively protruding leading edges but show less net nucleus locomotion in 3D-CoG. This setup imposes a higher spatial restriction on DCs compared to under-agarose assays due to its meshwork structure. Thus, the presence of multiple uncoordinated leading edges leads to rapid entanglement of the cell in the collagen matrix. In addition, contractility in the trailing edge is affected which is necessary for deforming the bulky nucleus for translocation through narrow pores. Lowering the collagen concentration – and by that lowering spatial restriction – partially alleviates cell migration of infected DCs. Spatial restriction of nucleus locomotion can also be observed for infected DCs initiating migration from the responder well in under-agarose assays towards the CCL19 gradient. Taken together, DCs lose their high plasticity immediately after contact with *Y. enterocolitica*.

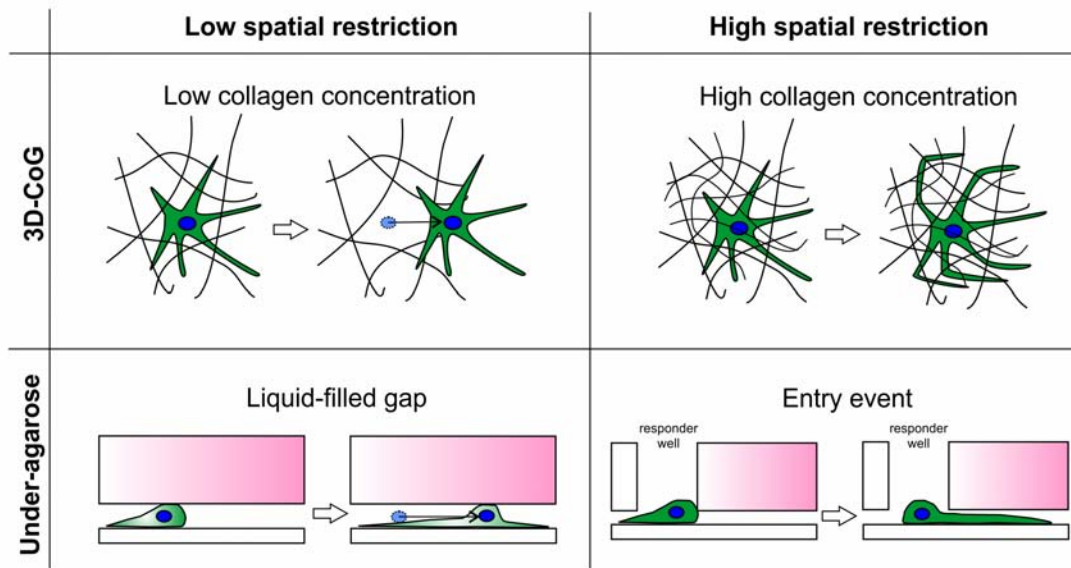


Figure 4.2: Effects of *Y. enterocolitica* YopT-mediated migration of inhibition. This schematic sketch illustrates the effect of YopT_{yen} on DC migration in setups with different spatial restriction. Contractility in the trailing edge of the cell is inhibited by inactivation of RhoA by YopT_{yen}. At low restriction, the entire cell body of YopT_{yen}-affected cells, including the nucleus (depicted in blue), can be translocated, whereas at high spatial restriction, the rigid nucleus is captured and anchors the moving cell body. In 3D-CoG, spatial restriction is dependent on collagen concentration; in under-agarose assays, the entry event of squeezing underneath the agarose obviously imposes high spatial restriction.

DCs were used as a model system, though the characteristic effect of YopT_{yen} was also observed with murine spleen neutrophils, migration-competent murine bone marrow cells and human neutrophils isolated from peripheral blood (Fig. 3.25, p. 75). This suggests that the observed morphotype is not cell-type specific and that the general mechanism of amoeboid cell migration is targeted by *Yersinia*.

Taken together, YopT_{yen} effects were analyzed in DCs and neutrophils in respect of amoeboid migration for the first time. Studies using Yop- β -lactamase fusion reporter constructs have shown that these cell types are preferentially targeted by *Yersinia* (Marketon *et al.*, 2005), emphasizing the importance of these cell types in *Yersinia* infection. Considering microcolony formation *in vivo*, YopT_{yen}-mediated paralysis of migrating immune cells might establish a protected niche for bacterial replication inside microcolonies as not only phagocytosis but also invasion of the microcolony structure is inhibited by WA(pYV) compared to WA(pYV Δ lcrD) (Fig. 3.18, p. 66). Furthermore, as WA(pYV) did not induce necrosis in host cells (Fig. 3.29, p. 80), it is conceivable that paralyzed but viable host cells support growth of *Y. enterocolitica* in tissue. Future studies in 3D-CoG/SSIM will focus on these aspects, as well as on cytokine release.

4.1.3.3 *Yersinia* species-dependent cellular effects of YopE and YopT

4.1.3.3.1 Effects on cell migration As mentioned above, differences in Rho GTPase specificities between YopT_{yen} and YopT_{ypp} have been reported: YopT_{yen} acts preferentially on RhoA (Zumbihl *et al.*, 1999), whereas YopT_{ypp} appears to exhibit a broader activity by additionally targeting Rac1, Cdc42 (Wong and Isberg, 2005) and RhoG (Mohammadi and Isberg, 2009). Different Rho GTPase targets are also discussed for YopE which functions as a GAP. YopE_{yen} inhibits Rac1-mediated actin rearrangements via direct downregulation of Rac1 (Andor *et al.*, 2001) or indirectly via inactivation of the Rac1-upstream RhoG/Elmo-Dock180 signaling complex (Roppenser *et al.*, 2009), whereas YopE_{ypp} is suggested to additionally target RhoA (Aili *et al.*, 2006).

YopT. It is conceivable that such *Yersinia* species-dependent specificity is reflected in unique cellular effects. Therefore the effects of *Y. enterocolitica*- or *Y. pseudotuberculosis*-derived YopE or YopT on amoeboid cell migration were studied using 3D-CoG and under-agarose assays. It could be demonstrated that both YopT_{ypp} and YopT_{yen} efficiently inhibited amoeboid migration (Fig. 3.26, p. 77). Strikingly, YopT_{ypp} prevented the formation of elongated DC protrusions, in contrast to YopT_{yen}. This discrepancy was

even more obvious in the under-agarose assay where YopT_{yps} caused unpolarized DCs with lamellipodia-like structures spanning the entire cell outline, while being unable to establish a functional uropode (Fig. 3.27, p. 79). ROCK inhibition caused a morphotype similar to that of YopT_{yen} (Fig. 3.24, p. 74). Complete inhibition of the Rho family by C3 exoenzyme (Aktories *et al.*, 2005) has been described in the literature to have a similar effect in various cell types (Narumiya *et al.*, 2009). Corresponding to this, the distinct YopT_{yps}-morphotype must be influenced by additional molecular mechanisms. Another highly interesting observation of YopT_{yps}-effects on DCs was that actin polymerization in the cell-spanning lamellipodium-like structure appeared to be at near maximal rates (>15 $\mu\text{m}/\text{min}$, Fig. 3.28, p. 80) when compared with published results on amoeboid DC migration (Renkawitz *et al.*, 2009). In the latter study it has also been shown that DCs increase actin polymerization rates in response to uncoupling force transduction from the actin cytoskeleton to integrin receptors. Thus, besides cell polarization, YopT_{yps} seems to affect also the force transduction of the actomyosin machinery of DCs to the underlying substrate. Whether this is due to disengagement of specific cellular receptors remains to be elucidated.

YopE. As has been reported previously, YopE_{yen} targets Rac1 and RhoG (Andor *et al.*, 2001; Roppenser *et al.*, 2009) and therefore it seems to be plausible that YopE_{yen} should affect cell migration. However, this was not observed with DCs using the mentioned cell migration assays. In contrast to this, YopE_{yps} severely affected migration of these cells (Fig. 3.26, p. 77 and Fig. 3.27, p. 79). Hentschke *et al.* (2007) showed that YopE_{yen} from serogroup O:8 is subjected to ubiquitination and subsequent proteasomal degradation and they could alleviate this effect by replacement of two lysin residues of YopE_{yen} which are crucial for polyubiquitination (K62, K75). Of note, these lysin residues are unique for YopE from *Y. enterocolitica* serotype O:8 and are not found in YopE_{yps}. An increased cytotoxicity (cell rounding) of YopE_{yenK62R,K75Q} in HEK293 cells has been shown (Gaus *et al.*, 2011). Using this modified YopE_{yenK62R,K75Q} with DCs, decreased migration of DCs in 3D-CoG was found in contrast to YopE_{yen} (Fig. 3.26, p. 77). However, YopE_{yps} had a considerably stronger effect on DCs than YopE_{yenK62R,K75Q}, which suggests additional functional differences between YopE_{yen} and YopE_{yps} besides protein stability in the cytosol. Another proposed mechanism to explain the Rho GTPase specificities is assigned to differences in intracellular localization of YopE. The region comprising amino acid residues 54-75 of YopE has been termed membrane localization domain (MLD) due to its involve-

ment in YopE association with cytoplasmic or endosomal membranes (Krall *et al.*, 2004; Roppenser *et al.*, 2009; Isaksson *et al.*, 2009). Rho GTPases have distinct localization inside the cell and MLD-mediated localization of YopE has been shown to determine YopE targeting to specific Rho GTPases (Roppenser *et al.*, 2009). The MLD of YopE_{yen} and YopE_{yps} differ in several amino acid residues (compare Fig. 3.31, p. 83). Future extensive cellular localization experiments could shed light on possible effects on localization and target specificity.

Taken together, this finding of unique cell biological morphotypes of YopE and YopT substantiates the hypothesis of species-dependent Rho GTPase-targeting patterns which has been suggested by other research groups previously (discussed above).

Finally, it has to be considered that the translocation rate of these Yops by the ‘toolbox strain’ WA(pTTSS, pYopX) has not been studied and differences in the actual amount of Yops in the host cytoplasm might account for some of these effects. For instance differential secretion and translocation of YopP from different *Yersinia* species has been described and attributed to polymorphisms of the N-terminus of YopP (Brodsky and Medzhitov, 2008). However, secretion of YopT_{yen} and YopT_{yps} was practically identical (Fig. 3.30 B, p. 81) and it is conceivable that the amount of translocated Yops is also dependent on *Yersinia*-DC contact time and frequency. During the presented experiments there was no indication that variation of incubation time or multiplicity of infection caused a transition between the *Y. enterocolitica*- or *Y. pseudotuberculosis*-specific morphotypes.

It is of note, that in contrast to *Y. pseudotuberculosis* serotype I, not all *Y. pseudotuberculosis* serotype III strains carry a functional *yopT* gene (Viboud *et al.*, 2006). However, both analyzed *Yps* strains, IP32953 and YPIII(pIB1) exhibited similar cytoskeletal morphotypes in migration assays, although YPIII(pIB1) is devoid of a *yopT* gene, suggesting a dominant effect of YopE_{yps}. In IP32953, the induction of near maximal rates of actin polymerization characteristic for the YopT_{yps} morphotype was obviously suppressed in the presence of YopE_{yps}. This might corroborate the finding that YopE and YopT compete for host substrates (Wong and Isberg, 2005), although effects of one Yop on the translocation rate of the other can not be ruled out yet. Future studies with single *yopE* or *yopT* mutants in IP32953 will further clarify this hypothesis. Whether the different effects of YopT_{yen} and YopT_{yps} observed *in vitro* with DCs can be translated to the *in vivo* infection process has to be demonstrated (e. g. by two photon *in vivo* microscopy).

4.1.3.3.2 Degradation of plasma membrane integrity The Yop translocation process is suggested to be initiated by the insertion of the YopB/YopD translocation pore into the host cell membrane and actin polymerization is suggested to be a prerequisite for stable pore formation. A role of YopE and YopT in closing the translocation pore via inactivation of the Rho GTPases Rac1 and RhoA in the host cell cytoplasm has been proposed for *Yersinia*-infected HeLa cells (Viboud and Bliska, 2001). As the results of the migration assays demonstrate *Yersinia* species-dependent differences of YopE- and YopT-effects on DC migration, and thereby suggest distinct molecular mechanisms, potentially due to Rho GTPase specificity, it was analyzed if these differences are also reflected in LDH release, indicating cell necrosis as a result of pore formation by the translocators.

HeLa cells responded with LDH release as expected in that only strain WA(pTTSS) lacking *yop* genes for translocation induced LDH release (Fig. 3.29, p. 80). However, neutrophils responded differently: WA(pTTSS) induced moderate release of LDH whereas strain WA(pTTSS, pYopT_{yps}) caused two-fold more LDH release than WA(pTTSS). These results might favor the hypothesis that the supposed strong Rho GTPase inhibiting activity of YopT_{yps} observed in DC migration assays is also responsible for this cytotoxicity and LDH release. The amount of YopT_{yen} and YopT_{yps} secreted into the medium upon induction was comparable, thus excluding fundamental differences in the secretion rate of both proteins. Assessing the involvement of the catalytic activity of YopT_{yps} led to surprising results (Fig. 3.30, p. 81): the necrotic effect of YopT_{yps} was mediated by the catalytic activity, whereas the ‘pore closing’ effect of YopT_{yen} was independent of it. However, it is still controversially discussed in the literature, if activity towards Rho GTPases is really needed for pore closure or if this effect is simply due to clogging by any translocated protein (Mejía *et al.*, 2008; Wölke *et al.*, 2011). Furthermore, YopQ, which has been suggested to play a role in regulating pore diameter or T3SS masking inside the host cell (Holmström *et al.*, 1997; Brodsky *et al.*, 2010; Dewoody *et al.*, 2011), is not present in strain WA(pTTSS). Thus, the results of the LDH release assay can not be transferred directly to the process of pore formation by wildtype *Yersinia*. In this context, the presented results have to be interpreted carefully and need further elucidation before drawing final conclusions.

However, some preliminary conclusions are reasonable: Firstly, the mechanism of the observed LDH release due to YopT_{yps} appears to be fundamentally different in neutrophils compared to HeLa cells. Secondly, this necrotic effect drastically differs between YopT_{yen} and YopT_{yps}, supporting the hypothesis that different members of the Rho GTPase family

might be targeted and involved in this process. Interestingly, the necrotic effect of YopT_{yps} is not seen in the *Y. pseudotuberculosis* wildtype strain IP32953, suggesting interference of another translocated Yop.

4.1.3.3.3 Homology modeling Several clear differences in the cellular effects of YopE and YopT from *Y. enterocolitica* and *Y. pseudotuberculosis* were found, the basics of which have to be biochemically characterized in subsequent studies. Chimeric proteins deriving of fragments from *Y. enterocolitica* or *Y. pseudotuberculosis*, as well as single amino acid exchange mutants, will be necessary in order to analyze the effect on potential Rho GTPase specificities. To facilitate the design of these experiments, structure models of YopE and YopT from *Y. enterocolitica* and *Y. pseudotuberculosis* were generated *in silico* and discussed in respect to sequence differences between both species (Fig. 3.31, p. 83).

YopT (Fig. 3.32, p. 84). No obvious candidates for mutagenesis could be deduced from the structure model. The most promising position in YopT is at the C-terminus of the protein, which is not included in the structure model: Interestingly, there are three amino acid exchanges in this area, which has been shown to be involved in the activity towards Rho GTPases (Sorg *et al.*, 2003). However, in the complete protein, the N-terminus (133 aa), which is not included in the structure but harbors 7 aa differences, might confer additional differences to the structure of the entire protein and should also be considered for mutagenesis studies.

YopE (Fig. 3.33, p. 85). It is of high interest, that all amino acid differences within the modeled structure are located on the opposite side of the arginine finger. Especially aa 213/214 have high preference for future site-directed mutagenesis studies as it has been shown that a deletion in this area of YopE_{yps} abrogates Rho GTPase inactivation but still mediates a cytotoxic effect on HeLa cells, a finding that has led to a debate of whether there are additional targets of YopE in the eukaryotic cell besides Rac1, RhoA and Cdc42 (Aili *et al.*, 2003). The accumulation of amino acid sequence differences within the MLD domain is a promising target for the construction of chimeric proteins containing either MLD_{yen} or MLD_{yps}. Analysis of subcellular localization of such chimeric proteins might reveal if such a mechanism plays a role for the different cellular effects, or if the above discussed differences in aa 213-214 contribute predominantly to the suggested target specificity.

4.2 Organ explant-based *ex vivo* model

4.2.1 Development of an *ex vivo* infection model

The study of host-pathogen interactions at mucosal interfaces by microscopy is a challenging venture. Cell culture systems provide only limited applicability due to the complexity of conditions at epithelial interfaces: Various different cell types are organized in a 3D context and form polarized cell layers. The isolation of single cell types can not represent *in vivo*-like conditions. The 3D architecture is based on a complex extracellular matrix which is produced by specific cell types. Taken together, a further development of cell culture systems to serve as epithelial models always faces the risk of over-simplification. Therefore, *in vivo* imaging based on two photon microscopy (TPM) in experimental animals, preferentially mice, has become a widely used method (Germain *et al.*, 2005, 2006). Here, experimental animals are anesthetized and fixed to a microscope stage. The tissue of interest is surgically exposed and brought in close proximity with the objective. While of great advantage for a multitude of applications, this method has serious restraints for the study of mucosal membranes: tissues like the urinary bladder or the gut are situated in sheltered locations of the body and not easily accessible to microscopy. Moreover, these hollow organs are subjected to autonomous muscle contractions of underlying smooth musculature. This can lead to motion artifacts in addition to those from respiration and circulation. Mechanical fixation of tissue can alleviate these disadvantages but oftentimes causes tissue trauma which may ultimately lead to unwanted inflammatory processes.

Another approach to study mucosal membranes is the use of explants: tissue is surgically removed from animals and cultivated *in vitro*. Thereby the 3D context of the tissue is preserved while vasculature, innervation and most other *in vivo* factors are sacrificed for the sake of high controllability. An early approach was the parabiotic chamber (Gabridge, 1974). However, this setup is not compatible with current confocal microscopes due to the lack of tissue fixation. Furthermore, perfusion of the tissue is rather basic and does not discriminate between apical and basal side of the epithelia.

Therefore, the presented mucosa explant-based model (Fig. 3.34, p. 87) was developed to permit dynamic imaging and measurements of secreted proteins. It can be used with both upright and inverted microscopes due to the isolation of the explant-containing compartment against the environment. A clear extension to previous models are the two independent compartments which are in contact with the basal and apical side of the or-

gan. By this, liquid composition and flow rate can be controlled independently for the two compartments and can be adapted to optimally mimic physiological conditions for different organs. Utilization of a custom-built membrane oxygenation device (Fig. 3.34 C, p. 87) allows for exact control of the gaseous contents of the medium. A similar approach has been used recently in a bioreactor (Vukasinovic *et al.*, 2009). Obviously, enrichment of medium with oxygen on the basal side of the tissue can only roughly compensate for oxygen supply by the vasculature, but for the application to relatively thin mucosal tissue diffusion is sufficient for basic supply. This is shown by a long-term experiment (8.5 h) for the urinary bladder (Fig. 3.36, p. 89): tissue preservation until 4-5 h is considered very good, subsequently single epithelial cells are detached from the organ but even after 8.5 h tissue condition was acceptable, judged from the integrity of the epithelial cell layer. This detachment of cells is probably enforced by endogenous organ movement which applies shear forces to cells in contact with the coverslip. These contractions could still be observed after 8 h, further confirming acceptable nutrient and gas supply to the organ. Other factors involved in tissue degradation could be late effects of surgical trauma, effects of fluorescence stains, as well as radicals formed due to laser irradiation (Lichtman and Conchello, 2005). Interestingly, all experiments could be performed using standard cell culture medium (RPMI / 10% FCS). Optimization of the medium to meet the specific needs of different organs is likely to improve incubation time.

Not only integrity and preservation of tissue depends on the culture conditions but also pathogens exhibit an intricate relationship with their environment. Changing conditions can be sensed rapidly and cause adapted gene expression within minutes. Thus, major differences in extracellular milieu between *in vivo* and *ex vivo* experiments are likely to produce divergent results (Hughes and Sperandio, 2008). The presented setup partially accounts for this fact by allowing different culture conditions for tissue on the basal side and for pathogens on the apical side of the explant. In the present experiments, the pathogen-challenged epithelia were perfused with PBS. Obviously, this was sufficient for the observed cellular events but for further studies, there is room for optimization as well. From the fact that *E. histolytica* trophozoites were not restricted in their migratory behavior for hours, it was concluded that for such short time frames the lack of anoxic conditions was tolerable. Still, for further studies it has to be considered that these settings contrast anoxic conditions in the caecum.

A feature which clearly distinguishes this model is the possibility to analyze the liquid composition of both the apical and the basal compartment before and after contact with the organ. In this work, this trait was used to measure the release of cytokines by urinary bladder tissue in real time (Fig. 3.39, p. 94), thereby supplementing visual data from dynamic imaging. Addition of live or heat-inactivated *E. coli* to native tissue mediated a release of KC, IL-8 and MCP-1 2 h after *ex vivo* infection. This observation further supports the good tissue preservation over this period of time. Native urinary bladder tissue released only minimal amounts of cytokines, contradicting a massive inflammatory response due to surgery or fixation trauma. Interestingly, TNF- α levels in the flow-through were low over 4 h, irrespective of infection. This is in contrast to previous results which showed strong TNF- α production as a result of *E. coli* infection (Ingersoll *et al.*, 2008). As strong cytokine production could be measured for KC, IL-8 and MCP-1, the lack of TNF- α secretion was considered to be specific for the used UPEC strain NU14 as the mentioned studies were based on infections with UTI89.

The performed *ex vivo* infection represents another valuable feature of the organ chamber: by infecting native organs directly on the microscope, it is possible to monitor early stages of infection, as for instance cell invasion, which are even more elusive in *in vivo* imaging due to the restricted spatial flexibility in these setups. Additionally, labeled cells could be injected to study the behavior of specific cell types in future studies. The additional inlet of the basal compartment could further be used to inject pharmacological compounds during experiments to study their effects on host-pathogen interactions. The main drawback of all explant-based systems in general is their inability to analyze any events based on immune cell extravasation from the vasculature, infiltration of cells into inflamed tissue and long-term effects of endocrinological interactions (Germain *et al.*, 2006). This is due to the complete disruption of the neural and vascular system by surgical explantation. Thus, the time frame qualified for *ex vivo* analysis is rather restricted. Nevertheless, this time frame can be shifted towards secondary inflammatory events by pre-infecting mice and explanting the organs shortly before the time point of interest. By this approach, IBC properties could be successfully studied in the present work. However, the lack of breathing and blood flow and the mechanical restraints imposed on the organ by fixation in the organ chamber considerably lessen motion artifacts compared to *in vivo* imaging.

Taken together, the present experimental setup is a valuable tool for studying host-pathogen interactions on mucous membranes by dynamic imaging at high spatial and

temporal resolution. It is a further development of explant-based systems by offering numerous advantages: Two independent compartments facilitate the establishment of more physiological conditions. Regulation of the two compartments is highly customizable in regard to liquid composition and flow rate. The secretion of proteins as a result of infection (for instance cytokines) can be analyzed at high temporal resolution. In comparison to TPM-based *in vivo* imaging, the presented model can be operated more easily, while at the same time offering higher image quality because a lower optical penetration depth into tissue is required (Germain *et al.*, 2006). Furthermore, it can lessen the amount and extent of animal infection experiments for specific questions. In this regard it represents an important intermediate step between *in vitro* and *in vivo* experiments from an ethical point of view by substituting for animal infection experiments. Nevertheless, it can not replace *in vivo* imaging for long-term experiments relying on intact vasculature, as for instance immune cell infiltration of tissues. Thus, the presented model fills a gap between conventional explant-based microscopical setups and *in vivo* imaging for the study of host-pathogen interactions on the cellular level.

4.2.2 Pathogenic mechanisms of uropathogenic *E. coli* and *E. histolytica*

In order to prove the applicability of the system, two representative pathogens of hollow organs were chosen: Uropathogenic *E. coli* (UPEC) infection of the urinary bladder and *E. histolytica* infection of the caecum. For both studies, the system produced new and intriguing results and perspectives.

UPEC invasion of urothelial cells leads to the formation of intracellular bacterial communities (IBCs). On the organ level, this is a rare event, complicating detection in histological sections (Mysorekar and Hultgren, 2006). In the present approach, the whole organ is mounted and can be analyzed, facilitating the study of IBCs. Conducting a co-infection experiment with two NU14 populations distinct in the expression of either GFP or mCherry, gained new insights into IBC formation: >90% of IBCs consisted of both GFP- and mCherry-expressing bacteria (Fig. 3.37 C, p. 90). This proves for the first time that IBCs are not the result of a single bacterial entry event into an urothelial cell. Even the <10% monochrome IBCs could have arisen from multiple entry events of bacteria of the same population. This evidence contradicts previous models which postulated the IBC formation process to be monoclonal (Garofalo *et al.*, 2007). Still, further studies have to show if simultaneous or sequential uptake of bacteria is prevalent for IBC formation. The dy-

dynamic component of the system was successfully employed for the finding of a new trait of IBCs: 5-6 h p.i., a significant proportion of the bacteria inside the IBC were motile (Movie 51). This contradicts a biofilm state and rather resembles movement of *Legionella* inside *Legionella*-containing vacuoles. This has so far not been described for UTI89, another UPEC strain (Anderson *et al.*, 2003). Furthermore, neutrophil interaction with infected urothelial cells could be visualized in this system at much higher spatial and temporal resolution compared to previous studies (Justice *et al.*, 2004). This achievement was the basis for the detection of phagocytic events of single bacteria (Fig. 3.38 D, p. 92).

In order to prove applicability of the model to protozoan parasites, *E. histolytica* was chosen. Invasion of trophozoites into epithelium and lamina propria could be detected after *ex vivo* infection of colon explants (Fig. 3.40, p. 95 and Movie 55). So far, C57BL/6 mice are considered resistant against *E. histolytica* invasion (Asgharpour *et al.*, 2005; Tsutsumi and Shibayama, 2006). An explanation for this success might be the thorough washing of the mucosa with PBS. This presumably removed a high amount of native gut flora, stool and also mucus, exposing the mucosa to trophozoite interactions. A similar mechanism has been described in a ‘washed-closed cecal loop’ model in hamsters and guinea pigs (Anaya-Velázquez *et al.*, 1985).

Finally, the model was applied to basic imaging of small intestine and stomach explants, in order to give an outlook on future perspectives. Considering the small intestine, dendritic cells (DC) play an important role in antigen sampling of the gut lumen (Chieppa *et al.*, 2006). Different subtypes have been shown to be involved (Lelouard *et al.*, 2010). The use of different transgenic mouse strains allows to differentiate between *CX₃CR1*- and *lysM*-positive cells. Both subtypes could be detected and in the case of *CX₃CR1*-positive cells, DC-like protrusions were found (Fig. 3.41 D, p. 97). The presented model might be an alternative to *in vivo* imaging for the study of these protrusions due to its higher resolution compared to *in vivo* imaging. Unexpectedly, some mice from the *lys-EGFP* strain were found to contain a significant amount of putatively small filamentous bacteria (SFB, Fig. 3.41 E, p. 97) (Gaboriau-Routhiau *et al.*, 2009). As these bacteria have not been cultured *in vitro*, this model might be an option to study their interaction with epithelia.

4.3 Conclusion

In conclusion, two independent *in vitro* and *ex vivo* infection models were established for the study of host-pathogen interactions on a cellular level by dynamic imaging in high spatial and temporal resolution.

As described in section 1.1 (p. 1), the establishment of new infection models should aim at the simulation of specific aspects of *in vivo*-like complexity. In this work, the three dimensional context was chosen as the variable which should be extended for an *in vitro* infection model. Specific host-pathogen interactions on the cellular level which demand a 3D context for correct interpretation are depicted in Fig. 1.1 (p. 1). This work achieves substantial progress in several of the described situations:

By providing a three dimensional environment, as well as a specific host plasma protein (fibrinogen), *in vivo*-like growth behavior of *S. aureus* could be simulated and new insights into the molecular basics were gained by revealing functional differences between secreted *S. aureus* coagulases.

The implications of such ‘collective growth behavior’ for establishing a protected niche for *S. aureus* by generating two sequential barriers impermeable for neutrophils was revealed. The finding that a thrombin inhibitor in clinical use is able to prevent encapsulation and thereby supports neutrophil invasion, demonstrates the important translational aspect of this surrogate infection model.

The targeting of immune cell migration machinery by *Yersinia* was analyzed in a proper context providing the prerequisites for *in vivo*-like amoeboid immune cell migration. A predominant role of the secreted cysteine protease YopT was found in *Y. enterocolitica* and furthermore, significant differences between YopE and YopT of *Yersinia enterocolitica* and *Y. pseudotuberculosis* were demonstrated in functional migration assays.

For the simulation of tissue-like dimensionality in regard to epithelia, an organ-explant based *ex vivo* infection model was established. Its functionality was proven for experimental UPEC infection of the bladder, during which neutrophil interaction with intracellular bacterial communities was analyzed. The broad applicability of this model was shown by its adoption for *E. histolytica* infection of caecum, for which epithelial penetration was successfully demonstrated in this *ex vivo* setup.

References

- Aepfelbacher, M. and Heesemann, J. (2001):** Modulation of Rho GTPases and the actin cytoskeleton by Yersinia outer proteins (Yops). *Int J Med Microbiol* **291**:269–276
- Aepfelbacher, M., Roppenser, B., Hentschke, M. and Ruckdeschel, K. (2011):** Activity modulation of the bacterial Rho GAP YopE: An inspiration for the investigation of mammalian Rho GAPs. *European Journal of Cell Biology* [**Epub ahead of print**]
- Aepfelbacher, M., Trasak, C. and Ruckdeschel, K. (2007):** Effector functions of pathogenic Yersinia species. *Thromb Haemost* **98**:521–9
- Aepfelbacher, M., Trasak, C., Wilharm, G., Wiedemann, A., Trulzsch, K., Krauss, K., Gierschik, P. and Heesemann, J. (2003):** Characterization of YopT effects on Rho GTPases in Yersinia enterocolitica-infected cells. *J Biol Chem* **278**:33217–23
- Aili, M., Isaksson, E.L., Hallberg, B., Wolf-Watz, H. and Rosqvist, R. (2006):** Functional analysis of the YopE GTPase-activating protein (GAP) activity of Yersinia pseudotuberculosis. *Cell Microbiol* **8**:1020–1033
- Aili, M., Telepnev, M., Hallberg, B., Wolf-Watz, H. and Rosqvist, R. (2003):** In vitro GAP activity towards RhoA, Rac1 and Cdc42 is not a prerequisite for YopE induced HeLa cell cytotoxicity. *Microb Pathog* **34**:297–308
- Aktories, K., Wilde, C. and Vogelsgesang, M. (2005):** Rho-modifying C3-like ADP-ribosyltransferases. *Reviews of Physiology, Biochemistry and Pharmacology*, Springer Berlin Heidelberg, 1–22
- Anaya-Velázquez, F., Martínez-Palomo, A., Tsutsumi, V. and González-Robles, A. (1985):** Intestinal invasive amebiasis: an experimental model in rodents using axenic or monoxenic strains of Entamoeba histolytica. *Am J Trop Med Hyg* **34**:723–30
- Anderson, G., Palermo, J., Schilling, J., Roth, R., Heuser, J. and Hultgren, S. (2003):** Intracellular bacterial biofilm-like pods in urinary tract infections. *Science* **301**:105
- Andor, A., Trülzsch, K., Essler, M., Roggenkamp, A., Wiedemann, A., Heesemann, J. and Aepfelbacher, M. (2001):** YopE of Yersinia, a GAP for Rho GTPases, selectively modulates Rac-dependent actin structures in endothelial cells. *Cell Microbiol* **3**:301–10
- Apodaca, G. (2004):** The uroepithelium: not just a passive barrier. *Traffic* **5**:117–28

- Asgharpour, A., Gilchrist, C., Baba, D., Hamano, S. and Houpt, E. (2005):** Resistance to intestinal *Entamoeba histolytica* infection is conferred by innate immunity and Gr-1+ cells. *Infect Immun* **73**:4522–9
- Autenrieth, I. and Firsching, R. (1996):** Penetration of M cells and destruction of Peyer's patches by *Yersinia enterocolitica*: an ultrastructural and histological study. *J Med Microbiol* **44**:285
- Barnes, P.D., Bergman, M.A., Mecsas, J. and Isberg, R.R. (2006):** *Yersinia pseudotuberculosis* disseminates directly from a replicating bacterial pool in the intestine. *J Exp Med* **203**:1591–601
- Bartlett, A. and Hulten, K. (2010):** *Staphylococcus aureus* Pathogenesis: Secretion Systems, Adhesins, and Invasins. *Pediatr Infect Dis J* **29**:860
- Barz, C., Abahji, T.N., Trülzsch, K. and Heesemann, J. (2000):** The *Yersinia* Ser/Thr protein kinase YpkA/YopO directly interacts with the small GTPases RhoA and Rac-1. *FEBS Letters* **482**:139–43
- Behnsen, J., Narang, P., Hasenberg, M., Gunzer, F., Bilitewski, U., Klippel, N., Rohde, M., Brock, M., Brakhage, A.A. and Gunzer, M. (2007):** Environmental dimensionality controls the interaction of phagocytes with the pathogenic fungi *Aspergillus fumigatus* and *Candida albicans*. *PLoS Pathog* **3**:e13
- Benabdillah, R., Mota, L.J., Lützelshwab, S., Demoinet, E. and Cornelis, G.R. (2004):** Identification of a nuclear targeting signal in YopM from *Yersinia* spp. *Microb Pathog* **36**:247–61
- Benvenuti, F., Hugues, S., Walmsley, M., Ruf, S., Fetler, L., Popoff, M., Tybulewicz, V.L.J. and Amigorena, S. (2004):** Requirement of Rac1 and Rac2 expression by mature dendritic cells for T cell priming. *Science* **305**:1150–3
- Billips, B.K., Forrestal, S.G., Rycyk, M.T., Johnson, J.R., Klumpp, D.J. and Schaeffer, A.J. (2007):** Modulation of host innate immune response in the bladder by uropathogenic *Escherichia coli*. *Infect Immun* **75**:5353–60
- Bjerketorp, J., Jacobsson, K. and Frykberg, L. (2004):** The von Willebrand factor-binding protein (vWbp) of *Staphylococcus aureus* is a coagulase. *FEMS Microbiol Lett* **234**:309–14
- Bokarewa, M.I., Jin, T. and Tarkowski, A. (2006):** *Staphylococcus aureus*: Staphylokinase. *Int J Biochem Cell Biol* **38**:504–9
- Bokoch, G. (2005):** Regulation of innate immunity by Rho GTPases. *Trends Cell Biol* **15**:163–171
- Borregaard, N., Sørensen, O.E. and Theilgaard-Mönch, K. (2007):** Neutrophil granules: a library of innate immunity proteins. *Trends Immunol* **28**:340–5
- Boxio, R., Bossenmeyer-Pourié, C., Steinckwich, N., Dournon, C. and Nüsse, O. (2004):** Mouse bone marrow contains large numbers of functionally competent neutrophils. *J Leukoc Biol* **75**:604–11

- Brinkmann, V., Reichard, U., Goosmann, C., Fauler, B., Uhlemann, Y., Weiss, D.S., Weinrauch, Y. and Zychlinsky, A. (2004): Neutrophil extracellular traps kill bacteria. *Science* **303**:1532–5
- Brodsky, I., Palm, N., Sadanand, S., Ryndak, M., Sutterwala, F., Flavell, R., Bliska, J. and Medzhitov, R. (2010): A Yersinia effector protein promotes virulence by preventing inflammasome recognition of the type III secretion system. *Cell Host Microbe* **7**:376–387
- Brodsky, I.E. and Medzhitov, R. (2008): Reduced secretion of YopJ by Yersinia limits in vivo cell death but enhances bacterial virulence. *PLoS Pathog* **4**:e1000067
- Chain, P., Carniel, E., Larimer, F., Lamerdin, J., Stoutland, P., Regala, W., Georgescu, A., Vergez, L., Land, M. and Motin, V. (2004): Insights into the evolution of Yersinia pestis through whole-genome comparison with Yersinia pseudotuberculosis. *Proc Natl Acad Sci USA* **101**:13826
- Charles, M., Pérez, M., Kobil, J. and Goldberg, M. (2001): Polar targeting of Shigella virulence factor IcsA in Enterobacteriaceae and Vibrio. *Proc Natl Acad Sci U S A* **98**:9871
- Chavakis, T., Wiechmann, K., Preissner, K.T. and Herrmann, M. (2005): Staphylococcus aureus interactions with the endothelium: the role of bacterial "secretable expanded repertoire adhesive molecules" (SERAM) in disturbing host defense systems. *Thromb Haemost* **94**:278–85
- Cheng, A.G., DeDent, A.C., Schneewind, O. and Missiakas, D. (2011): A play in four acts: Staphylococcus aureus abscess formation. *Trends Microbiol* **19**:225–32
- Cheng, A.G., Kim, H.K., Burts, M.L., Krausz, T., Schneewind, O. and Missiakas, D.M. (2009): Genetic requirements for Staphylococcus aureus abscess formation and persistence in host tissues. *FASEB J* **23**:3393–404
- Cheng, A.G., McAdow, M., Kim, H.K., Bae, T., Missiakas, D.M. and Schneewind, O. (2010): Contribution of coagulases towards Staphylococcus aureus disease and protective immunity. *PLoS Pathog* **6**:e1001036
- Cheung, A.L., Bayer, A.S., Zhang, G., Gresham, H. and Xiong, Y.Q. (2004): Regulation of virulence determinants in vitro and in vivo in Staphylococcus aureus. *FEMS Immunol Med Microbiol* **40**:1–9
- Chieppa, M., Rescigno, M., Huang, A.Y.C. and Germain, R.N. (2006): Dynamic imaging of dendritic cell extension into the small bowel lumen in response to epithelial cell TLR engagement. *J Exp Med* **203**:2841–52
- Cornelis, G.R. (2002): The Yersinia Ysc-Yop 'type III' weaponry. *Nat Rev Mol Cell Biol* **3**:742–52
- Croft, D.R., Coleman, M.L., Li, S., Robertson, D., Sullivan, T., Stewart, C.L. and Olson, M.F. (2005): Actin-myosin-based contraction is responsible for apoptotic nuclear disintegration. *J Cell Biol* **168**:245–55

- Cruz, M.A., Yuan, H., Lee, J.R., Wise, R.J. and Handin, R.I. (1995):** Interaction of the von Willebrand factor (vWF) with collagen. Localization of the primary collagen-binding site by analysis of recombinant vWF A domain polypeptides. *J Biol Chem* **270**:19668
- Cvetanovic, S. (2011):** In vitro und in vivo Analyse der Yersinia enterocolitica Yop-Translokation mittels beta-Laktamase-Reporter. Dissertation, Ludwig-Maximilians-Universität München
- Dahlbäck, B. (2000):** Blood coagulation. *Lancet* **355**:1627–1632
- Datsenko, K.A. and Wanner, B.L. (2000):** One-step inactivation of chromosomal genes in Escherichia coli K-12 using PCR products. *Proc Natl Acad Sci U S A* **97**:6640–5
- Dewoody, R., Merritt, P.M., Houppert, A.S. and Marketon, M.M. (2011):** YopK regulates the Yersinia pestis type III secretion system from within host cells. *Mol Microbiol* **79**:1445–61
- Diamond, L.S., Harlow, D.R. and Cunnick, C.C. (1978):** A new medium for the axenic cultivation of Entamoeba histolytica and other Entamoeba. *Trans R Soc Trop Med Hyg* **72**:431–2
- Diep, B.A., Gill, S.R., Chang, R.F., Phan, T.H., Chen, J.H., Davidson, M.G., Lin, F., Lin, J., Carleton, H.A., Mongodin, E.F., Sensabaugh, G.F. and Perdreau-Remington, F. (2006):** Complete genome sequence of USA300, an epidemic clone of community-acquired methicillin-resistant Staphylococcus aureus. *Lancet* **367**:731–9
- Drecktrah, D., Levine-Wilkinson, S., Dam, T., Winfree, S., Knodler, L., Schroer, T. and Steele-Mortimer, O. (2008):** Dynamic Behavior of Salmonella-Induced Membrane Tubules in Epithelial Cells. *Traffic* **9**:2117–2129
- Duthie, E.S. and Lorenz, L.L. (1952):** Staphylococcal coagulase; mode of action and antigenicity. *J Gen Microbiol* **6**:95–107
- e Sousa, C.R. (2006):** Dendritic cells in a mature age. *Nat Rev Immunol* **6**:476–483
- Evdokimov, A.G., Tropea, J.E., Routzahn, K.M. and Waugh, D.S. (2002):** Crystal structure of the Yersinia pestis GTPase activator YopE. *Protein Sci* **11**:401–8
- Falkow, S. (2004):** Molecular Koch's postulates applied to bacterial pathogenicity—a personal recollection 15 years later. *Nat Rev Microbiol* **2**:67–72
- Faust, N., Varas, F., Kelly, L.M., Heck, S. and Graf, T. (2000):** Insertion of enhanced green fluorescent protein into the lysozyme gene creates mice with green fluorescent granulocytes and macrophages. *Blood* **96**:719–726
- Feuk-Lagerstedt, E., Jordan, E.T., Leffler, H., Dahlgren, C. and Karlsson, A. (1999):** Identification of CD66a and CD66b as the major galectin-3 receptor candidates in human neutrophils. *J Immunol* **163**:5592–8
- Forst, C.V. (2006):** Host-pathogen systems biology. *Drug Discov Today* **11**:220–7

- Förster, R., Schubel, A., Breitfeld, D., Kremmer, E., Renner-Müller, I., Wolf, E. and Lipp, M. (1999): CCR7 coordinates the primary immune response by establishing functional microenvironments in secondary lymphoid organs. *Cell* **99**:23–33
- Foster, T.J. and Höök, M. (1998): Surface protein adhesins of *Staphylococcus aureus*. *Trends Microbiol* **6**:484–8
- Foti, M., Granucci, F., Aggujaro, D., Liboi, E., Luini, W., Minardi, S., Mantovani, A., Sozzani, S. and Ricciardi-Castagnoli, P. (1999): Upon dendritic cell (DC) activation chemokines and chemokine receptor expression are rapidly regulated for recruitment and maintenance of DC at the inflammatory site. *Int Immunol* **11**:979–986
- Freund, S., Czech, B., Trülzsch, K., Ackermann, N. and Heesemann, J. (2008): Unusual, virulence plasmid-dependent growth behavior of *Yersinia enterocolitica* in three-dimensional collagen gels. *J Bacteriol* **190**:4111–20
- Friedl, P., Maaser, K., Klein, C.E., Niggemann, B., Krohne, G. and Zänker, K.S. (1997): Migration of highly aggressive MV3 melanoma cells in 3-dimensional collagen lattices results in local matrix reorganization and shedding of alpha2 and beta1 integrins and CD44. *Cancer Res* **57**:2061–70
- Friedl, P. and Weigelin, B. (2008): Interstitial leukocyte migration and immune function. *Nat Immunol* **9**:960–9
- Friedrich, R., Panizzi, P., Fuentes-Prior, P., Richter, K., Verhamme, I., Anderson, P.J., Kawabata, S.I., Huber, R., Bode, W. and Bock, P.E. (2003): Staphylocoagulase is a prototype for the mechanism of cofactor-induced zymogen activation. *Nature* **425**:535–9
- Friedrich, R., Panizzi, P., Kawabata, S.I., Bode, W., Bock, P.E. and Fuentes-Prior, P. (2006): Structural basis for reduced staphylocoagulase-mediated bovine prothrombin activation. *J Biol Chem* **281**:1188–95
- Frigault, M.M., Lacoste, J., Swift, J.L. and Brown, C.M. (2009): Live-cell microscopy - tips and tools. *J Cell Sci* **122**:753–67
- Fueller, F. and Schmidt, G. (2008): The polybasic region of Rho GTPases defines the cleavage by *Yersinia enterocolitica* outer protein T (YopT). *Protein Sci* **17**:1456–62
- Furie, B. and Furie, B. (1988): The molecular basis of blood coagulation. *Cell* **53**:505–518
- Gaboriau-Routhiau, V., Rakotobe, S., Lécuyer, E., Mulder, I., Lan, A., Bridonneau, C., Rochet, V., Pisi, A., Paepe, M.D. and Brandi, G. (2009): The key role of segmented filamentous bacteria in the coordinated maturation of gut helper T cell responses. *Immunity* **31**:677–689
- Gabridge, M.G. (1974): Parabiotic chamber for organ cultures: improved model. *Appl Microbiol* **28**:774–7
- Galán, J.E. and Wolf-Watz, H. (2006): Protein delivery into eukaryotic cells by type III secretion machines. *Nature* **444**:567–73

- Garofalo, C.K., Hooton, T.M., Martin, S.M., Stamm, W.E., Palermo, J.J., Gordon, J.I. and Hultgren, S.J. (2007): Escherichia coli from urine of female patients with urinary tract infections is competent for intracellular bacterial community formation. *Infect Immun* **75**:52–60
- Garrett, W., Chen, L., Kroschewski, R., Ebersold, M., Turley, S., Trombetta, S., Galán, J. and Mellman, I. (2000): Developmental control of endocytosis in dendritic cells by Cdc42. *Cell* **102**:325–334
- Gaskill, M.E. and Khan, S.A. (1988): Regulation of the enterotoxin B gene in Staphylococcus aureus. *J Biol Chem* **263**:6276–80
- Gaus, K., Hentschke, M., Czymmeck, N., Novikova, L., Trulzsch, K., Valentin-Weigand, P., Aepfelbacher, M. and Ruckdeschel, K. (2011): Destabilization of YopE by the Ubiquitin-Proteasome Pathway Fine-Tunes Yop Delivery into Host Cells and Facilitates Systemic Spread of Yersinia enterocolitica in Host Lymphoid Tissue. *Infect Immun* **79**:1166–1175
- Geiman, Q. and Becker, C. (1953): In vitro growth and metabolism of Endamoeba histolytica. *Ann N Y Acad Sci* **56**:1048–1056
- Germain, R., Miller, M., Dustin, M. and Nussenzweig, M. (2006): Dynamic imaging of the immune system: progress, pitfalls and promise. *Nat Rev Immunol* **6**:497–507
- Germain, R.N., Castellino, F., Chieppa, M., Egen, J.G., Huang, A.Y.C., Koo, L.Y. and Qi, H. (2005): An extended vision for dynamic high-resolution intravital immune imaging. *Semin Immunol* **17**:431–41
- Giraud, A.T., Cheung, A.L. and Nagel, R. (1997): The sae locus of Staphylococcus aureus controls exoprotein synthesis at the transcriptional level. *Arch Microbiol* **168**:53–8
- Goerke, C., Fluckiger, U., Steinhuber, A., Zimmerli, W. and Wolz, C. (2001): Impact of the regulatory loci agr, sarA and sae of Staphylococcus aureus on the induction of alpha-toxin during device-related infection resolved by direct quantitative transcript analysis. *Mol Microbiol* **40**:1439–47
- Grosdent, N., Maridonneau-Parini, I., Sory, M.P. and Cornelis, G.R. (2002): Role of Yops and adhesins in resistance of Yersinia enterocolitica to phagocytosis. *Infect Immun* **70**:4165–76
- Hanahan, D. (1983): Studies on transformation of Escherichia coli with plasmids. *J Mol Biol* **166**:557–80
- Harraghy, N., Kormanec, J., Wolz, C., Homerova, D., Goerke, C., Ohlsen, K., Qazi, S., Hill, P. and Herrmann, M. (2005): sae is essential for expression of the staphylococcal adhesins Eap and Emp. *Microbiology* **151**:1789–800
- Hartleib, J., Köhler, N., Dickinson, R., Chhatwal, G., Sixma, J., Hartford, O., Foster, T., Peters, G., Kehrel, B. and Herrmann, M. (2000): Protein A is the von Willebrand factor binding protein on Staphylococcus aureus. *Blood* **96**:2149

- Hauert, A.B., Martinelli, S., Marone, C. and Niggli, V. (2002):** Differentiated HL-60 cells are a valid model system for the analysis of human neutrophil migration and chemotaxis. *Int J Biochem Cell Biol* **34**:838–54
- Heasman, S.J. and Ridley, A.J. (2008):** Mammalian Rho GTPases: new insights into their functions from in vivo studies. *Nat Rev Mol Cell Biol* **9**:690–701
- Heesemann, J., Keller, C., Morawa, R., Schmidt, N., Siemens, H. and Laufs, R. (1983):** Plasmids of human strains of *Yersinia enterocolitica*: molecular relatedness and possible importance for pathogenesis. *J Infect Dis* **147**:107
- Heesemann, J., Sing, A. and Trülsch, K. (2006):** *Yersinia*'s stratagem: targeting innate and adaptive immune defense. *Curr Opin Microbiol* **9**:55–61
- Heit, B. and Kubes, P. (2003):** Measuring chemotaxis and chemokinesis: the under-agarose cell migration assay. *Sci STKE* **2003**:PL5
- Hentschke, M., Trulzsch, K., Heesemann, J., Aepfelbacher, M. and Ruckdeschel, K. (2007):** Serogroup-Related Escape of *Yersinia enterocolitica* YopE from Degradation by the Ubiquitin-Proteasome Pathway. *Infect Immun* **75**:4423–4431
- Higgins, J., Loughman, A., van Kessel, K.P.M., van Strijp, J.A.G. and Foster, T.J. (2006):** Clumping factor A of *Staphylococcus aureus* inhibits phagocytosis by human polymorphonuclear leucocytes. *FEMS Microbiol Lett* **258**:290–6
- Hijikata-Okunomiya, A. and Kataoka, N. (2003):** Argatroban inhibits staphylothrombin. *J Thromb Haemost* **1**:2060–2061
- Hiramatsu, K., Cui, L., Kuroda, M. and Ito, T. (2001):** The emergence and evolution of methicillin-resistant *Staphylococcus aureus*. *Trends Microbiol* **9**:486–493
- Holmström, A., Pettersson, J., Rosqvist, R., Håkansson, S., Tafazoli, F., Fällman, M., Magnusson, K., Wolf-Watz, H. and Forsberg, Å. (1997):** YopK of *Yersinia pseudotuberculosis* controls translocation of Yop effectors across the eukaryotic cell membrane. *Mol Microbiol* **24**:73–91
- Hughes, D.T. and Sperandio, V. (2008):** Inter-kingdom signalling: communication between bacteria and their hosts. *Nat Rev Microbiol* **6**:111–20
- Hultgren, S., Schwan, W., Schaeffer, A. and Duncan, J. (1986):** Regulation of production of type 1 pili among urinary tract isolates of *Escherichia coli*. *Infect Immun* **54**:613
- Hunstad, D.A. and Justice, S.S. (2010):** Intracellular lifestyles and immune evasion strategies of uropathogenic *Escherichia coli*. *Annu Rev Microbiol* **64**:203–21
- Hunstad, D.A., Justice, S.S., Hung, C.S., Lauer, S.R. and Hultgren, S.J. (2005):** Suppression of bladder epithelial cytokine responses by uropathogenic *Escherichia coli*. *Infect Immun* **73**:3999–4006
- Hussain, M., Becker, K., von Eiff, C., Schrenzel, J., Peters, G. and Herrmann, M. (2001):** Identification and characterization of a novel 38.5-kilodalton cell surface protein of *Staphylococcus aureus* with extended-spectrum binding activity for extracellular matrix and plasma proteins. *J Bacteriol* **183**:6778–86

- Hussain, M., Hagggar, A., Heilmann, C., Peters, G., Flock, J.I. and Herrmann, M. (2002): Insertional inactivation of Eap in *Staphylococcus aureus* strain Newman confers reduced staphylococcal binding to fibroblasts. *Infect Immun* **70**:2933–40
- Ingersoll, M.A., Kline, K.A., Nielsen, H.V. and Hultgren, S.J. (2008): G-CSF induction early in uropathogenic *Escherichia coli* infection of the urinary tract modulates host immunity. *Cell Microbiol* **10**:2568–78
- Isaksson, E.L., Aili, M., Fahlgren, A., Carlsson, S.E., Rosqvist, R. and Wolf-Watz, H. (2009): The Membrane Localization Domain Is Required for Intracellular Localization and Autoregulation of YopE in *Yersinia pseudotuberculosis*. *Infect Immun* **77**:4740–4749
- Islam, L., McKay, I., Wilkinson, P. and 3D-CoG (1985): The use of collagen or fibrin gels for the assay of human neutrophil chemotaxis. *J Immunol Methods* **85**:137–151
- Jaffe, A. and Hall, A. (2005): Rho GTPases: biochemistry and biology. *Annu Rev Cell Dev Biol* **21**:247–269
- Jain, S., Ulsen, P.V., Benz, I., Schmidt, M., Fernandez, R., Tommassen, J. and Goldberg, M. (2006): Polar localization of the autotransporter family of large bacterial virulence proteins. *J Bacteriol* **188**:4841
- Janeway, Jr, C.A. and Medzhitov, R. (2002): Innate immune recognition. *Annu Rev Immunol* **20**:197–216
- Johnson, M., Cockayne, A. and Morrissey, J.A. (2008): Iron-regulated biofilm formation in *Staphylococcus aureus* Newman requires *ica* and the secreted protein Emp. *Infect Immun* **76**:1756–65
- Jung, S., Aliberti, J., Graemmel, P., Sunshine, M.J., Kreutzberg, G.W., Sher, A. and Littman, D.R. (2000): Analysis of fractalkine receptor CX(3)CR1 function by targeted deletion and green fluorescent protein reporter gene insertion. *Mol Cell Biol* **20**:4106–4114
- Justice, S., Hung, C., Theriot, J., Fletcher, D., Anderson, G., Footer, M. and Hultgren, S. (2004): Differentiation and developmental pathways of uropathogenic *Escherichia coli* in urinary tract pathogenesis. *Proc Natl Acad Sci U S A* **101**:1333
- Kaisho, T. and Wagner, H. (2008): Host-pathogen interactions. *Curr Opin Immunol* **20**:369–70
- Kobayashi, S.D., Braughton, K.R., Palazzolo-Ballance, A.M., Kennedy, A.D., Sampaio, E., Kristosturyan, E., Whitney, A.R., Sturdevant, D.E., Dorward, D.W., Holland, S.M., Kreiswirth, B.N., Musser, J.M. and DeLeo, F.R. (2010): Rapid neutrophil destruction following phagocytosis of *Staphylococcus aureus*. *J Innate Immun* **2**:560–75
- Kobayashi, S.D. and DeLeo, F.R. (2009): Role of neutrophils in innate immunity: a systems biology-level approach. *Wiley Interdiscip Rev Syst Biol Med* **1**:309–33
- Krall, R., Zhang, Y. and Barbieri, J.T. (2004): Intracellular membrane localization of *Pseudomonas* ExoS and *Yersinia* YopE in mammalian cells. *J Biol Chem* **279**:2747–53

- Kreiswirth, B.N., Löfdahl, S., Betley, M.J., O'Reilly, M., Schlievert, P.M., Bergdoll, M.S. and Novick, R.P. (1983): The toxic shock syndrome exotoxin structural gene is not detectably transmitted by a prophage. *Nature* **305**:709–12
- Kroh, H.K., Panizzi, P. and Bock, P.E. (2009): Von Willebrand factor-binding protein is a hysteretic conformational activator of prothrombin. *Proc Natl Acad Sci U S A* **106**:7786–91
- Kropec, A., Maira-Litran, T., Jefferson, K.K., Grout, M., Cramton, S.E., Götz, F., Goldmann, D.A. and Pier, G.B. (2005): Poly-N-acetylglucosamine production in *Staphylococcus aureus* is essential for virulence in murine models of systemic infection. *Infect Immun* **73**:6868–76
- Kwieciński, J., Josefsson, E., Mitchell, J., Higgins, J., Magnusson, M., Foster, T., Jin, T. and Bokarewa, M. (2010): Activation of plasminogen by staphylokinase reduces the severity of *Staphylococcus aureus* systemic infection. *J Infect Dis* **202**:1041–9
- Laemmli, U.K. (1970): Cleavage of structural proteins during the assembly of the head of bacteriophage T4. *Nature* **227**:680–5
- Lämmermann, T., Bader, B.L., Monkley, S.J., Worbs, T., Wedlich-Söldner, R., Hirsch, K., Keller, M., Förster, R., Critchley, D.R., Fässler, R. and Sixt, M. (2008): Rapid leukocyte migration by integrin-independent flowing and squeezing. *Nature* **453**:51–5
- Lämmermann, T., Renkawitz, J., Wu, X., Hirsch, K., Brakebusch, C. and Sixt, M. (2009): Cdc42-dependent leading edge coordination is essential for interstitial dendritic cell migration. *Blood* **113**:5703–10
- Lee, W.Y., Chin, A.C., Voss, S. and Parkos, C.A. (2006): In vitro neutrophil transepithelial migration. *Methods Mol Biol* **341**:205–15
- Lelouard, H., Henri, S., Bovis, B.D., Mugnier, B., Chollat-Namy, A., Malissen, B., Méresse, S. and Gorvel, J.P. (2010): Pathogenic Bacteria and Dead Cells Are Internalized by a Unique Subset of Peyer's Patch Dendritic Cells That Express Lysozyme. *YGAST* **138**:173–184.e3
- Lichtman, J.W. and Conchello, J.A. (2005): Fluorescence microscopy. *Nat Methods* **2**:910–9
- Logsdon, L.K. and Mecsas, J. (2003): Requirement of the *Yersinia pseudotuberculosis* effectors YopH and YopE in colonization and persistence in intestinal and lymph tissues. *Infect Immun* **71**:4595–4607
- Lowy, F.D. (1998): *Staphylococcus aureus* infections. *N Engl J Med* **339**:520–32
- Lutz, M.B., Kukutsch, N., Ogilvie, A.L., Rössner, S., Koch, F., Romani, N. and Schuler, G. (1999): An advanced culture method for generating large quantities of highly pure dendritic cells from mouse bone marrow. *J Immunol Methods* **223**:77–92
- Mainiero, M., Goerke, C., Geiger, T., Gonser, C., Herbert, S. and Wolz, C. (2010): Differential target gene activation by the *Staphylococcus aureus* two-component system saeRS. *J Bacteriol* **192**:613–23

- Maniatis, T., Fritsch, E. and Sambrook, J. (1989):** Molecular cloning: A Laboratory Manual. Cold Spring Harbor Laboratory Press, Cold Spring Harbor, New York
- Mann, B.J. (2002):** Structure and function of the *Entamoeba histolytica* Gal/GalNAc lectin. *Int Rev Cytol* **216**:59–80
- Mantovani, A., Cassatella, M.A., Costantini, C. and Jaillon, S. (2011):** Neutrophils in the activation and regulation of innate and adaptive immunity. *Nat Rev Immunol* **11**:519–31
- Marketon, M.M., DePaolo, R.W., DeBord, K.L., Jabri, B. and Schneewind, O. (2005):** Plague bacteria target immune cells during infection. *Science* **309**:1739–41
- Mascari, L.M. and Ross, J.M. (2003):** Quantification of staphylococcal-collagen binding interactions in whole blood by use of a confocal microscopy shear-adhesion assay. *J Infect Dis* **188**:98–107
- McDevitt, D., Vaudaux, P. and Foster, T.J. (1992):** Genetic evidence that bound coagulase of *Staphylococcus aureus* is not clumping factor. *Infect Immun* **60**:1514–23
- McDonald, C., Vacratsis, P.O., Bliska, J.B. and Dixon, J.E. (2003):** The yersinia virulence factor YopM forms a novel protein complex with two cellular kinases. *J Biol Chem* **278**:18514–23
- Mejía, E., Bliska, J.B. and Viboud, G.I. (2008):** Yersinia controls type III effector delivery into host cells by modulating Rho activity. *PLoS Pathog* **4**:e3
- Merrell, D.S. and Falkow, S. (2004):** Frontal and stealth attack strategies in microbial pathogenesis. *Nature* **430**:250–6
- Mittal, R., Peak-Chew, S.Y. and McMahon, H.T. (2006):** Acetylation of MEK2 and I kappa B kinase (IKK) activation loop residues by YopJ inhibits signaling. *Proc Natl Acad Sci U S A* **103**:18574–9
- Mohammadi, S. and Isberg, R.R. (2009):** Yersinia pseudotuberculosis virulence determinants invasin, YopE, and YopT modulate RhoG activity and localization. *Infect Immun* **77**:4771–82
- Mosesson, M.W. (2005):** Fibrinogen and fibrin structure and functions. *J Thromb Haemost* **3**:1894–904
- Mysorekar, I. and Hultgren, S. (2006):** Mechanisms of uropathogenic *Escherichia coli* persistence and eradication from the urinary tract. *Proc Natl Acad Sci U S A* **103**:14170
- Narumiya, S., Tanji, M. and Ishizaki, T. (2009):** Rho signaling, ROCK and mDia1, in transformation, metastasis and invasion. *Cancer Metastasis Rev* **28**:65–76
- Nathan, C. (2006):** Neutrophils and immunity: challenges and opportunities. *Nat Rev Immunol* **6**:173–182
- Nauseef, W.M. (2007):** How human neutrophils kill and degrade microbes: an integrated view. *Immunol Rev* **219**:88–102
- Navarro, L., Alto, N.M. and Dixon, J.E. (2005):** Functions of the Yersinia effector proteins in inhibiting host immune responses. *Curr Opin Microbiol* **8**:21–7

- Oberhettinger, P., Schütz, M., Raddatz, G., Keller, H., Autenrieth, I.B. and Linke, D. (2011): The sequence of the pYV virulence plasmid from *Yersinia enterocolitica* strain WA-314 biogroup 1B serotype O:8. *Plasmid* **65**:20–4
- Oellerich, M.F., Jacobi, C.A., Freund, S., Niedung, K., Bach, A., Heesemann, J. and Trülsch, K. (2007): *Yersinia enterocolitica* infection of mice reveals clonal invasion and abscess formation. *Infect Immun* **75**:3802–11
- Palma, M., Hagggar, A. and Flock, J.I. (1999): Adherence of *Staphylococcus aureus* is enhanced by an endogenous secreted protein with broad binding activity. *J Bacteriol* **181**:2840–5
- Peters, N.C., Egen, J.G., Secundino, N., Debrabant, A., Kimblin, N., Kamhawi, S., Lawyer, P., Fay, M.P., Germain, R.N. and Sacks, D. (2008): In vivo imaging reveals an essential role for neutrophils in leishmaniasis transmitted by sand flies. *Science* **321**:970–4
- Pishchany, G., Mccoy, A.L., Torres, V.J., Krause, J.C., Jr, J.E.C., Fabry, M.E. and Skaar, E.P. (2010): Specificity for Human Hemoglobin Enhances *Staphylococcus aureus* Infection. *Cell Host Microbe* **8**:544–550
- Platt, C.D., Ma, J.K., Chalouni, C., Ebersold, M., Bou-Reslan, H., Carano, R.A.D., Mellman, I. and Delamarre, L. (2010): Mature dendritic cells use endocytic receptors to capture and present antigens. *Proc Natl Acad Sci U S A* **107**:4287–4292
- Prehna, G., Ivanov, M.I., Bliska, J.B. and Stebbins, C.E. (2006): *Yersinia* virulence depends on mimicry of host Rho-family nucleotide dissociation inhibitors. *Cell* **126**:869–80
- Prentki, P. and Krisch, H.M. (1984): In vitro insertional mutagenesis with a selectable DNA fragment. *Gene* **29**:303–13
- Pritt, B.S. and Clark, C.G. (2008): Amebiasis. *Mayo Clin Proc* **83**:1154–9; quiz 1159–60
- Que, X. and Reed, S. (2000): Cysteine proteinases and the pathogenesis of amebiasis. *Clin Microbiol Rev* **13**:196
- Renkawitz, J., Schumann, K., Weber, M., Lämmermann, T., Pflücke, H., Piel, M., Polleux, J., Spatz, J.P. and Sixt, M. (2009): Adaptive force transmission in amoeboid cell migration. *Nat Cell Biol* **11**:1438–43
- Renkawitz, J. and Sixt, M. (2010): Mechanisms of force generation and force transmission during interstitial leukocyte migration. *EMBO Rep* **11**:744–50
- Ridley, A.J. (2006): Rho GTPases and actin dynamics in membrane protrusions and vesicle trafficking. *Trends Cell Biol* **16**:522–9
- Riedl, J., Flynn, K.C., Raducanu, A., Gärtner, F., Beck, G., Bösl, M., Bradke, F., Massberg, S., Aszodi, A., Sixt, M. and Wedlich-Söldner, R. (2010): Lifeact mice for studying F-actin dynamics. *Nat Methods* **7**:168–169
- Roberts, J., Marklund, B., Ilver, D., Haslam, D., Kaack, M., Baskin, G., Louis, M., Möllby, R., Winberg, J. and Normark, S. (1994): The Gal (alpha 1-4) Gal-specific tip adhesin of *Escherichia coli* P-fimbriae is needed for pyelonephritis to occur in the normal urinary tract. *Proc Natl Acad Sci U S A* **91**:11889

- Roggenkamp, A., Neuberger, H.R., Flügel, A., Schmoll, T. and Heesemann, J. (1995): Substitution of two histidine residues in YadA protein of *Yersinia enterocolitica* abrogates collagen binding, cell adherence and mouse virulence. *Mol Microbiol* **16**:1207–19
- Roppenser, B., Röder, A., Hentschke, M., Ruckdeschel, K. and Aepfelbacher, M. (2009): *Yersinia enterocolitica* differentially modulates RhoG activity in host cells. *J Cell Sci* **122**:696–705
- Rosenbaum, D.M., Rasmussen, S.G.F. and Kobilka, B.K. (2009): The structure and function of G-protein-coupled receptors. *Nature* **459**:356–363
- Ruckdeschel, K., Roggenkamp, A., Schubert, S. and Heesemann, J. (1996): Differential contribution of *Yersinia enterocolitica* virulence factors to evasion of microbicidal action of neutrophils. *Infect Immun* **64**:724–33
- Rüssmann, H., Shams, H., Poblete, F., Fu, Y., Galán, J. and Donis, R. (1998): Delivery of epitopes by the *Salmonella* type III secretion system for vaccine development. *Science* **281**:565
- Saltzman, W., Parkhurst, M., Parsons-Wingerter, P. and Zhu, W. (1992): Three-Dimensional Cell Cultures Mimic Tissues. *Ann N Y Acad Sci* **665**:259–273
- Sawai, T., Tomono, K., Yanagihara, K., Yamamoto, Y., Kaku, M., Hirakata, Y., Koga, H., Tashiro, T. and Kohno, S. (1997): Role of coagulase in a murine model of hematogenous pulmonary infection induced by intravenous injection of *Staphylococcus aureus* enmeshed in agar beads. *Infect Immun* **65**:466–71
- Schmidt, G. (2011): *Yersinia enterocolitica* outer protein T (YopT). *European Journal of Cell Biology* [Epub ahead of print]
- Shao, F. (2008): Biochemical functions of *Yersinia* type III effectors. *Curr Opin Microbiol* **11**:21–9
- Shao, F., Merritt, P.M., Bao, Z., Innes, R.W. and Dixon, J.E. (2002): A *Yersinia* effector and a *Pseudomonas* avirulence protein define a family of cysteine proteases functioning in bacterial pathogenesis. *Cell* **109**:575–88
- Shao, F., Vacratsis, P.O., Bao, Z., Bowers, K.E., Fierke, C.A. and Dixon, J.E. (2003): Biochemical characterization of the *Yersinia* YopT protease: cleavage site and recognition elements in Rho GTPases. *Proc Natl Acad Sci U S A* **100**:904–9
- Skurnik, M. and Toivonen, S. (2011): Identification of distinct lipopolysaccharide patterns among *Yersinia enterocolitica* and *Y. enterocolitica*-like bacteria. *Biochemistry (Mosc)* **76**:823–831
- Söding, J., Biegert, A. and Lupas, A. (2005): The HHpred interactive server for protein homology detection and structure prediction. *Nucleic Acids Res* **33**:W244
- Sorg, I., Hoffmann, C., Dumbach, J., Aktories, K. and Schmidt, G. (2003): The C terminus of YopT is crucial for activity and the N terminus is crucial for substrate binding. *Infect Immun* **71**:4623–32
- Stanley, S.L. (2001): Pathophysiology of amoebiasis. *Trends Parasitol* **17**:280–5

- Stanley, S.L. (2003):** Amoebiasis. *Lancet* **361**:1025–34
- Stecher, B., Hapfelmeier, S., Muller, C., Kremer, M., Stallmach, T. and Hardt, W. (2004):** Flagella and chemotaxis are required for efficient induction of *Salmonella enterica* serovar Typhimurium colitis in streptomycin-pretreated mice. *Infect Immun* **72**:4138
- Sun, F., Li, C., Jeong, D., Sohn, C., He, C. and Bae, T. (2010):** In the *Staphylococcus aureus* two-component system *sae*, the response regulator *SaeR* binds to a direct repeat sequence and DNA binding requires phosphorylation by the sensor kinase *SaeS*. *J Bacteriol* **192**:2111
- Swartz, M.A. and Fleury, M.E. (2007):** Interstitial flow and its effects in soft tissues. *Annu Rev Biomed Eng* **9**:229–256
- Trcek, J., Fuchs, T.M. and Trülsch, K. (2010):** Analysis of *Yersinia enterocolitica* invasins expression in vitro and in vivo using a novel luxCDABE reporter system. *Microbiology* **156**:2734–45
- Trosky, J.E., Liverman, A.D.B. and Orth, K. (2008):** *Yersinia* outer proteins: Yops. *Cell Microbiol* **10**:557–65
- Trülsch, K., Roggenkamp, A., Aepfelbacher, M., Wilharm, G., Ruckdeschel, K. and Heesemann, J. (2003):** Analysis of chaperone-dependent Yop secretion/translocation and effector function using a mini-virulence plasmid of *Yersinia enterocolitica*. *Int J Med Microbiol* **293**:167–77
- Trülsch, K., Sporleder, T., Igwe, E.I., Rüssmann, H. and Heesemann, J. (2004):** Contribution of the major secreted yops of *Yersinia enterocolitica* O:8 to pathogenicity in the mouse infection model. *Infect Immun* **72**:5227–34
- Tsutsumi, V. and Shibayama, M. (2006):** Experimental amebiasis: a selected review of some in vivo models. *Arch Med Res* **37**:210–20
- Vanassche, T., Verhaegen, J., Peetermans, W.E., Hoylaerts, M.F. and Verhamme, P. (2010):** Dabigatran inhibits *Staphylococcus aureus* coagulase activity. *J Clin Microbiol* **48**:4248–50
- Viana, D., Blanco, J., Tormo-Más, M.Á., Selva, L., Guinane, C.M., Baselga, R., Corpa, J.M., Lasa, Í., Novick, R.P., Fitzgerald, J.R. and Penadés, J.R. (2010):** Adaptation of *Staphylococcus aureus* to ruminant and equine hosts involves SaPI-carried variants of von Willebrand factor-binding protein. *Mol Microbiol* **77**:1583–1594
- Viboud, G.I. and Bliska, J.B. (2001):** A bacterial type III secretion system inhibits actin polymerization to prevent pore formation in host cell membranes. *EMBO J* **20**:5373–82
- Viboud, G.I. and Bliska, J.B. (2005):** *Yersinia* outer proteins: role in modulation of host cell signaling responses and pathogenesis. *Annu Rev Microbiol* **59**:69–89
- Viboud, G.I., Mejía, E. and Bliska, J.B. (2006):** Comparison of YopE and YopT activities in counteracting host signalling responses to *Yersinia pseudotuberculosis* infection. *Cell Microbiol* **8**:1504–15

- Vicente-Manzanares, M., Ma, X., Adelstein, R. and Horwitz, A. (2009): Non-muscle myosin II takes centre stage in cell adhesion and migration. *Nat Rev Mol Cell Biol* **10**:778–790
- Vukasinovic, J., Cullen, D.K., Laplaca, M.C. and Glezer, A. (2009): A microperfused incubator for tissue mimetic 3D cultures. *Biomed Microdevices* **11**:1155–65
- Wang, L. and Zheng, Y. (2007): Cell type-specific functions of Rho GTPases revealed by gene targeting in mice. *Trends Cell Biol* **17**:58–64
- Weber, K. and Osborn, M. (1969): The reliability of molecular weight determinations by dodecyl sulfate-polyacrylamide gel electrophoresis. *J Biol Chem* **244**:4406–12
- Wieser, A., Guggenberger, C., Pritsch, M., Heesemann, J. and Schubert, S. (2011): A novel ex vivo set-up for dynamic long-term characterization of processes on mucosal interfaces by confocal imaging and simultaneous cytokine measurements. *Cell Microbiol* **13**:742–51
- Witko-Sarsat, V., Rieu, P., Descamps-Latscha, B., Lesavre, P. and Halbwachs-Mecarelli, L. (2000): Neutrophils: molecules, functions and pathophysiological aspects. *Lab Invest* **80**:617–53
- Wölke, S., Ackermann, N. and Heesemann, J. (2011): The *Yersinia enterocolitica* type 3 secretion system (T3SS) as toolbox for studying the cell biological effects of bacterial Rho GTPase modulating T3SS effector proteins. *Cell Microbiol* **13**:1339–57
- Wong, K.W. and Isberg, R.R. (2005): *Yersinia pseudotuberculosis* spatially controls activation and misregulation of host cell Rac1. *PLoS Pathog* **1**:e16
- Yang, D., Chen, Q., Stoll, S., Chen, X., Howard, O.M. and Oppenheim, J.J. (2000): Differential regulation of responsiveness to fMLP and C5a upon dendritic cell maturation: correlation with receptor expression. *J Immunol* **165**:2694–702
- Yoshinaga-Ohara, N., Takahashi, A., Uchiyama, T. and Sasada, M. (2002): Spatiotemporal regulation of moesin phosphorylation and rear release by Rho and serine/threonine phosphatase during neutrophil migration. *Exp Cell Res* **278**:112–122
- Zhou, G., Mo, W., Sebbel, P., Min, G., Neubert, T., Glockshuber, R., Wu, X., Sun, T. and Kong, X. (2001): Uroplakin Ia is the urothelial receptor for uropathogenic *Escherichia coli*: evidence from in vitro FimH binding. *J Cell Sci* **114**:4095
- Zhu, M., Shao, F., Innes, R.W., Dixon, J.E. and Xu, Z. (2004): The crystal structure of *Pseudomonas avirulence* protein AvrPphB: a papain-like fold with a distinct substrate-binding site. *Proc Natl Acad Sci U S A* **101**:302–7
- Zumbihl, R., Aepfelbacher, M., Andor, A., Jacobi, C.A., Ruckdeschel, K., Rouot, B. and Heesemann, J. (1999): The cytotoxin YopT of *Yersinia enterocolitica* induces modification and cellular redistribution of the small GTP-binding protein RhoA. *J Biol Chem* **274**:29289–93

Appendix: Movie legends

Movie 1: GFP-positive cells from the spleen emigrate from the tissue slice and migrate on the coverslip. The spleen from a *lys-EGFP* mouse was removed, embedded in 4% agarose and cut into 300 μm thin tissue slices with a vibrating blade microtome. The tissue slice was mounted in a dish (μ -slide 8 well, ibidi) and analyzed on a confocal microscope equipped with an incubation chamber. Green: GFP-expressing cells. Duration 41 min.

Movie 2: GFP-positive cells from the spleen are able to take up bacteria after emigration from the tissue slice. The spleen from a *lys-EGFP* mouse was removed, embedded in 4% agarose and cut into 300 μm thin tissue slices with a vibrating blade microtome. The tissue slice was mounted in a dish (μ -slide 8 well, ibidi) pre-incubated with *Y. enterocolitica* WA-C(pRFP) and analyzed on a confocal microscope equipped with an incubation chamber. GFP-positive cells exhibit migratory behavior and efficient phagocytosis of bacteria. Green: GFP-expressing cells. Red: DsRed-expressing *Y. enterocolitica* WA-C. Duration 22 min.

Movie 3: Bone marrow-derived macrophages in 3D-CoG. Bone-marrow derived macrophages were incorporated into 3D-CoG together with WA-C. The migratory behavior of macrophages in 3D-CoG is different from that of spleen-derived GFP-positive cells. Duration 69 min.

Movie 4: Degradation of pseudocapsule and MAM by plasmin. *S. aureus* Newman colonies were grown in 3D-CoG/Fib for 16 h. Subsequent addition of plasmin (8 $\mu\text{g}/\text{ml}$) to the 3D-CoG/Fib surface led to rapid degradation of both pseudocapsule and MAM surrounding Newman microcolonies within few minutes. Duration: 22 min.

Movie 5: Fibrinolysis of CA-MRSA strain USA300. A single USA300 microcolony degrading pseudocapsule and MAM 21 h after inoculation in 3D-CoG/Fib (10x bacterial density compared to normal assays to provoke fibrinolysis). This is a time lapse movie representing the bottom left area of Fig. 3.11 C. Fibrin structures are degraded, whereas collagen fibers are unaffected. A projection of several sections spanning a total depth of 11 μm is shown. Confocal reflection microscopy shows collagen and fibrin fibers. Duration: 140 min.

Movie 6: Interaction of neutrophils with *S. aureus* Newman in 3D-CoG/Fib. *S. aureus* Newman was grown in 3D-CoG/Fib for 17 h and then challenged with neutrophils. Neutrophils migrated within the 3D-CoG but did not approach the colonies within 3 h of observation. Fig. 3.12 E shows a time projection of the entire observation period. Green: GFP-neutrophils; White: confocal reflection microscopy showing collagen fibers. A projection of 3 sections spanning a total depth of 10.3 μm is shown. Duration: 3 h.

Movie 7: Interaction of neutrophils with *S. aureus* Newman *sae* mutant in 3D-CoG/Fib. Newman *sae* mutant (Newman-29) clusters grown in 3D-CoG/Fib for 17 h were immediately invaded and phagocytosed by neutrophils. Fig. 3.13 shows a time projection of the entire observation period. Green: GFP-neutrophils; White: confocal

reflection microscopy showing collagen fibers. A projection of two sections spanning a total depth of 5.3 μm is shown. Duration: 87 min.

Movie 8: Interaction of neutrophils with *S. aureus* Newman *vWbp emp* mutant in 3D-CoG/Fib. Newman *vWbp emp* mutant was grown in 3D-CoG/Fib for 17 h and then challenged with neutrophils. Neutrophil migration in the vicinity of the microcolony was not inhibited. Neutrophils approached the microcolony but were prevented from invading by the pseudocapsule. Fig. 3.12 H shows a time projection of the entire observation period. Green: GFP-neutrophils; White: confocal reflection microscopy showing collagen fibers. A projection of 3 sections spanning a total depth of 10.3 μm is shown. Duration: 3 h.

Movie 9: Protective function of the pseudocapsule. Pseudocapsules protected *S. aureus* from direct invasion by neutrophils into the microcolony. This is shown here with the *vWbp emp* double mutant. 17 h after inoculation, bacterial microcolonies were challenged with neutrophils. After approximately 5 h 15 min of neutrophil challenge, the first neutrophils invaded the microcolony and started phagocytosis. Green: GFP-neutrophils; Blue: Sytox Blue-stained DNA; White: confocal reflection microscopy showing collagen fibers. Duration: 45 min.

Movie 10: Pseudocapsule rupture. Pseudocapsules protected *S. aureus* from direct invasion by neutrophils into the microcolony. This is shown here with the *vWbp emp* double mutant. 17 h after inoculation, bacterial microcolonies were challenged with neutrophils. After approximately 5 h the pseudocapsule ruptured and released huge amounts of staphylococci which are phagocytosed by surrounding neutrophils. Green: GFP-neutrophils; Blue: Sytox Blue; White: confocal reflection microscopy. Duration: 45 min.

Movie 11: Neutrophil cell lysis/necrosis after pseudocapsule rupture. Direct contact of neutrophils with staphylococci due to pseudocapsule rupture or invasion led to massive neutrophil cell lysis/necrosis, visualized by Sytox Blue staining of nuclei. The *vWbp emp* double mutant was grown in 3D-CoG/Fib for 17 h and then challenged with neutrophils. 5 h later this movie was taken. Green: GFP-neutrophils; Blue: Sytox Blue-stained DNA; White: confocal reflection microscopy showing collagen fibers. Duration: 45 min.

Movie 12: The irregularly shaped pseudocapsule of the *coa* mutant retains residual barrier function. The *coa* mutant was grown in 3D-CoG/Fib for 17 h and then challenged with neutrophils. 3 h later this movie was taken. Residual barrier function of the irregularly shaped pseudocapsule could be detected in some sections of the microcolony. Green: GFP-neutrophils; Blue: Sytox Blue-stained DNA; White: confocal reflection microscopy showing collagen fibers. Duration: 35 min.

Movie 13: CA-MRSA USA300 barrier function in 3D-CoG/Fib. USA300 was grown in 3D-CoG/Fib for 17 h and then challenged with neutrophils. 3.5 h later this movie was taken. A barrier function of the MAM and the pseudocapsule could be demonstrated. Green: GFP-neutrophils; Blue: Sytox Blue-stained DNA; White: confocal reflection microscopy showing collagen fibers. Duration: 87 min.

Movie 14: DC migration in a CCL19 gradient. DCs were incorporated into 3D-CoG. After polymerization of the 3D-CoG, a CCL19 gradient was established and cell migration was recorded using time lapse microscopy. The majority of cells migrate towards the gradient decreasing from right to left. Duration 2 h 45 min.

Movie 15: DC migration in a CCL19 gradient after infection with WA(pYV). DCs were infected with WA(pYV) *in vitro* for 30 min (MOI 20). Cells were then washed and incorporated into 3D-CoG. After polymerization of the 3D-CoG, a CCL19 gradient was established and cell migration was recorded using time lapse microscopy. Most cells are unable to migrate towards the gradient but get stuck in the 3D-CoG by formation of several leading edges in parallel. CCL19 gradient decreases from right to left. Duration 2 h 45 min.

Movie 16: DC migration in a CCL19 gradient after infection with WA(pYV Δ lcrD). DCs were infected with WA(pYV Δ lcrD) *in vitro* for 30 min (MOI 20). Cells were then washed and incorporated into 3D-CoG. After polymerization of the 3D-CoG, a CCL19 gradient was established and cell migration was recorded using time lapse microscopy. Migratory behavior of DCs is not different from uninfected cells: approximately 70 % of all cells migrate constantly towards the CCL19 gradient. CCL19 gradient decreases from right to left. Duration 2 h 45 min.

Movie 17: DC migration in a CCL19 gradient after infection with WA(pYV Δ yopT). DCs were infected with WA(pYV Δ yopT) *in vitro* for 30 min (MOI 20). Cells were then washed and incorporated into 3D-CoG. After polymerization of the 3D-CoG, cell migration was recorded using time lapse microscopy. Migratory behavior of DCs is not inhibited and resembles cells infected with WA(pYV Δ lcrD). CCL19 gradient decreases from right to left. Duration 3 h.

Movie 18: DC migration in a CCL19 gradient after infection with WA(pTTSS, pYopT). DCs were infected with WA(pTTSS, pYopT) *in vitro* for 30 min (MOI 20). Cells were then washed and incorporated into 3D-CoG. After polymerization of the 3D-CoG, cell migration was recorded using time lapse microscopy. Migratory behavior of DCs is not different from cells infected with WA(pYV). CCL19 gradient decreases from right to left. Duration 3 h.

Movie 19: Migratory behavior of DCs transfected with MLC-GFP constructs after contact with WA(pYV, pRFP) in under-agarose assays. DCs and bacteria were inoculated under agarose using pipet tips. DCs were inoculated at a distance of 4-5 mm from the attractor well. Bacteria were inoculated between responder and attractor well. Green: MLC-GFP. Red: yersiniae with pRFP. Duration: 18 min.

Movie 20: Migratory behavior of DCs transfected with MLC-GFP constructs after contact with WA(pYV Δ lcrD, pRFP) in under-agarose assays. DCs and bacteria were inoculated under agarose using pipet tips. DCs were inoculated at a distance of 4-5 mm from the attractor well. Bacteria were inoculated between responder and attractor well. Green: MLC-GFP. Red: yersiniae with pRFP. Duration: 11 min.

Movie 21: Elongated cell shape of DCs after contact with WA(pYV, pRFP). DCs and bacteria were inoculated under agarose using pipet tips. While the cell body

containing the nucleus is paralyzed, cell protrusions are highly active even 3 h after first cell elongation events occurred. Green: MLC-GFP. Red: yersiniae with pRFP. Duration: 32 min.

Movie 22: YopT_{yen}-dependent morphotype is dependent on type III secretion, demonstrated with a β -lactamase (*bla*) reporter system. CCF4-loaded DCs were infected in under-agarose assays with WA(pYV, pYopH-*bla*) carrying a plasmid encoding for a fusion of YopH and β -lactamase. Successful translocation of this construct cleaves the FRET substrate CCF4 inside the DCs. Green: fluorescence of the CCF4. Red: fluorescence of CCF4 after cleavage by β -lactamase. Overlaid with bright field channel. CCL19 gradient decreases from top to bottom. Duration 68 min.

Movie 23: YopT_{yen}-dependent morphotype is not induced by WA(pYV Δ *lcrD*, pYopH-*bla*). CCF4-loaded DCs were infected in under-agarose assays with WA(pYV Δ *lcrD*, pYopH-*bla*) carrying a plasmid encoding for a fusion of YopH and β -lactamase. Successful translocation of this construct cleaves the FRET substrate CCF4 inside the DCs. Green: fluorescence of the CCF4. Red: fluorescence of CCF4 after cleavage by β -lactamase. Overlaid with bright field channel. CCL19 gradient decreases from bottom to top. Duration 68 min.

Movie 24: Migratory behavior of murine bone marrow cells (Lifeact mice) after contact with WA(pYV) in an under-agarose assay. Bone marrow was prepared from Lifeact-GFP mice (depicted in green). After bacterial contact cell elongation similar to that observed in DCs can be observed. Green: Lifeact-GFP. Duration: 95 min.

Movie 25: Migratory behavior of murine bone marrow cells (Lifeact mice) after contact with WA(pTTSS, pYopT_{yen}) in an under-agarose assay. Bone marrow was prepared from Lifeact-GFP mice (depicted in green). After bacterial contact cell elongation similar to that observed in DCs can be observed. Green: Lifeact-GFP. Duration: 40 min.

Movie 26: Migratory behavior of human neutrophils isolated from peripheral blood after contact with WA(pYV) in an under-agarose assay. Neutrophils were isolated and incubated in under-agarose assays in the presence of WA(pYV). Contact leads to massive cell elongation. Duration 120 min.

Movie 27: DC migration in a CCL19 gradient after infection with *Y. pseudotuberculosis* IP32953. DCs were infected with *Y. pseudotuberculosis* IP32953 *in vitro* for 30 min (MOI 20). Cells were then washed and incorporated into 3D-CoG. After polymerization of the 3D-CoG, cell migration was recorded using time lapse microscopy. Migratory behavior of DCs is strongly affected but residual protrusion dynamics can be observed. CCL19 gradient decreases from right to left. Duration 3 h.

Movie 28: DC migration in a CCL19 gradient after infection with *Y. pseudotuberculosis* YPIII(pIB1). DCs were infected with *Y. pseudotuberculosis* YPIII(pIB1) *in vitro* for 30 min (MOI 20). Cells were then washed and incorporated into 3D-CoG. After polymerization of the 3D-CoG, cell migration was recorded using time lapse microscopy. Migratory behavior of DCs is strongly affected but residual protrusion dynamics can be observed. CCL19 gradient decreases from right to left. Duration 3 h.

Movie 29: DC migration in a CCL19 gradient after infection with WA(pTTSS, pYopT_{yps}). DCs were infected with WA(pTTSS, pYopT_{yps}) *in vitro* for 30 min (MOI 20). Cells were then washed and incorporated into 3D-CoG. After polymerization of the 3D-CoG, cell migration was recorded using time lapse microscopy. Migratory behavior of DCs is strongly affected and protrusion dynamics were almost completely abrogated. CCL19 gradient decreases from right to left. Duration 3 h.

Movie 30: DC migration in a CCL19 gradient after infection with WA(pTTSS, pYopE_{yps}). DCs were infected with WA(pTTSS, pYopE_{yps}) *in vitro* for 30 min (MOI 20). Cells were then washed and incorporated into 3D-CoG. After polymerization of the 3D-CoG, cell migration was recorded using time lapse microscopy. Migratory behavior of DCs is strongly affected but residual protrusion dynamics can be observed. CCL19 gradient decreases from right to left. Duration 3 h.

Movie 31: Migratory behavior of DCs after contact with IP32953 in an under-agarose assay. DCs and bacteria were inoculated under agarose using pipet tips. DCs were inoculated at a distance of 4-5 mm from the attractor well. Bacteria were inoculated between responder and attractor well. Cell migration is severely affected after contact with bacteria. Green: Lifeact-GFP. Duration: 40 min.

Movie 32: Detail from Movie 31.

Movie 33: F-actin dynamics of a DC after contact with IP32953 in an under-agarose assay. The cell appears paralyzed, no lamellipodia formation can be observed. White: Lifeact-GFP. Duration: 75 s.

Movie 34: Migratory behavior of DCs after contact with YPIII(pIB1) in an under-agarose assay. DCs and bacteria were inoculated under agarose using pipet tips. DCs were inoculated at a distance of 4-5 mm from the attractor well. Bacteria were inoculated between responder and attractor well. Cell migration is severely affected after contact with bacteria. Green: Lifeact-GFP. Duration: 40 min.

Movie 35: Detail from Movie 34.

Movie 36: F-actin dynamics of a DC after contact with YPIII(pIB1) in an under-agarose assay. The cell appears paralyzed, no lamellipodia formation can be observed. White: Lifeact-GFP. Duration: 78 s.

Movie 37: Migratory behavior of DCs after contact with WA(pTTSS, pYopE_{yen}) in under-agarose assays. DCs and bacteria were inoculated under agarose using pipet tips. DCs were inoculated at a distance of 4-5 mm from the attractor well. Bacteria were inoculated between responder and attractor well. Cell migration is unaffected by contact with bacteria. Green: Lifeact-GFP. Duration: 40 min.

Movie 38: Detail from Movie 37.

Movie 39: F-actin dynamics of a DC after contact with YPIII(pIB1) in an under-agarose assay. The cell front is protruding by actin polymerization towards the CCL19 gradient. White: Lifeact-GFP. Duration: 78 s.

Movie 40: Migratory behavior of DCs after contact with WA(pTTSS, pYopE_{yps}) in under-agarose assays. DCs and bacteria were inoculated under agarose using pipet tips. DCs were inoculated at a distance of 4-5 mm from the attractor well. Bacteria were inoculated between responder and attractor well. Cell migration is severely affected after contact with bacteria. Green: Lifeact-GFP. Duration: 40 min.

Movie 41: Detail from Movie 40.

Movie 42: F-actin dynamics of a DC after contact with WA(pTTSS, pYopE_{yps}) in an under-agarose assay. Overall, the cell appears to be paralyzed, residual lamellipodia formation can be observed. White: Lifeact-GFP. Duration 78 s.

Movie 43: Migratory behavior of DCs after contact with WA(pTTSS, pYopT_{yen}) in an under-agarose assay. DCs and bacteria were inoculated under agarose using pipet tips. DCs were inoculated at a distance of 4-5 mm from the attractor well. Bacteria were inoculated between responder and attractor well. Migration of the cell front seems uninhibited whereas the trailing edge gets stuck to the substrate after contact with bacteria. This leads to massive cell elongation. Green: Lifeact-GFP. Duration: 29 min.

Movie 44: Detail from Movie 43.

Movie 45: F-actin dynamics of a DC after contact with WA(pTTSS, pYopT_{yen}) in an under-agarose assay. High rates of actin polymerization in lamellipodia can be observed, whereas the trailing edge is rather static. White: Lifeact-GFP. Duration 78 s.

Movie 46: Migratory behavior of DCs after contact with WA(pTTSS, pYopT_{yps}) in an under-agarose assay. DCs and bacteria were inoculated under agarose using pipet tips. DCs were inoculated at a distance of 4-5 mm from the attractor well. Bacteria were inoculated between responder and attractor well. Forward movement of cells is stopped after contact with bacteria and cells take a circular shape. Green: Lifeact-GFP. Duration: 40 min.

Movie 47: Detail from Movie 46.

Movie 48: F-actin dynamics of a DC after contact with WA(pTTSS, pYopT_{yps}) in an under-agarose assay. Cell shape is rather circular, lamellipodia are highly active in regard to actin polymerization without actual translocation. White: Lifeact-GFP. Duration 107 min.

Movie 49: F-actin dynamics of a DC after contact with WA(pTTSS, pYopT_{yps}) in an under-agarose assay. The cell shows no polarization, the lamellipodium spans the entire cell outline and actin treadmilling takes place at a high rate. White: Lifeact-GFP. Cell diameter approximately 40 μm . Duration: 87 s.

Movie 50: F-actin dynamics of a native DC in an under-agarose assay. The native cell is clearly polarized and migrates towards a CCL19-gradient by lamellipodium protrusion. White: Lifeact-GFP. Duration: 220 s.

Movie 51: Single bacteria in IBCs (NU14) exhibit motility. A *lys-EGFP* mouse was infected intravesically with $\sim 3 \times 10^8$ cfu NU14(pM965-4 eGFP), sacrificed 5 h p.i. and the urinary bladder was removed. Blue: DAPI-stained nuclei. Green: NU14(pM965-4 eGFP). White: Confocal reflection microscopy. 1 h after explantation. Duration 59 s.

Movie 52: Recruitment of neutrophils to an IBC and subsequent phagocytosis. A *lys-EGFP* mouse was infected intravesically with 3×10^8 cfu NU14(pFPV-mCherry/2), sacrificed 5 h p.i. and the urinary bladder was removed. Some neutrophils appear to be inside the IBC. z projection of 10 z sections spanning a total depth of 31.5 μm . 30 min after explantation. Duration 1.5 h.

Movie 53: *E. histolytica* trophozoites migrate on caecum explants. Caecum explants from C57BL/6 mice were infected with 3.8×10^4 amoebae and analyzed by confocal microscopy. Yellow: FM 4-64-stained cell membranes. Red: rWGA-Alexa680-stained *E. histolytica* trophozoites. z projection of 5 z sections spanning a total depth of 26 μm . Duration 26 min.

Movie 54: *E. histolytica* interacting with cecal mucosa surface. Caecum explants (*lys-EGFP* mouse) were infected with 3.8×10^4 amoebae and analyzed by confocal microscopy. Flow rate in the apical compartment is increased to 4 ml/h until the trophozoite is flushed from the area of view due to increased shear stress. Red: FM 4-64-stained cell membranes. Yellow: rWGA-Alexa680-stained *E. histolytica* trophozoites. Blue: DAPI-stained nuclei. Green: GFP-positive cells. White: Confocal reflection microscopy. Duration 5 min.

Movie 55: An amoeba having successfully invaded caecum mucosa. 3D reconstruction from Fig. 3.40 C proves localization of the trophozoite inside the mucosa. z projection of 15 z sections spanning a total depth of 22 μm .

Movie 56: Neutrophils interacting with SFBs on the gut surface. Gut tissue from a naive *lys-EGFP* mouse was explanted and mounted in the organ chamber. SFBs were found anchored in the mucosa. Neutrophils were associated with SFBs, obviously trying to ingest them. During the movie, the tissue deforms and partly ruptures. From this, a strong adherence of neutrophils to SFBs can be deduced. Yellow: FM 4-64-stained cell membranes. Green: GFP-positive cells. Blue: DAPI-stained nuclei. z projection of 5 z sections spanning a total depth of 7.2 μm . 45 min after explantation. Duration 22 h.

Movie 57: Neutrophils after contact with *Y. enterocolitica* in 3D-CoG. WA(pYV Δ yadA) grown in 3D-CoG was challenged with neutrophils from a *lys-EGFP* mouse. After 2 h most neutrophils in contact with bacteria were elongated with their trailing edge often fixed to the 3D-CoG or bacteria. Duration: 40 min.

List of Publications

The following publications, manuscripts and contributions to symposia originated from this thesis:

Peer reviewed journals

- **Wieser, A.***, **Guggenberger, C.***, **Pritsch, M.**, **Heesemann, J.** and **Schubert, S.** (2011): A novel ex vivo set-up for dynamic long-term characterization of processes on mucosal interfaces by confocal imaging and simultaneous cytokine measurements. *Cell Microbiol* **13**:742-51

* contributed equally

- **Guggenberger, C.**, **Wolz, C.**, **Morrissey, J.A.** and **Heesemann, J.**: Two Distinct Coagulase-Dependent Barriers Protect *Staphylococcus aureus* from Neutrophils in a Three Dimensional in vitro Infection Model. *PLoS Pathog*, Submitted: June 29, 2011, in revision

Conferences and Symposia: Poster presentations

- **Guggenberger, C.**, **Czech, B.**, **Freund, S.** and **Heesemann, J.**
Establishment of a 3D dynamic imaging system for ex vivo analysis of host-pathogen interactions.
Munich Interact 2009, PhD Symposium, Munich, April 2, 2009
- **Guggenberger, C.**, **Czech, B.**, **Freund, S.** and **Heesemann, J.**
Host-pathogen interactions in a three dimensional context – a novel system for dynamic imaging of infectious processes.
Annual Conference of the German Society for Hygiene and Microbiology, Göttingen, August 20-23, 2009
- **Guggenberger, C.**, **Freund, S.** and **Heesemann, J.**
Characterisation of host-pathogen interactions in a three dimensional context.
Munich Interact 2010, PhD Symposium, Munich, March 23, 2010

- **Guggenberger, C., Freund, S. and Heesemann, J.**
Dynamics of host-pathogen interactions studied in a 3D collagen gel model.
Pathogenomics – From Basic Research to Application,
Pécs, Hungary, April 22-24, 2010
- **Guggenberger, C., Freund, S. and Heesemann, J.**
Characterisation of host-pathogen interactions in a three dimensional context.
EMBO Summer School Host-Microbes Interactions,
Spetsai, Greece, September 1-9, 2010
- **Guggenberger, C. and Heesemann, J.**
Interaction of bacterial pathogens with immune cells in a three dimensional context.
II. Summer School Pathogen-Host Interactions at Cellular Barriers,
Münster, June 8-10, 2011

Conferences and Symposia: Talks

- **Guggenberger, C. and Heesemann, J.**
Studying Yersinia virulence mechanisms in a three dimensional collagen gel setup.
2nd German Yersinia Meeting, Herrsching, September 17-18, 2010
- **Guggenberger, C. and Heesemann, J.**
Interaktion von Neutrophilen mit Staphylokokken im 3D-Collagen-Gel.
2. Süddeutsches Chemotherapiegespräch, Ulm, July 8, 2011

Acknowledgements

First of all, I would like to thank Prof. Dr. Michael Boshart for representing this thesis in the faculty of Biology at the University of Munich.

I am most grateful to my supervisor Prof. Dr. Dr. Jürgen Heesemann for giving me the opportunity to work on this highly interesting topic, his continuous and full support and his openness for discussion at any time. He granted me the freedom to develop and pursue my own ideas – even outside of the *Yersinia* world.

I would like to thank Prof. Dr. Michael Sixt for his help with everything ‘migration-related’, Prof. Dr. Christiane Wolz for access to *Staphylococcus* methods and Dr. Daniel Hilger for his help with protein structure homology modeling.

Many thanks to Andreas for our collaboration on the *ex vivo* microscopy project.

I would like to thank all present and former members of the AG Heesemann who I shared office or lab space with or who helped me in any way: Beate, Bettina, Sandra, Kristina, Julia, Stefan, Gigi, Steffi, Eva, Julia, Kathrin, Anette, Katja, Klaus, Susi, Hicham.

I am grateful to the team of the MvPI animal facility, to Sabine Tost at the Anatomical Institute for electron microscopy and to the Protein Analysis Unit for MALDI-TOF analysis.

Many thank to my friends for their moral support over the years, especially Uli, Daniel and Tobi.

Most importantly, I sincerely thank Steffi and my family, in particular my parents and grandparents, for supporting me in every possible way. It was you who made this possible for me.

Eidesstattliche Erklärung

Hiermit versichere ich ehrenwörtlich, dass die vorliegende Dissertation von mir selbständig und nur unter Verwendung der angegebenen Quellen und Hilfsmittel angefertigt wurde. Desweiteren erkläre ich, dass ich nicht anderweitig ohne Erfolg versucht habe, eine Dissertation einzureichen oder mich der Doktorprüfung zu unterziehen. Die vorliegende Dissertation liegt weder ganz, noch in wesentlichen Teilen einer anderen Prüfungskommission vor.

München, den 8. August 2011

Christoph Guggenberger